Developing protein conjugation techniques to enhance cell delivery of therapeutic enzymes

By:

Rosalyn Hart

PhD

December 2017

The University of Sheffield

Faculty of Life Sciences

Department of Biomedical Science

Abstract

The focus of disease research often surrounds therapeutic pathway identification and the subsequent investigation of proteins or compounds that potentially interfere with disease mechanisms. However, finding targets and effective therapeutic domains often overshadows another important aspect of drug delivery and efficacy; the method of domain conjugation. Unfortunately the combination of good therapeutic components and good therapeutic design can often be amiss, with differing skills and groups needed to marry the two together. In recognition of this, there are new techniques emerging that aim to not only address old problems of stable conjugation, but incorporating new knowledge of drug design.

This research takes a reverse approach to drug design in order to better comprehend requirements which are often an afterthought; first looking at conjugation technique and then how it can best be exploited. Thereby, exploring how different conjugation methods can be used to complement existing therapeutic and internalisation strategies.

Here, two methods of conjugation were investigated through attachment of bacterial toxin domains derived from botulinum A and diphtheria, with the intention of targeting neuroblastoma cells using a variety of specific and non-specific pathways. Both conjugation techniques proved to be stable *in vitro* and capable of binding a variety of domains consistently. The data here also emphasized the importance of endosomal escape proteins to increase the translocation of catalytic domains into the cytosol. It was demonstrated that the conjugates formed were able to facilitate the binding between targeting and catalytic domains, enabling specific neuroblastoma internalisation. Moreover, that three domains were able to conjugate together using a linking method and could form a co-operative triple-functioning complex.

Table of Contents

Tables and Figures

List of Abbreviations

AA	Amino acid
Ahx	6-aminohexanoic acid
AU	Arbitrary Unit
ADC	Antibody drug conjugate
ADCC	Antibody dependent cell-mediated cytotoxicity
APS	Ammonium Persulfate
B	Boiled
BLF1	Burkholderia lethal factor 1
BotLC	Botulinum Light Chain
BotLcTd/A	Botulinum Light Chain Translocation domain, serotype A
BotNT	Botulinum neurotoxin
BotNT/A	Botulinum neurotoxin, serotype A
Bq	Becquerel
Brevin	Synaptobrevin
BSA	Bovine serum albumin
Ci	Curie
CNTF	Ciliary neurotrophic factor
CNTFR	Ciliary neurotrophic factor receptor
COSHH	Control of Substances Hazardous to Health
CPM	Counts per Minute
CPP	Cell Penetrating Peptides
CRD	Cysteine rich domain
CRH	Corticotrophin releasing hormone
cSNAP25	Cleaved SNAP25
DARPins	Designed Ankyrin repeat proteins
Dermo	Dermorphin
dH_2O	Deionized water
DMEM	Dulbecco's modified Eagle medium
DPM	Disintegrations per Minute
DT	Diphtheria toxin
DipLC	Diphtheria Light Chain
DipLcTd	Diphtheria Light Chain Translocation Domain

eEF-2	eukaryotic elongation factor-2
eIF	eukaryotic Initiation factor
EGF	Epithelial growth factor
EGFR	Epithelial growth factor receptor
ER	Endoplasmic reticulum
ERAD	Endoplasmic-reticulum-associated protein degradation
FBS	Foetal bovine serum
FPLC	Fluid phase liquid chromatography
GST	Glutathione S-transferases
HA2	Hemagglutinin 2
HEPES	4-(2-hydroxyethyl)-1-piperazineethanesulfonic acid
HV	High Voltage
ICC	Immunocytochemistry
IFP	Interstitial fluid pressure
IL-2	Interleukin 2
Int.	Intensity
L	Litres
LC	Light Chain
LcTd	Light chain and translocation domain
LF3000	Lipofectamine 3000
$MgCl_2$	Magnesium Chloride
MES	2-(*N*-morpholino)ethanesulfonic acid
M	Molar concentration per litre
ms	Millisecond
MTT	(3-(4,5-Dimethylthiazol-2-yl)-2,5-Diphenyltetrazolium Bromide)
MWCO	Molecular weight cut off
n	Number of repeats within an experiment
N	Number of separate experiments
NEAA	Non-essential amino acids
NEB	New England Biolabs
NPY	Neuropeptide Y
NS	Not Significant
NSF	N-ethylmaleimide-sensitive factor
Obj.	Objective

OD	Optical density
OG	Octyl β-D-glucopyranoside
P	Passage number
Pass.	Passage number
P/S	Penicillin/streptomycin
PACAP	Pituitary adenylate cyclase-activating polypeptide
PBS	Phosphate buffered saline
PBS-T	Phosphate buffered saline- Tween20
PenStrep	Penicillin Streptomycin
PI	Propidium iodide
Rbd	Receptor binding domain
Rcf	Relative centrifugal force
RIP	Ribosome inactivating protein
RT	Room Temperature (22˚C)
S25	SNAP25
SDS	Sodium dodecyl sulphate
SH	Sulfhydryl
SNAP	Soluble NSF attachment protein
SNAP25	Synaptosomal-associated protein of 25kDa
SNARE	Soluble *N*-ethylmaleimide sensitive factor attachment protein receptor
SubP	Substance P
SV2	Synaptic vesicle protein 2
Syx	Syntaxin
TCEP	Tris(2-carboxyethyl)phosphine
Td	Translocation domain
TEMED	Tetramethylethylenediamine
Temp.	Temperature
Thio	Pyridyldithio
TNFα	Tissue Necrotic Factor α
tRNA	transfer RNA
Trunc	Truncated
Tub	Tubulin
U	Unboiled
UN	Units of protein

VAMP	Vesicle associated membrane protein
VEGF	Vascular endothelial growth factor
VIP	Vasoactive intestinal peptide
VLS	Vascular leak syndrome
Vol	Volume
WB	Western blot
WT	Wild Type

Acknowledgements

Firstly, I'd like to thank Professor Bazbek Davletov for supervising me during this project and for all the help and support he has given me throughout my PhD. I would also like to thank the other members of the Davletov lab who have been a source of helpful suggestions and advice. I would like to thank Charlotte Leese for her help in discussing and troubleshooting the more challenging areas of this project, and also Rebecca Bresnahan for being a constant source of support and friendship.

I would also like to acknowledge my advisors Carl Smythe and Mohammed Nassar for giving me good support and advice as well as keeping me focused throughout. Thank you also to Elizabeth Smythe and the members of her laboratory for donating antibodies along with their help and advice with slide fixing and imaging.

Additionally, I would like to thank my friends and family for their support and love which was invaluable throughout the project. My parents and siblings especially were always there with encouragement and praise which really helped keep morale high. Finally, I would like to thank my wonderful partner Tom, who was always on hand with pep-talks, laughter, tea and biscuits, and never doubted for a second that I would see the finish line.

Declaration

I declare that all data within this thesis has been completed by the author. Some proteins, plasmids and reagents which have been helpfully made by others have been referenced where necessary.

Chapter 1: Introduction

1.1 Considering Conjugation

Combining protein domains allows synthesis of novel drugs for treatment of various diseases (Sandvig & van Deurs 2005; Yeh et al. 2011). Such novel drugs may exploit proteins that bind cells specifically and catalytic domains which could exert a potent therapeutic effect within the cell. A number of factors need to be contemplated in drug construction; if the conjugation between different protein domains is unstable then the drug will fall apart in the bloodstream, not target the cells and cause side effects. On the other hand, if it is not cleavable then the domains will not break apart inside the lysosomes of cells and could interfere with the efficiency of the catalytic domain. There are also issues with making multidomain drugs, for instance if an optimal ratio of particular therapeutic domains is required then there is difficulty in ensuring that the particular ratio is synthesised without heterogeneity or the different domains interfering with each other.

The consideration of conjugation technique between protein domains for the production of therapeutics is an important step in drug design, where the consequences can influence stability and efficiency of the therapeutic product (Stephanopoulos & Francis 2011). As technology and understanding of therapeutic construction evolves so does specifications for desirable protein linking; therefore, there is an ongoing need to investigate methods of conjugation in order to develop drugs, methods of probing or tagging. From this, it is important that many avenues of protein conjugation are investigated to allow the greatest efficiency in a designed therapeutic.

1.1.1 Bioconjugation methods

A suitable linker between drug components should be stable in the blood, but not interfere with the effects of the attached drug once it has reached the desired location, often the cytosol. There have been many reported methods of protein conjugation, but the appropriate modification strategy is influenced by the desired supramolecular properties. Broadly, conjugation types can be divided into non-cleavable and cleavable (Srinivasarao et al. 2015). Non-cleavable bonds, such as maleimide bonds or recombinant fusion, can be used to conjugate a variety of domains consisting of drug and probes (McCombs & Owen 2015). For instance, antibody drug conjugates (ADCs) function through the conjugation of an antibody to various cytotoxic drugs; antibodies are a commonly used way to specifically

target receptors on cells *in vivo* and *in vitro*, therefore ADCs developed to exploit this through targeting and internalising specifically diseased cells and delivering their payload (Kitson et al. 2013; Huennekens 1994). Once the ADC enters the lysosomes its structure degrades leaving an amino acid chain attached to the drug; the drug can then exert its function (McCombs & Owen 2015). However, the conjugated amino acid chain can interfere with drug efficacy; therefore, there is a growing trend for cleavable linkers between drugs and carriers in order for drugs to function unimpeded (McCombs & Owen 2015; Lee et al. 2013). Cleavable bonds are those where either chemical, photolytic or enzymatic activity can cause breakage, examples which have been investigated for this purpose include disulphide and hydrazone bonds (Leriche et al. 2012). Hydrazone bonds are stable at neutral pHs, however have shown in some studies to readily hydrolyse and have a short biological half-life (Kovaříková et al. 2008; Hruskova et al. 2011).

The uncleavable maleimide bonds is the most commonly used protein conjugation strategy owing to their ability to stably bind to lysine and cysteine residues in a single step process (Fontaine et al. 2015). Whilst there are maleimide-conjugated FDA approved drugs such as the ADCs Brentuximab vedotin and Trastuzumab emtansine, the long term stability of these drugs is poor (Fontaine et al. 2015; Ponte et al. 2016). Because of this, there is a demand for simple yet physiologically more stable alternatives.

The maleimide reaction is shown in figure 1.1:A, where either the sulfhydryl (SH) or amino group (NH_2) can bind to the maleimide group via Michael addition to conjugate the two proteins (Kalia & Raines 2007). However, at neutral pH the conjugate can undergo the retro-Michael reaction, causing the product to separate; there are also reports of favourable binding to albumin and glutathione in plasma, making this instability a particular issue *in vivo* (Tumey et al. 2014; Kitagishi et al. 2015; Wei et al. 2016). This unfavourable stability has been investigated, with reports of between 35-67% break down in mouse plasma over 3 days (Christie et al. 2015; Badescu et al. 2014). There have been many ways where maleimides have been altered to increase the stability, for instance hydrolysing the maleimide ring, hence preventing the retro-Michael reaction from occurring (fig 1.1:A). However, this then turns a one-step protocol into multi-step protocol, where increased temperatures or pHs are needed for efficient hydrolysis or catalysts are used which could disrupt the proteins conjugated (Lyon et al. 2014; Kalia & Raines 2007).

Disulphide bonds have been shown to form and retain stability at neutral and acidic pH, but are reduced in the lysosomes via lysosomal enzymes (Lee et al. 2013; Arunachalam et

al. 2000). Disulphide bonds are usually formed when sulfhydryl (SH) groups on chemicals or on cysteine amino acids bind together. Their stability makes them favourable to use for conjugating proteins or chemicals, however they are often overlooked in favour of maleimide because cysteines are often less present than lysines within proteins and because of the uncontrolled homo and heterodimerisation between SH groups.

Succinimidyl 3-(2-Pyridyldithio)Propionate (SPDP) is a chemical used to facilitate the introduction of a cysteine onto a protein, where an NH_2 residue displaces the succinimidyl group at one end, leaving a pyridyldithio group at the other end in order to 'cap' the reactive sulfhydryl group. This 'cap' can then be removed by reducing the disulphide bridge through reagents such as DTT, and the released SH group can then conjugate to another protein, often via a maleimide group (Shi et al. 2009; Manjappa et al. 2011) (fig. 1.1:B).

It has been shown in examples that the pyridyl-disulphide (pyridyldithio) group on SPDP can be bound directly to SH groups, forming a disulphide bond and a pyridyl thione, which does not interfere with the conjugated proteins and is small enough to be easily filtered (Carlsson et al. 1978; Stuchbury et al. 1975) (fig. 1.1C). Whilst this technique has been identified, the conjugation and stability of pyridyl-disulphide formed disulphide bonds have yet to be thoroughly explored from a biological perspective independent of SPDP, or as a way to potentially modify proteins and enzymes with peptides (Eby et al. 2012; Van Der Vlies et al. 2010).

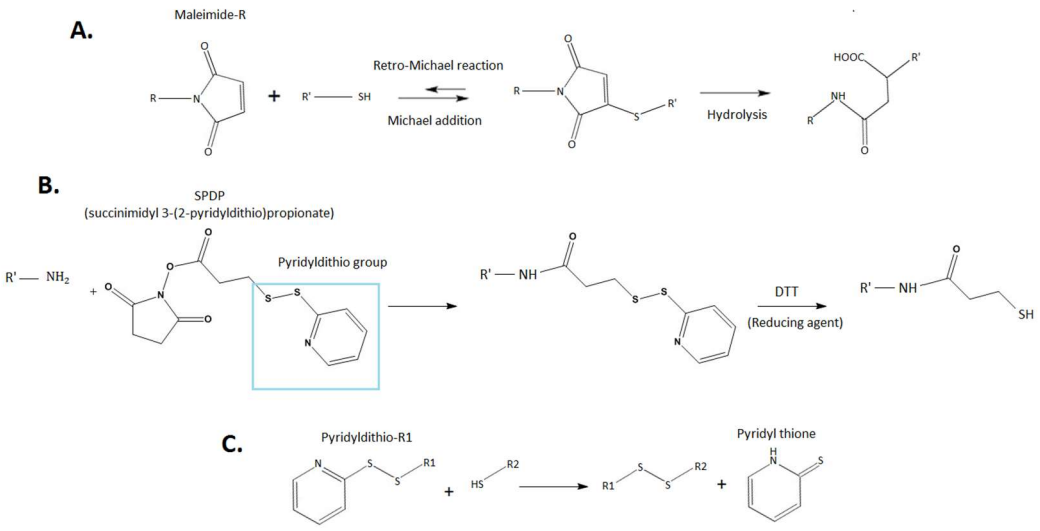

Figure 1.1 – Diagrams of bioconjugation methods

A) Shows the maleimide reaction with a sulfhydryl (SH) group forming a conjugation between the two proteins, via Michael addition, represented by R and R', joined by a succinimide ring. The retro-Michael reaction is a slow reaction which reverses the Michael addition. Hydrolysis can occur to the succinimide ring, where it breaks open and this stabilises the structure preventing the retro-Michael reaction. B) Succinimidyl 3-(2-Pyridyldithio)Propionate (SPDP) structure. This is composed of a succinimidyl group one end which is displaced by NH_2 residues. The pyridyldithio end can then be reduced by DTT to expose an SH group, which is often then bound to maleimide domain. C) SH groups on cysteine residues can be sufficient to displace the pyridyl disulphide, forming a disulphide bridge between desired proteins and releasing pyridine-2-thione.

1.1.2 Alternative linking strategies

As well as using chemical covalent attachment between therapeutically relevant domains to synthesise drugs, there are numerous alternative conjugation strategies which could be appropriate to use depending on the requirements of the product. For instance, there are examples where proteins in nature bind extremely stably and specifically through either covalent or non-covalent means, some of these have then been hijacked to bring together drug domains, probes or targeting domains, using these stably binding proteins as 'glue' (Hartley 1989; Reddington & Howarth 2015). Examples of these protein-derived conjugation techniques include 'SpyCatcher/SpyTag'. Derived from bacterial fibronectin binding proteins, there have been reports showing that by having either the 'SpyCatcher' or the 'SpyTag' attached to various domains in a library, the conjugation between select proteins could be done on demand, making a useful and flexible conjugation tool (Moon et al. 2016; Zakeri et al. 2012). Other proteins which have been similarly used include the barnase-barstar module and an adapter/docking-tag system based on mutated fragments of RNAse (Rossi et al. 2012).

There are however examples where protein conjugation can be facilitated by enzymes; for instance, it has been demonstrated that the bacterial transpeptidase sortase A will cleave between the threonine and glycine in a LPCTG motif, generating an acyl-enzyme intermediate. This then reacts with N-terminal glycines to create an amide bond. Therefore, proteins can be expressed with the recognition motifs before sortase A is added

(Levary et al. 2011). Whilst the reaction is quick and efficient, because enzymes are required there are added reagents and conditions which need to be considered for this conjugation technique which are not required in spontaneous reactions. Therefore, for the purpose of this work, spontaneous reactions are preferable.

Another example of protein-derived conjugation is SNARE stapling; this is a method which uses the self-assembling potential of the SNARE complex (Sudhof & Rothman 2009) (fig. 1.2). Endogenously, the SNARE complex forms between the SNARE peptides on vesicles and docking membranes, where the complex formation overcomes the forces required to merge the two membranes together, forming pores between the two compartments; because of this function, SNARE complexes are extremely stable (Montecucco & Molgó 2005; Zhang et al. 2016). The SNARE complex relies on the formation of the complex through three or more different helical proteins. This could be an advantage, because there are instances within drug design where more than two domains are needed to conjugate, for instance in dual targeting or where more than one drug needs to be used; a suitable method to design such a multidomain complex has yet to be thoroughly developed. Hypothetically, it should be possible to attach each of these SNARE proteins to variety of different therapeutic and targeting proteins and link them together.

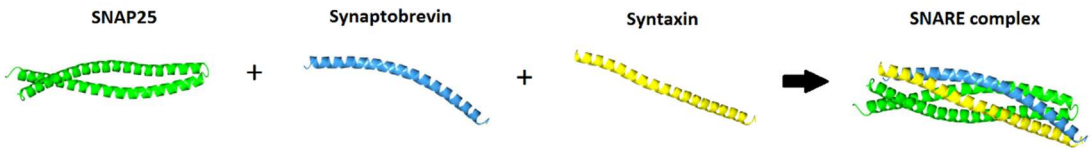

Figure 1.2 – Diagram of the formation of the SNARE complex

Diagram showing three SNARE proteins which come together and form the SNARE complex; a supercoiled quasi-irreversible structure. SNARE PDB ID: 5W5D (McNicholas et al. 2011; Berman et al. 2000)

SNARE-stapled conjugation research has previously shown that catalytic domains derived from botulinum can be linked via the SNARE complex to growth factors and other receptor binding domains to target and internalise into specific cells (Arsenault et al. 2013; Darios et al. 2010). However, the data currently is limited to attaching botulinum domains and

there has only been utilisation of two out of the four available SNARE helices. Therefore, there is an interest in determining whether SNARE-stapling could be used to link numerous different targeting and catalytic proteins together; moreover, whether three or more separate proteins could be attached to the SNARE helices and successfully form a triple-functioning complex.

1.2 *In Vitro* cancer cell targeting

Synthesised complexes were to be tested on cells to determine how well the constructs are able to internalise their attached catalytic proteins. For this, it was decided to utilise adherent cell lines which can be grown, incubated with samples and assayed easily *in vitro*. Owing to the nature of the botulinum neurotoxin research and neuronal cell models used previously in this laboratory, neuroblastoma cells were chosen as the main test model.

1.2.1 Neuroblastoma pathology

Neuroblastoma is a rare cancer of the brain, but the most common form of death from paediatric cancer of children between the ages of 1 and 5 (Louis & Shohet 2015). It is a neuroendocrine tumour arising from the neural ganglia of the peripheral nervous system which often exhibits extreme heterogeneity. Mostly, it originates in the adrenal glands but can arise from nerve tissues in the neck, abdomen, chest and pelvis; however, it can develop anywhere along the sympathetic nervous system, as it arises from the neuroblasts (Louis & Shohet 2015). The prognosis of the cancer is primarily dependant on the stage of differentiation; whilst low-risk tumours can have good outcomes simply from surgery or observation only, high risk tumours can be difficult to successfully treat even with the most intensive treatment (Pinto et al. 2015).

Prognosis for developed cancer in children over 18 months remains poor, even if aggressive multimodal therapy is used, with high risk cancer prognosis rates remain at 30% with relapse being common (Hoy 2016). However, in 2015 the FDA approved the first antibody therapy for neuroblastoma. Dinutuximab (Unituxan) is a monoclonal antibody which targets the glycolipid GD2 on cancer cells and is used in a combined therapy with IL-2, 13-cis-Retinioic acid and GM-CSF (Hoy 2016). Whilst there are side effects such as

neuropathy, there was significant increase in event-free survival in Phase III trials (Ploessl et al. 2016). That said, there is still plenty of potential for using neuroblastoma within this research, not just as a proof of concept for drug construct delivery, but to identify and investigate alternative receptors which can be exploited for therapeutic targeting (Megison et al. 2013).

1.2.2 Neuroblastoma cell lines

There are numerous cell lines which can be used as an *in vitro* model of neuroblastoma; it is a very heterogeneous cancer, therefore cells taken from a variety of sources each have their own behaviour and signalling pathways (Ngan 2015). For instance, Neuro2A are a fast-growing mouse derived neuroblastoma cell line which is commonly used for differentiation into neurite-like morphology (Ma'ayan et al. 2009). SH-SY5Y and LA-N-5 cells on the other hand are slower growing human derived neuroblastoma that can be differentiated with a variety of adrenergic, cholinergic and dopaminergic features, with SH-SY5Y being often used for Parkinson's disease models (Biedler et al. 1978; Lopes et al. 2010; Hill & Robertson 1998). However, by keeping the cells undifferentiated they maintain their proliferative cancer-like phenotype in an adherent monolayer and are a suitable model for delivering conjugated complexes (Shastry et al. 2000).

1.2.3 Alternative useful cell models

The J774.2 mouse macrophage cell line has been found to have an increased sensitivity to numerous therapeutic toxins, most likely due to enhanced macropinocytosis (Rust et al. 2015). This feature is useful for the initial identification of potential internalisation strategies through increased likelihood of observing effects which a less sensitive cell line, such as a neuroblastoma, would not measure. Thereby can be used as a foundation upon which internalising strategy amendments can be built upon.

1.3 Enzymatic toxins for targeted therapy

Enzymatic toxins, both derived from plants and bacteria, have emerged as strong candidates for cancer therapy owing to their high potency, their intracellular stability and

high turnover rate (Siegall 1994; Antignani & FitzGerald 2013). However, their size often makes them a challenge to deliver without their endogenous binding domains. Nonetheless, there is a drive to harness their unique catalytic properties, attaching them to targeting moieties to increase their efficiency of internalising into the cells (Liu et al. 2014; Pastan et al. 1993). In addition, the proteinous nature of toxin-derived therapeutics makes it possible to manipulate them through reduction and plasmid engineering. Therefore, this project adopted toxin-derived enzymes to investigate their effects upon neuroblastoma cells and as a means of determining whether conjugated complexes can successfully deliver their payload.

1.3.1 Botulinum Neurotoxins

Botulinum neurotoxins (BotNT) are a product of *Clostridium botulinum* and other Clostridium bacteria. These toxins are proteases, and catalytically cleave SNARE peptides at specific locations. SNARE proteins endogenously are used to dock and fuse vesicles with intracellular compartments or the plasma membrane, cleaving these proteins is sufficient to inhibit exocytosis and can result in paralysis and death (Tighe & Schiavo 2013). Thereby, the botulinum toxin is usually used clinically for a variety of hypersecretory syndromes or hyperexcitibility disorders of peripheral nerve terminals (Luvisetto et al. 2015).

Like many other bacterial toxins, Botulinum Neurotoxin serotype A (BotNT/A) is composed of 2 chains: A light chain which is the catalytic domain, and a heavy chain which contains the translocation domain and the receptor binding domain (Montal 2010) (fig. 1.3:A). Unlike other bacterial toxins, the full length toxin is often used in treatment, as opposed to utilising only certain domains of the toxin. BotNT/A is the isoform most often used both at bench and clinic and it has been FDA approved since 1989 for numerous conditions such as strabismus and blepharospasm, with it later being also approved for chronic migraine, spasticity and cosmetic procedures (Chen 2012; Jost et al. 2015). At a cellular level, BotNT/A is not toxic to cells, instead it has been shown to cleave SNAP25 and inhibit exocytosis. There is potential that BotNT/A could also have therapeutic applications in cancer; because it inhibits exocytosis there are findings suggesting that this could alter signalling in the tumour microenvironment causing a decrease in cancer cell growth or even blood vessel dilation, potentially allowing enhancement of chemotherapy delivery (Arnold et al. 2009; Karsenty et al. 2009).

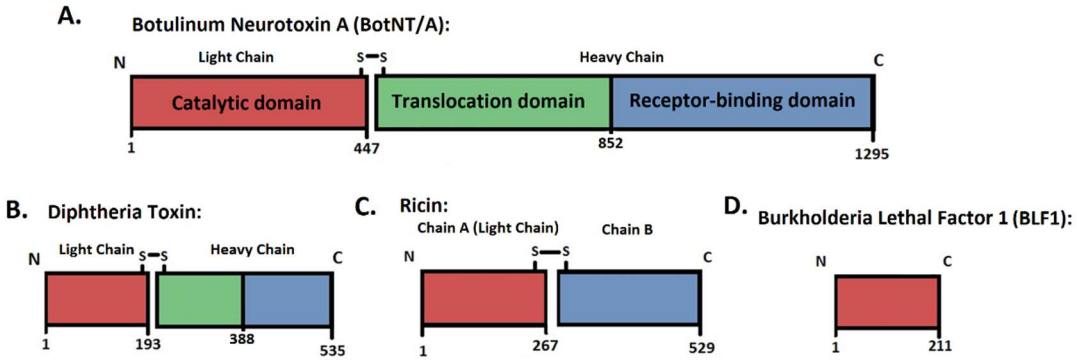

Figure 1.3 – Schematics of the structures of various toxins

A-D) Layout of the domains of Botulinum Neurotoxin A, Diphtheria toxin, Ricin and BLF1 respectively. Red: Catalytic domain, Green: Translocation domain, Blue: Receptor binding domain (Greenfield et al. 1983; Thompson et al. 1990; Halling et al. 1985; Lee et al. 2007).

1.3.2 Diphtheria Toxin

Diphtheria toxin (DT) is endogenously produced by the bacteria *Corynebacterium diphtheria* and shares a similar structural layout to BotNT/A, with a light chain catalytic domain and a covalently attached heavy chain (fig. 1.3:B). Its catalytic domain has ADP-ribosylation activity to inactivate eukaryotic elongation factor 2 (eEF-2), preventing the translocation of t-RNA through the ribosome thus inhibiting protein synthesis, eventually killing the cell (Bell & Eisenberg 1996). DT belongs to a family of proteins called Ribosomal inactivating proteins (RIPs), which target the specific pathways of protein synthesis and can be used to target cancer (Siegall 1994). DT is also particularly useful as within the cytosol it is estimated to inactivate up to 2000 eEF-2s/min; from this, a single diphtheria toxin molecule is able to kill a cancer cell (Yamaizumi et al. 1978; Moynihan & Pappenheimer 1981).

Because of its toxic effects and extreme potency, DT has been extensively researched as an effective treatment for a variety of cancer types with there being many clinical trials of DT conjugated drug candidates (Y. M. Li et al. 2013; Frankel et al. 1995). To date, there is only one diphtheria-conjugated drug on the approved by the FDA: Denileukin diftitox (Ontak) is approved for treatment of human cutaneous T-cell lymphoma and is composed of the first 389 amino acids of DT recombinantly fused to IL-2 to bind to upregulated IL-2

receptors in T- cells, thus facilitating internalisation and resulting in cell death (Fuentes et al. 2015; Duvic & Tapur 2008). This construct contains the catalytic light chain and the translocation domain of DT, but not the endogenous binding domain so as to avoid undesired cell targeting, this technique is common with most toxin-derived therapeutics (Frankel et al. 1995).

However there are limitations of using DT, for instance DT is commonly vaccinated against in the first world. Moreover, there have been reported side effects for DT-conjugated drugs such as flu-like symptoms or vasculitis (Cohen et al. 2005; Duvic & Tapur 2008). However, solutions are being explored to overcome the immunogenicity of the toxin by mutating with point mutations or wrapping in immunoliposomes (Schmohl et al. 2015; Vingerhoeds et al. 1996).

1.3.3 Ricin

Ricin is a cytotoxic protein isolated from castor bean seeds. Like DT and BotNT/A is exists in subunits, a catalytic A-chain and a targeting B-chain which are linked together via disulphide bond (Tyagi et al. 2015). Unlike DT and BotNT/A there is no translocation domain (fig. 1.3:C), nonetheless it is one of the most toxic proteins in nature (Halling et al. 1985). Ricin is an N-glycosidase which removes an adenine residue from a highly conserved loop of rRNA. This prevents the subsequent binding of eukaryotic elongation factor 1 and 2, halting protein synthesis resulting in cell death and making it part of the RIP family along with DT (Endo & Tsurugi 1987; Dever & Green 2012).

There are numerous examples of ricin A-chain being attached to targeting domains as a candidate for cancer therapy, some of which have managed to progress to clinical trial phase, however there are currently no FDA approved drug based on ricin (Słomińska-Wojewódzka & Sandvig 2013; Frankel et al. 1995). Part of this is because there have been problems with off target effects such as vascular leak syndrome due to inappropriate toxin entry into the endothelial cells, which can cause issues such as multiple organ failure and oedema (Baluna et al. 1999; Polito et al. 2016). Another issue with ricin and other RIPs is that they can be highly immunogenic, stimulating patients to produce antitoxin antibodies which decreases the half-life, and therefore efficacy, of the construct (Kreitman 1998; Antignani & FitzGerald 2013). Nonetheless, with modifications to reduce immunogenicity, ricin could still be a useful therapeutic protein for cancer research (Li et al. 2009).

1.3.4 BLF and alternative toxins

In addition to those listed above, there are other toxins that are also used for re-targeting to cancer cells such as pseudomonas exotoxin, produced by the bacteria *Pseudomonas aeruginosa*, which inhibits eEF-2 in a manner similar to DT (Shimamura et al. 2010; Weldon & Pastan 2012). Saporin on the other hand is more comparable to ricin; derived from the seeds of the *Saporin officinalis*, it is another RIP that depurinates adenine residues on ribosomal subunits which irreversibly inhibits protein synthesis (Polito et al. 2011; Quadros et al. 2013).

RIPs remain some of the most toxin proteins in nature; they come in numerous structures, sizes and functions from both plant and bacterially derived sources and there has yet to be a completely uniform classification of them due to their variety (Schrot et al. 2015). Nonetheless, their protein synthesis inhibiting function and the consequent cell death resulting from their internalisation has enabled them to be attractive for targeting to cancer cells; however, drug candidates containing these toxins still have issues with side-effects and unwanted toxicity.

Interestingly, it has emerged that a newly identified RIP toxin inhibits protein synthesis potentially without killing cells. Burkholderia Lethal Factor1 (BLF1) is a toxin derived from the bacteria *Burkholderia pseudomallei*. Whilst the bacteria has been associated with melioidosis and infection often resulting in death, BLF1 is an inhibitor of the eukaryotic initiation factor 4A (eIF-4A) which has been identified as an oncogene and as a potential druggable target (Cruz-Migoni et al. 2011; Chu & Pelletier 2014). Significantly, BLF1 has been shown to prevent growth of cells *in vitro* without activation of the caspase pathway (Rust et al. 2015). It had been previously identified as a new tool for targeted delivery (Walsh et al. 2013), however the findings that BLF1 may inhibit growth of cells without killing could offer new drug candidates with reduced toxicity and side effects.

1.4 Internalisation techniques

Most therapeutic agents target proteins and mechanisms within the cell cytosol, this requires them to be internalised into cells efficiently and be able to reach the location within the cell needed to induce catalytic effect. This process often involves delivery strategies to first internalise the drug and then allow it to escape cellular compartments to

reach the therapeutic target. There have been numerous diverse methods developed to internalise drugs into cells; their efficiency can depend on a variety of pathways, both specific and non-specific to particular cell types depending on their external receptors or protein signature (Böhme & Beck-Sickinger 2015). Because of the size of therapeutic protein drugs it is difficult for them to pass through the cell membrane, hence internalisation strategies are needed to overcome biological barriers and improve both the efficiency and specificity of drug targeting (Sandvig & van Deurs 2005). Most often, the strategy for efficient internalisation is to conjugate internalisation proteins or peptides to the therapeutic domain, so that as the targeting domain binds to cell receptors and is endocytosed, so too is the therapeutic domain (fig. 1.4). There are a large variety of internalisation domains which have been investigated for this purpose.

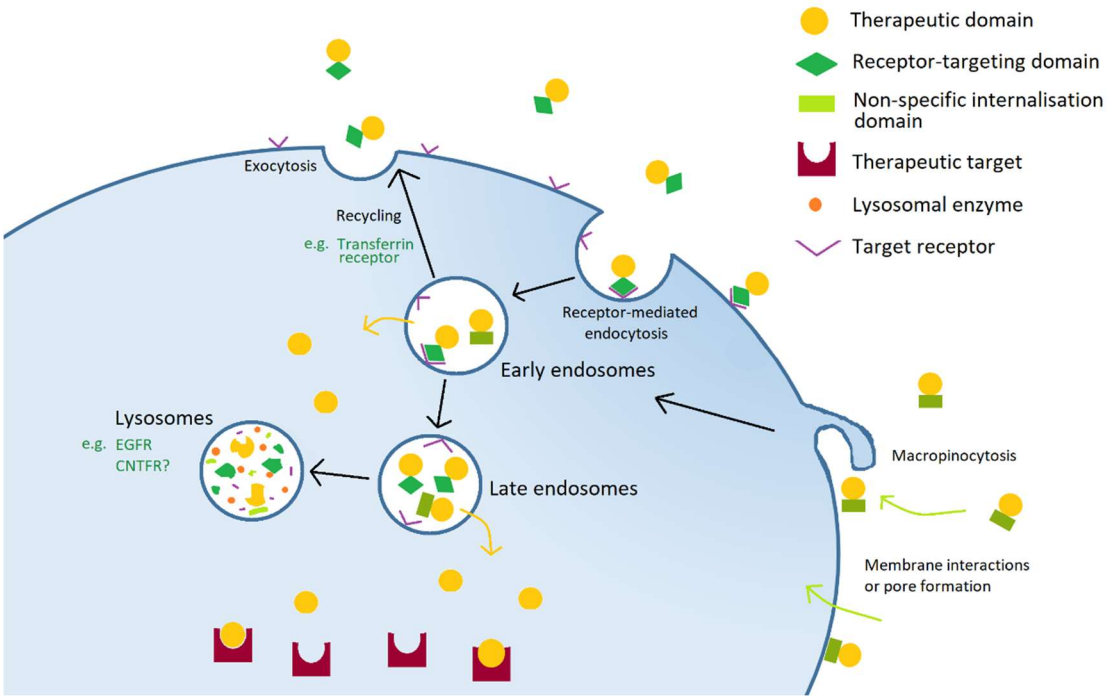

Figure 1.4 – Schematic showing basic drug internalisation pathway

Diagram showing the strategy most adopted by researchers for drug construction and internalisation: A therapeutic domain is conjugated to an internalisation domain to facilitate uptake into cells. This method can be used through proteins using non-specific pathways internalisation pathways such as CPPs (Reissmann 2014) or receptor mediated endocytosis where receptors are either recycled back to the cell surface (e.g. transferrin receptor) (Tortorella & Karagiannis 2014) or degraded in the lysosomes to prevent further signalling (e.g. EGF receptor) (Seshacharyulu et al. 2013).

1.4.1 Cell penetrating peptides

Cells are known for their ability to prevent non-specific entry of proteins and macromolecules, and only employs specific pathways for the transport of desired proteins. About 30 years ago there was the discovery of small sequences which were able to pass through the membranes of cells unhindered via non-specific delivery, these were referred to as cell penetrating peptides (CPPs) (Reissmann 2014) These short sequences are traditionally composed of either numerous positively charged amino acids such as lysine or arginine (polycationic CPPs) or have an alternating structure of polar and non-polar amino acids (amphipathic CPPs), however many different varieties of CPPs have been developed over recent years (Bechara & Sagan 2013) (Table 1.1). These were developed as a new drug delivery method and several have been established as ways of efficiently translocating a variety of cargo into cells, such as small molecule drugs, proteins and fluorescent labels (Koren & Torchilin 2012; Young Kim et al. 2015).

Initially CPPs were derived from proteins such as HIV and *drosophila antennapedia*, resulting in Penetratin and TAT, however since then there have been numerous forms artificially synthesised (Nischan et al. 2015; Ma et al. 2012). As well as being shown to bind and deliver small proteins and nucleic acids, some CPPs have also been shown to deliver larger proteins into cells *in vitro*, such as BotNT/A (1-448) and β-galactosidase (Farkhani et al. 2014; Montrose et al. 2013; Saffarian et al. 2016).

There is a lot of dispute regarding the mechanisms of cell entry, enabling them to internalise and deliver cargo before being broken down by lysosomes or recycled. There are reports showing that chlorpromazine or other macropinocytosis inhibitors will inhibit CPP uptake at low concentrations (< 5 μM), but at higher concentrations it appears that they internalise via non-endocytic mechanisms (Fischer et al. 2004; Chao & Raines 2011). There is further evidence that CPPs interact with the cell membrane and can form pores suggesting that fatty acids on the surface of the cell interact with arginine residues (R), common in CPPs. This then leads to the formation of channels, where on the cytosolic side the pH decreases and the fatty acids are protonated, releasing the peptides and resealing the channel (Herce et al. 2009; Herce et al. 2014). There is also a proposed 'inverted-micelle' mechanism which suggests that electrostatic interactions between the lipid bilayer and CPPs trigger conformational changes in the peptide, causing it to bind to the bilayer and changing its properties causing encapsulation (Alves et al. 2008; Cardoso et al. 2012).

In reality, uptake is probably a mixture of many cell entry pathways depending on concentrations and the individual amino acid structure.

Cell penetrating peptide	Type	Origin	Charge	Sequence	Reference
Penetratin	Protein	Antennapedia (43–58)	Cationic	RQIKIWFQNRRMKWKK	(Derossi et al. 1994)
TAT peptide	Protein	HIV (48-60)	Cationic	GRKKRRQRRRPPQ	(Vives et al. 1997)
TAT peptide	Protein	HIV (47-57)	Cationic	YGRKKRRQRRR	(Ignatovich et al. 2003)
pVEC	Protein	Cadherin(615–632)	Amphipathic	LLIILRRRIRKQAHAHSK	(Elmquist et al. 2001)
KFGF	Protein	Kaposi's sarcoma fibroblast growth factor	Hydrophobic	AAVALLPAVLLALLAP	(Lin et al. 1995)
Polyarginines	Synthetic	N/A	Cationic	RRRRRR	(Mitchell et al. 2000)
(W/R) nonapeptide	Synthetic	N/A	Cationic	RRWWRRWRR	(Delaroche et al. 2007)
Transportan	Chimeric	Galanine/ Mastoparan	Amphipathic	GWTLNSAGYLLGKINLKALAALAKKIL	(Pooga et al. 1998)

Table 1.1 – Table of Cell penetrating peptides (CPPs) and their sequences

Whilst these peptides were designed to enter into cells efficiently and indiscriminately, this has been a double-edged sword as specific delivery into diseased cells is most often preferable. There are reports of attempts to develop tissue specific CPPs through using *in vivo* or *in vitro* phage display; for example, motifs have been identified in peptides for targeting tumour vasculature in particular cancers (Zahid & Robbins 2015; Arap et al. 2012; Lim et al. 2013). However this supports a more receptor-based method of entry, as opposed to a non-specific, therefore questioning the definition of a CPP. Whilst there have been positive results in various disease models which in some cases have prompted clinical trials, there are currently no CPP drugs approved by the FDA (Guidotti et al. 2017)

Nonetheless, their ability to be taken up in a variety of cell lines makes them particularly useful for investigation into proof of concept delivery.

1.4.2 Ligand-receptor interaction and internalisation

In order to give targeted toxins more specificity in selecting cancer tissue over healthy tissue there is an established method where ligands or ligand-like peptides are conjugated to therapeutic domains and bind to receptors specific to disease (Allen 2002; Toporkiewicz et al. 2015). It is known that many varieties of cancer have particular upregulated receptors on the surface of the cells, these receptors can be exploited by using endogenous or synthetic proteins to target the upregulated receptors and attaching drugs (Srinivasarao et al. 2015). Once the ligand is bound to the overexpressed receptors, the conjugate can be endocytosed into endosomes where it is then either recycled, processed or directed to the lysosomes to be degraded. However, via endosomal escape the internalised toxin is able to translocate into the cytosol where it can exert its function.

There have been many successful examples of ligand directed toxins, the most successful of which have made it to clinical trials and even FDA approval (Duvic & Tapur 2008; Böhme & Beck-Sickinger 2015). As previously mentioned, Ontak is a drug which has IL-2 conjugated to a portion of DT, but there have been other examples of interleukins used to target toxins owing to their overexpression in numerous cancer cell types (Cohen et al. 2005; Kunwar et al. 2010). Additionally, there have been a variety of examples where other ligands have been utilised for cancer targeting, such as EGF or transferrin, and have been able to deliver toxin domains to neuroblastoma cells and others (Raso & Basala 1984; Yotsumoto et al. 2009). Table 1.2 list some of the ligands which have been previously identified for neuroblastoma targeting, and others which have been shown to target other cancers but may have potential to target neuroblastoma.

Sometimes however, it is undesirable when developing drugs to use endogenous ligands. Despite the fact that they can have high specificity and potentially efficient internalisation they can activate undesired pathways, for instance increased cell growth; these receptors are of course upregulated in cancer for a reason. Therefore, once the target receptors have been identified through endogenous ligands or otherwise, peptides or proteins can be engineered which bind to the receptor and still internalise without the unwanted increase in pathway activation (Nicklin et al. 2000; Li & Mao 2014). Like CPPs, peptide ligands are

selected from phage-display libraries or chemical synthesis. This technique has resulted in peptide ligands being identified which specifically bind to receptors (Guardiola et al. 2015). It should be noted that this method can have a lot of overlap with CPPs, as there are peptides which have been identified which share similar sequences to CPPs but with more receptor-dependent internalisation (Arap et al. 2012).

Targeting of cancer tissue increases intratumoural accumulation of drug, increasing the toxicity; it is also aided partially by the dense, leaky vascular system which accompanies most solid tumours. However, it does rely on the external signature of the cell remaining unchanged throughout, as if it does change then it could lead to tumour resistance (Toporkiewicz et al. 2015). Unfortunately, many cancers in later stages are highly unstable and therefore can repeatedly mutate to alter their receptor make-up over time, meaning that populations of cancer cells remain resistant to chemotherapy (Kuczynski et al. 2015). Alternatively, heterogeneity is a problem in many types of cancer and is especially known in neuroblastoma, where a population of cancer cells will have numerous clusters of cells each expressing different receptors making targeting the whole population a significant challenge (Ngan 2015).

To address this, most courses of cancer treatment employ more than one individual therapy, although there are strategies emerging to incorporate more than one targeting method into a single therapy. Whilst antibody based dual-targeting is now being established as an important strategy to combat the resistance of cancer, ligand based dual-targeting has not been explored to the same extent because the means of conjugating two ligands together with one therapeutic domain remains a complex process (Kontermann 2012; Chester et al. 2015). Bulk delivery carriers such as liposomes and nanoparticles have touched upon coating the surfaces with numerous ligands, however these are often heterogeneous and bulk delivery is not always desired (Rangger et al. 2013; Gao et al. 2014). The need remains therefore to develop a conjugation method which is able to bring together two targeting domains together with a therapeutic domain to produce a homogenous, ratio-controlled product, where all components of the complex retain their function and can behave co-operatively in the same way as a ligand-toxin conjugate.

Ligand – Receptor Target	**Toxin/ conjugated**	**Disease target(s)**	**References**
Dermorphin – μ opioid receptor	--	Neuroblastoma	(Glaser et al. 1981; Arttamangkul et al. 2000)
Substance P – Neurokinin 1	Botulinum Light Chain,	Neuropathic pain, Neuroblastoma	(Mustafa et al. 2008; Muñoz et al. 2005)
Corticotrophin-releasing hormone (CRH) – CRH receptor 1	Botulinum Light Chain + Translocation domain	Neuroblastoma	(Arsenault et al. 2013)
Vasoactive intestinal peptide (VIP) – VIP receptors 1 and 2	Micelles	Neuroblastoma, Breast Cancer	(Ding et al. 2013; Pence & Shorter 1992)
Neuropeptide Y (NPY) – NPY receptors 1-5	Nanoparticles	Neuroblastoma, Breast cancer	(J. Li et al. 2015; Lu et al. 2010)
Pituitary adenylate cyclase-activating polypeptide (PACAP) and PACAP 2 – PACAP receptor, VIP receptors 1 and 2	--	Neuroblastoma	(De Boisvilliers et al. 2016; Falktoft et al. 2009)
Ciliary neurotrophic factor (CNTF) – CNTF receptor, IL-6	Botulinum Light Chain + Translocation domain	Neuroblastoma	(Kuroda et al. 2001; Arsenault et al. 2013)
Epidermal Growth Factor (EGF) – EGF receptor	Nanoparticles, Ricin light chain, Botulinum Light Chain + Translocation domain	Neuroblastoma, Numerous Cancers	(Seshacharyulu et al. 2013; Master & Gupta 2012; Herschman 1984)
Tumour necrosis factor alpha (TNFα) – TNFα receptors 1 and 2	Botulinum Light Chain + Translocation domain	Gastric cancer, metastasis, Numerous cancers	(Oshima et al. 2014; Bigatto et al. 2015; Arsenault et al. 2013)
Adrenomedullin – calcitonin receptor like receptor (CLR), Receptor activity-modifying proteins (RAMP) 2 and 3	--	Colorectal Cancer, Osteosarcoma	(Wang et al. 2014; Wu et al. 2015)

Table 1.2 – Ligands with either identified or potential use for internalisation into neuroblastoma

1.4.3 Antibody directed cell internalisation

Antibodies possess numerous attributes which make them desirable to be used for cancer targeting. For instance they can be selectively developed for high binding affinity whilst being molecularly homogenous, they can also be humanised or chimeric to decrease immunogenic reactions and can be engineered in very versatile ways (Becker & Benhar 2012; Smaglo et al. 2014). From these, antibody-drug conjugates (ADCs) have developed, where, instead of ligands, antibodies are conjugated to toxins in order to target and deliver to specific cells; these are referred to as immunotoxins (Kreitman 1998; Antignani & FitzGerald 2013).

Antibody therapy often uses ligand internalisation studies as a foundation in order to design and develop an immunotoxin with specific binding characteristics in mind. Antibody production is expensive, and this limits its usefulness at early stages of drug target research. Nonetheless, in recent years there has been a boom in antibody therapy production because of their specificity to receptors, even those without endogenous ligands, without the unwanted receptor-pathway activation. This has led to numerous antibody based drugs being FDA approved through targeting receptors such as EGF, TNFα and others (Scott et al. 2012; X.-X. Li et al. 2015; Deeks 2016). Whilst antibodies have been used to target cells, often instead of drug attachment they retain the endogenous sequence in the antibody to activate the immune system to kill the cell; out of over 65 monoclonal antibody drugs which have been approved, only two of them currently available are conjugated to a drug (Beck & Reichert 2014).

On the other hand, there is no shortage of research or demand for antibody-drug conjugates; unstable and inefficient conjugation has been named as one of the reasons for their current lack of success (Perez et al. 2014; Thomas et al. 2016). There have been many examples where antibody drug conjugates have been developed to meet different cancer varieties, however there has yet been a method developed to consistently synthesise stable ADCs which optimise disease targeting and drug action (Bornstein 2015; Ducry & Stump 2017; Beck & Reichert 2014). As antibodies and antibody derived domains have emerged as the targeting method of choice, it is clear that solutions are needed to address these issues.

1.5 Endosomal escape and cytosolic delivery

All of the approved ADCs until now have only used small molecule drugs as their payload, this is because once antibodies internalise and the payload released it is more likely to translocate to the cytosol if it is a small molecule than if it is a large protein. Because of this, endosomal escape is not a current consideration in ADC design (Perez et al. 2014; Bornstein 2015). However, there new methods being explored to aid the cytosolic delivery of large proteins, allowing immunotoxins to fully develop as a successful avenue of drug research (Fuchs et al. 2016; Becker & Benhar 2012).

Most therapeutic enzymes target proteins in the cytosol, so after cell internalisation there needs to be a way for the toxin to escape endosomes and reach its target for there to be a catalytic effect. As previously mentioned, the endocytic pathway takes up proteins and other components from the surrounding environment, often into endosomes, and then does one of three things: (i) it can degrade the internalised proteins through passage to the lysosomes where proteins undergo enzymatic degradation, or (ii) it can be recycled and transported out of the cell via exocytosis. The third option, is that the internalised proteins undergo endosomal escape, where the proteins pass into the cytosol (Varkouhi et al. 2011). Endosomal escape is an important and currently an intensively researched area, it is critical to the pharmaceutical efficiency of many drugs, as most targeted proteins and pathways of pharmaceutical relevance are within the cytosol. However, a ubiquitous method of cytosolic translocation has yet to be identified. As is, endosomal escape is often a limiting factor in drug delivery, hence there is a shift in focus from only targeting cells to also focusing on efficient cytosolic delivery (Fuchs et al. 2016; Bostad et al. 2015; Shete et al. 2014)

There are several researched methods of endosomal escape, for instance, viruses and bacteria have evolved ways of efficiently translocating inside of cells. In enveloped viruses there can be fusion directly between the envelope and cell membrane which encourages endocytosis and there is subsequent cell lysis, whereas viruses without an envelope have been known to create pores (Medina-Kauwe 2003; Hogle 2002). Pore formation is also a common way which bacteria get from the endosomes or phagosomes to the cytosol, using proteins which are activated by reducing agents or low the pH found in vesicles to allow cytosolic escape without compromising the endosomal membrane (Mandal & Lee 2002). Another endosomal escape method triggered by low pH is the proton sponge effect, this is facilitated by agents with a high buffering capacity. For instance, histidine-rich molecules

can show a buffering effect upon protonation of their imidazole ring; it induces ion and water intake into the endosomes, which swell then ruptures the endosomal membrane (Pack et al. 2000). A similar example exists where tertiary amine groups containing a hydrophobic chain can accumulate in endosomes and become detergents upon protonation caused by the low pH, resulting in a disruption of the endosomal membrane (Miller et al. 1983). However, it is worth noting that some of these endosomal escape methods which involve the lysis or disruption of the membrane may result in cell death, which can be undesirable (Lönn et al. 2016).

1.5.1 Utilising toxin cytosolic translocation proteins

By researching the translocation domains which are already present in toxins such as botulinum and diphtheria, an understanding has developed on their mechanism of function and how they can be exploited to enhance drug delivery. It has been suggested that the change in pH when the botulinum translocation domain is internalised into early endosomes causes it to interact with the membrane and allows pores to form (Nagahama et al. 2014) (fig. 1.5). This pore allows the catalytic light chain domain of botulinum to get into the cytosol whilst chaperoned by the translocation domain to retain its stability (Fischer et al. 2012; Araye et al. 2016; Koriazova & Montal 2009). It is proposed that this is the same mechanism used for the diphtheria translocation domain (Murphy 2011; Chassaing et al. 2011); although, there is additional data supporting that the translocation domain of diphtheria also inhibits the early endosome maturation, hence increasing the time available for escape before lysosomal degradation (Antignani & Youle 2008). It has also been reported that within the translocation domains of botulinum A, C and D and diphtheria there is a 10 amino acid loosely conserved sequence, which is also seen in anthrax and could account for the similarity in translocation mechanisms (Trujillo et al. 2006; Jiang et al. 2015). The fact remains that some of the most toxic known proteins in negligible amounts are being still efficiently translocated into cells through their translocation domains; it was even noted that without the receptor binding domain, the light chain and the translocation domain of BotNT/A were able to enter particular cells independent of any targeting domain (Fischer et al. 2008).

The research into how bacterial and plant agents escape into the cytosol has given way to the translocation domain being used as a way to increase drug translocation. For instance, Ontak is composed of the first 391 amino acids of diphtheria, which is both the catalytic

and translocation domain, attached to IL-2 (Fuentes et al. 2015). There are also examples of research and patents where the translocation domains of these toxins are harnessed; the translocation domain of diphtheria has been attached to alternative catalytic domains, including botulinum, to increase translocation (Sutton & Shone 2004; Shone et al. 2003). Moreover, it has even been shown that the conjugation of the translocation domain of diphtheria to plasmids increases gene transfection (Kakimoto et al. 2009). This strongly indicates that particular translocation domains on toxic proteins can assist in cytosolic delivery, and therefore would be a useful avenue to explore through conjugation to targeting and therapeutic domains.

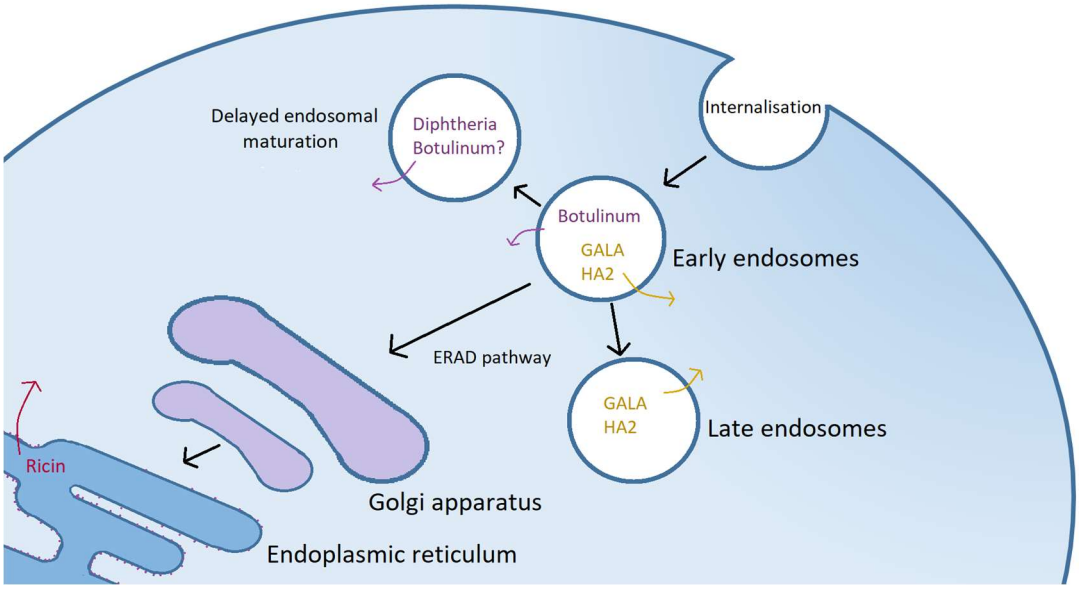

Figure 1.5 – Endosomal escape of toxins and peptides

Schematic showing the endosomal escape of toxins and peptides. Both botulinum and diphtheria have endosomal escape facilitated by their translocation domains which insert into the endosomal membranes in response to the pH of the early endosome and form channels (Koriazova & Montal 2009; Antignani & Youle 2008). Ricin has not got a translocation domain, but its A chain facilitates protein folding which leads it through the ERAD pathway to the endoplasmic reticulum where it then escapes (Sun et al. 2004). Peptides can escape the endosomes through a variety of mechanisms depending on its amino acid composition, however GALA and HA2 fuse with the membrane in response to low pH (Varkouhi et al. 2011).

1.5.2 Utilising peptides for endosomal escape

Additionally, there are several peptides which have been reported to increase the presence of attached proteins into cytosol. For instance, GALA is a short anionic synthetic amphipathic peptide sequence which, when in the endosome, is protonated due to the low pH causing a conformational change which allows it to fuse with the lipid bilayer. The proposed mechanism is that the inserted GALA peptides then aggregate together and form pores, allowing endosomal proteins to cross into the cytosol (Nicol et al. 2000; Lewis 2014; Parente et al. 1988). The attachment of GALA has also been shown to increase the cytosolic location of nanocapsules and increase transfection efficiency (Futaki et al. 2005; Nishimura et al. 2014).

Influenza virus hemagglutinin (HA) is a glycoprotein which fuses the influenza virus capsid with cell membranes for internalisation. A 20 amino acid peptide within the subunit HA2 was identified as a sequence which under acidic conditions will bind and disrupt endosomal membranes leading to endosomal escape (Wiley & Skehel 1987; Neundorf et al. 2009). There are also reports that CPPs with histidine rich domains are able to successfully translocate into the cytosol and can be used as a transfection peptides (Järver et al. 2007). It has been demonstrated that when cationic CPPs are exposed to acidic environments within endosomes they are able to bind to the endosome bi-layer and leak through the membrane following a pH gradient (Yang et al. 2010; Madani et al. 2013). However, this method of endosomal escape is limited in that it may not facilitate the cytosolic translocation of attached proteins, therefore, CPPs are being used in combination with other endosomal escape peptides such as HA2 (Neundorf et al. 2009; Liou et al. 2012; Tünnemann et al. 2006). This sort of combination of internalisation domains, endosomal escape domains and therapeutic domains is becoming more popular because it addresses the bottleneck of cytosolic translocation. Through new conjugation methods, it is hoped that these processes can be explored more efficiently.

1.6 Aims of Thesis

This introduction has laid out four main themes: conjugation, toxins, cell internalisation methods and endosomal escape. This thesis aims to use pyridyl disulphide conjugation and SNARE linking to be able to further understand the nature of particular therapeutic toxins,

identify cell internalisation peptides or proteins for neuroblastoma targeting, and investigate how to enhance conjugate cytosolic translocation through endosomal escape. In doing so, it is hoped that new findings will be made in these areas, but also that it will identify the limitations and potential of particular conjugation methods for drug construction. Furthermore, it is the ambition of this project that these findings will aid the development of other conjugation methods in wider research, that it may contribute to strategies for the optimisation of antibody-drug conjugate development and future methods of targeted delivery.

Chapter 2: Materials and Methods

2.1 Materials

2.1.1 Reagents

Reagent	**Supplier**
2-YT powder	Invitrogen - Thermo Fisher Scientific
Acetic acid (Glacial)	Thermo Fisher Scientific
Agar	Scientific Lab Supplies
Agarose	Biogene
Ammonium persulphate (APS)	Thermo Fisher Scientific
Ampicillin	Panreac
Benzonase Nuclease	Sigma-Aldrich
Bovine Serum Albumin (BSA)	Thermo Fisher Scientific
Bromophenol Blue	BDH Chemical
Calcium Chloride ($CaCl_2$)	Sigma-Aldrich
Coomassie Brilliant Blue	BDH Chemical
Chloramphenicol	Panreac
Desipramine	Sigma-Aldrich
Deoxyribonuclease I from bovine pancreas	Sigma-Aldrich
DMSO	Sigma-Aldrich
EDTA	Thermo Fisher Scientific
Ethanol	Thermo Fisher Scientific
Fish skin gelatine	Sigma-Aldrich
D-Glucose	Sigma-Aldrich
Glycerol	Thermo Fisher Scientific
HEPES	Thermo Fisher Scientific
Hydrochloric acid (HCl)	Thermo Fisher Scientific
IPTG	Melford
Lipofectamine 3000	Invitrogen
Magnesium Chloride ($MgCl_2$)	Acros Organics
Magnesium Sulphate ($MgSO_4$)	Merck
MES running buffer (x20)	Life Technologies - Thermo Fisher Scientific
Methanol	Thermo Fisher Scientific
Skimmed milk powder	Sigma-Aldrich
MTT - (3-(4,5-Dimethlthiazol-2-yl)-2,5-Diphenyltetrazolium)	Sigma-Aldrich
Octyl β-D-glucopyranoside (OG)	Thermo Fisher Scientific

Pargyline hydrochloride	Sigma-Aldrich
Paraformaldehyde (PFA)	Sigma-Aldrich
Phosphate Buffered Saline (PBS) (x10)	Thermo Fisher Scientific
Protogel	National Diagnostics
Resolving gel buffer	Bio-Rad Laboratories
Sodium Chloride (NaCl)	Thermo Fisher Scientific
Sodium Dodecyl Sulphate (SDS)	Thermo Fisher Scientific
Sodium Hydrocarbonate ($NaHCO_3$)	Sigma-Aldrich
Sodium Hydroxide NaOH	Sigma-Aldrich
Stacking gel buffer	Bio-Rad Laboratories
TCEP	Sigma-Aldrich
TEMED	Sigma-Aldrich
Transfer Buffer (x10)/ Tris-glycine buffer	Fluka
Triton-X-100	Thermo Fisher Scientific
Tween-20	Thermo Fisher Scientific
Xylene cyanol	Sigma-Aldrich

Table 2.1 – Reagents used

2.1.2 Buffers

All made at Room Temperature (RT) unless otherwise stated. RT was measured at 20˚C.

Buffer A: Made with 10 mL 1 M HEPES pH 7.3 (20 mM – final concentration), 10 mL 5 M NaCl (100 mM), made up to 500 mL with deionised water (dH_2O).

Lysis Buffer (Protein purification): Made with 10 mL 1 M HEPES pH 7.3 (20 mM), 50 mL 5 M NaCl (500 mM), 1 mL 0.5 M EDTA (1 mM), made up to 500 mL with dH_2O.

Low Salt Buffer: Made with 10 mL 1 M HEPES pH 7.3 (20 mM), 10 mL 5 M NaCl (100 mM), 2.5 mL 20 % Triton-X-100 (0.1 %), 1 mL 0.5 M EDTA (1 mM), made up to 500 mL with dH_2O.

High Salt Buffer: Made with 10 mL 1 M HEPES pH 7.3 (20 mM), 100 mL 5 M NaCl (1 M), 2.5 mL 20 % Triton-X-100 (0.1 %), 1 mL 0.5 M EDTA (1 mM), made up to 500 mL with dH_2O.

4x loading Buffer (SDS-PAGE gel): Made with 3.2g SDS (approx. 12 %), 20 mL 0.5 M Tris-HCl pH6.8 (approx. 0.25 M), 640 µL 0.5 M EDTA, 16 mL 50 % Glycerol (approx. 20 %),

2.5 mL dH_2O, 1.5 tips Bromophenol Blue. This is then diluted in water to make x1 and x2 loading buffers.

SDS-PAGE staining solution: Made in the following order- 200 mL Methanol, 1 tip Coomassie Brilliant Blue, 700 mL dH_2O, 100 mL Glacial Acetic acid.

4x Sample Lysis Buffer (Westerns): 4g SDS (8 %), 25 mL 0.5 M Tris-HCl pH6.8, 800 µL 0.5 M EDTA (8 mM), 10 mL 50 % Glycerol (10 %), 1.5 tips Bromophenol Blue, up to 50 mL dH_2O.

Membrane Transfer Buffer: Made with 700 mL dH_2O, 100 mL 10x Transfer buffer, 200 mL Methanol.

PBS-T: Made with 100 mL 10x PBS, 900 mL dH_2O, 0.5 mL Tween (0.05 %).

Membrane blocking solution: 5 mL (vol) Milk powder, made up to 50 mL PBS-T.

MES running buffer: Made with 950 mL dH_2O, 50 mL MES running buffer (x20).

Tris-Glycine Running buffer (x10): 500 mL 10x transfer buffer, 5g SDS. Diluted to x1 in deionised water when running gels.

SDS-PAGE 12 % resolving gel: made with 1.33 mL dH_2O, 2.0 mL 50 % Glycerol (sterilised), 2.5 mL Resolving Gel buffer (1.5 M Tris pH 8.8), 4 mL Protogel (30 % (w/v) Acrylamide, 0.8 % (w/v) Bis-Acrylamide), 100 µL 10 % SDS (in water) **To be added just before pouring gel:** 80 µL 10 % (w/v) Ammonium persulphate (APS), 8 µL TEMED.

SDS-PAGE stacking gel: made with 3.8 mL dH_2O, 1.5 mL Stacking gel buffer (0.5 M Tris pH 6.8), 600 µL Protogel (30 % (w/v) Acrylamide, 0.8 % (w/v) Bis-Acrylamide), 60 µL 10 % SDS (in water). **To be added just before pouring gel:** 80 µL 10 % (w/v) Ammonium persulphate (APS), 8 µL TEMED.

TAE buffer (x50): 242 g Tris base is dissolved in dH_2O, 57.1 mL glacial acetic acid is then added and 100 mL EDTA 500 mM (pH 8.0) solution. The final volume is then bought up to 1 L. Diluted in dH_2O before use.

Basal Buffer (Radiation experiments): 132 mM NaCl, 5 mM KCl, 0.6 mM $MgSO_4.7H_2O$, 5 mM $NaHO_3$, 2 mM $CaCl_2$, 10 mM D-glucose, 20 mM HEPES, pH 7.4.

Release Buffer (Radiation experiments): 67 mM NaCl, 70 mM KCl, 0.6 mM $MgSO_4.7H_2O$, 5 mM $NaHO_3$, 2 mM $CaCl_2$, 10 mM D-glucose, 20 mM HEPES, pH 7.4.

4% PFA (1L) – made by Rebecca Bresnahan (Davletov Lab) - Heat 0.7 L of 1xPBS to 55-57 ˚C (do not allow to go over 60 ˚C). Add 40 g of PFA powder, then add 2 M NaOH dropwise until all PFA has dissolved (~1-1.5 mL). Cool on ice to RT, then add 1xPBS to make up to 1 L. Add HCl (5 M) dropwise to return pH to 7.4. Filter through 0.45 µm filter. Aliquot into 10 mL falcons and freeze -20C.

Blocking solution – made by Rebecca Bresnahan (Davletov Lab) – The following reagents are added before being made up to 400 mL in water, the solution is stirred for a few hours until all reagents are dissolved before being aliquoted into 10 mL stocks and stored at -20 ˚C: 8 g BSA (2 %), 8 mL fish skin gelatine (2 %), 0.4 mL Tween-20 (0.1 %), 40 mL 10x PBS (x1).

2.1.3 Broths and antibiotic stocks

2-YT Media: Made with 16 g 2-YT powder, 500 mL dH_2O (2-YT used at 32 g/L). Autoclaved.

2-YT Agar: Made with 6.4 g 2-YT powder, 200 mL dH_2O, 3 g Bacto-Agar. Autoclaved, the antibiotics were added when cooling, or carefully microwave until melted and add the antibiotics and pour into dishes after 30 minutes cooling.

Ampicillin 100mg/mL: 1 g Ampicillin in 10 mL dH_2O.

Chloramphenicol 50mg/mL: 0.5 g Chloramphenicol in 10 mL 100% Ethanol.

IPTG 100mM: 238.3 mg IPTG in 10mL dH_2O.

2.1.4 Enzymes and Proteins

Unless otherwise stated, all proteins listed here were expressed and purified in-house by myself from existing plasmids (see section 2.2 for protein synthesis and purification). All plasmids were pGEX based. For those which are marked with (*) the plasmid sequences can be found in Appendix 1. Molarity is calculated through protein size: If protein size is XDa, then 1 M = X g/L, so 1 µM= X µg/L.

The concentration (mg/ml) of pure stocks was measured through Nanodrop (Thermo Fisher Scientific). The concentration of mixed samples and formed complexes was

measured relative to BSA standards on SDS-PAGE via ChemiDoc XRS (Bio-Rad) (see section 2.3.4).

Protein	Approx. protein Size	Supplier of Plasmid	Additional Notes
Burkholderia Lethal Factor 1 (BLF1)	23.4 kDa	Gift from Professor David Rice – University of Sheffield	Expressed and purified by Charlotte Leese
Diphtheria Light Chain (aa. 1-193)	23 kDa	Generated by Dhevahi Niranjan (Davletov lab)	
Diphtheria Light Chain Translocation Domain (aa. 1-388)*	48 kDa	Generated by Dhevahi Niranjan (Davletov lab)	
Diphtheria Light Chain Translocation Domain (aa. 1-388) – SNAP25B*	68 kDa	Ordered from Dundee Cell products	
Diphtheria Light Chain Translocation Domain (aa. 1-388) - Diphtheria Light Chain (aa. 1-196)*	67 kDa	Ordered from Dundee Cell products	
Diphtheria Light Chain Translocation Domain (aa. 1-388) – Diphtheria (aa. 179-190) – Cysteine rich domain *	60 kDa	Ordered from Dundee Cell products	Restriction sites: XbaI-NcoI-Dip fragment (aa.179-190)-NcoI-SalI-Cysteine rich domain-SalI—XhoI
Ricin Light Chain (aa. 1-267)	29.6 kDa	Generated by Dhevahi Niranjan (Davletov lab)	
Botulinum/A Light Chain (aa. 1-438)	48.6 kDa	Gift from Thomas Binz 2015	Protein only received, not plasmid
Botulinum/A Light Chain Translocation Domain (aa. 1-852)*	100 kDa	Generated by Dhevahi Niranjan (Davletov lab)	Restriction sites: SmaI- BotLcTd/A-XbaI
Botulinum/A Light Chain Translocation Domain (1-852) – SNAP25B *	120 kDa	Generated by Dhevahi Niranjan (Davletov lab)	
Botulinum/A Light Chain Translocation Domain (1-852)-S25CRD	123 kDa	Generated by Rose Hart (See Chapter 3)	Restriction sites: SmaI- BotLcTd/A-XbaI-NcoI-S25CRD-HindIII
SNAP25B- Cysteine rich domain (S25-CRD)*	2.7 kDa	Generated by Dhevahi Niranjan (Davletov lab)	Restriction sites: NcoI-S25CRD-HindIII
Synaptobrevin (aa.2-94)*	10.5 kDa	Generated by Dhevahi Niranjan (Davletov lab)	
SNAP25 trunc (aa.2-204)*	20 kDa	Generated by Dhevahi Niranjan (Davletov lab)	Cysteine residues substituted to Alanine

SNAP25 wildtype	25 kDa	Generated by Dhevahi Niranjan (Davletov lab)	
mCherry	24 kDa	Generated by Dhevahi Niranjan (Davletov lab)	Restriction sites: EcoRI-mCherry-EcoRI
mCherry-4cys	27 kDa	Generated by Rose Hart (See Chapter 3)	Restriction sites: EcoRI-mCherry-EcoRI- XbaI-NcoI-S25CRD-HindIII
Synaptobrevin (25-84) – Ciliary neurotrophic factor (Brevin-CNTF)*	27 kDa	Generated by Jason Arsenault (Davletov lab)	
Syntaxin 3 (195-253) -Ciliary neurotrophic factor (Syx-CNTF)*	27 kDa	Generated by Jason Arsenault (Davletov lab)	
Synaptobrevin (25-84)-Epidermal Growth Factor (Brevin-EGF)	15 kDa	Generated by Jason Arsenault (Davletov lab)	
Botulinum/A Light Chain Translocation Domain (aa. 1-852)- Ciliary neurotrophic factor	120 kDa	Generated by Jason Arsenault (Davletov lab)	
Botulinum/A Light Chain Translocation Domain (aa. 1-852)- Epidermal Growth Factor	106 kDa	Generated by Jason Arsenault (Davletov lab)	
Botulinum/A Light Chain Translocation Domain (aa. 1-852)-NPY	103 kDa	Generated by Jason Arsenault (Davletov lab)	Protein taken from existing stocks at -80˚C
Botulinum/A Light Chain Translocation Domain (aa. 1-852)-PACAP	103.5 kDa	Generated by Jason Arsenault (Davletov lab)	Protein taken from existing stocks at -80˚C
Botulinum/A Light Chain Translocation Domain (aa. 1-852)-PACAP2	103.5 kDa	Generated by Jason Arsenault (Davletov lab)	Protein taken from existing stocks at -80˚C
Botulinum/A Light Chain Translocation Domain (aa. 1-852)-Adrenomedullin	Predicted: 106 kDa	Generated by Jason Arsenault (Davletov lab)	Protein taken from existing stocks at -80˚C
Botulinum/A Light Chain Translocation Domain (aa. 1-852)-VIP	103 kDa	Generated by Jason Arsenault (Davletov lab)	Protein taken from existing stocks at -80˚C
Botulinum/A Light Chain Translocation Domain (aa. 1-852)-TNFα	Predicted: 117 kDa	Generated by Jason Arsenault (Davletov lab)	Protein taken from existing stocks at -80˚C

Table 2.2 – Plasmids and proteins used.

2.1.5 Peptides

All peptides were synthesised to order by PeptideSynthetics. 6-aminohexanoic acid (Ahx) is composed of six inert linear carbon atoms which are used to insert space between the peptide and attachments. All stocks arrive lyophilised and are diluted to 10 mg/ml stocks in 100 % DMSO and stored at -20 ˚C. Peptides are further diluted to working concentrations in Buffer A before use.

Peptide	Sequence
FITC-Ahx-Cellulobrevin (aa.12-37)	FITC-Ahx-RLQQTQNQVDEVVDIMRVNVDKVLE-NH_2
Bio-FITC-Ahx-TAT	Biotin-FITC-K-Ahx-GRKKRRQRRRPPQ-NH_2
Bio-FITC-Ahx-CPPenetratin	Biotin-FITC-K-Ahx-RQIKIWFQNRRMKWKK-NH_2
FITC-Ahx-HA2	FITC-Ahx-GLFGAIAGFIENGWEGMIDGWYG-NH_2
FITC-Ahx-CPBrevinMM	FITC-K-Ahx-AAKLKRKYWWKNLKMM-NH_2
Bio-FITC-Ahx-CPBrevin	Biotin-FITC-K-Ahx-AAKLKRKYWWKNLK-NH_2
CPBrevinMM-Ahx-Thio	Ac-AAKLKRKYWWKNLKMM-Ahx-C(pyridyldithio)-NH2
Thio-Ahx-CPBrevinMM	Ac-(pyridyldithio)C-Ahx- AAKLKRKYWWKNLKMM -NH2
CPBrevinMM	Ac-AAKLKRKYWWKNLKMM-NH2
CPPenetratin-Ahx-Thio	Ac-RQIKIWFQNRRMKWKK-Ahx-C(pyridyldithio)-NH2
Thio-Ahx-CPPenetratin	Ac-(pyridyldithio)C-Ahx-RQIKIWFQNRRMKWKK-NH2
CPPenetratin	Ac-RQIKIWFQNRRMKWKK-NH2
Dermo-Ahx-Thio	YaFGYPS-Ahx-C(pyridyldithio)-NH2
SubstanceP-Ahx-Thio	RPKPQQFFGLM-Ahx-C(Pyridyldithio)-NH2
VIP-Ahx-Thio	HSDAVFTDNYTRLRKQMAVKKYLNSILN-Ahx-C(pyridyldithio)-NH2
Thio-Ahx-CRH	Ac-C(pyridyldithio)-Ahx-SEEPPISLDLTFHLLREVLEMARAEQLAQQAHSNRKLMEII-NH2
Syntaxin45-Ahx-Thio	Ac-EIIKLENSIRELHDMFMDMAMLVESQGEMIDRIEYNVEHAVDYVE-Ahx-C(pyridyldithio)-NH2

Table 2.3 – Sequences of Peptides used

2.1.6 Cell lines

All cell lines used for experiments are listed below:

Cell line	Species	Disease derived from	Cell type	Supplier	Pass. number received
J774.2	Mouse	Reticulum cell sarcoma	Macrophage	Gift from Lynda Partridge, originally from ECACC	pass.4
Neuro2a	Mouse	Neuroblastoma	Neuroblast	ATCC	pass.3
SH-SY5Y	Human	Neuroblastoma	Neuroblast	Sigma	pass.21
LA-N-5	Human	Neuroblastoma	Neuroblast	Boston Children's Oncology Group	pass.21

Table 2.4 – Details of cell lines used

2.1.7 Antibodies

Antibodies were used either with western blot (WB) or Immunocytochemistry (ICC)

Primary Antibody	Species	Dilutions	Supplier
SNAP25	Rabbit	1:4000 (WB), 1:500 (ICC)	In-house
SNAP25	Mouse	1:4000 (WB), 1:500 (ICC)	Biolegend – SMI81
Cleaved SNAP25 (cSNAP25)	Rabbit	1:5000 (WB), 1:1000 (ICC)	In-house – further purified by Charlotte Leese
Syntaxin 1	Rabbit	1:1000 (WB)	In-house
β-III-tubulin	Mouse	1:2000 (WB), 1:1000 (ICC)	R&D Systems – MAB1195
CNTFR	Mouse	1:1000 (WB), 1:200 (ICC)	R&D Systems – MAB303
EGFR	Rabbit	1:1000 (WB), 1:200 (ICC)	Gift from Liz Smythe Cell Signalling – 2232S

Table 2.5 – Details of primary antibodies used

Secondary Antibody	Dilutions	Supplier
Sheep anti-mouse (HRP tag)	1:24000 (WB)	Amersham
Donkey anti-rabbit (HRP tag)	1:24000 (WB)	Amersham
Goat anti-mouse (Alexa Fluor 488 tag)	1:2000 (ICC)	Life Technologies
Goat anti-rabbit (Alexa Fluor 488 tag)	1:2000 (ICC)	Life Technologies
Goat anti-mouse (Alexa Fluor 594 tag)	1:2000 (ICC)	Life Technologies
Goat anti-rabbit (Alexa Fluor 594 tag)	1:2000 (ICC)	Life Technologies

Table 2.6 - Details of secondary antibodies used

2.2 Recombinant protein generation

To set up the restriction digests for recombinant plasmid formation, 4 µL of each of the donor and recipient plasmid DNA was mixed with 1 µL of each required restriction enzyme, 1 µL of each required 10x enzyme buffer and made up to 10 µL in DNase free water (Thermo Fisher Scientific) (table 2.7). All plasmids used in these experiments were pGEX-KG (fig. 2.1). The sample was then incubated for 1 hour at the required incubation temperature. After incubation finished, 5 µL FastAP (Thermo Fisher Scientific) was added to the recipient DNA only and is then left to incubate at 37 ˚C for a further 10 minutes.

To make the 1 % agarose gel, 0.5 g of electrophoresis grade agarose was added to 50 mL of 1x TAE buffer, then microwaved until the agarose had dissolved. After leaving to stand for 20 minutes, 1 µL sybrsafe DNA gel stain (Thermo Fisher Scientific) was added and agarose was poured into casing and the comb was inserted. The gel was then inserted into the tank (Bio-Rad) and is filled up with 1X TAE buffer as running buffer.

Once restriction reactions were ready, 2.5 µL of 5X agarose loading buffer (Bioline) was added to reactions. Samples were run on 1 % agarose gel at 70 mV for 45 minutes with DNA ladder (Hyperladder 1 kb – Bioline). An image was taken by gel imaging with blue light as opposed to UV (U:Genius3 - Syngene). The relevant bands were then cut from the gel and weighed. A gel extraction kit (Sigma-Aldrich) was used to purify the DNA.

Restriction enzyme	Supplier	Incubation time and temp.	Buffer	Notes
SmaI	NEB	25 ˚C, 1 hour	CutSmart (NEB)	Used in double Digest with XbaI for BotLcTd/A restriction, SmaI was added first then after 1 hour at 25 ˚C XbaI was added and incubated for a further hour at 37 ˚C
XbaI	Promega	37 ˚C, 1 hour	CutSmart (NEB)	See above
EcoRI	NEB	37 ˚C, 1 hour	NEBuffer 2.1 (NEB)	Used for mCherry restriction
SalI	NEB	37 ˚C, 1 hour	NEBuffer 3.1 (NEB)	Used for the removal of the cysteine rich domain from Diphtheria Light Chain Translocation Domain (aa. 1-388) – Diphtheria (aa. 179-190) – Cysteine rich domain *

Table 2.7 – Restriction enzymes and their conditions of use.

After DNA purification, the DNA concentrations were measured by Nanodrop and a ligation reaction set up using 100 ng Donor plasmid DNA, 3x molar ratio of Insert DNA (calculated through NEBioCalculator – NEB), DNase free H_2O up to 9 µL, 10 µL T4 DNA ligase buffer (NEB) and 1 µL T4 DNA ligase (NEB). Reactions were left at room temperature for 30 minutes then 5 µL was used to transform 30 µL of DH5α cells. DH5α cells (Thermo Fisher Scientific) were grown and made competent in house by Charlotte Leese through Rubidium Chloride incubation, they are not resistant to any antibiotics. Transformation of DNA into DH5α cells was done in the same way as detailed in section 2.2.1, however chloramphenicol is not added.

After colonies grew, 4 from each plate were used to inoculate 5 mL 2-YT culture broth with ampicillin and grown overnight at 37 ˚C with shaking. The bacteria was then harvested and mini-prepped using a kit (Qiagen). The DNA extracted from the mini-prep was then be run agarose gel with and without restriction digestion to ensure that the plasmid has the desired inserts. Once the desired plasmids were identified they were then transformed into BL21-gold (DE3) pLysS bacteria competent cells and the protein synthesised as described in section 2.2.

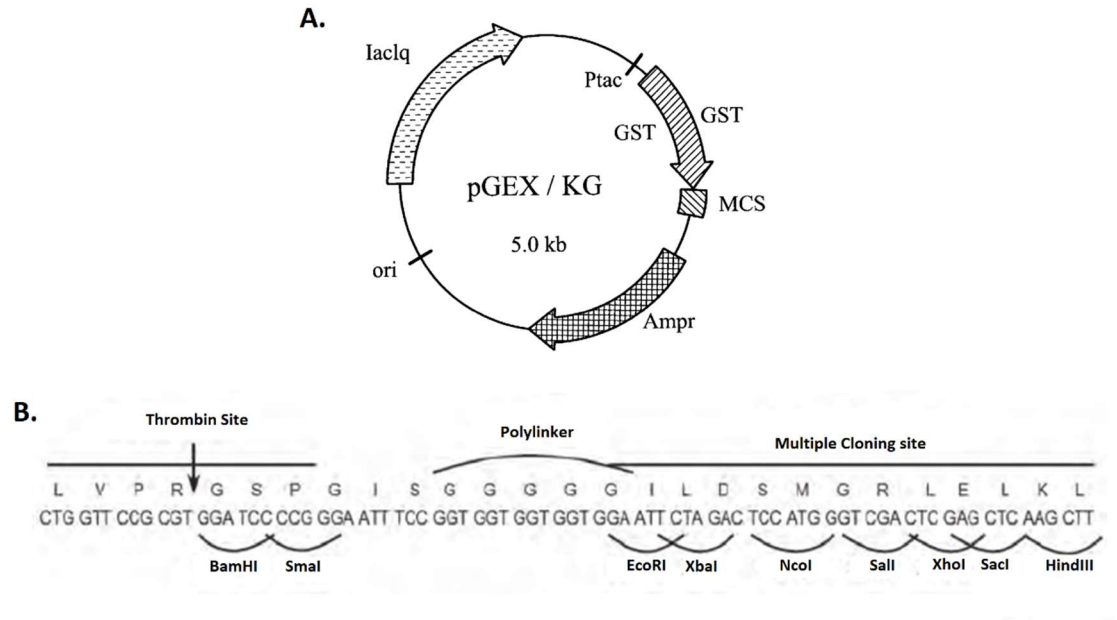

Figure 2.1 – Map of pGEX-KG plasmid with restriction sites

A) Overall map of pGEX-KG plasmid, showing the location of the Lac1 initiator, the Glutathione S-Transferase site (GST), the Multiple Cloning Site (MCS) and the Ampicillin resistance site (Ampr). B) Diagram showing DNA sequence of the MCS and the restriction enzyme sites.

2.3 Expression and purification of recombinant proteins cloned in pGEX-KG vector

2.3.1 Transformation of BL21-gold (DE3) pLysS competent cells

BL21-gold (DE3) pLysS (Agilent) were made competent for transformation by Charlotte Leese (Davletov lab) through Rubidium Chloride incubation. The cells are resistant to chloramphenicol, whilst the pGEX plasmid is resistant to Ampicillin.

Agar plates were first made by mixing 2-YT Agar before autoclaving and storing. Agar was then melted in microwave before mixing 1:1000 with ampicillin 100 mg/mL and chloramphenicol 50 mg/ml and approximately 15 mL placed in each 100 mm x 15 mm plate (Thermo Fisher Scientific). These are then allowed to set before storing at 4 ˚C for up to 1 month.

To transform pGEX-KG vectors into competent cells for expression of proteins, an aliquot was first defrosted on ice before 25-30 µL was put in one tube for each vector sample. 1 µL DNA was added to each competent cell sample and gently mixed, then incubated for 30 minutes on ice and mixed twice meanwhile. The samples are then heat shocked for 30 seconds at 42 ˚C and returned to the ice for a further 5 minutes. 300 µL of 2-YT media, pre-warmed at 37 ˚C, was added to samples then incubated in a shaker at 37 ˚C for 1 hour. The media and cells are then spread on ampicillin and chloramphenicol agar plates and incubated overnight at 37 ˚C.

After colonies had grown, some were harvested and grown overnight in 5 mL 2-YT media with antibiotics at 37 ˚C shaking. In order to store the bacteria without need for re-transformation, stocks could then be made by mixing 600 µL 50 % glycerol (sterilised) with 400 µL bacteria overnight culture.

2.3.2 Low temperature expression and purification of proteins

All pGEX-KG plasmids which were expressed contained not just the protein of interest but also GST with a thrombin cleavage site. To grow and express the GST-proteins whose vectors had been transformed into competent cells, firstly a colony from a plate or a glycerol stock pinch was placed in 5 mL 2-YT media and 5 µL of both ampicillin 50 mg/mL and chloramphenicol 50 mg/mL and incubated overnight with shaking at 37 ˚C. The following day the overnight culture was poured into a 2 L flask with 500 mL sterile 2-YT media with 500 µL of both ampicillin 50 mg/mL and chloramphenicol 50 mg/mL, and grown for a further 3 hours (approximately) at 37 ˚C until the OD_{600} reached between 0.5 and 0.7 as measured by Colorimeter (WPA Biowave). 0.5 mL IPTG (Melford) 100 mM was then added and the flask was incubated overnight shaking at between 18-20 ˚C.

The bacteria was then pelleted using a centrifuge at approximately 5000 rcf for 15 minutes, and supernatant was discarded into empty flasks and Virkon added to sterilise any remaining bacteria. The pellet was re-suspended in 5 mL lysis buffer and cOmplete EDTA-free protease inhibitor cocktail (Roche) through shaking (50 mL Lysis buffer has 1 Protease inhibitor tablet dissolved into it before use to make 1x stock), keeping the samples on ice when not on the shaker. Re-suspended pellet was then converted into a 50 mL falcon tube while another 5 mL lysis buffer + PI was used to re-suspend any pellet remaining in the

centrifuge container. The cell suspension was then snap frozen either in dry ice with ethanol or in -80 °C freezer for 15 minutes and then put it in RT water for 20-30 min.

12 µL of 1 M $MgCl_2$ stock and ~ 2 mg of deoxyribonuclease I from bovine pancreas was then added once thawed and the samples then rotate at room temperature for 10 min. Triton X-100 is then added for a final concentration of 2 % (approx. 1.5 mL of 20 %) and rotated for 20 minutes at 4 ˚C.

Meanwhile 0.5mL of Glutathione Sepharose beads (GE Healthcare) was pipetted into two 15 mL falcon tubes, these were washed twice in low salt buffer by centrifuging at 2000 rcf for 1 min. The cell sample was then centrifuged for 20 minutes at 7000 rcf at 4˚C, 3 µL of supernatant was saved for gel analysis and the rest poured on the beads and incubated for at least 1 hour rotating at 4˚C. The sample was then centrifuged at 2000 rcf for 1 minute and 3 µL of the flow through saved for gel analysis. The beads were then washed twice in high salt buffer and twice in low salt buffer before re-suspending in 7.5 mL low salt buffer, with 10 µL saved for gel analysis. The beads then had a further 7.5 mL glycerol added, which was mixed well at 4 ˚C before storing at -20 ˚C.

Loading buffer was then added to the gel analysis samples and run on an in-house SDS-PAGE gel as described in section 2.5.

2.3.3 Thrombin cleavage of GST

To separate the protein from the glutathione beads, GST was cleaved by thrombin (Sigma-Aldrich). The beads were first washed twice with buffer A to remove the glycerol, then transferred to a 2 mL tube where the beads were further washed once with buffer A and made up to 2 mL, 5 µL was kept for gel analysis. 20 µL thrombin (diluted 250 units into 1 mL dH_2O) was then added and incubated for 30 minutes at 37 ˚C shaking. It should be noted that proteins containing a translocation domain have a thrombin cleavage site between the light chain and the translocation domain in addition to the one between the GST and protein N-terminus. Because of this, after thrombin incubation both of these sites are cleaved and these proteins exist as two subunits held together by a disulphide bond (see Appendix 1).

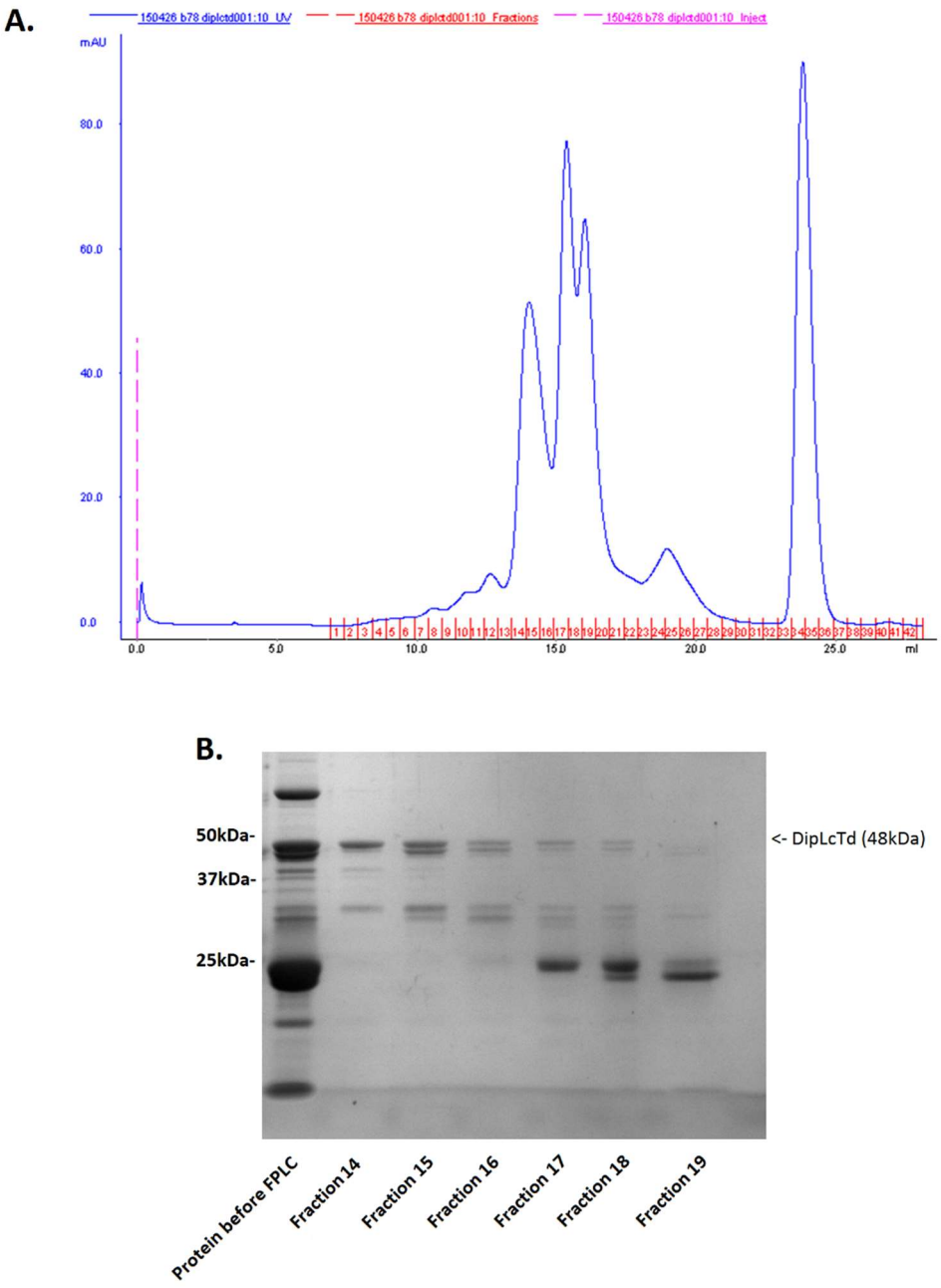

Figure 2.2 – Diphtheria Light Chain Translocation FPLC purification example

A) UV trace showing relative protein detected in each filtrate fraction, with the expressed protein leaving the FPLC column between fractions 9-28, and the xylene cyanol tracer in fractions 34-36. B) SDS-PAGE showing fractions taken from FPLC and their protein content: the band near 50 kDa is likely to correspond to diphtheria Light Chain Translocation domain (DipLcTd), which has a molecular weight of around 48 kDa, and so for this example fraction 14 is the purest. The band near 25 kDa is likely to be a breakdown product of the polypeptide, most likely corresponding to the 23 kDa diphtheria light chain.

Beads were then transferred to Spin Columns (Generon) and spun down multiple times (maximum volume is 700 µL) to separate beads from protein sample for 1 minute at 13,000 rpm. 5 µL of both the beads and elute was saved for gel analysis. Some proteins such as those with free cysteines, require the addition of tris(2-carboxyethyl)phosphine (TCEP) at 4 mM for 30 minutes at room temperature to reduce binding. The elute was then concentrated with a concentration column (Vivaspin 10,000 MWCO) to 0.5 mL using centrifugation at 5000 rcf (progress checked every 5 minutes). The concentrated sample was then transferred to a spin column for 1 minute to remove bubbles and foam for Fluid Phase Liquid Chromatography (FPLC). FPLC was used on most of the proteins to ensure purity, but especially on those where there are excessive undesirable protein fragments in which have been expressed, for instance diphtheria Light Chain Translocation Domain (DipLcTd) (fig. 2.2).

Xylene cyanol was sometimes added to the concentrated eluate in order to see protein sample whilst loading onto the FPLC (AKTA UPC-900) to be filtered through the column (GE Healthcare: Superdex 200 Increase 10/300 GL). The FPLC makes a UV trace and the relevant fractionations were taken and 5 µL from each taken for gel analysis. The 5 µL gel analysis samples were then run on an in-house SDS-PAGE gel. Figure 2.2 uses dipLcTd as an example of the FPLC trace and fractionations on lab-made SDS-PAGE gel. These are done individually for almost every protein made.

2.4 Protein conjugation

2.4.1 Pyridyl disulphide binding

In order to allow conjugation to form between pyridyl disulphide containing peptides and proteins with unbound cysteine residues, the proteins which were believed to contain free cysteine groups were incubated with the pyridyldithio-peptide in an equivalent or excess molar ratio for 1 hour at room temperature (20 ˚C) diluted in buffer A. The incubation time and particular incubation reagents varied between experiments, but unless otherwise mentioned 1 hour incubation at RT in buffer A is the standard incubation condition.

2.4.2 SNARE formation

SNARE complexes were formed by combining an equal molar ratio of syntaxin, synaptobrevin and SNAP25, or proteins containing these sequences. The method was optimised to 1 hour incubation in buffer A containing 0.4 % OG (See Chapter 3), however there may be variation. These are the conditions which are used unless otherwise mentioned.

A.

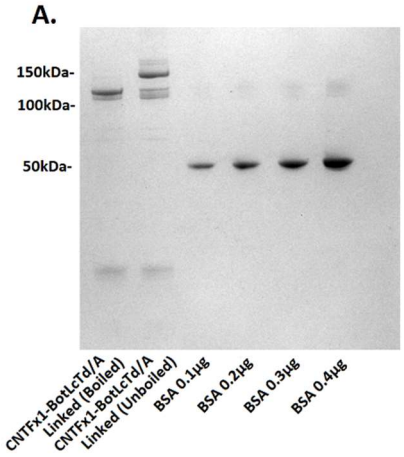

B.

BSA µg	Int. x mm
0.1	6302.681
0.2	7010.763
0.3	7790.506
0.4	8564.488

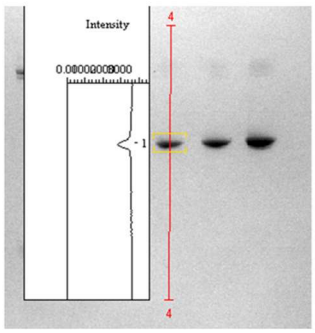

C.

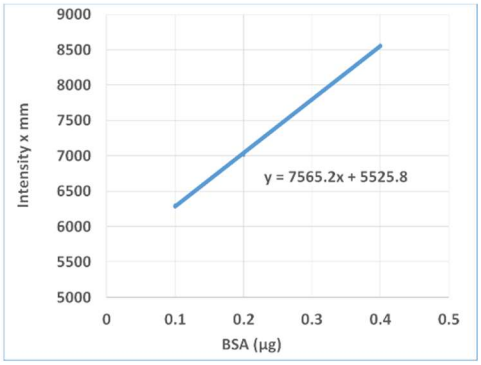

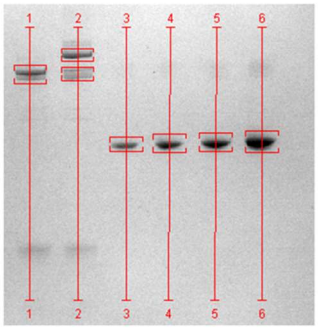

D.

	Int. x mm (µg)	Size kDa	Protein Quantity (µL)	Concentration (nM)
BotLcTd/A	7205.856	0.222077	3	592.205
CNTFx1-BotLcTd/A Linked	7017.805	0.19722	3	438.266

Figure 2.3 – Example of calculating protein concentrations using BSA standards.

A) Progression of SDS-PAGE with samples and BSA standards through band analysis on ChemiDoc XRS (Bio-Rad). The botLcTd/A put into the linked sample was measured at 600 nM as diluted from Nanodrop (Thermo) reading. B) Table of band intensities of subfigure A rows 3-6 measured by band analysis software. C) Graph of BSA standard concentrations against band intensity with linear trendline and trendline equation. D) Table of band intensities of the boiled CNTFx1-BotLcTd/A linked sample, taking the botLcTd/A-S25 band, and the formed CNTFx1-BotLcTd/A linked sample (unboiled) (rows 1 and 2 from subfigure A). Using the trendline equation, the amount of protein in µg could be calculated. From this and the size (kDa) of the protein the concentration in nM of the samples can be calculated. Note that the botLcTd/A-S25 concentration has been measured as close to the predicted 600 nM.

2.4.3 Reduction through TCEP

All TCEP reactions were done through incubating proteins up to 0.2 mg/ml in 4 mM TCEP for half an hour at RT unless stated otherwise. TCEP was filtered out of sample through FPLC

2.4.4 Measuring protein concentration

Pure protein stock concentrations were measured through Nanodrop (Thermo Fisher Scientific). When there is a mix of proteins in a sample, for instance in linked samples, samples were run on SDS-PAGE with BSA standards 0.1-0.4 µg (fig. 2.3). The bands were then analysed on the ChemiDoc XRS which were then used to make a standard curve to measure the approximate concentration of the protein band. The size of the protein (kDa) was then used to determine the molarity. Figure 2.3 gives an example of CNTFx1-BotLcTd/A linked complex being formed and the consequent analysis which was typical of analysing stocks.

2.5 Cell culture

2.5.1 Cell line cultures

All cell lines were cultured in a 37 °C, 5 % CO_2 humidified incubator (Panasonic – Incusafe) and passaged twice a week. J774.2, SH-SY5Y and Neuro2A cell lines were cultured in Dulbecco's modified Eagle medium + GlutaMax (DMEM) (Life Technologies) supplemented with 10 % foetal bovine serum (FBS) (Life Technologies). LA-N-5 cell line was cultured in RPMI 1640 + GlutaMax (Life Technologies) with 10 % FBS. The cell stocks were not grown in any antibiotics. Cell stocks were maintained in T25 flasks (Thermo Fisher Scientific)

All cell lines were passaged using Trypsin-EDTA 0.25 % (Sigma), apart from the J774.2 cell line which was passaged by cell scraping. For viable cell counting, cells were diluted 1:1 in trypan blue dye (Bio-Rad) and counted in duplicate using an automated cell counter (Bio-Rad).

Cells were kept for either 10 weeks or 20 passages (whichever is shorter) before disposing and defrosting new batch of cells.

Incubators and culture hoods (Esco – Airstream) were cleaned monthly to prevent infection. All cells were spot-checked for mycoplasma annually by Jackie Price using PCR detection kit (Sigma-Aldrich); there was no significant mycoplasma infection detected in any of the cell cultures over the project.

2.5.2 Cell line freezing and defrosting

Cells were removed from liquid nitrogen and incubated for 1 minute in a 37 ˚C water bath before defrosting and diluting in 5 mL pre-warmed media. The cells were then centrifuged for 5 minutes at 3000 rpm before aspirating the media and replacing with fresh media and placing in culture flasks for incubation. Cells were passaged at least twice to recover from liquid nitrogen before use.

Cells were frozen by growing to confluency in a T75 flask before trypsinising and cell counting. Cells were centrifuged and re-diluted in FBS + 10 % DMSO before placing 1.5 mL in cryo-tubes (Thermo Fisher Scientific) each containing $2x10^6$ cells. The cryo-tubes were then put in a freezing container (Nalgene) and frozen overnight at -80 ˚C and then placed in liquid nitrogen.

2.5.3 Cell plating and sample addition

Unless otherwise indicated, Neuro2A and J774.2 were seeded at a density of $5x10^3$ cells per well in 96-well plates, $1.5x10^4$ cells per well in 48-well plates and $5x10^4$ cells per well in 6 well plates (All plates were purchased from Corning). SH-SY5Y were seeded at a density of $1x10^4$ cells per well in 96-well plates, $3x10^4$ cells per well in 48-well plates, $2.5x10^4$ in 24 well plate and $8x10^4$ cells per well in 6 well plates. LA-N-5 cells were seeded at $2x10^4$ cells per well in 96-well plates, $6x10^4$ cells per well in 48-well plates and $1.5x10^5$ in 6 well plate. In 96 and 24 well plates the wells around the edge were not used and were instead filled with sterile PBS. All cells seeded for incubating with samples were dosed with Penicillin-Streptomycin cocktail (PenStrep) (Sigma-Aldrich) diluted 1:100. All plates after seeding remained at RT for around 10 minutes to allow to settle before putting into 37 ˚C incubator to prevent cells clustering into the centre of wells (Lundholt et al. 2003).

Cells seeded into 96 well plates had a volume of 90 µL, 48 well plates had a volume of 270 µL, 24 well plates had a volume of 900 µL and 6 well plates were seeded with a minimum volume of 2 mL. All cells were incubated for a minimum of 4 hours after plating before samples were added, unless stated otherwise, all plates had sample added on the same day as seeding. Samples which had been previously diluted in either cell media or PBS were then further diluted x10 into plate wells. Standard incubation time before assaying or harvesting was 3 days unless stated otherwise. All 96 well plates had the samples added in triplicate, whereas other plates were always incubated singularly with each sample.

Samples containing OG at either 0.4 % or 0.2 %, depending on cell type and sample concentration, were further diluted in OG at a constant concentration before diluting 1 in 10 in cell media + PenStrep and vortexing. Half of the media was then removed from all wells to be dosed before sample taken from the top and diluted into plate well media 1 in 2. It was important that the samples were made with more than 50 % excess. The reason for this was to allow any OG which has not fully solubilised to sink to the bottom of the sample, so the sample to be added into the wells could be taken off the top without there being excess insoluble OG, which was toxic to cells.

Where there were samples containing Lipofectamine3000 (LF3000), samples to be added had LF3000 added to make an overall concentration of 5 % before incubating for 15 minutes. The samples were then added into wells, diluting the sample 1 in 10.

2.6 SDS-PAGE and Western blotting

2.6.1 Cell harvesting and lysis

To lyse cells for Western blot samples, 1X western lysis buffer was made by mixing 250 µL 4X lysis buffer with 750µL dH_20, 10 µL 1 M $MgCl_2$ and 1 µL ≥250 units / µL Benzonase Nuclease (added just before use). The cells (seeded in 48 well plate) were aspirated and 60 µL 1X Western lysis buffer added to each well. The plate was then shaken for 10 minutes shaker 850 rpm on Grant Bio PMS-1000i plate shaker before mixing and each sample placed into a 1.5 mL tube. Tubes were then boiled at 95-100 ˚C for 3 minutes before centrifuging at 13,000 rpm for 1 minute. The samples could then be used for western blot, or frozen at -20 ˚C until use.

2.6.2 Making SDS-PAGE gels

Gel plates were assembled into cassettes, ensuring bottom of plates were level and had formed a seal with the rubber in holder. 5 mL resolving gel buffer was then put between the glass plates, and small volume of water layered on top of setting gel using 1 mL syringe before the gel was left to set for 20 minutes. The excess water was later removed once set by tipping and drying with tissue paper.

2 mL stacking gel was then placed on top of the resolving gel and a 15 lane comb immediately inserted in the stacking gel, inserting diagonally to avoid bubbles. Gel was then left to set for 20 minutes. The combs were removed after setting and the wells are washed with dH_2O. The gels could be used immediately or wrapped in wet towel and stored at 4 ˚C until use for up to a week (Bio-Rad cassettes and tank used).

2.6.3 SDS-PAGE and protein staining

Samples of approx. between 0.1 and 0.5 µg protein were loaded onto a gel with a maximum sample size of 10 µL. 3 µL 4x Sample buffer was then added to each sample and vortexed before loading into pre-cast gel (Novex NuPage 12 % Bis-Tris gel – Invitrogen) or lab-made gel with a ladder (5 µl for SDS-PAGE and 15 µl for western blot – Bio-Rad Precision Plus Dual colour protein standard). Pre-cast gels were run using MES x1 buffer and lab-made gels were run using Tris-Glycine x1 running buffer, both were prepared by diluting the concentrated stocks with appropriate amounts of dH_2O.

Standard gels or Western blots were typically run at 180 mV for 50 minutes until the bromophenol blue reached the bottom. Western blots and gels requiring the separation of cleaved SNAP25 band from whole SNAP25 were run at 180 mV for 110 minutes.

Gels containing SNAREs required them to be run with cold (+4 ˚C) 1x MES buffer in a bucket of ice for 110 minutes at 180 mV to prevent breakage. SNAREs were pipetted into two Eppendorf tubes before adding loading buffer, one was boiled at 95 ˚C for 3 minutes before centrifuging, cooling and loading, whereas the other was loaded as normal; together these samples gave the 'before' and 'after' samples for SNARE formation.

Lab-made gels as shown in section 2.3.2 were used for protein analysis after running through the FPLC. These gels were run at 200 mV for 40 minutes.

After gel running had completed the gel was removed from the cassette and submerged in SDS-PAGE staining solution, it was then microwaved for 30 seconds and then placed on a rocker at RT for 20 minutes. The gel was then removed from the stain and then de-stained in water overnight. Images of the gels were taken on the ChemiDoc imager for record keeping and any band analysis required.

2.6.4 Western Blotting

8-15 µL of each sample was loaded onto pre-cast gel and run at 180 mV for appropriate amount of time (as described in section 2.3.3). Transfer membrane (Immobilon-P – Merck) was activated by soaking with methanol then placing with 2 sheets of whatman paper (GE Healthcare) into transfer tank (Bio-Rad) containing cold membrane transfer buffer. After gel had run, the following were then layered onto the Black side of transfer cassette: Sponge, 1 whatman paper, Gel (flipped so ladder was on the right), membrane, whatman

paper, sponge. The cassette was closed and placed in transfer tank along with a freezer block and 4 ˚C membrane transfer running at constant 250 mA for 1 hour. The membrane was removed and washed with water, then placed in blocking solution rocking for 30 minutes. Primary antibody was added, then rocked overnight in cold room. The following morning the membrane was washed with PBS-T for 5 minutes three times before fresh blocking solution containing secondary antibody was added. Membrane was then rocked at room temperature for 30 minutes. The membrane was then further washed with PBS-T for 5 minutes three times before SuperSignal West (Dura Extended Duration substrate-Thermo Fisher Scientific) was prepared (600 µL per membrane). The membranes were placed on visualisation tray, then SuperSignal West solution was added and distributed evenly by tipping the tray. Cling film was placed over membranes, which were then processed in a dark room using exposure to photofilm (Amersham Hyperfilm – GE Healthcare) before placing through X-ray film processor (Optimax 2010). Images were then taken by ChemiDoc for digital storage and band quantification.

A.

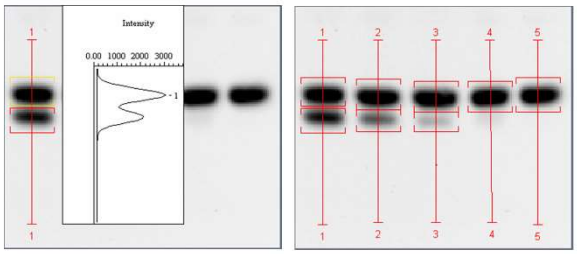

B.

Lane	Band 1 int. x mm	Band 2 int. x mm	Band 2 %
1	4661.213	2927.338	38.57572
2	4962.488	1726.338	25.80928
3	4942.288	693.663	12.30783
4	4757.775	0	0
5	4473.225	0	0

Figure 2.4 – Demonstration of Band analysis for Western blot

A) Images of band detection software drawing around protein bands. B) Quantification of the band intensities and subsequent calculation of the % cleaved SNAP25 band based off the total band intensity detected.

2.6.5 Western blot band quantification

To measure band intensity or % SNAP25 cleavage in Western Blots, images taken of the blot on the Bio-Rad were quantified by band analysis software. A densitometric analysis was performed on the band, setting the background intensity to 100 before, then creating a report which gave a value for the relative band intensities. The % was taken by taking the

value for the cleaved band and then dividing it by the value for the combined bands added together (fig. 2.4). All error bars on band densitometric analysis graphs represent standard deviation.

2.7 Cell count and viability assays

2.7.1 Automated cell counts

Cell concentration and % viability was measured before plating by automated cell counter. 10 µL cells was mixed with 10 µL trypan blue solution (Sigma-Aldrich) and 10 µL of the mix was inserted into cassettes (Bio-Rad) which was then inserted into an automated cell counter (TC20 – Bio-Rad). This was done in duplicate and the average taken. The machine calculated the values for the total cell concentration, the alive cell concentration and the % alive cells.

2.7.2 MTT assay

A 12 mM MTT stock solution was prepared by adding 1 mL of sterile PBS to 5 mg of MTT and mixed through vortexing, often overnight incubation at 4 ˚C would fully dissolve the solution however occasionally it would need to be centrifuged to remove any particulate material that did not dissolve. An SDS-HCl solution was made by adding 10 mL of 0.01 M HCl to 1 g of SDS which was gently shaken until fully dissolved.

Cell media was removed through careful aspiration from the cells to be analysed (in 96 well plate) and it replaced with 100 µL of phenol red free DMEM (Gibco – Thermo Fisher Scientific) + 10 % FBS. 10 µL of the 12 mM MTT stock solution was then added to each well, including a medium only negative control well. . The plate was then incubated at 37 ˚C 5 % CO_2 for 4 hours. 100 µL of the SDS-HCl solution was added to each well and mixed thoroughly using the pipette, the plate was then further incubated for 37 °C for 4 hours. Each sample was then mixed again using a pipette and end point absorbance read using a microplate reader at 560 nm (iMark – Bio-Rad). Plates were analysed by removing the background values and the % reading was based off the wells containing untreated cells.

2.7.3 AlamarBlue

10 µL DeepBlue Cell Viability solution (Biolegend) was added to each well to be analysed, including 3 background wells, and the plate was placed at 37 ˚C, 5 % CO_2 for 4 hours. After, plate was removed and analysed for fluorescence, measuring the absorbance at 560 nm and the emission at 590 nm (Fluoroskan Ascent – Labsystems). Plates were analysed by removing the background values and the % reading was based off the wells containing untreated cells. All error bars on alamarBlue assay graphs represent standard deviation.

2.7.4 Hoescht/PI viability assay

Cells which were intended for fluorescence were seeded in 96 well glass bottomed imaging plates (Greiner). At appropriate time points, the cells were then washed with phenol-red free DMEM media before adding Hoechst 33342 (Life Technologies) (1:2000) and propidium iodide (PI) (Life Technologies) (1:2000) stains to investigate cell viability. Hoechst dye is cell permeable and stains the DNA of all cells, whereas PI is cell impermeable and only stains the DNA of dead cells. Cells were incubated at 37 °C for 15 minutes before imaging using an epifluorescence microscope (DMIRB, Leica). 3 images were taken per well using 20x objective and both total cells and PI stained cells were counted using image J. Cell viability was calculated as a ratio of dead cells compared to overall cell count.

2.8 Microscopy

2.8.1 Live cell imaging

Cells were seeded in 96 well glass bottomed imaging plates (Greiner) and left overnight. Samples were then incubated with fluorescent proteins for the time stated. In the case of live cell microscopy, the cells were then washed twice with PBS, before incubating a further 10 minutes in phenol red-free media with Hoechst 33342 (Life Technologies) (1:2000). The cells were then imaged at x20 or x40 on epifluorescence microscope (DMIRB, Leica) for intervals ranging between 10 ms and 800 ms (see figures for specifics).

2.8.2 Fixing cells on plates or glass coverslips

Glass cover slips (radius 25 mm, Marienfeld, Germany) were sterilised by plating in 6 well plates and rocking for 1 hour in 100 % ethanol, before washing three times in sterile PBS. The coverslips were then aspirated and left to dry in the sterile hood under ultraviolet light for 1 hour. The plates could then be sealed and stored at 4 ˚C until needed.

Wells and coverslips for cell seeding were laminin coated at 10 µg/mL (Sigma-Aldrich) for over 1 hour at 37 ˚C incubation. 40 µL laminin in PBS was used to coat in 96 well glass bottomed imaging plate, 1 mL in 6 well plate with glass cover slips. Unless stated otherwise, cells were seeded as described in section 2.4.3.

After cell growth and sample addition (if required), cells were then washed twice with PBS before fixing for 10 minutes at room temperature with PFA 4 %. The PFA was then removed and the samples permeabilised for 15 minutes with PBS-0.3 % Triton X-100. The cells were then washed twice with PBS before being saturated with blocking solution for at least 1 hour at RT, if coverslips were being used then pieces of parafilm were used as 'coverslips' to avoid dehydration. The primary antibody was then incubated for 1 hour at room temperature. The samples were washed twice with PBS before the secondary antibody was added at a concentration of 1:2000 along with DAPI (Sigma-Aldrich) if needed at 1:1000 for 45 minutes whilst protected from light. Samples were then washed twice with PBS. The 96 well glass bottomed imaging plates were left in the third wash of PBS, wrapped in foil and stored at 4 ˚C

Glass coverslips were mounted by removing excess PBS with tissue paper after washing, before placing face down on glass slides (Menzel Glaser 76 x 26 mm) with 20 µL mounting media (DAPI Fluoromount-G-SouthernBiotech). The slides were left to dry for over 24 hours before imaging. The slides were protected from light and stored at 4 ˚C.

2.8.3 Microscopes

The two microscopes used throughout this project were an inverted epifluorescence microscope (DMIRB, Leica) and a confocal microscope (Nikon A1 TIRF).

The most often used microscope was the Leica, which used a mercury vapour lamp to pass light through an R4 filter cube for fluorescent images. In addition to this, all brightfield images were taken on this microscope. This microscope could be used with both slides and

96 well imaging plates. Image J was used to analyse the images. The scaling was set by Rebecca Bresnahan (Davletov lab) using a micro-ruler, the following scaling was applied manually to all images.

Objective	Size	Units
5x	468.7114	Pixels / mm
10x	0.928	Pixels / µm
20x	1.88	Pixels / µm
40x	3.7667	Pixels / µm

Table 2.8 – Scaling for epifluorescent microscope

The confocal microscope was only used to image the slides, this employed a hyper selector to select laser wavelengths based on the specific secondary antibody used. Laser intensity, offset and HV were conserved between experiments. Scaling was automatically inputted onto images using the NDi6d plug-in on image J.

2.8.4 Image J analysis

Image J was used to draw around cells and have the average cell intensity calculated, this was done freehand on all cells which had visible boundaries within a defined random area. The cells were drawn around on the brightfield image, and the overlay was then compared to the DAPI image before finally placing it over the image to be analysed (either FITC or mCherry) (fig. 2.5:A). The software would produce a value of the average pixel intensity across the cells drawn around, for these images no adjustment tool was used and all images were taken in the same session with the same exposure. Image J was used to count cells manually using the counting tool (fig. 2.5:B). It should be noted that it was sometimes difficult to judge where the boundaries of the cell lay so this method is not 100 % accurate, especially taking into account that some cells clumped together when confluent or during apoptosis. Nonetheless the images were analysed consistently. The values were then exported to Microsoft excel for analysis.

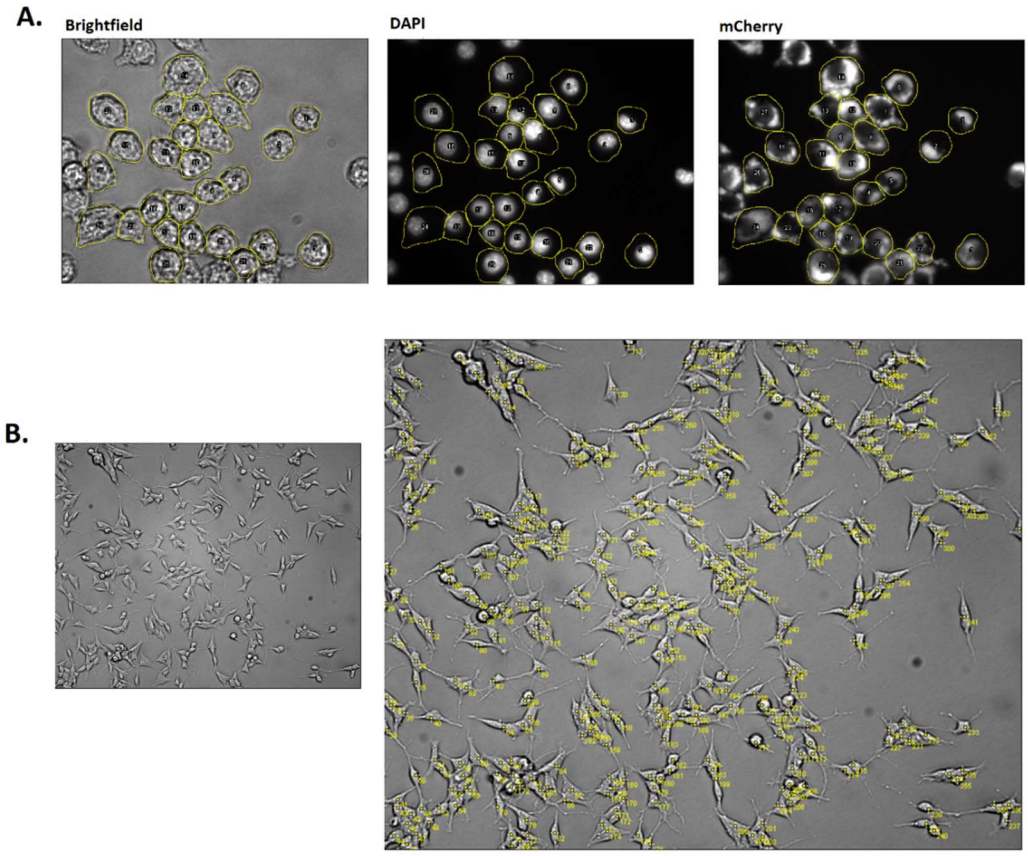

Figure 2.5 – Figure demonstrating the techniques used in ImageJ

A) Images showing hand-drawn traces around brightfield images, before comparing the overlay to the DAPI images and then placing the overlay over the image to be measured for average intensity. B) Image showing LA-N-5 cells before and after counting tool was used.

2.9 Radioactivity assay

Radiation measurements were completed by samples being placed in 6 mL scintillation tubes (Sarstedt). All samples were made up to 1 mL in basal buffer before placing in tubes and topped up with 4 mL scintillation fluid per tube (Emulsifier-Safe – PerkinElmer). The tubes were then put in racks and placed in a scintillation counter (WinSpectral 1414 α/β – PerkinElmer). Scintillation counter was calibrated using provided [H3] and [C14] sources. Every experiment used controls containing either no radiation or known concentrations of radiation. Wipe tests were done after every experiment using lint-free paper soaked in ethanol, wiping areas, and then placing in scintillation vials with scintillation fluid. Quench curves were done manually to compare between the predicted Disintegrations per Minute

(DPM) and the received Counts per minute (CPM). All buffers and experimental protocols were based off previous experiments: (Shone & Melling 1992; Géraldine et al. 2010; Atcheson et al. 1994; Davletov et al. 1998; Biedler et al. 1978)

All buffers used had their pHs measured at between 7.3-7.4. Quench curves were made by titrating known concentrations of [3H]-NA (Noradrenaline, levo-[ring-2,5,6-^{3}H] – Perkin Elmer) into 1 mL basal buffer before scintillation analysis. Alternatively, known concentrations of cell lysates were mixed with known concentrations of [3H]-NA before scintillation analysis. There was no measured difference between the quench of release buffer and basal buffer. When basal buffer was incubated for 45 minutes with cells there was no measured difference in the quench between the incubated and non-incubated basal buffer, therefore the same quench values could be used. The quench value for cell lysates was taken with 3 or more known values of [3H]-NA at each experiment attempt owing to the variety of the values, this was done by seeding and harvesting excess untreated wells. In addition, other wells not to be tested with [3H]-NA were incubated with equivalent botulinum domain containing samples to get approximate representative cleavage of the radiation added wells.

Unless stated otherwise, cells were seeded at $2.5x10^{4}$ cells in culture media in laminin coated 24 well plates, after 4 hours any samples to be added were diluted 1 in 10 into the wells. Wells were added in triplicate: one well to measure basal release, one to measure stimulated release, and one to be lysed and the SNAP25 cleavage measured on western blot. Cells were incubated for 72 hours at 37 ˚C 5 % CO_2. After 72 hours the incubation media was removed and replaced with basal buffer with 20 mM pargyline, 0.2 mM ascorbic acid and 1.25 µCi [3H]-NA (46.25 kBq) for 45 minutes at 37 ˚C. There was always at least 1 well without [3H]-NA added as a control. After 45 minutes, a control well had the [3H]-NA containing incubation buffer removed and placed in a scintillation vial. The well was then washed 3x 1 minutes with basal buffer before incubating for 5 minutes with Trypsin-EDTA, then a further 5 minutes with 0.4 % triton X-100 + 0.2 % Benzonase nuclease in PBS added 1 in 2. The cell homogenate was then extracted and placed in a scintillation vial for analysis. Once the CPM readings have been converted to DPM through factoring quench, the % cell uptake was determined.

For wells to be analysed for [3H]-NA release, all incubation media was removed and placed in scintillation vials before the wells were washed 3 x 2 minutes with basal buffer. Release was then measured by incubating the cells for 5 minutes with either basal buffer or release

buffer. The buffer was then removed and kept for scintillation radioisotope counting. The well was then washed 3 x 1 minute with basal buffer before incubating for 5 minutes with Trypsin-EDTA, then a further 5 minutes with 0.4 % triton X-100 + 0.2 % Benzonase nuclease in PBS added 1 in 2. The cell homogenate was then extracted and placed in a scintillation vial for analysis. Through using quench and converting CPM to DPM, the % release of the samples was determined.

2.10 Rat blood harvesting

The harvesting of rat blood was done by Rebecca Bresnahan on a deceased 3-4 week old male untreated Sprague-Dawley. This was done in accordance with Home Office regulations.

2.11 Statistics

N refers to the number of completely independent experiments, n is the number of repeats within the experiments.

The null hypothesis is that there is no significant difference between specific populations of data; this was tested throughout the project through two different statistical tests:

Student's T-Test were done through GraphPad Prism to determine whether the null hypothesis was correct when there were two data sets. On the other hand, one-way ANOVA tests were also done through GraphPad Prism was used to determine whether the null hypothesis was correct when there were 3 or more data sets. Sometimes, if the null hypothesis was indicated to be false then additional Student's T-Tests would be done to further determine relationships.

These are both used to determine the *p*-value of the relationship, which in turn denotes the level of significance, or put another way, the chance that the null hypothesis is correct. A *p*-value of 0.05 (or 5 % chance that the null hypothesis is correct) was used as the

threshold for significance, with further levels of significance also noted, denoted at the following: $P>0.05$ = NS $P<0.05$ = * $P<0.01$ = ** $P<0.001$=***, where NS = Not significant.

The statistical test used and the levels of significance are stated in the figure legends of each appropriate figure.

Anomalies were rare but did occur, most often due to human error or mis-dosing of cells. Anomalies were judged to be outside ± 3.5 standard deviations of the mean assuming that all data points were normally distributed (99.7 % of data points are within 3 standard deviations if data is normally distributed). Anomalies were removed from data sets.

All error bars shown in this project represent 1 standard deviation of the mean, assuming that all data was normally distributed.

2.12 Safety

Good Laboratory practise was employed at all times throughout this project. Lab coat and gloves were worn at all times at the bench. Masks and goggles were worn when working with PFA. Control of Substances Hazardous to Health (COSHH) forms were kept up to date and new ones written when needed (e.g. Radioactive substances). Proteins or complexes which contained toxins were first deactivated with 0.5 M HCl + 2 % SDS before disposing of. Experiments involving radioactive substances adhered to the University of Sheffield Policy and Procedures and the Work Certificate obtained for unsealed sources; full training was provided. Wipe tests were completed after every experiment and radioactive waste was disposed of correctly.

Chapter 3: Establishing protein modification and binding techniques for controlled protein conjugation.

3.1 Introduction

As previously discussed, conjugation is an important yet often overlooked factor within drug design. There is prevailing preference for cleavable linkers over fused linkers as there is the advantage that the targeting domain can be cleaved away and will not therefore interfere with the therapeutic domain (Böhme & Beck-Sickinger 2015; Chen et al. 2014). Whilst conjugation via pyridyl disulphide has already been established as a method of conjugation, there is very little focus on the biological aspects of it: its limitations and how it influences proteins, its stability and conjugation efficiency. However there are drawbacks to pyridyl disulphide binding, such as that only two components can be brought together, whereas there is a demand for a protein platform which can assemble multiple domains. In this regard, SNARE complexes could offer an avenue of research to address this need (Arsenault et al. 2013).

Therefore, both pyridyl disulphide modification and SNARE linking will be individually investigated as techniques for conjugation, each having the potential to meet different demands for drug construction. Here, both methods are explored, optimised and compared to determine their properties and their suitability for use in drug design.

3.2 Results

3.2.1 Enzymatic domains of therapeutic enzymes can have unbound sulfhydryl groups on cysteine residues.

Many toxins such as diphtheria and ricin are formed from a Light Chain (LC) enzymatic subunit attached via disulphide bridges to a targeting heavy chain, sometimes with the addition of a translocation domain (fig. 3.1:A-C) (Bell & Eisenberg 1996). The enzymatic domains of ricin, diphtheria, burkholderia lethal factor 1 (BLF1) and botulinum have shown potential as therapeutics for cancer treatment, with botulinum also being investigated for the alleviation of chronic pain and migraine (Tyagi et al. 2015; Dressler & Benecke 2007; Walsh et al. 2013).

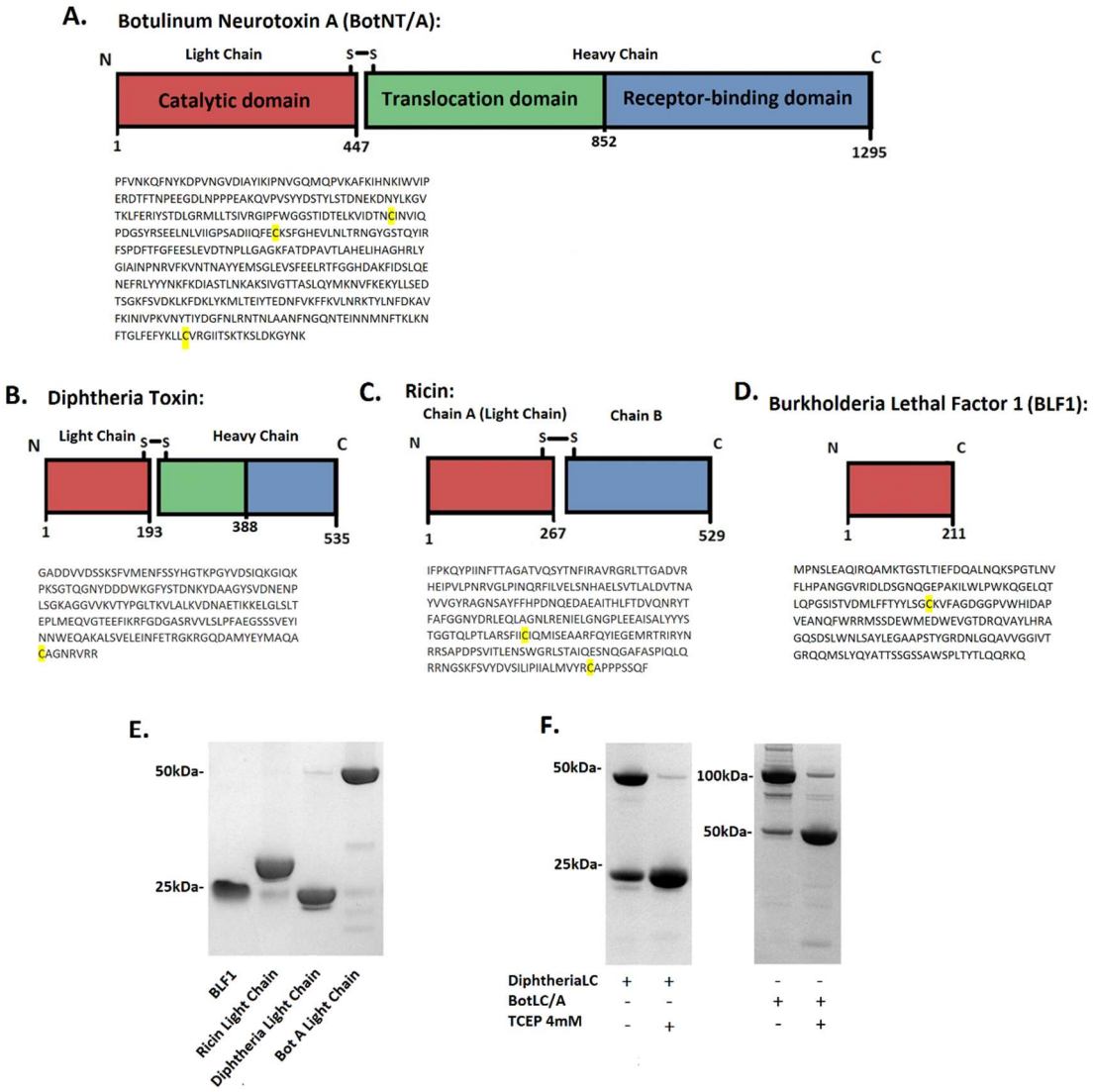

Figure 3.1 - Numerous therapeutic enzymes contain cysteine residues for potential modification

A-D) Schematics showing the structure of toxins and the amino acid sequences of their catalytic (enzymatic) Light Chain (LC) domains with the cysteine residues highlighted (Greenfield et al. 1983; Thompson et al. 1990; Halling et al. 1985; Lee et al. 2007). E) SDS-PAGE of Catalytic domains of toxins shown in A-D after 3 hours at 22˚C (Bot = Botulinum). F) SDS-PAGE showing dimerisation of light chains (LCs) after 1 month at -20˚C and the subsequent breaking of the dimers after incubation with TCEP 4 mM.

By preparing plasmids with the light chain domain of these toxins, it is possible to express the enzyme with the cysteines unbound by the heavy chain, leaving them potentially free to conjugate to other proteins. This could also theoretically happen by expressing the full length toxin and incubating with a reducing agent such as TCEP, however the heavy chain would then need to be separated from the rest of the sample and also there is the added risk of exposure to the full length toxin. The enzyme alone, without the heavy chain, has lost the ability to efficiently translocate inside cells, thereby decreasing the toxic risk to the user.

Figures 3.1:A-D shows the subunit layout of the toxins botulinum A, ricin, diphtheria and BLF1 and the amino acid sequences for the enzymatic domains, highlighting the cysteine residues with potentially unbound SH groups. Because of the unbound cysteines on the enzymes there is a risk of aggregation; figure 3.1:E shows the toxin LCs after 3 hours at room temperature, with minimal aggregation, indicating relative stability of LC samples. However, it was noted that prolonged storage above -80 ˚C resulted in dimerisation, whilst this was avoided, the aggregated protein could be reduced back to its monomeric state through incubation at RT for 30 minutes with 4 mM TCEP (fig. 3.1:F). The protein would then need to undergo filtering through Fast Protein Liquid Chromatography (FPLC) in order to separate the TCEP from the protein before further use.

3.2.2 Selection of Cell-Penetrating peptides for pyridyl disulphide attachment

Cell Penetrating Peptides (CPPs) are short amphipathic peptides which are used for the non-specific delivery of drugs and proteins via conjugation (Koren & Torchilin 2012; Farkhani et al. 2014) Previously established CPPs Penetratin and TAT were attached to the fluorophore FITC as well as endosomal escape sequence HA2, and a 25 amino acid cytoplasmic portion of the SNARE protein cellulobrevin (VAMP3) (aa.12-37) as a control (fig. 3.2:B) (Ramsey & Flynn 2015; Dunican & Doherty 2001). CP-BrevinMM was previously investigated by Violeta Ruipérez of Bazbek Davletov's lab as a potential CPP due to its numerous cationic residues over a portion of the synaptobrevin sequence; this short sequence was isolated and shown *in vitro* to increase the internalisation of siRNA through non-covalent complex formation (Appendix 2). It was hypothesised that that CP-BrevinMM would be better at internalising into cells than CP-Brevin due to the hydrophobic methionine residues at the C-terminus, which are part of the transmembrane domain of

synaptobrevin and potentially encourages interaction with plasma membranes; therefore both CP-BrevinMM and CP-Brevin were labelled with FITC to compare.

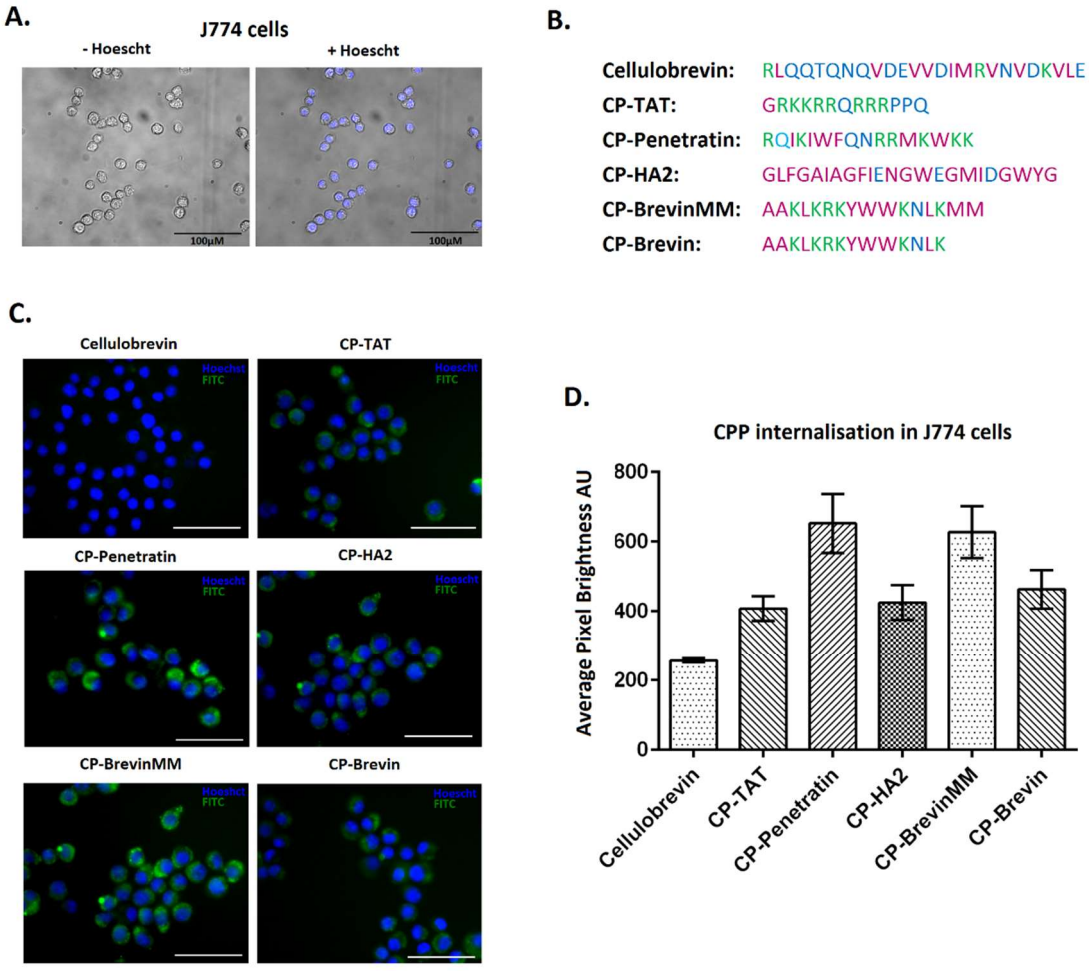

Figure 3.2 - Identification of usable Cell Penetrating Peptides

A) Showing J774.2 cells stained with and without Hoechst, image taken at x40 objective.. B) Amino acid structures of the peptides which were attached to FITC. Green=cationic amino acid, blue=polar/hydrophilic amino acid, pink=non-polar/hydrophobic amino acid. C) Live cell imaging after 2 hours in 500 nM FITC-peptide samples green=FITC-peptide (400 ms), blue= Hoechst (20 ms). Scale bars represent 100 µM, image taken at x40 objective. D) Quantification of the fluorescent intensity of FITC attached peptides using image J (n=2, N=2).

J774.2 macrophage cells were incubated with the 500 nM (approx. 1µg/ml) FITC-peptides for 2 hours to allow internalisation before the cells were washed, incubated with Hoechst for 10 minutes then immediately imaged. Images of each well were taken and the cells were drawn around the raw images in Image J to acquire the average pixel intensity for quantification. Figure 3.2:C-D shows that CP-Penetratin and CP-BrevinMM were the most efficient at internalising into J774.2 cells. It also showed that CP-BrevinMM was taken up more than CP-Brevin, indicating that the hydrophobic C-terminus influenced uptake. Figure 3.1:B shows that both CP-Penetratin and CP-BrevinMM had around 40% of their amino acids as positive (green) mixed with numerous hydrophobic (purple) and other hydrophilic (blue) residues. This combination of cationic and amphipathic sequencing may be the reason for their successful internalisation. Because there appeared to be the most FITC present in the cells, it was decided that CP-Penetratin and CP-BrevinMM were to be synthesised with a pyridyl disulphide domain at either the N or C terminus.

3.2.3 Pyridyldithio-peptides conjugate to the cysteine residues on enzymes.

The two selected CPPs were synthesised externally with pyridyl disulphide domains on either the N or C terminus to establish whether they could bind to the free cysteines on proteins (fig. 3.3:A). When ricinLC was incubated with excess pyridyldithio-CPPenetratin (thio-CPPenetratin) and loaded with SDS into an SDS-PAGE gel there was complete shift in the protein band, even at only 15 minutes incubation (fig 3.3:B). This strongly indicates that all of the ricinLC managed to successfully conjugate to the thio-CPPenetratin, and was shown to be the case in 10% DMSO in water, buffer A and buffer A with 0.4% Octyl β-D-glucopyranoside (OG), a non-ionic surfactant (fig. 3.3:C). It should be noted that as well as a large primary band where ricinLC conjugated to thio-CPPenetratin, a small secondary band formed above the main band. This is because the ricinLC has 2 free cysteines (fig. 3.1:C), therefore a small proportion of the protein has managed to bind thio-CPPenetratin to both the free SH groups. The formation of the second band does not noticeably increase on further incubation (fig. 3.3:B). It is likely that one of the cysteines is more internal than the other in the ricinLC structure, hence decreasing the chance that thio-CPPenetratin will bind. On the other hand, figure 3.3C shows when the enzyme BLF1 was incubated with thio-CPPenetratin in the same environments, there was no conjugation noted despite the 1 cysteine residue in the amino acid chain. It was hypothesised that this was because the cysteine was within the internal structure, therefore BLF1 was boiled for 3 minutes at 95˚C

with SDS to disrupt the structure before incubating with thio-CPPenetratin. Figure 3.3:D shows that after boiling, there is approximately 50% conjugation between BLF and thio-CPPenetratin, indicating that the hypothesis was correct; this makes sense as BLF1 is the only enzyme tested which does not endogenously associate with other domains.

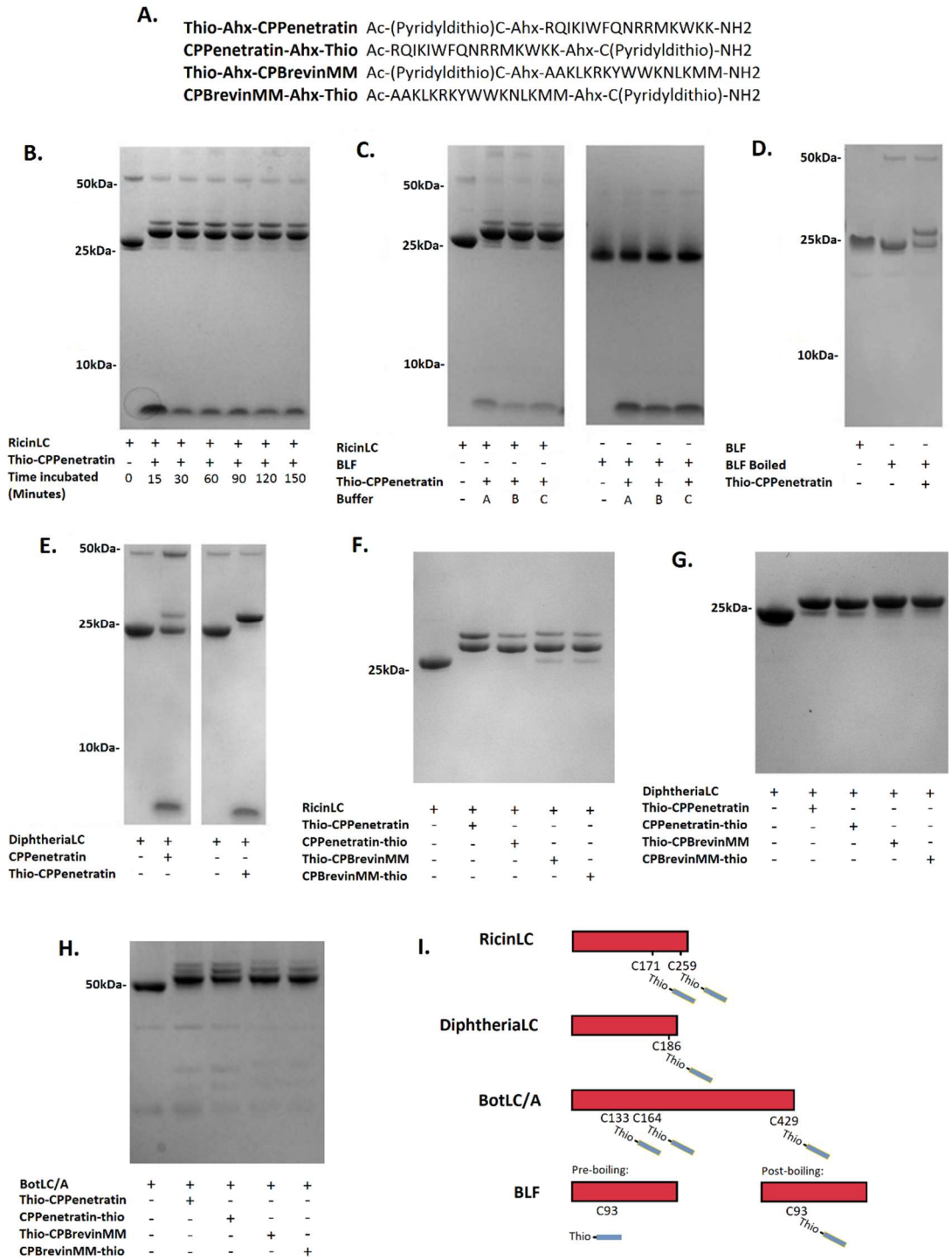

Figure 3.3 - Cysteine groups are needed for pyridyldithio binding

A) The amino acid sequence of CP-Penetratin and CP-BrevinMM with pyridyldithio domains. B) SDS-PAGE looking at the how incubation time influences disulphide bond formation; ricinLC was incubated with thio-CPPenetratin at a variety of time points. C) SDS-PAGE comparing the pyridyldithio conjugation between ricinLC and BLF. This was done at 2 hours incubation at room temperature where the peptide had been diluted in a variety of buffers before incubation. Buffers: A- 10% DMSO in water. B- Buffer A. C- Buffer A + OG 0.4%. D) SDS-PAGE showing BLF boiled at 95 ˚C incubated with thio-peptide enabling it to form 50% conjugation. E) SDS-PAGE showing that both the cysteine and the pyridyldithio group are needed to form an efficient bond, however small amounts of non-specific binding occur. F,G and H) SDS-PAGE showing ricinLC, diphtheriaLC and botulinumLC/A incubated with thio-peptides and peptide-thios to determine whether the orientation of the pyridyldithio domain influenced binding, these samples were incubated at 95 ˚C for 3 minutes prior to gel loading. I) Schematic summarising findings of the figure: The light chains of ricin, diphtheria and botulinum A from figure 3.1 were able to have all their cysteine residue bound to thio-peptides with varying efficiency. BLF however did not find to any thio-peptide conjugation unless it was first boiled to denature the protein structure. Red: protein LCs. Blue: thio-peptides.

DiphtheriaLC is shown in figure 3.3:E to also conjugate to thio-CPPenetratin, forming 1 band on the SDS-PAGE gel owing to its 1 free cysteine. When CP-Penetratin with no pyridyldithio group was incubated with diphtheriaLC there was a small amount of non-specific binding, which is unsurprising given the reactive nature of cysteines; however, there is a clear difference between conjugations of diphtheriaLC to the -thio and non-thio peptides.

Figures 3.3:F-H show that there was no difference in conjugation when the pyridyldithio domain was attached to the N or C terminus of either CP-Penetratin or CP-BrevinMM with ricinLC, diphtheriaLC or botulinumLC/A. BotulinumLC/A was also able to form multiple bands, with up to 3 bands forming where the 3 free cysteine residues; however, like ricinLC, only one of the cysteine residues was able to efficiently conjugate. The size of the protein did not appear to influence the efficiency of conjugation. It should be noted that some

dimerisation of the enzymes was visible over time due to the reactivity of the SH groups, however when stored at -80°C and with minimisation of freeze-thaw cycles, a monomeric stock was sustained. There was no dimerisation within the pyridyldithio-attached stocks. Together, the data here clearly shows that cysteines can bind efficiently to pyridyldithio-peptides (fig. 3.3:I); moreover, that the cysteines on the proteins will bind to the pyridyldithio-peptides preferentially rather than homodimerising.

3.2.4 The length of peptide-thio potentially influences binding efficiency

A variety of peptide-thio samples of different sizes were accumulated to determine whether the length of the peptide influences the binding efficiency. Because of the nature of the synthesis, 45 amino acids was the maximum number of peptides used as each amino acid was added in separate reactions, therefore increased amino acid size lead to increased cost and potential decrease in quality. Figure 3.4:A shows the amino acid sequence of the CPPs, ligands and peptides which had pyridyl disulphide bound to them.

The results in figure 3.4:B shows that after 1 hour incubation there was full binding of the smaller peptides, however syntaxin45-thio did not bind as efficiently. Then the same samples spent 24 hours at 4 ˚C and there was an increase in the amount of syntaxin45-thio conjugated to ricinLC. It is unclear whether this is because of the increased length of the peptide or because of the quality of the peptide sample, which may have been hindered due to the size of the peptide. Alternatively, the reason for differences in binding may have been due to the different amino acid composition of the peptides, each with different charges and isoelectric points, meaning that the interactions between ricinLC and each peptide would have been different and could potentially influence the efficiency of conjugation. Whilst inconclusive, length or peptide charge may be factors which need to be considered when attempting to conjugate peptides. It is noted that there is a difference of only 4 amino acids between the length of CRH and syntaxin45, suggesting that potentially protein charge or quality of stock may be the more influential factor than length, but that by 24 hours at 4˚C there was little discernible difference.

A.

Peptide	No. of amino acids	Sequence
Dermo-Ahx-Thio:	7	YaFGYPS-Ahx-C(Pyridyldithio)-NH2
SubstanceP-Ahx-Thio:	11	RPKPQQFFGLM-Ahx-C(Pyridyldithio)-NH2
CPPenetratin-Ahx-Thio:	16	Ac-RQIKIWFQNRRMKWKK-Ahx-C(Pyridyldithio)-NH2
VIP-Ahx-Thio:	28	HSDAVFTDNYTRLRKQMAVKKYLNSILN-Ahx-C(Pyridyldithio)-NH2
Thio-Ahx-CRH:	41	Ac-C(Pyridyldithio)-Ahx-SEEPPISLDLTFHL LREVLEMARAEQLAQQAHSNRKLMEII-NH2
Syntaxin45-Ahx-Thio:	45	Ac-EIIKLENSIRELHDMFMDMAMLVESQGE MIDRIEYNVEHAVDYVE-Ahx-C(Pyridyldithio)-NH2

B.

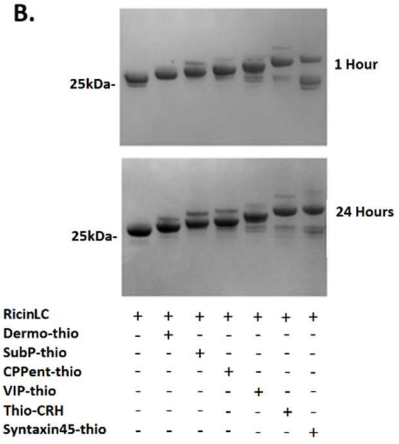

Figure 3.4 - Peptide length potentially influences binding efficiency

A) Peptides of different amino acid lengths were synthesised with the pyridyl disulphide group attached (-thio). B) SDS-PAGEs showing conjugation of differing length thio-peptides at 1 hour and 24 hours, showing increase of binding at 24 hours of the largest peptide syntaxin45-Ahx-Thio (N=2).

3.2.5 The disulphide conjugation between peptide-thio and protein is stable at all tested physiological pHs, and does not influence the catalytic activity of botulinumLC/A

The stability of the disulphide bond formed through pyridyl disulphide binding to cysteines was measured through monitoring breakdown of the conjugation at a variety of physiological pHs for 3 hours shaking at 37 ˚C. Through SDS-PAGE it was shown that at none of the conditions tested was there any observable breakdown of conjugation throughout the time interval (fig. 3.5:A).

Additionally, it was important to establish whether the conjugation of small peptides to proteins influenced the function of the enzymes themselves. Botulinum A endogenously cleaves SNAP25 and this can be mimicked by botulinumLC/A *in vitro* through incubation with SNAP25 (Vaidyanathan et al. 1999). Because only 9 amino acids are cleaved off SNAP25 by botulinumLC/A there is little size difference between the full length protein and the cleaved version, however this cleavage can be seen by running on SDS-PAGE for longer to sufficiently separate the cleaved band from the uncleaved band. BotulinumLC/A either

on its own or previously incubated with CPPenetratin-thio was added at particular concentrations to 0.5 mg native SNAP25 and the relative proportion of SNAP25 cleavage was observed. Figure 3.5:B shows that there was no difference in the amount of SNAP25 cleavage at any of the concentrations tested, indicating that the binding of small peptides to the enzyme via the cysteine has no influence on enzyme efficiency.

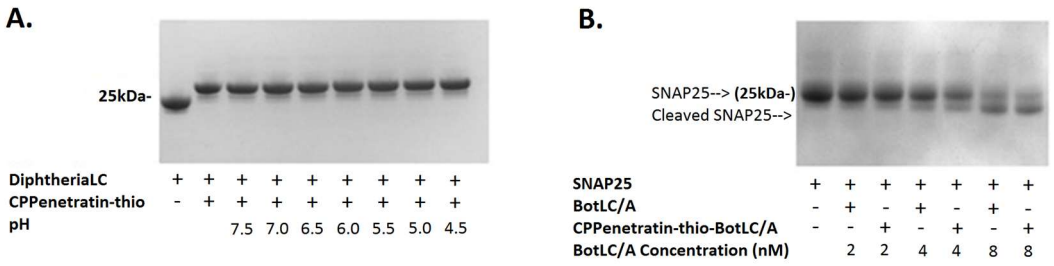

Figure 3.5 - The disulphide bond formed between cysteines and pyridyl disulphide group is stable at physiological pHs and does not influence catalytic activity

A) SDS-PAGE gel showing that there was no breakdown of the disulphide bond at a variety of physiological pHs over 3 hours at 37˚C (N=2). B) The catalytic function of bound vs unbound botulinumLC/A was tested through incubating with SNAP25 for 1 hour at RT (N=2).

3.2.6 A cysteine-rich domain can be recombinantly fused to proteins without endogenous cysteine groups to conjugate pyridyldithio-peptides

There are numerous proteins which potentially have useful therapeutic or experimental benefit that do not have cysteines. For instance, in order to further determine stability of peptide-protein conjugations, such as in rat plasma or cell lysates, a fluorescent protein or sequence that could be picked up by western blot would have to be used. MCherry protein is similar in size to both ricinLC and diphtheriaLC, it is fluorescent on SDS-PAGE gels as well as can be used as a protein for imaging in cells, so would be useful to be able to attach small peptides to in order to see the effects particular peptides have on delivery. However, mCherry does not have any cysteines in its amino acid structure. It was therefore hypothesised that a mCherry could me made with cysteines by cloning a cysteine rich sequence into the mCherry plasmid and expressing it to form a mCherry that would be able

to bind to pyridyldithio-peptides. Wild type (WT) SNAP25B has a cysteine rich domain between amino acids 84 and 92 (Oyler et al. 1989). Through restriction digest, the sequence for mCherry was inserted into a pGEX plasmid containing the SNAP25 cysteine rich domain (S25-CRD) (fig. 3.6:A). This was then transformed into bacteria, mini-prepped and expressed as mCherry-S25CRD (fig. 3.6:B-C). It was shown in figure 3.6:D that the expressed mCherry-S25CRD was able to conjugate to CPPenetratin-thio whereas the mCherry without the free cysteines was not; thereby creating a useful tool for further investigating modification of proteins and how peptide binding influences their behaviour.

3.2.7 Disulphide bridges formed between pyridyl disulphide groups and cysteine residues are stable in rat plasma, but break apart in cell lysates.

As previously mentioned, drugs need to remain stable in a variety of physiological environments such as the blood stream. The disulphide bond has been reported to remain stable in the blood, but it is reduced intracellularly by reducing proteins such as Gamma-interferon-inducible lysosomal thiol reductase and glutathione reductase (Arunachalam et al. 2000; Patil et al. 2015). Therefore, it is important to determine the stability of the constructs synthesised both in rat plasma and in the cell lysates, now possible using the previously constructed mCherry-S25CRD.

To determine whether the pyridyldithio bond was stable in physiological conditions such as plasma or cell lysates it was first important to acquire the cell lysates. Cells are often lysed through a combination of triton x-100 and benzonase nuclease, however it is important to also check that the disulphide conjugation is stable in a sample containing both these reagents. Harvested Neuro2A neuroblastoma cells ($2x10^6$) were incubated for half an hour at room temperature with 1mL either buffer A or buffer A containing 0.2% triton x-100 + 0.1% benzonase nuclease (Merck 2017), the samples were then centrifuged for 5 minutes at 5000 rpm and the supernatant removed and run on a western blot with β-III Tubulin antibody. The Western blot shows that β-III Tubulin was released when incubated with triton x-100 and benzonase nuclease, therefore concluding that this was a sufficient method of cell lysis (fig. 3.7:A). To ensure that the pyridyldithio conjugation is stable in lysis buffer, ricinLC-thio-CPPenetratin was incubated in either 0.2% triton x-100, 0.1% benzonase nuclease or both for two hours before running on SDS-PAGE gel. Figure 3.7:B shows that there was no observable breakdown in the conjugation in these conditions.

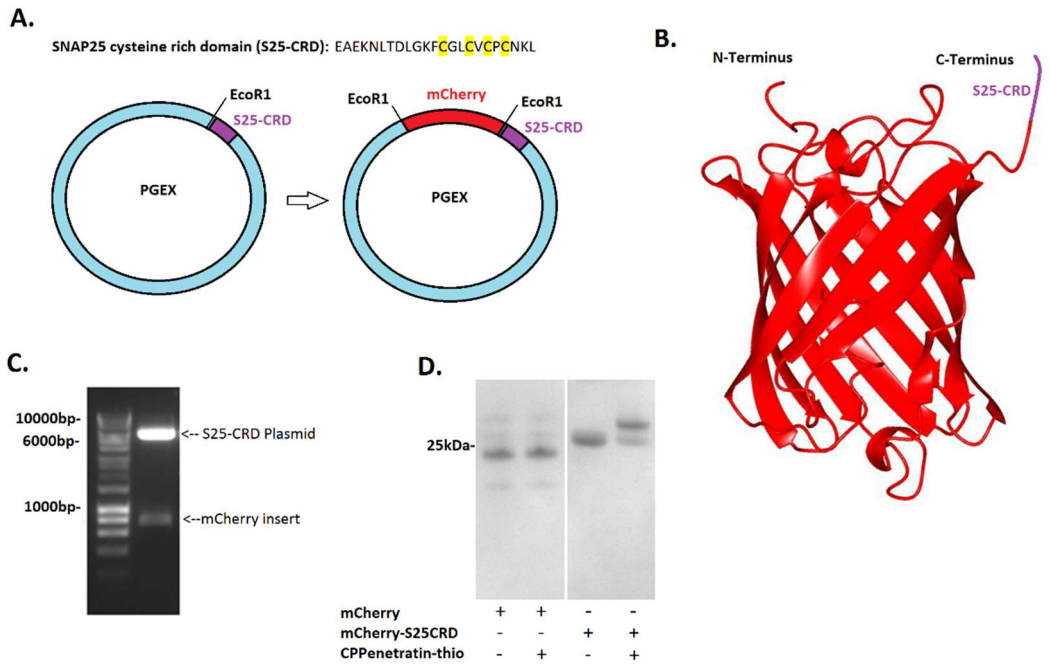

Figure 3.6 - A cysteine rich domain from SNAP25 can be attached to non-cysteine containing proteins so they can be further modified with thio-peptides

A) Schematic showing the insertion of mCherry into a pGEX plasmid containing the sequence for the cysteine rich domain of SNAP25. B) Diagram showing S25-CRD sequence recombinant fusion to the C-terminus of mCherry, forming mCherry-S25CRD. C) UV luminescent image of DNA plasmid after mini-prep and further digestion by EcoR1 showing successful insertion of mCherry insert. D) SDS-PAGE showing the binding of CPPenetratin-thio to mCherry and mCherry-S25CRD after 1 hour incubation (N=2). PDB ID: 2H5Q. S25-CRD was hand drawn (McNicholas et al. 2011; Berman et al. 2000)

Rat blood was taken immediately after the culling of untreated male rats (see methods) and immediately centrifuged for 5 minutes at 5000 rpm. The supernatant was then diluted 1:5 in buffer A before running on a SDS-PAGE gel with the extracted lysates to determine relative protein concentrations (fig. 3.7:C)

MCherry-S25CRD was incubated either with or without CPPenetratin-thio in buffer A, rat plasma or Neuro2A cell line lysates (fig 3.7:D). Whilst the unconjugated mCherry-S25CRD at 0 hours could be seen at approximately 25 kDa, after 3 days at 37 ˚C in buffer A it had

completely dimerised to around 50 kDa. On the other hand, the conjugated mCherry-S25CRD after 3 days at 37 ˚C in buffer A remained at around 25 kDa, this shows therefore that it is only when the disulphide bond between the pyridyldithio peptide and the protein is reduced that the protein is free to dimerise. In rat plasma, the CPPenetratin-thio attached mCherry-S25CRD remained at approximately 25kDa with only little increase in the 50kDa band, indicating that the majority of CPPenetratin-thio was still bound, preventing it from dimerising. However, when combined with the cell lysates for 3 days, there was complete dimerisation, suggesting that the disulphide linker had been cleaved allowing the mCherry-S25CRD to dimerise. Together, this shows that the conjugation is relatively stable in rat plasma, however is cleaved within cells.

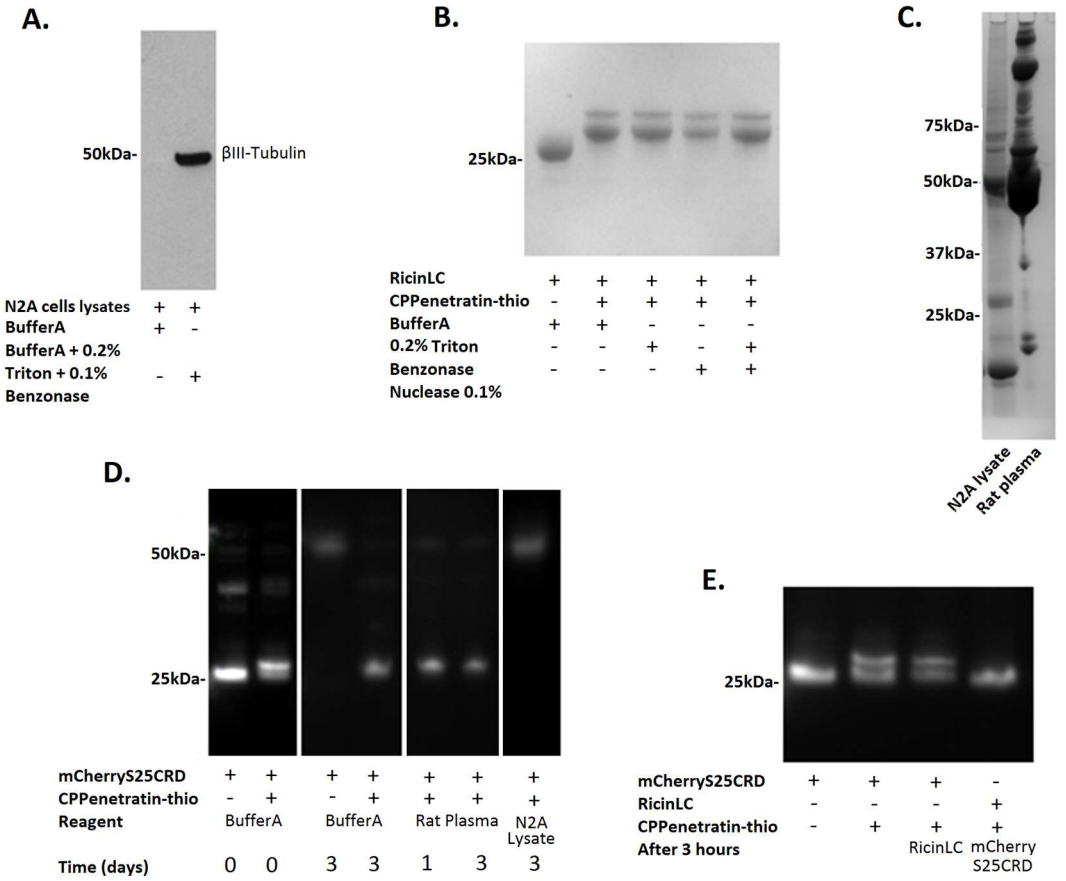

Figure 3.7 - Pyridyl disulphide conjugation is stable for 3 days in rat plasma but is broken down in cell lysates

A) Western blot showing 0.4% Triton + 0.1% Benzonase nuclease is sufficient for breaking open cells to release cell lysate. B) *SDS-PAGE showing ricinLC binding to CPPenetratin-thio and being stable after 3 hours incubation at RT with triton x-100 0.2% and benzonase nuclease 0.1%. C) SDS-PAGE showing lysates on from cells and rat plasma as a representation of the relative concentration of samples. D) UV trace of mCherry-S25CRD and the attachment of CPPenetratin-thio showing that stability of the pyridyldithio formed disulphide bond in rat plasma, cell line lysates and buffer A at 37 ˚C (N=2) E) UV trace showing mCherry-CRD conjugation; excess mCherry-S25CRD was bound to CPPenetratin-thio over 3 hours so only 50% was bound, when ricinLC was added and incubated for a further 3 hours there was no difference to the % mCherry-S25CRD which was conjugated. Additionally, mCherry-S25CRD for was added to CPPenetratin-thio-ricinLC and incubated for 3 hours; there was no noted conjugation of mCherry-S25CRD, indicating that existing bonds are not disrupted by excess SH groups (N=2).*

It is also possible to look at the nature of the bond through using mCherry-S25CRD. For instance, whether it falls apart and reforms or if it is constantly stable. In order to observe, this mCherry-S25CRD was incubated with enough CPPenetratin-thio to conjugate half; after 3 hours ricinLC was added yet there was no decrease in the amount of mCherry-S25CRD bound. Likewise, excess ricinLC was incubated with CPPenetratin-thio and after 3 hours mCherry-S25CRD was added; yet after another 3 hours there was no observable mCherry-S25CRD conjugation (fig. 3.7:E). This supports previous evidence that the disulphide bond formed between pyridyl disulphide groups and cysteines is stable.

3.2.8 Octyl β-D-glucopyranoside (OG) can expose unbound cysteines in within protein structures

As previously discussed, botulinum A exists in three subunits, the catalytic light chain, the translocation domain and the binding domain. Until this point only the catalytic ability and modification of the LC has been investigated; however, there have been studies which suggest that the translocation domain could potentially increase the cytosolic translocation of the light chain, so may improve cytosolic effect (Araye et al. 2016; Fischer

et al. 2008). Along with being a much larger protein at 100 kDa, the botulinum A light chain translocation domain (botLcTd/A) (amino acids: 1-872) has 5 cysteines, although two of them are conjugated to form the disulphide bridge which endogenously exists between the two subunits (fig. 3.8:A). Therefore, there are three cysteines remaining for potential thio-conjugation. Figure 3.8:B shows that when CRH-thio peptide was incubated with botLcTd/A there was little conjugation, however when Octyl β-D-glucopyranoside (OG) was introduced at a variety of concentrations there appeared to be an increase in conjugation, with 100% conjugation to at least 1 cysteine at 1.2% OG after 1 hour at RT.

Octyl β-D-glucopyranoside (OG) is a mild non-ionic surfactant which disrupts the hydrogen binding within the secondary protein structure without denaturing the proteins or affecting protein catalytic activity (Koley & Bard 2010; Morandat & El Kirat 2007); these disruptions decreases the integrity of the protein structure, potentially allowing thio-peptides to bind to the newly exposed cysteines. Thio-CRH was used as it is the largest quick binding thio-peptide in possession and would therefore give a greater difference in size if it conjugated. Conclusively, there were three bands for the three free cysteines. There was increased conjugation as the OG concentration increased, suggesting that OG influences the exposure of the cysteines in a concentration dependant manner. The most likely reason that botLC/A was able to conjugate without the assistance of the OG whereas botLcTd/A required OG could be because botLC/A endogenously binds to its heavy chain and therefore needs to have the cysteines available on the edge of the protein after post-translational modification. On the other hand, botLcTd/A does not endogenously conjugate to other domains via cysteines, and the reactive nature of cysteines means that it is far more stable to keep the unconjugated cysteines inside the post-translational structure. This is then altered by OG 'loosening' the structure of the proteins through disruption of hydrogen bonds to give access to the cysteines. Using OG to expose some of the internal structure is far more preferable to the boiling which was used in figure 3.3:D because through this method there is still the potential to have the same catalytic activity.

To further investigate the potential for S25-CRD to be attached to proteins, and whether botLcTd/A could bind to cysteines without the need for OG, botLcTd/A-S25CRD was made in the same way as mCherry-S25CRD was in figure 3.5 (fig. 3.8:C). Gel analysis of the restriction enzyme digested plasmid purified after mini-prep strongly indicates that botLcTd/A-S25CRD was successfully made (fig. 3.8:D). Additionally, after expression, both botLcTd/A and botLcTd/A-S25CRD were reduced with TCEP then run on SDS-PAGE gel,

which showed that the botLcTd/A-S25CRD had a larger translocation domain subunit than botLcTd/A (fig. 3.8:E). When incubated with thio-CRH only for 24 hours at 4 ˚C, approximately 50% of the botLcTd/A-CRD was conjugated (fig. 3.8:F). When the thio-CRH was incubated with botLcTd/A-S25CRD in the presence of OG there was a similar increase in the amount of conjugation; however it should be noted that 4 bands formed instead of 3.

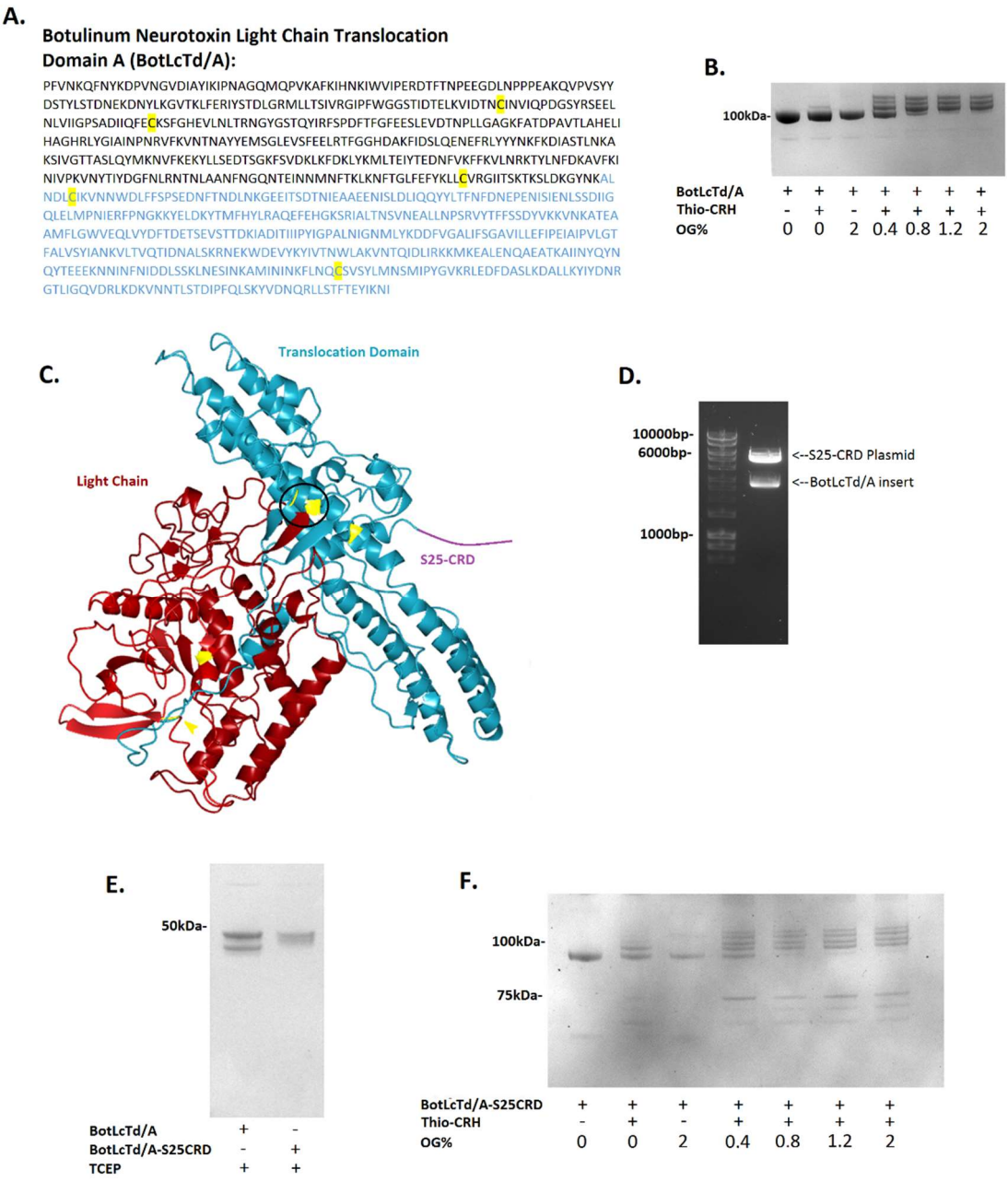

Figure 3.8 - Octyl β-D-glucopyranoside (OG) can expose cysteines within protein structures

A) Amino acid sequence of botulinum A light chain and translocation domain (botLcTd/A) with the cysteine residues highlighted. B) SDS-PAGE showing no conjugation between thio-CRH and botLcTd/A without OG but 100% botLcTd/A was conjugated to at least 1 thio-CRH peptide at 1.2% OG at 24 hours at 4˚C N=2. C) Schematic of the botLcTd/A with S25-CRD added which was made in the same way as mCherry-S25CRD, showing all 5 of the cysteines in the botLcTd/A structure (yellow) excluding those in the S25-CRD. Circled are the two cysteines which form a disulphide bridge between the LC and Td domains. D) UV illumination of plasmid samples run after mini-prep and digestion with SmaI and XbaI. E) Both botLcTd/A and botLcTd/A-S25CRD run on SDS-PAGE after reducing by TCEP, showing the different sizes of the reduced subunits. F) SDS-PAGE showing approximately 50% of botLcTd/A-S25CRD was conjugated to thio-CRH after 24 hours at 4 ˚C, whilst almost 100% of the botLcTd/A-S25CRD was conjugated to at least one thio-CRH at 0.8% OG (N=2). BotLcTd/A PDB ID: 3BTA, S25-CRD was hand drawn (McNicholas et al. 2011; Berman et al. 2000).

It can therefore be concluded that S25-CRD attachment is possible and can be used for the conjugation to thio-peptides, however in neither mCherry-S25CRD nor botLcTd/A-S25CRD was there 100% attachment, with botLcTd/A being around 50% and mCherry at about 75%. This difference in conjugation is probably due to a variety between the two proteins in how the added domain folded or reacted with the existing structure, but the S25-CRD is receptive to OG addition.

3.2.9 Proteins attached to SNARE helices could potentially be used to form multifunctioning complexes

Whilst cysteine rich domains can be fused to proteins to allow thio-peptide modification, it would be difficult to get the pyridyl disulphide group on proteins, as opposed to chemically synthesised peptides, for a protein-protein conjugation. This is because they are too big to be made reliably synthetically. Additionally there is the limitation with pyridyl disulphide conjugation where only two components can be brought together, but there is

a demand for methods which will allow more proteins to be brought together in a controlled ratio to form multidomain complexes. This requires a system where particular components can be used and react to form a homogenous sample of multidomain drug.

SNARE proteins are a family of proteins which are involved in the endogenous mechanisms surrounding vesicular transport. Four helices come together to form a supercoiled complex; There is 1 helix in synaptobrevin, 1 in syntaxin and 2 in SNAP25 (Sudhof & Rothman 2009). Because of the spontaneous and quasi-irreversible binding, it is possible to attach therapeutically relevant proteins to different SNARE proteins and then as the SNARE complex forms the individual proteins will be bought together in a controlled ratio, forming a multifunctioning complex (Darios et al. 2010; Arsenault et al. 2013). For example, figure 3.9:A shows how a SNARE forms normally, but then in figure 3.9:B botLcTd/A is recombinantly fused to SNAP25 and the ligand EGF is recombinantly attached to synaptobrevin. When incubated together with syntaxin45 they could theoretically form a complex which would combine the therapeutic potential of botLcTd/A with the receptors and cell internalisation potential of EGF.

Initially, it was vital to investigate the conditions needed for efficient SNARE complex formation. An alternative SNAP25 was used, SNAP25trunc, due to better protein expression than the wild-type version; all the cysteine domains in this version were substituted to remove potential unwanted thio-conjugation. In figure 3.9:C the helix domains of all three SNARE proteins, SNAP25trunc (aa.2-204), syntaxin45 (aa.1-45) and synaptobrevin2 (aa.2-94) were incubated together for 2 hours at RT with different concentrations of OG. Half of the sample was then boiled to break apart any SNARE complex that may have formed and this was then compared to the unboiled sample. It was found that in the absence of OG, SNARE components on their own formed little SNARE complex after 2 hours, however with increased OG% there was increased SNARE formation. At 0.4% OG all of the synaptobrevin was used up, whereas at lower concentrations there was still a proportion of protein left over from all of the visible components, indicating that there was still potential for further complex formation. It should be noted that syntaxin45 is small and was often run off the end of the gel in these experiments. It was also highlighted in this figure the importance of using correct ratios of individual proteins for SNARE complex formation, otherwise there is a lot of excess of any one particular protein. The ratio for adding protein had to be in mM rather than mg protein because of the different sizes of proteins, and in this instance 1 mM of one component

reacts with 1 mM of the other components independent of size. Figure 3.9:D showed that the SNARE complex formation reaction was fully complete after 1 hour at RT, as indicated by the absence of synaptobrevin at this time. From this data, unless specified all SNARE complexes will be made with the syntaxin45 (syx45), synaptobrevin (brevin) and SNAP25trunc used here for 1 hour in the presence of OG 0.4%.

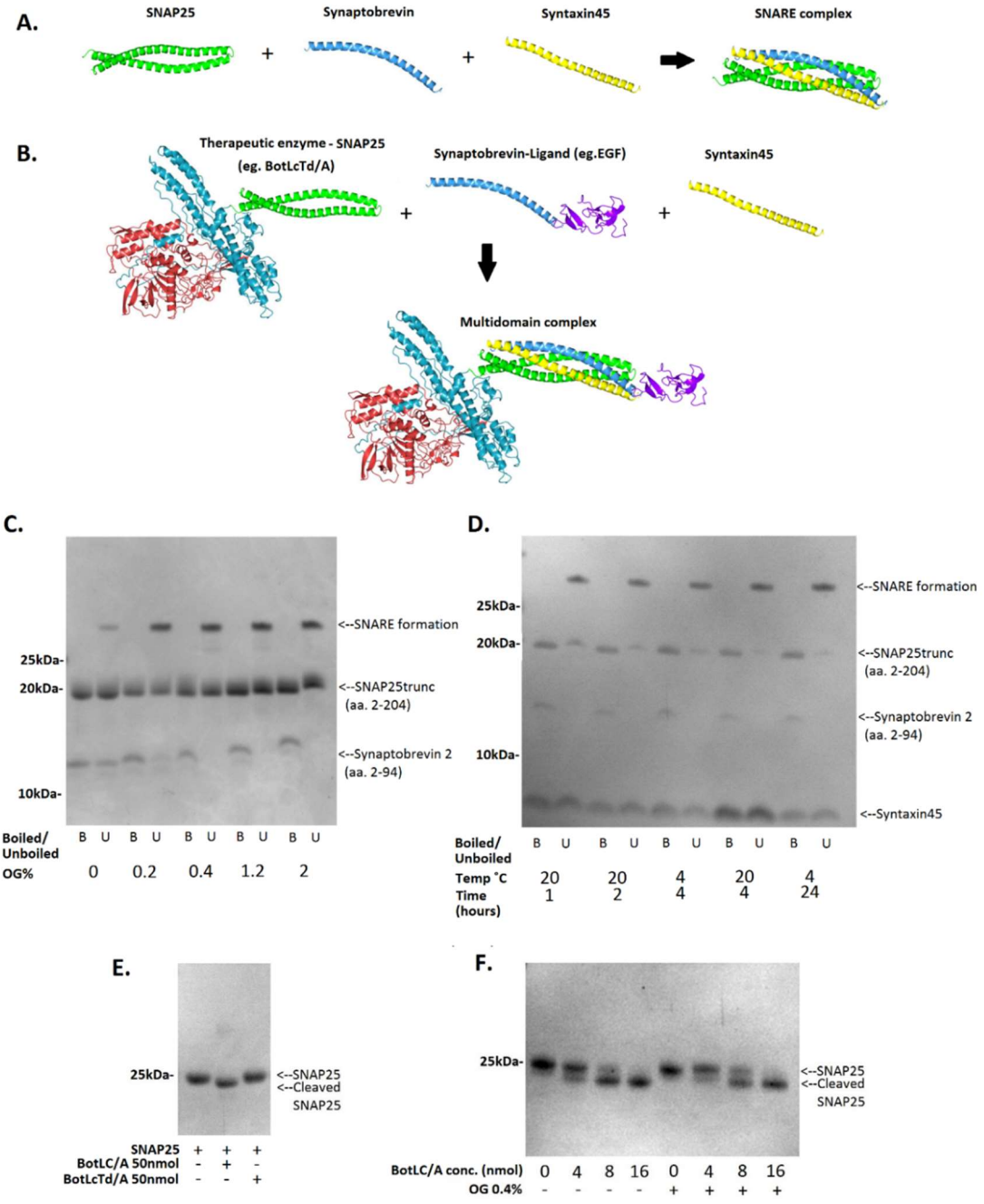

Figure 3.9 – Investigating SNARE complex formation

A) Schematic of SNARE complex being formed from individual SNARE proteins. B) Schematic of SNARE complex being formed from SNARE proteins which have been recombinantly fused to therapeutic proteins and targeting proteins. C) SDS-PAGE showing SNARE formation after 2 hours with various concentration of OG, showing complete SNARE formation at 0.4% OG (n=2). D) SDS-PAGE showing SNARE formation with 0.4% OG at a variety of timepoints, showing complete SNARE formation even at 1 hour at room temperature (N=2). E) SNAP25 after being incubated with botLC/A and LcTd/A for 30 minutes. F) SNAP25 after being incubated for 1hr at RT with botLC/A and botLC/A which had been pre-incubated with OG 0.4% for one hour, showing no observable difference in the cleavage (N=2). EGF PDB ID: 1JL9. BotLcTd/A PDB ID: 3BTA. PDB ID: 5W5D (McNicholas et al. 2011; Berman et al. 2000).

Because it was found that OG 0.4% was necessary for the efficient formation of SNARE complexes it was important to determine whether this OG addition would have any influence on the catalytic function of enzymes. Initially, this was to be investigated botLcTd/A, but it was shown that botLcTd/A did not have any catalytic effect on SNAP25 within 30 minutes of incubation, unlike botLC/A (fig. 3.9:E). This is either because the botLcTd/A which has been expressed is not functional, or more likely because the LC domain is unable to function if the Td is attached; this is also seen in diphtheria (Ariansen et al. 1993). Like when previously determining whether thio-conjugation influenced catalytic activity (fig. 3.5:B), a naked SNAP25 assay was used to investigate OG effects on catalytic activity. It was found that there was no noticeable difference between the cleavage of full length SNAP25 when incubated with botLC/A on its own or botLC/A which had been pre-incubated for 1 hour with 0.4% OG (fig. 3.9:F). This data is in agreement with previous studies showing that OG addition does not denature proteins, however direct catalytic activity had not been measured in these examples (Morandat & El Kirat 2007).

3.2.10 SNARE complexes are stable at a variety of physiological pHs, rat plasma and cell lysates.

It is important to determine whether SNAREs are stable at a range of physiological pHs to investigate their suitability as a drug platform. SNAREs were formed in buffer A for 1 hour before incubating at 37 ˚C in a variety of physiological pHs for 3 hours. There was no noticeable breakdown of the SNARE complex in any of the conditions tested (fig. 3.10:A). In order to further determine the stability of the SNAREs in physiological conditions, they were subjected to 3 day stability tests in rat plasma and lysates. Instead of using mCherry, this was done using full length SNAP25 and measuring breakdown through western blot with a SNAP25 antibody (αSNAP25). The SNAP25 containing proteins that were successfully expressed are shown in figure 3.10:B. Figure 3.10:C shows that αSNAP25 will bind to SNAP25 cleanly in Neuro2A and SH-SY5Y and cell lysates, but not J774.2 lysates owing to the lack thereof. Also, that the αSNAP25 will only bind to the full length SNAP25 and not the truncated version. Additionally, botulinumLcTd/A-SNAP25 (botLcTd/A-SNAP25) was able to be detected by αSNAP25 because it contains the full length sequence. When botLcTd/A-SNAP25 is reduced by TCEP it forms two bands, the botLC/A (50 kDa) and the remaining Td-SNAP25 (75 kDa); as expected, the western blot shows that the αSNAP25 antibody only binds to the Td-SNAP25 portion. Together, this shows that αSNAP25 is clean and does not exhibit non-specific binding.

Like figure 3.7:A, figure 3.10:D shows that SNARE complex stability is not influenced by the presence of 0.2% triton x-100 and 0.1% benzoase nuclease. Figure 3.10:E shows that after 3 days in buffer A there was no observable breakdown of the SNARE complex. In rat plasma, there was comparable amounts of SNARE to the buffer A samples at day 1, with minimal SNARE degradation between day 1 and 3. Additionally, there was no significant SNARE breakdown between 1 and 3 days in J774.2 cell lysate. This was expected as the breaking of SNARE complexes is done by the specialised ATPase NSF, which endogenously unfolds the SNARE complex in an ATP dependant reaction to their initial form; as there was no added ATP in the system there was no breakdown. Interestingly there appeared to be a decrease in the amount of SNAP25 after 3 days in rat plasma which was repeatable. This only happened in the rat plasma, so it could be possible that SNAP25 is binding to an alternative protein, or was denatured; nonetheless, there was no influence on the amount of formed SNARE. This data therefore shows that there is good stability of SNAREs, however this data may not be representative of what happens inside cells due to the SNARE breaking down being an ATP dependant reaction.

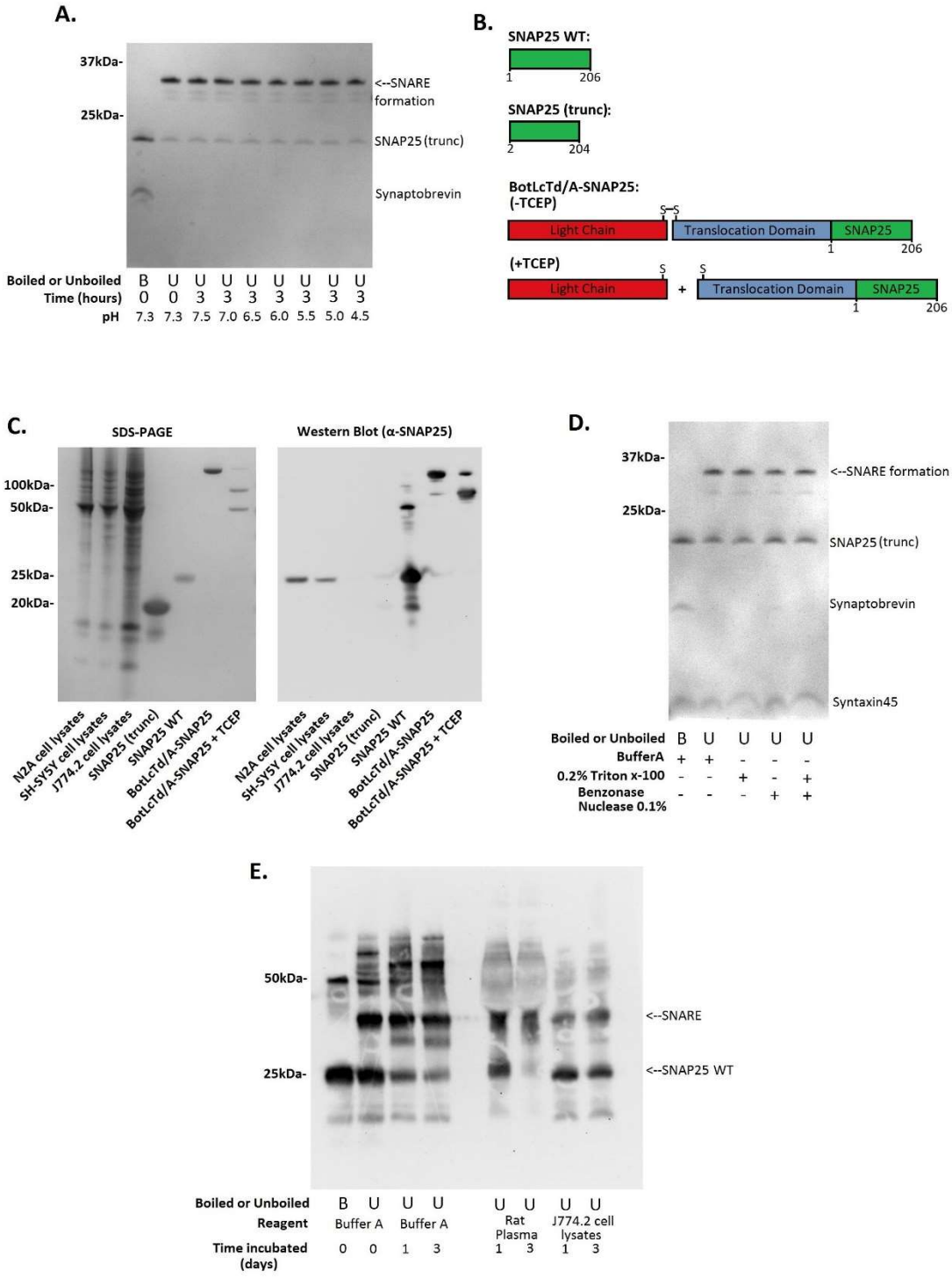

Figure 3.10 - SNARE complexes are stable at a variety of physiological pHs, rat plasma and cell lysates

A) SNARE complexes were formed over 1 hour before incubating for a further 3 hours in a variety of biological pHs; there was no noticeable breakdown of the SNARE complex within this time (N=2). B) Schematic of the 3 SNAP25 containing proteins expressed, and the reduction of botLcTd/A-SNAP25 after incubation with TCEP. C) SDS-PAGE gel and an

accompanying western blot of the same gel with αSNAP25 antibody, showing that the antibody is specific, also that J774.2 cell lysate does not have SNAP25. D) Control SDS-PAGE gel showing SNARE stability in buffers containing 0.2% triton x-100 and benzonase nuclease 0.1%. E) Western blot showing SNARE stability in buffer A, rat plasma and J774.2 cell lysates over 3 days at 37˚C (N=2).

3.2.11 Proteins can be attached to SNARE complexes through pyridyldithio or recombinant conjugation.

The purpose of these investigations into the formation and stability of the SNARE complex has been to determine the suitability of the SNARE complex for a potential multidomain drug platform. Thus far it appears that there is adequate efficiency in the assembly and that they are stable enough in various pHs and rat plasma for SNARE stapling to be utilised as a conjugation method. Therefore, it now can be determined whether proteins or peptides can be bound to the SNARE complex.

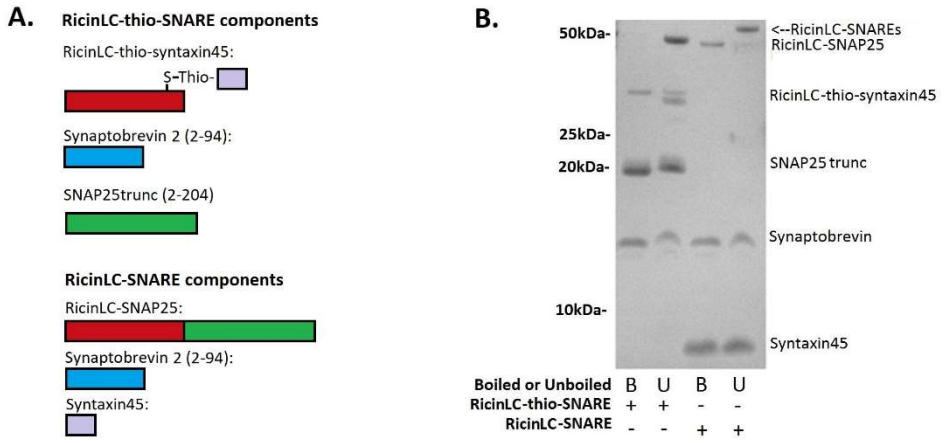

Figure 3.11 – Proteins can be attached to the SNARE complex through recombinant and pyridyldithio mediated conjugation

A) Schematic of protein components needed to form ricinLC-thio-SNARE and ricinLC-SNARE. B) SDS-PAGE showing formation of ricinLC-SNAREs where ricinLC is attached either via disulphide binding to syntaxin45-thio or recombinant expression to SNAP25 (N=2).

RicinLC-thio-syntaxin45 was formed by adding syntaxin45-thio in excess to ricinLC then filtering excess thio-syntaxin45. The resulting sample was then incubated with synaptobrevin (brevin) and SNAP25 and OG 0.4% for 1 hour to form ricinLC-thio-SNARE. This was then compared with ricinLC-SNAP25 (recombinantly fused), syntaxin45 and brevin formed complex, ricinLC-SNARE (fig. 3.11:A). The SDS-PAGE shows that both ricinLC-thio-SNARE and ricinLC-SNARE formed well. One of the issues however with the ricinLC-thio-SNARE was that a small band can be seen under the ricinLC-thio-syntaxin45 band which disappears when boiled; this indicates that not all of the syntaxin45-thio was filtered properly and that it is forming complexes without the ricinLC attached. Also, in the ricinLC-thio-SNARE one can see that after 1 hour there are still remaining components of all three of the SNARE proteins, whereas for ricinLC-SNARE the ricinLC-SNAP25 was completely used up, indicating that the reaction had finished (fig. 3.11:B). This indicates that the ricinLC could be bound to syntaxin45-thio in a way which potentially obscures the reaction site, giving either a slower reaction or making a proportion of the protein no longer functional. Additionally, there appears to be issues with filtering the ricinLC-thio-syntaxin45 from excess syntaxin45-thio which could be problematic if there is competition in formation. Either way it can be seen that attaching proteins to SNAREs recombinantly is more efficient process than doing it through thio-reactions because there are fewer components to be added. This demonstrates that proteins can be conjugated to SNARE proteins and the complex is still able to link together. Further investigations will determine whether more domains can be added and which domains are best for targeting neuroblastoma cells.

3.3 Discussion

Conjugation between therapeutic and targeting domains is an important consideration within drug design; however, problems have arisen when conjugation methods are not adequate for long term stability in plasma, leading to drug degradation and an increase in side effects. This chapter has identified two usable methods for either the modification of proteins through peptides or attaching multiple proteins into large complexes. The data here has investigated the optimum conjugation conditions and the stability in a variety of conditions. Both pyridyl disulphide and SNARE formation methods were successfully

formed and shown to be stable in the conditions tested, however have yet to be introduced to cells to determine their effectiveness at delivering therapeutic enzymes to targeted cells.

Disulphide bonds have long been recognised as a stable method of conjugation as it is one of the main ways which various endogenous proteins stabilise their structure (Braakman & Hebert 2013; Srinivasarao et al. 2015). It has been shown in these experiments, as well as wider literature, that the bond is stable in plasma, but that there are enzymes in the cytosol which are able to reduce them after endosomal escape such as glutathione reductase (Koriazova & Montal 2009; Patil et al. 2015). These properties make disulphide bonds ideal for drug construction, where the targeting domain of the therapeutic can be cleaved from the drug domain in order for it to function efficiently, but without it breaking apart in the plasma leading to side effects. Endogenously, synthesised proteins form the disulphide bonds within their structure before the proteins are cleaved into separate subunits, therefore there is control in how they are formed (Patil et al. 2015). However, controlled disulphide binding between two separate proteins is difficult as the chances of homodimerisation is equal to that of heterodimerisation, making the reaction inefficient. Therefore, it has been proposed in this chapter that pyridyl disulphide group is an efficient yet underutilised method to ensure efficient heterodimerisation in conjugated protein samples as the reaction between pyridyldithio and cysteine residues appeared to be preferential to cysteine-cysteine reactions whilst there was no dimerisation in between pyridyldithio groups.

Provided that there is an available cysteine, up to 100% binding efficiency was detected from 15 minutes between proteins and pyridyldithio-peptides. The attachment of a recombinant cysteine rich domain to proteins was successful through plasmid manipulation, but unfortunately, neither of the S25-CRD attached proteins were able to bind more than 75% over 1 hour. This could be because of interactions between the S25-CRD domain and the protein or that the tertiary structure of the overall protein meant that the S25-CRD was internally folded. Although there are 4 cysteines on the S25-CRD, there was only 1 band showing conjugation in both examples; this is most likely to be because the cysteines are within close proximity to each other and therefore there was not space for more than one to bind. However, another reason may be that they have internally conjugated or the protein folding does not allow binding to other cysteines. Significantly, when OG was added there was still only an addition of 1 band which does suggest that the

lack of more bands is not because of protein folding. It may be that smaller peptides or chemicals would be able to conjugate to more than one of the 4 cysteines. Both the BotulinumLcTd-S25CRD and mCherry-S25CRD showed that cysteines can be added to proteins and that they can be used to bind, however it may be worth considering using alternative cysteine rich domains in the hope that a better binding efficiency can be achieved.

It has also been investigated here whether existing cysteines in a protein which are buried within the structure can be accessed through OG. The data shows there is increased binding in the presence of OG in most proteins tested and that when OG is added there is no influence on the function. However, only botulinumLC/A was tested and it could be that OG may influence function of other enzymes at particular concentrations, but this has not been investigated. It should be noted that OG mediated binding was not always successful, as when BLF was tested with OG there was no conjugation of thio-peptides despite the internal cysteine being bound through boiling in figure 3.3:D. Another significant matter with using OG is its toxicity in cells; therefore, to test OG containing complexes in cells it will be necessary to highly dilute the samples and test the cell threshold for OG tolerance. Whilst it was possible to modify existing cysteines of some proteins using OG, whether the modifications are functional have not yet been tested. There is the hypothesis that after the peptide has bound and the OG been diluted for adding onto cells, the tertiary structure recovers and this may mean that the modification is internalised and therefore would not be functional as a targeting peptide. This is something which has yet to be determined and will be addressed in future chapters.

Once the disulphide bridge has formed, the data showed that addition of alternative SH groups does not interfere with the existing binding, therefore purification to a homogeneous product would result from the addition of beads or other large proteins to mop up excess pyridyldithio-peptides. Encouragingly, there was no degradation of the disulphide bridge at pHs between 4.5 and 7.5 and little noticeable cleavage after 3 days at 37˚C in rat plasma, yet the bond was cleaved in cell lysates. Taken together, this strongly indicates that they would be stable in the blood stream and only break down once inside the cell, most likely through lysosomal enzymes. This finding however does bring into question why the protein dimerised in cell lysates if the disulphide bonds were reduced, as the dimerisation would have been because of cysteine residues forming homodimers though disulphide bonds. This should not have been possible if intracellular enzymes were

reducing all disulphide bonds. Reasons for this could be because over the three days the disulphide bond was cleaved but then the reducing enzyme responsible for this then denatured, allowing disulphide bridges to re-form. It is also possible that the thio-peptides were broken down or denatured so in these conditions there was preferable binding of the homodimer. Had an analysis been taken after 1 day in cell lysates this speculation would be more conclusive.

Pyridyl disulphide conjugation is most often used only in reactions with SPDP. Because of the succinimidyl group on the SPDP, this linker is attached non-uniformly to the numerous and sporadic lysine residues which are often present in proteins and peptides. It is therefore important to consider the use of peptides which have been synthesised and fused with pyridyl disulphide groups without the rest of the SPDP linker. It should be noted that there are numerous publications which utilise the pyridyl disulphide group as a method of conjugation, however the method is not a focus and the techniques vary (Stuchbury et al. 1975; Van Der Vlies et al. 2010). Therefore, this section aimed to solely focus on the efficiency of pyridyldithio conjugation, its potential applications and stability. An unfortunate consequence of using pyridyl disulphide without SPDP is that it can be only attached to specially manufactured peptides whereas the point of SPDP is that it can utilise the readily available lysines on proteins. Therefore, whilst a protein that needs to be conjugated can be modified with cysteines if required, the modification with the pyridyl disulphide needs to be a short peptide, polymer or chemical.

The other conjugation method in this chapter which was investigated was SNARE stapling. Like pyridyldithio conjugation, OG was needed to efficiently assemble the helices together into the complex; therefore, for these samples there also needs to be concerns addressed about potential OG-related toxicity. Endogenously formed SNARE complexes are regulated and assisted by a variety of proteins, such as SM proteins, which direct their fusogenic action and ensure specificity when docking (Sudhof & Rothman 2009). This however was unsuitable for the system here, but OG removes the regulation and specificity allowing the SNARE complexes to form completely and efficiently.

As previously discussed, SNARE complexes are quasi-irreversible because of the high energy input required to disassemble them. It is facilitated mostly by N-ethylmaleimide-sensitive factor (NSF), which is an ATPase and dissociates the SNARE complex through the energy released by ATP hydrolysis (Sollner et al. 1993). It was therefore unsurprising to find that the SNARE complex is stable for 3 days in rat plasma. It was shown that unlike the

thio-binding there was no observable breakdown of the SNARE complex in lysates, however the reaction for breaking down the complex is ATP dependant, so without the addition of ATP it would not be expected. The fact that SNARE complexes require particular enzymes to dissociate them is potentially interesting because NSF only exists in the cytosol. So where the thio-constructs will break down in endosomes, there is the possibility for the complex to be stable in the endosomes and only break down in the cytosol, which could be a useful feature. It should be mentioned however that just because the SNARE complex itself is stable does not mean that attached therapeutic domains are definitely stable. *In vivo* the domains will be exposed to plasma and potential immunogenic reaction and therefore may be subjected to various protein eroding forces which the SNARE complex is more resistant to.

It has been demonstrated here that as yet only ricinLC has been attached to the SNARE complex and there as only been the attachment of one domain. Before attaching other domains it is useful to determine which targeting proteins could be best utilised for internalising into neuroblastoma, which will be addressed in another chapter. It has yet to be seen whether there will be success in adding more than one component to the SNARE complex, however there are published examples of two domains being successfully added (Ferrari et al. 2011; Arsenault et al. 2013). Within this project it is eventually hoped that all three SNARE proteins can be conjugated to different domains and still link together into a complex. There is a concern regarding the method of domain attachment to the SNARE complex; whilst ricinLC was conjugated to the SNARE both recombinantly and through pyridyldithio binding, the syntaxin45-thio-ricinLC did not fully react with the other SNARE peptides, whereas this was not the case with the recombinant sample. It is not known how recombinant attachment to the toxins may influence the effects of the protein function. For instance, it has been shown that diphtheriaLC is only functional once cleaved from its heavy chain (Ariansen et al. 1993), and similar results were seen here where botulinumLcTd/A was not able to cleave SNAP25 but botulinumLC/A was in a 30 minute reaction. Therefore if there is a possibility that with the recombinant addition of a SNARE protein the diphtheriaLC would no longer function. On the other hand, it should be noted that the use of ricinLC-SNAP25 means that only one reaction needs to take place, as syntaxin45-thio-ricinLC needs to be formed separately.

Lack of purity of the SNARE complexes is a potential issue as it is difficult to purify the SNARE-linked sample in the small quantities which are being made. Whilst not an issue at

this stage, un-stapled proteins later on may interfere with the fully linked product when incubated with cells. This reiterates the importance of forming the complexes through the correct molar ratio of each individual component, something which needs to be improved before cell dosing. Whilst having three components coming together opens up a new dimension of potential for protein conjugation, it adds another degree of complexity in the synthesis of the linked complexes. However, this complexity will hopefully prove to be overshadowed by the benefits of a unique system where numerous proteins can be linked together in a mix-and-match system using complementary SNARE proteins.

Moving forward, this chapter has explored and established two methods of protein conjugation and modification. From this, they can be investigated separately *in vitro* with alternative targeting domains and toxins to identify which targeting domains best internalise into neuroblastoma, the effects of toxins in different cell lines, and the limitations of attachment and delivery in both conjugation types.

Chapter 4: Investigating peptide-based cell delivery of enzymes through pyridyldithio group conjugation

4.1 Introduction

There is a universal demand for there to be more efficient methods of delivering large proteins, such as enzymes, into the cell cytosol *in vivo* without disrupting the cell behaviour or function. The plasma membrane is a barrier which separates the controlled internal environment of cells from the outside environment; because of this, the methods of internalisation into cells is highly regulated, making drug delivery a primary issue. Membranes normally are only permeable to small hydrophobic compounds, anything large or alternatively charged needs to use alternative means (Garnacho 2016). Therefore, there have been several methods developed to enhance the delivery of drugs, enzymes and other proteins or probes into cells. As explored previously in Section 1.4 the simplest of these methods is conjugation between a targeting domain and a therapeutic domain. Here, the pyridyl disulphide conjugation method established in Chapter 3 is further explored to determine whether it can be used to target therapeutic enzymes into cells via attached internalisation peptides. It is hypothesised that both CPPs and peptide ligands which have been pyridyldithio-conjugated to enzymes are able to direct them into the cytosol of cells *in vitro* in a concentration dependant way, where the enzymatic activity can be measured through biological assays.

4.2 Results

4.2.1 Cell growth and assay controls

Cells to be used to investigate the hypothesis were first established through a series of controls to observe their growth and behaviour and how they responded to cell death assays. The murine and human neuroblast cells lines Neuro2A and SH-SY5Y derived from neuroblastoma were investigated as the main cell models to be used in these future experiments. J774.2 cells are a macrophage cell line derived from mouse lymphoma that have been previously shown to have enhanced protein uptake and would therefore be more sensitive to any changes in the amount of toxin given (Rust et al. 2015). Whilst not a

neuroblastoma cell, J774.2 is a useful tool to gauge potentially more subtle catalytic effects of delivered drugs that may not be measured in neuroblastoma cells, and is therefore more suited to initial investigations.

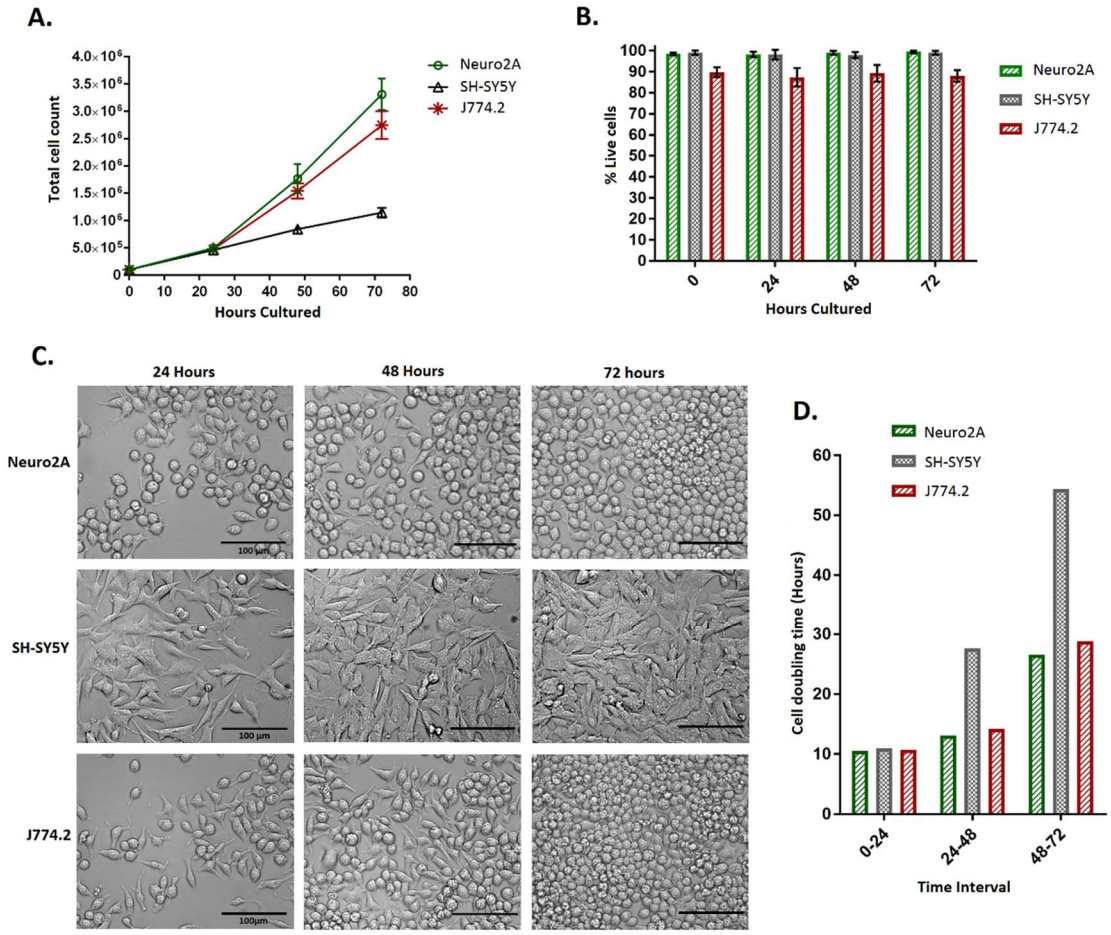

Figure 4.1 – Controls for cell line growth and growth assays

A) Graph showing cell growth of two neuroblast cell lines, Neuro2A and SH-SY5Y and the macrophage cell line J774.2 measuring at 24 hour time points through Bio-Rad automated cell counter (n=2, N=3). B) Overall % of live cells recorded at each time point for each cell type. C) Images taken at each 24 hour time point of the three cell lines investigated (n=3, N=3) (x40 objective, all scale bars 100 µm). D) Graph showing the doubling times measured at each recorded interval of cell counting.

Cells were seeded into 6 well plates at 1x10^5 alive cells per well. Over the following three days one well each day was harvested and the overall cell count measured by Bio-Rad automated cell counter in duplicate (n=2), this experiment was then repeated in triplicate (N=3). The media was not changed over the 3 days. All cells formed an adherent monolayer over the bottom of the well. The data shows that the initial rate of cell growth was similar in all three cell lines, but that after this the rate of growth in SH-SY5Y cells was slower than J774.2 and Neuro2A (fig. 4.1:A). The cell count also showed that there was no significant increase in cell death over the time intervals measured (fig. 4.1:B). Images were taken of all wells before harvesting, showing the relative confluency, morphology and overall health of the cell samples (fig. 4.1:C). Figure 4.1:D was derived from the data in figure 4.1:A, which measured the doubling time through using the following formula to get an approximation in hours (Roth 2006):

$$DoublingTime = \frac{Duration * \log(2)}{\log(final\ concentration) - \log(initial\ concentration)}$$

Figure 4.1:D shows that initially all of the cells had doubling time of about 10 hours, but as confluency increased and media nutrients decreased the doubling time increased, which is to be expected. J774.2 and Neuro2A were less sensitive to the changes than SH-SY5Y, which massively increased its doubling time over three days. These growth behaviours are factors which need to be considered when plating and passaging, that more SH-SY5Y cells will be needed in a plate to reach full confluency in a desired interval than either J774.2 or Neuro2A. However, it is understood that this data is not the full picture, as higher or lower seeding density will most likely alter the growth rate. Through trial and error, it was calculated the cell concentrations needed for seeding each cell type which would result in approximately 80-100% confluency after 72 hours (see methods).

4.2.2 Suitability of alamarBlue and MTT assays for measuring cell death in selected cell lines

In order to determine the effects of catalytic domains of diphtheria and ricin, assays such as MTT and alamarBlue were be used. MTT is a yellow tetrazole which is reduced in living cells to a purple formazan through cellular oxidoreductase enzymes present in living cells.

AlamarBlue also uses reduction as a live cell indicator, with the blue dye resazurin being reduced to the highly fluorescent resorufin (Hayon et al. 2003; Rampersad 2012). Both assays use this metabolic activity to determine the relative number of live cells in a sample and can be used in 96 well plates allowing a high data throughput.

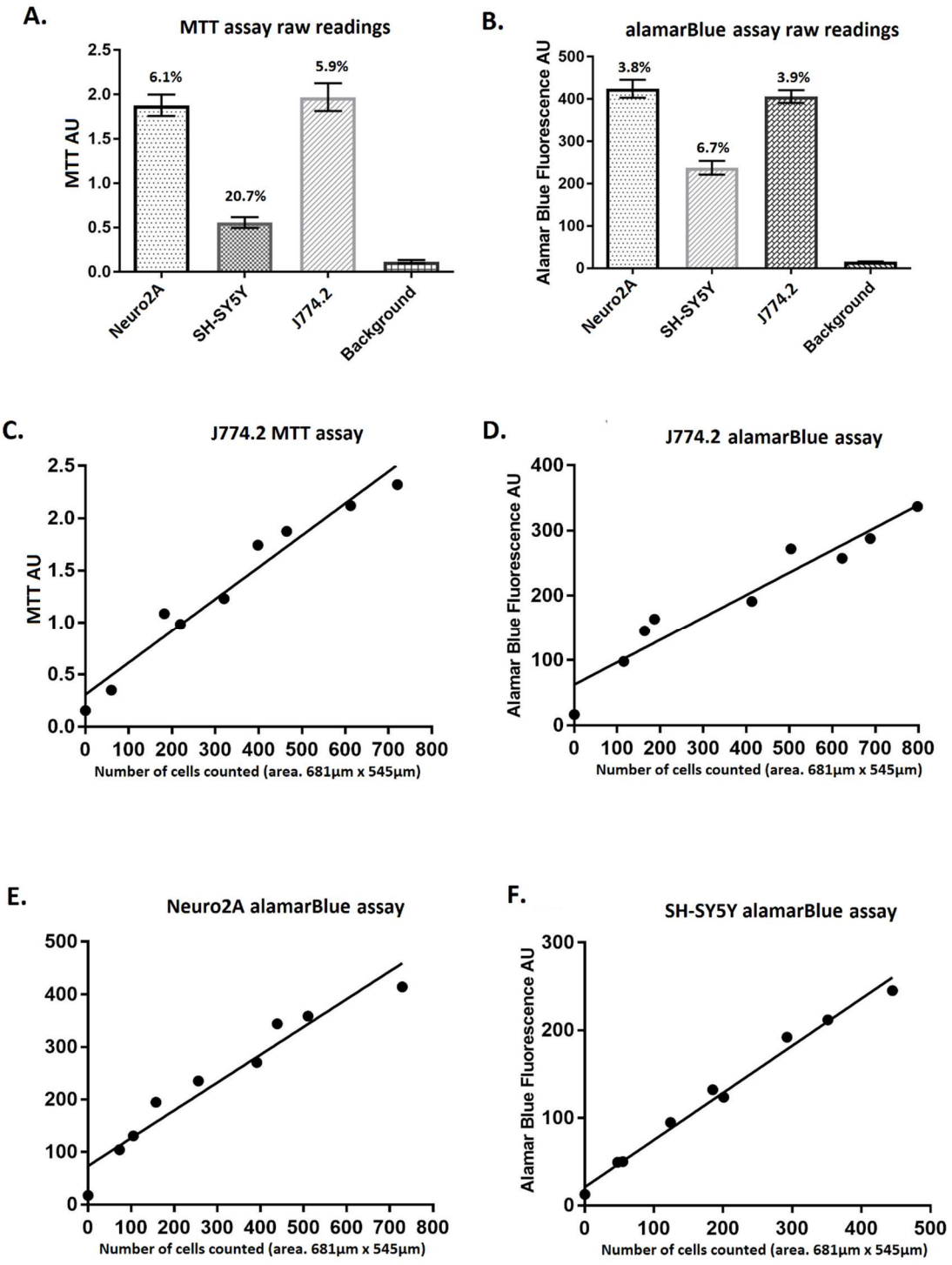

Figure 4.2 – Establishing MTT and alamarBlue assays

A) MTT assays showing cells grown in 96 well plate for 72 hours to confluency between 80-100% and measured with a background reading. % values are the proportion of the MTT assay reading which consisted of the background reading (n=3, N=3). B) AlamarBlue assay showing cells grown in 96 well plate for 72 hours to confluency between 80-100% and measured with a background reading. % values are the proportion of the alamarBlue assay reading which consisted of the background reading (n=3, N=3). C) Graph showing the relationship between MTT AU and the number of J774.2 cells counted in images at x20 (n=2, N=9). D-F) Graph showing the relationship between alamarBlue AU and the number of J774.2, Neuro2A and SH-SY5Y cells respectively counted in images at x20 (n=2, N=9).

Different individual cell lines have individual metabolic rates, and therefore cannot be directly compared against one another. But to ensure that assays were suitable for a particular cell line the cells were each seeded in 96 well plate in triplicate along with a background which contained media without any cells. After 72 hours, each plate was subjected to either MTT or alamarBlue assay where the absorbance or fluorescence of each of the cell types and the background was measured. The raw data was placed into graphs as shown in figures 4.2:A-B and the % of the value which was background was stated above each of the bar. Whilst MTT assays are widespread there was a low MTT AU value relative to background in the wells containing SH-SY5Y. This would mean that MTT assay would be unsuitable for measuring SH cells because there would be less precision in the data and higher error. A background reading of less than 10% was deemed suitable for use, therefore J774.2 and Neuro2A cells could be used with MTT, but not SH-SY5Y. All of the cell types could be used with an alamarBlue assay.

It is generally assumed that metabolic rate is directly proportional to live cell count. However this is not always the case as factors such as cell confluency or media condition could influence metabolism. Figure 4.2:C-F show that for both MTT and alamarBlue assays in J774.2, Neuro2A and SH-SY5Y cells the cell number counted manually through well imaging was directly proportional to the AU recorded. It is understood however that different toxins may affect the metabolic rates of cells as well as the number, so for good

practise imaging of wells are taken alongside MTT and alamarBlue assays to ensure assay results are representative.

4.2.3 Diphtheria light chain conjugated to CPPs via pyridyldithio groups can increase uptake of toxin in J774.2 cell line.

The J774.2 macrophage cell line has been shown to internalise toxic enzymes more efficiently than neuroblastoma cells (Rust et al. 2015); because of this, J774.2 cells were initially incubated with either diphtheriaLC (dipLC) or thio-CPP conjugated dipLC to determine whether there was a difference in cytotoxicity. It was shown through MTT assay that none of the CPPs alone altered J774.2 % MTT AU either with or without pyridyldithio attachment (fig. 4.3:A). However, when dipLC was added at 100nM there was a decrease in MTT AU to about 40% of control levels, not dissimilar to that which had been previously reported (Rust et al. 2015). Figure 4.3:B shows that the MTT AU% decreases significantly between dipLC and dipLC-thio-CPPs, with both CP-Penetratin and CP-BrevinMM yielding similar results. This strongly indicates that both CPPs are enhancing the translocation of dipLC into the cell, where it remains functional and is therefore increasing the rate of cell death due to its enhanced internalisation. There was a small yet significant decrease in the MTT AU % when CPPs were added without the pyridyldithio group, showing that the non-specific binding demonstrated in figure 3.3:E is capable of enhancing internalisation. However, the CPPs needed to be completely conjugated to the dipLC for there to be a large increase in internalisation.

The effect of decreased MTT AU % between dipLC-thio-CPPs and dipLC was seen across numerous concentrations in figure 4.3:C, with the EC_{50} in these conditions being 50nM for dipLC and approximately 7nM for both dipLC-thio-CPPs when incubated for 72 hours. Further results showed that there was no difference in toxicity of the construct when the orientation of the pyridyldithio domain was moved between the N and the C termini of the CP-Penetratin. On the other hand, this was not the case with CP-BrevinMM (fig. 4.3:D). This is most likely because of the MM amino acids on the C-terminus of the peptide which caused the increase in FITC-peptide uptake in figure 3.2. Therefore, further experiments need to take into consideration the nature and function of the peptides involved, for instance the location of receptor binding domains or hydrophobic sequences, to consider which end is best for attachment without compromising the conjugation.

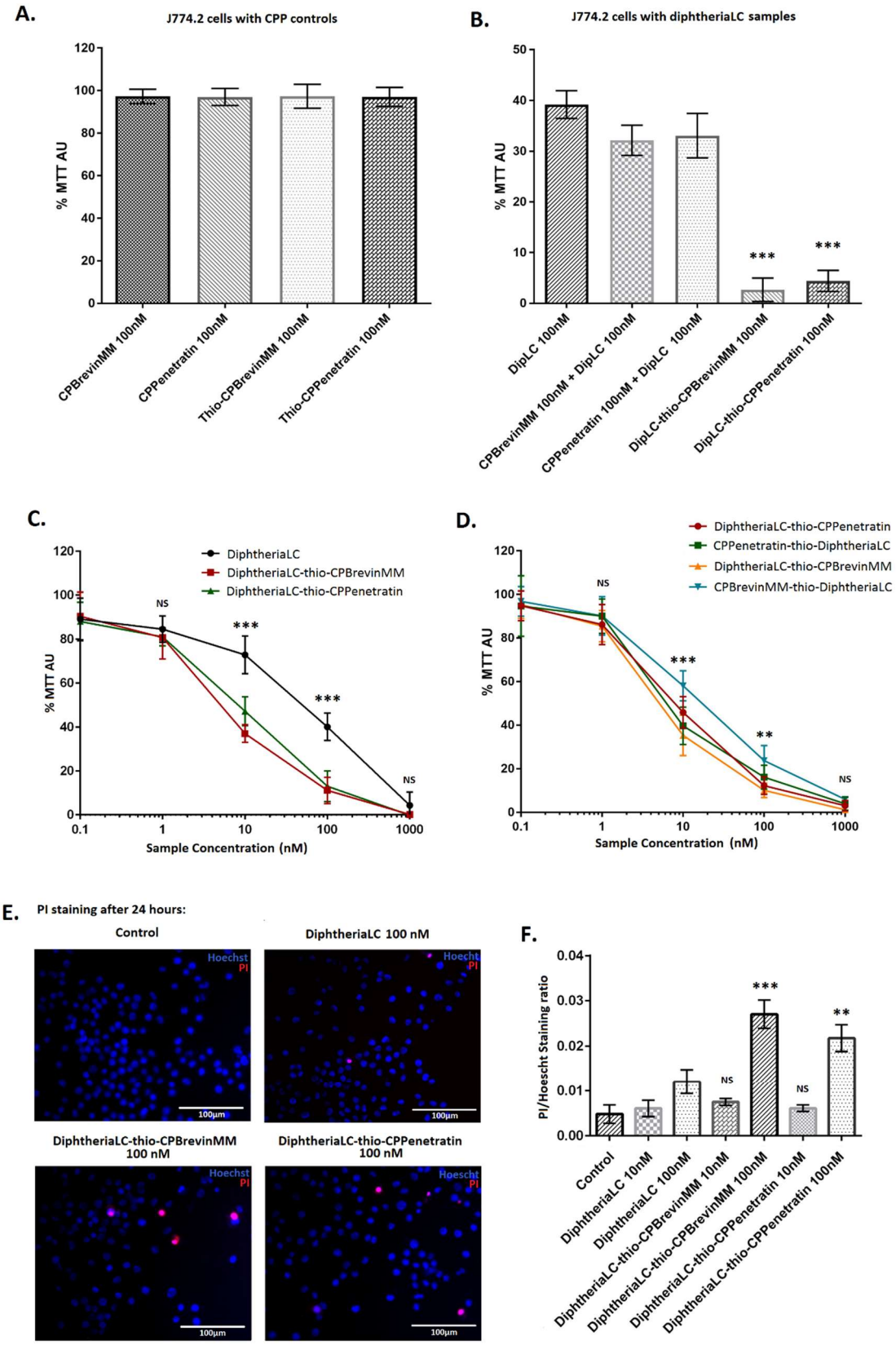
A.
J774.2 cells with CPP controls
% MTT AU
CPBrevinMM 100nM
CPPenetratin 100nM
Thio-CPBrevinMM 100nM
Thio-CPPenetratin 100nM
B.
J774.2 cells with diphtheriaLC samples
% MTT AU
DipLC 100nM
CPBrevinMM 100nM + DipLC 100nM
CPPenetratin 100nM + DipLC 100nM
DipLC-thio-CPBrevinMM 100nM
DipLC-thio-CPPenetratin 100nM
***
C.
DiphtheriaLC
DiphtheriaLC-thio-CPBrevinMM
DiphtheriaLC-thio-CPPenetratin
% MTT AU
Sample Concentration (nM)
NS
***
D.
DiphtheriaLC-thio-CPPenetratin
CPPenetratin-thio-DiphtheriaLC
DiphtheriaLC-thio-CPBrevinMM
CPBrevinMM-thio-DiphtheriaLC
% MTT AU
Sample Concentration (nM)
**
E.
PI staining after 24 hours:
Control
DiphtheriaLC 100 nM
DiphtheriaLC-thio-CPBrevinMM 100 nM
DiphtheriaLC-thio-CPPenetratin 100 nM
Hoechst
PI
100µm
F.
PI/Hoescht Staining ratio
Control
DiphtheriaLC 10nM
DiphtheriaLC 100nM
DiphtheriaLC-thio-CPBrevinMM 10nM
DiphtheriaLC-thio-CPBrevinMM 100nM
DiphtheriaLC-thio-CPPenetratin 10nM
DiphtheriaLC-thio-CPPenetratin 100nM

Figure 4.3 – Investigating the effect of thio-CPP conjugation to diphtheriaLC in J774.2 cells

*A) Control showing that the CPPs and thio-CPP are not toxic in J774.2 macrophages when measured by MTT assay. B) MTT assay showing metabolic activity when 100nM samples are added, significance is shown compared between dipLC with unconjugated CPPs and dipLC with CPPs conjugated via pyridyl disulfide using Student's T-test. C) Graph showing sample titrations measured against MTT assay readings after 72 hours incubation. Significance measured by one-way ANOVA for each concentration. D) Comparison of the activity of CPPs when thio-conjugated to either the N or C terminus. Significance measured by one-way ANOVA for each concentration. E) Images showing propidium iodide (PI) staining after 24 hours incubated with dipLC samples (x40 objective). F) Graph showing ratio of Hoescht stained and PI stained cells. Significance was measured compared to dipLC alone at the same concentration. Significance measured by Student's T-test comparing against dipLC at the same concentration. Significance for statistical analysis: P>0.05 = NS P<0.05 = * P<0.01 = ** P<0.001=***.*

In order to further support the proposal that thio-CPP conjugation could efficiently deliver dipLC, dipLC and dipLC-thio-CPPs were incubated with cells for 24 hours at either 10 nM or 100 nM before they were stained with propidium iodide (PI) (fig. 4.3:E). PI is a fluorescent DNA and RNA stain which cannot permeate through living cell membranes, therefore is a useful stain to detect cells which are apoptotic or necrotic. The PI staining was quantified as ratio, dividing the number of PI stained cells by the overall cells which were stained with hoescht. This showed that there was an increase in the cell death when thio-CPPs were conjugated to the dipLC at 10 nM but not at 1nM, supporting the previous MTT assay results (fig. 4.3:F). Whilst there was an increase in the cell death between dipLC and dipLC-thio-CPP, overall there was very little PI staining. The reason for this most is most likely that whilst the dipLC may have been delivered into the cell and inhibiting translation, most of the cells have not yet apoptosed.

An important consideration however, is that there are references showing that one single dipLC enzyme is sufficient to kill cells (Yamaizumi et al. 1978). Therefore, it should be asked why there is not an even bigger increase in cell toxicity with the conjugation of CPPs than has been shown in this data, especially taking into account the enhanced uptake behaviour

of J774.2. There could be numerous explanations for this; for one, whilst CPPs can internalise normally themselves, they are unable to efficiently internalise as one would hope when conjugated to dipLC. Alternatively, conjugated dipLC-thio-CPPs are entering into cells but that either the dipLC or the CPP or both are trapped in the endosomes or other vesicles and are not entering into the cytosol efficiently. In this case, the CPP may not be able to escape the endosomes whilst attached to dipLC, or the CPP can escape the endosomes but is unable to facilitate the translocation of dipLC. On the other hand, it is possible that the dipLC that is being used here is not fully functional due to errors in protein synthesis, or has been denatured in storage.

4.2.4 Lipofectamine 3000 drastically enhances diphtheriaLC internalisation compared to diphtheriaLC-thio-CPP

Lipofectamine 3000 (LF3000) is a transfection reagent which has been reported to efficiently deliver proteins and DNA into cells (Rust et al. 2015; Yu et al. 2016). In order to determine the functionality of the dipLC used, LF3000 was incubated with dipLC before adding onto J774.2 cells for 72 hours. LF3000 added at 0.5% dilution was shown not to be significantly toxic to J774.2 cells (fig. 4.4:A). When the same amount was added to various concentrations of dipLC with or without thio-CPbrevinMM conjugation there was complete toxicity at all concentrations tested (fig. 4.4:B). These data strongly indicate that the dipLC being used is fully functional even when conjugated to thio-peptides.

Similarly as with dipLC, ricinLC was conjugated to thio-CPBrevinMM and thio-CPPenetratin and incubated at a variety of concentrations with J774.2 cells for 72 hours in order to compare toxicity and enzyme internalisation. Interestingly, unlike dipLC, there was no significant alteration in the cells when measured by MTT assay (fig. 4.4:C). However, when ricinLC was incubated with 0.5% concentration of LF3000 there was a massive shift in EC_{50} compared to ricinLC alone. Together this strongly suggests that it is not the enzymes lacking function, but that either the CPPs are unable to transport the enzymes into the cells efficiently, or that the enzymes are transported into the cells yet cannot escape into the cytosol efficiently.

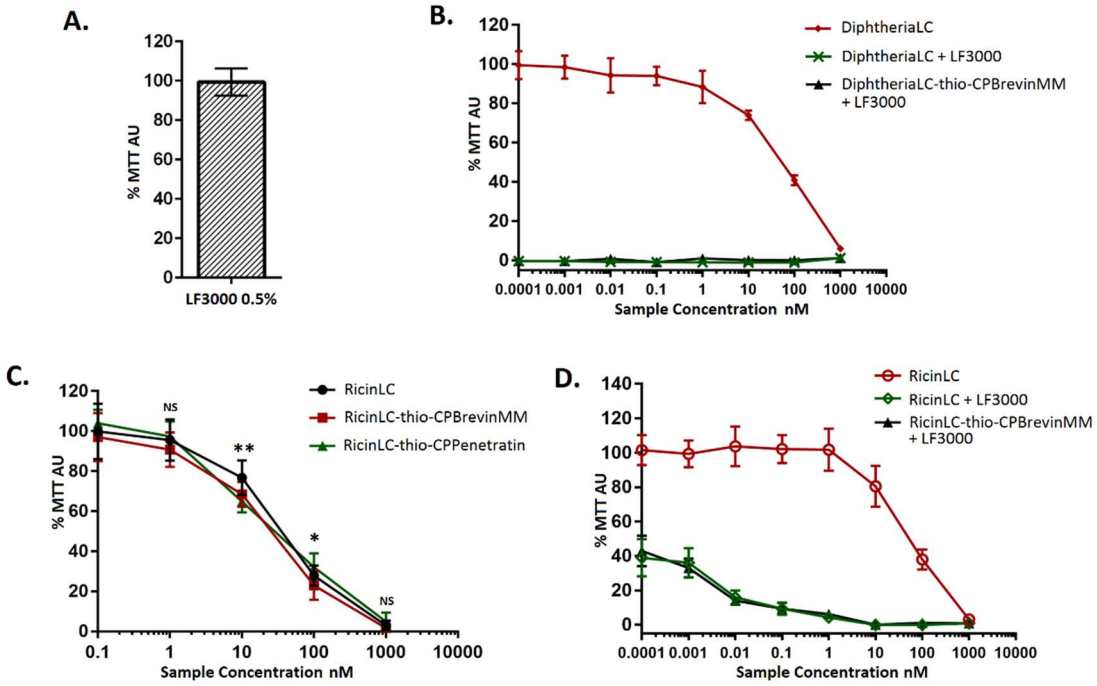

Figure 4.4 - Lipofectamine 3000 enhances diphtheriaLC internalisation compared to diphtheriaLC-thio-CPP

A) *MTT assay of J774.2 cells incubated for 72 hours in 0.5% LF3000 and measured by MTT assay (n=3, N=3). B) J774.2 cells incubated with concentrations of diphtheriaLC with or without thio-CPBrevinMM conjugation and 0.5% LF3000 after 72 hours incubation (n=3, N=2). C) Titrations of ricinLC with or without CPPs conjugated, measured by MTT assay. Significance measured by one-way ANOVA for each concentration (n=3, N=3). D) J774.2 cells incubated with concentrations of ricinLC with or without thio-CPBrevinMM conjugation and 0.5% LF3000 after 72 hours incubation (n=3, N=2). Significance for statistical analysis: P>0.05 = NS P<0.05 = * P<0.01 = ** P<0.001=***.*

4.2.5 Both thio-CPPenetratin and thio-CPBrevinMM increase the uptake of mCherry-S25CRD in J774.2 cells

MCherry-S25CRD, first synthesised in chapter 3, was conjugated to thio-CPBrevinMM and thio-CPPenetratin similar to that in figure 3.6 before being incubated at 500 nM in J774.2 cells and subsequently washed, hoescht stained and live imaged. Figure 4.5:A showed that there was a large increase in the amount of intracellular mCherry-S25CRD detected after 2 hours when CPPs were conjugated. The result was quantified by analysing the average

pixel intensity over the cells in the raw images (fig. 4.5:B). Interestingly, when imaged at a higher magnification it was observed that the mCherry-S25CRD appeared vesicular inside the cell, as opposed to having a consistent presence throughout the cytosol (fig. 4.5:C).

The images clearly show that the CPPs are enhancing the delivery of conjugated mCherry-S25CRD into the cells, whereas the vesicular localising of the peptide seems to suggest that the protein is remaining in the endosomes and phagosomes instead of being delivered into the cytosol. This is in agreement with previous figures and would account for the lack of major increase in catalytic activity within the cytosol. Whilst it is true that there was a significant difference in the EC_{50} between dipLC and dipLC-thio-CPP constructs, as there would be more dipaLC entering into the intracellular compartments of the cell it could be assumed that the difference is because of small amounts of leakage from the endosomes. Whatever the particulars of the mechanisms, it can be concluded that whilst CP-Penetratin and CP-BrevinMM conjugation both do increase uptake of conjugated protein into particular cells, it is not an efficient delivery method due to lack of efficient cytosolic translocation.

4.2.6 CP-Penetratin and CP-BrevinMM are internalised significantly less in neuroblastoma cell lines SH-SY5Y and Neuro2A than J774.2 cells

To determine whether the previously observed effects of the CPPs and their transportation properties could be applied to other cells, it was decided to investigate FITC-CPP and dipLC-thio-CPP effects in neuroblastoma cell lines Neuro2A and SH-SY5Y. Figure 4.6:A shows that there is limited entry of FITC-CPP peptides after 2 hours incubation and subsequent washing, hoescht staining and live cell imaging. It should be noted that the images taken here had a higher exposure than in figure 3.2. It is unsurprising that there is less thio-CPP in the neuroblastoma cells compared to J774.2 given the phagocytic nature of macrophages and previous data relating to their increased internalisation rates (Lunov et al. 2011; Rust et al. 2015). For these following experiments, alamarBlue assay was used owing to the lack of sensitivity of the MTT assay with these cell lines. It was necessary to determine whether either cell line had resistance to dipLC; it was found in figure 4.6:B that dipLC added with 0.5% LF3000 significantly decreased the alamarBlue AU % in both cell lines.

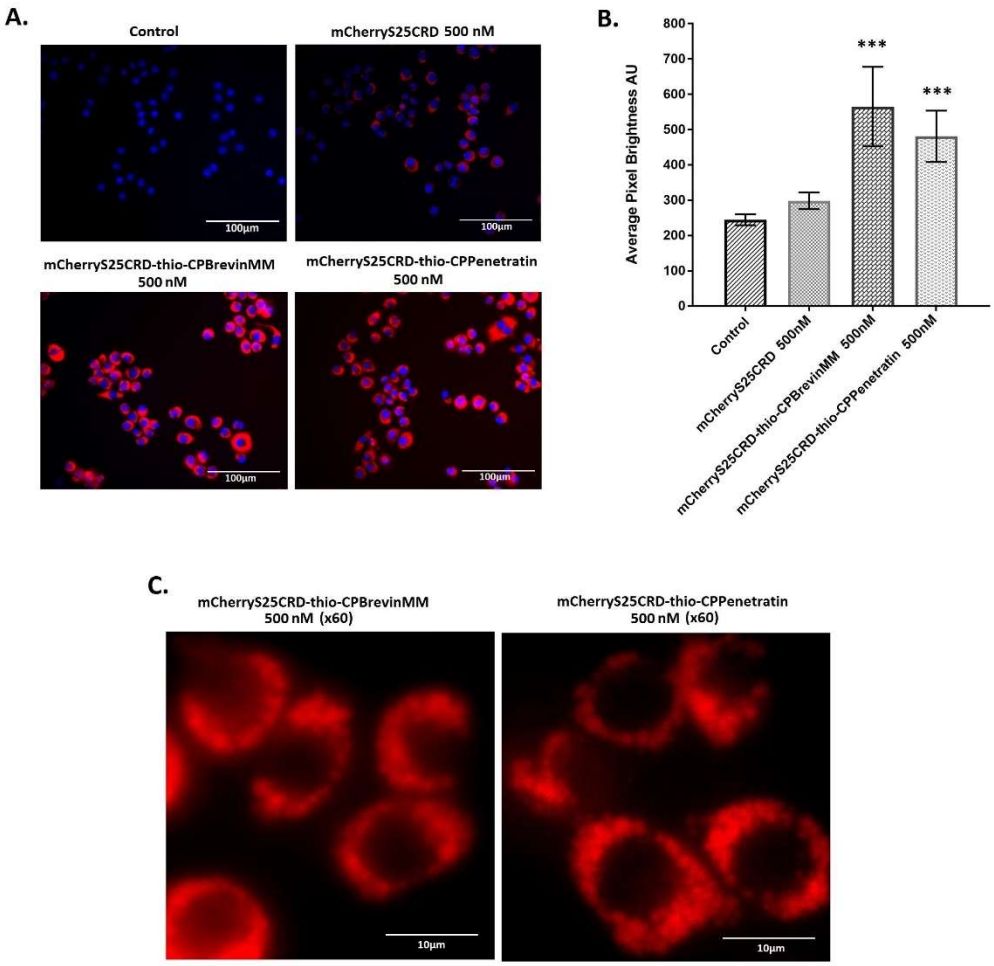

Figure 4.5 - Both CPPenetratin-thio and CPBrevinMM-thio increase the uptake of mCherry-S25CRD in J774.2 cells

*A) Objective 40x images showing mCherry-S25CRD internalisation into J774.2 with and without attachment of thio-CPPenetratin and thio-CPBrevinMM (n=2, N=2). B) Graph showing average pixel intensity within the cells, using the raw images, which were taken live cell at 300 ms exposure after 2 hours incubation inside the cells. Significance measured by Student's T-test comparing against mCherry-S25CRD. C) 60x images of mCherry-S25CRD when attached to CPPs, showing punctated appearance of mCherry-S25CRD within the cells (600 ms) (N=2). Significance for statistical analysis: P>0.05 = NS P<0.05 = * P<0.01 = ** P<0.001=***.*

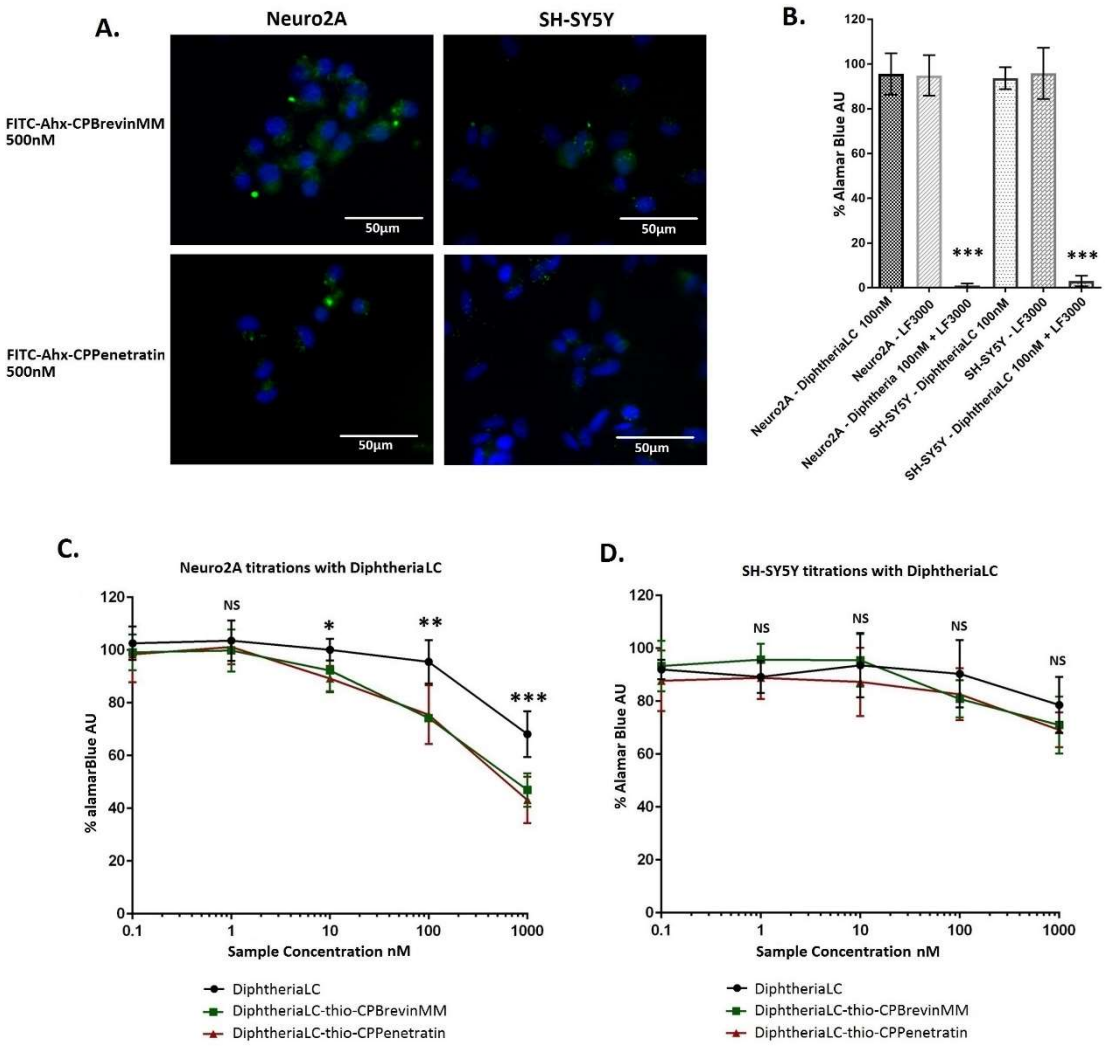

Figure 4.6 - Fluorescent CPPenetratin and CPBrevinMM are internalised less in neuroblastoma cell lines than in J774.2

*A) Live cell imaging of Neuro2A and SH-SY5Y after 2 hours in 500nM FITC-peptide samples green=FITC-peptide (1200 ms), blue= Hoechst (20 ms) (x40 obj.) (n=3, N=2). B) Neuro2A and SH-SY5Y cells with LF3000 (0.5%), diphtheriaLC, or diphtheriaLC+LF3000 after 72 hours. Significance measured by Student's T-test against diphtheriaLC in each cell (n=3, N=3). C and D) Neuro2A and SH-SY5Y cells with diphtheriaLC and diphtheriaLC-thio-CPP conjugates after 72 hours incubation. Significance measured by one-way ANOVA for each concentration (n=3, N=3). Significance for statistical analysis: P>0.05 = NS P<0.05 = * P<0.01 = ** P<0.001=***.*

Through alamarBlue assay, the data in figure 4.6:C-D indicated that with Neuro2A there was a decrease in the number of live cells between the dipLC-thio-CPP and the dipLC incubated cells at high concentrations when incubated over 72 hours, but there was no observable difference with SH-SY5Y cells. Like J774.2, this shift in the dose-response curve is not toxicity that one would expect from an efficiently functioning cell entry tool. Because of this, this study will investigate alternative methods of endosomal escape for the efficient delivery of enzymes to their therapeutic targets within the cell.

4.2.7 Translocation domains of both diphtheria and botulinum/A increase the cytosolic internalisation of enzyme without attached internalisation sequence.

To increase the translocation of toxin domains into the cytosol of the cells, endosomal escape methods were explored. As mentioned in the introduction, there are peptides which have been designed and investigated as a means of enhancing cytosolic translocation, such as GALA (Li et al. 2004; Haas & Murphy 2004). GALA-thio was acquired and was shown to successfully conjugate to dipLC (fig. 4.7:A). Additionally, diphtheriaLcTd (dipLcTd)was successfully expressed with a thrombin cleavage sequence between the two domains, allowing the cysteines to form a disulphide bridge that is endogenously present on the native toxin which in turn can be reduced (fig. 4.7:B-C). Unfortunately, aside from the cysteines which form the disulphide bridge, there are no other cysteine residues on dipLcTd, therefore thio-peptides are unable to bind (fig. 4.7:D).

DipLC, dipLcTd and GALA-thio-dipLC were added to J774.2, Neuro2A and SH-SY5Y cell lines and incubated for 72 hours, these proteins along with an example of the reduction of dipLcTd, are shown as a schematic in figure 4.7:E. There was no noticeable difference in the alamarBlue AU % between dipLC and GALA-thio-dipLC in any of the cells tested after this timepoint (fig. 4.7:F-H). However, there was a significant difference at higher concentrations between dipLC and dipLcTd. Interestingly, the effects of the translocation domain was different for each cell type: SH-SY5Y cells were far more sensitive to the dipLcTd than Neuro2A cells, with J774.2 cells showing no decrease in % alamarBlue AU between the dipLC and dipLcTd samples.

To further investigate translocation domains, both botulinumLC/A (botLC/A) and botulinumLcTd/A (botLcTd/A) were added onto Neuro2A and SH-SY5Y cells to compare the

cleavage of SNAP25. Both cell lines showed increased cleavage between botLC/A and botLcTd/A (fig. 4.7:I-J). Although there appears to be variation in the response to the translocation domains between the cell lines and the toxins, it is evident here that translocation domains are able to increase the cytosolic location of the catalytic domains of toxins.

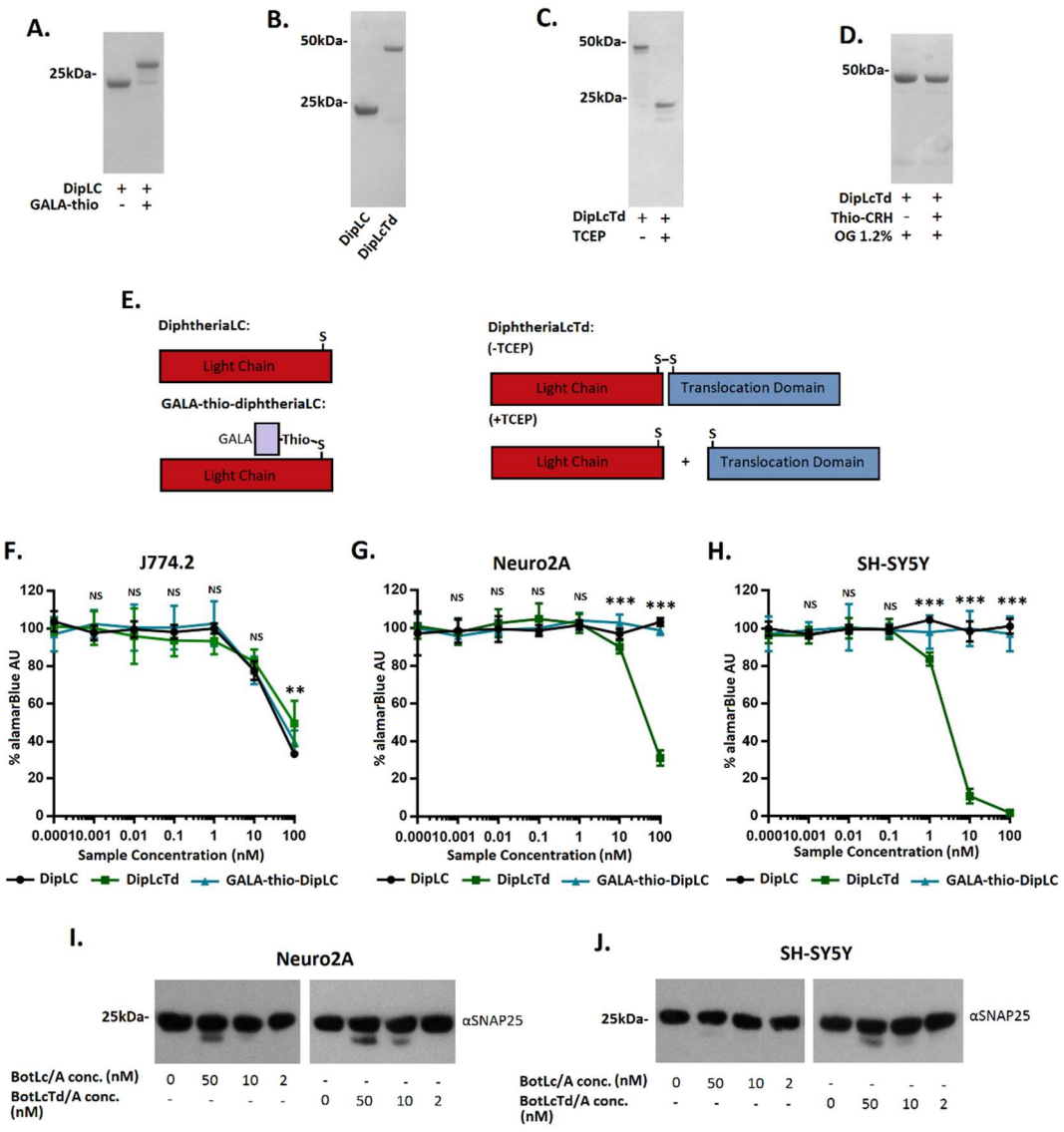

Figure 4.7 – Investigating cytosolic translocation methods

*A) SDS-PAGE gel showing conjugation between dipLC and GALA-thio. B) SDS-PAGE gel showing both dipLC and dipLcTd. C) SDS-PAGE showing the reduction of dipLcTd using TCEP to confirm the presence of disulphide bridged domains. D) SDS-PAGE showing attempted conjugation between dipLcTd and thio-CRH in the presence of OG 1.2%. E) Schematic of the proteins and conjugates to be incubated with cells, and of the reduction reaction of dipLcTd when incubated with TCEP. F-H) AlamarBlue assays of J774.2, Neuro2A and SH-SY5Y incubated with dipLC, GALA-thio-dipLC and dipLcTd over 72 hours. Significance measured by one-way ANOVA for each concentration (n=3, N=3). I-J) Western Blot of Neuro2A and SH-SY5Y cells showing SNAP25 cleavage after incubating with botLC and botLcTd after 72 hours incubation (N=2). Significance for statistical analysis: P>0.05 = NS P<0.05 = * P<0.01 = ** P<0.001=***.*

4.2.8 Thio-Ligand and thio-CPP conjugation via Octyl β-D-glucopyranoside (OG) does not enhance cell uptake

Having determined that pairing catalytic light chains with their native translocation domains can enhance cytosolic translocation, it was to be determined whether CPPs and other ligands with the pyridyl disulphide group attached would be able to conjugate to the LcTd toxins. Because CPPs only marginally increase the internalisation in neuroblastoma, it was decided that other ligands which were previously investigated for conjugation in figure 3.4 should also be investigated for internalisation. The aim of this was to investigate the hypothesis that a combination of cell internalisation and translocation is required for effective delivery.

In figure 3.8, it was demonstrated that botLcTd/A was able to conjugate its internal 3 free cysteines with the assistance of OG. OG is a light detergent and therefore has the potential to be toxic to cells, because of this it was important to first determine the cytotoxic threshold that could be used for incubating cells with OG containing samples. Both Neuro2A and SH-SY5Y were incubated with a particular % OG which was diluted a further 1 in 20 into wells (see methods). It was found that both cell types could be incubated with 0.2% OG, and SH-SY5Y could be incubated with 0.4% (fig. 4.8:A). Next, it was important to determine whether it was possible for the entire SNAP25 population within the cells could be cleaved by botLcTd/A. This positive control was set up using LF3000 0.5% with the

added sample over 72 hours. It was found by western blot that after 72 hours all of the cells incubated with LF3000 + botLcTd/A had fully cleaved SNAP25 in both cell lines (fig. 4.8:B).

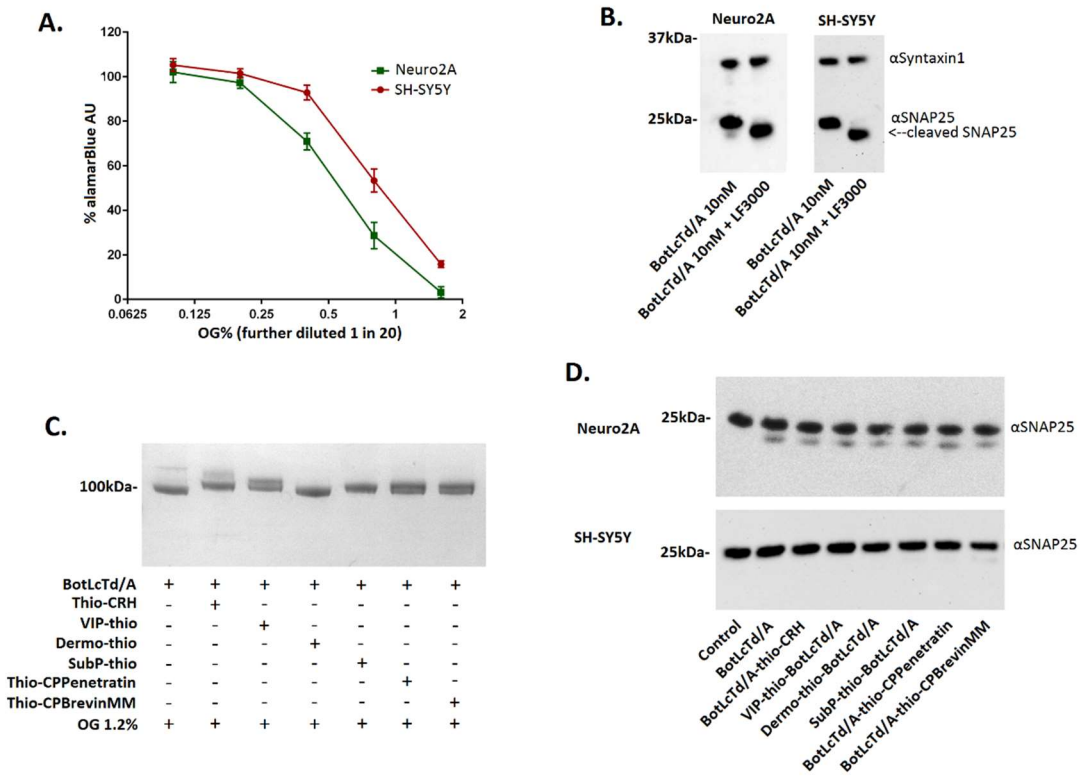

Figure 4.8 – Thio-Ligand and thio-CPP conjugation via OG is not able to direct botulinumLcTd/A into cells.

A) *AlamarBlue graph showing the sensitivity of Neuro2A and SH-SY5Y to OG (n=3, N=2). B) Western Blot showing the cleavage of SNAP25 when cells have been incubated for 72 hours with either botLcTd/A or botLcTd/A+LF3000. αSyntaxin1 was used as a loading control (N=2). C) SDS-PAGE gel showing the conjugation between the thio-peptides and botLcTd/A after 1 hour incubation with 1.2% OG (N=3). D) Western blots showing the cleavage of SNAP25 when cells have been incubated for 72 hours with peptide-thio-botLcTd/A at 10 nM (N=2).*

Samples of botLcTd/A-thio-peptides were made using 1.2% OG as described in figure 3.8; the peptides were incubated with botLcTd/A and OG for 1 hour before running on SDS-PAGE for two hours to allow effective band separation (fig. 4.8:C). Interestingly, whilst it

appeared that all the botLcTd/A had peptide-thio conjugated (although with dermo-thio this was difficult to tell) it appeared that the different peptide-thios were able to be conjugated in different ways. For instance, thio-CRH mainly conjugated once to the botLcTd/A as indicated by the one prominent band, yet VIP-thio was spread equally across 2 bands. This may be because the larger size of thio-CRH inhibits further conjugation. These samples were then diluted to ensure that the OG was less than 0.2% and that the samples were at the correct concentration for incubating with cells once diluted 1 in 20 into wells. All the samples were then incubated for 72 hours with Neuro2A and SH-SY5Y cells before harvesting and analysing for SNAP25 cleavage on a western blot. It was found that there was no increase in the amount of the SNAP25 cleaved between conjugated and unconjugated botLcTd/A. This result was not entirely unexpected as it is likely that as the OG concentration decreased the hydrogen bonds within the botLcTd/A re-formed, potentially allowing the protein to fold back over the ligand.

4.2.9 Thio-CPP attachment via S25-CRD domain on botulinumLcTd/A slightly increases neuroblastoma cell internalisation

Figure 3.8:F showed that it was possible to attach a S25-CRD to botLcTd/A and that after 1 hour 50% could be conjugated to thio-CRH; this was repeated with incubation increased to determine whether a high proportion of botLcTd/A-S25CRD could be conjugated. Figure 4.9:A shows that there is no difference in the conjugation of thio-CRH to botLcTd/A-S25CRD between 1 and 24 hours. Interestingly, when the thio-peptides were conjugated to botLcTd/A-S25CRD, it appeared that the efficiency of binding was different for each of the peptides. For instance, 50% thio-CRH was conjugated, however substanceP-thio appeared as if there was 100% binding and there also appeared to be 2 bands forming with the CPP samples. Like figure 4.8:C, this is most influenced by size, however it is difficult to fully conclude because of the tiny difference in band sizes even after running the SDS-PAGE for over 2 hours (fig. 4.9:B). To determine the function of botLcTd/A-S25CRD in comparison to botLcTd/A, Neuro2A cells were incubated with both. Figure 4.9:C shows that the internalisation and SNAP25 cleavage of botS25-S25CRD in Neuro2A cells is comparable to that of botLcTd/A.

A Western blot was then used to analyse the SNAP25 cleavage of cells incubated with the thio-peptide samples conjugated to botLcTd/A-S25CRD. It was found that unfortunately

there was no observable increase in SNAP25 cleavage with the attachment of thio-ligands (fig 4.9:D). However, for Neuro2A there was an increase between the non-CPP and CPP versions. There was negligible increase in cleavage in SH-SY5Y cells. It is worth bearing in mind that the % attachment of CPPs compared to the % attachment of the larger ligands may have influenced the internalisation, as ideally a fair comparison would be for the same amount of peptide to be conjugated across all the samples. Whilst there was some cleavage at the 72 hour timepoint in the thio-CPP samples, it is possible that optimum SNAP25 cleavage occurs at a different timepoint. For instance, botLcTd/A could have internalised and cleaved SNAP25 by 24 hours, but by 72 hours the cells have proliferated and the botLcTd/A may have been degraded; in this case there would be proportionally less SNAP25 cleavage at 72 hours. Therefore, at 24 hours the cells incubated with botLcTd/A-S25CRD were harvested and run on a western blot (fig. 4.9:E). There was no cleavage in any of the samples at 24 hours, hence supporting the use of the 72 hour timepoint.

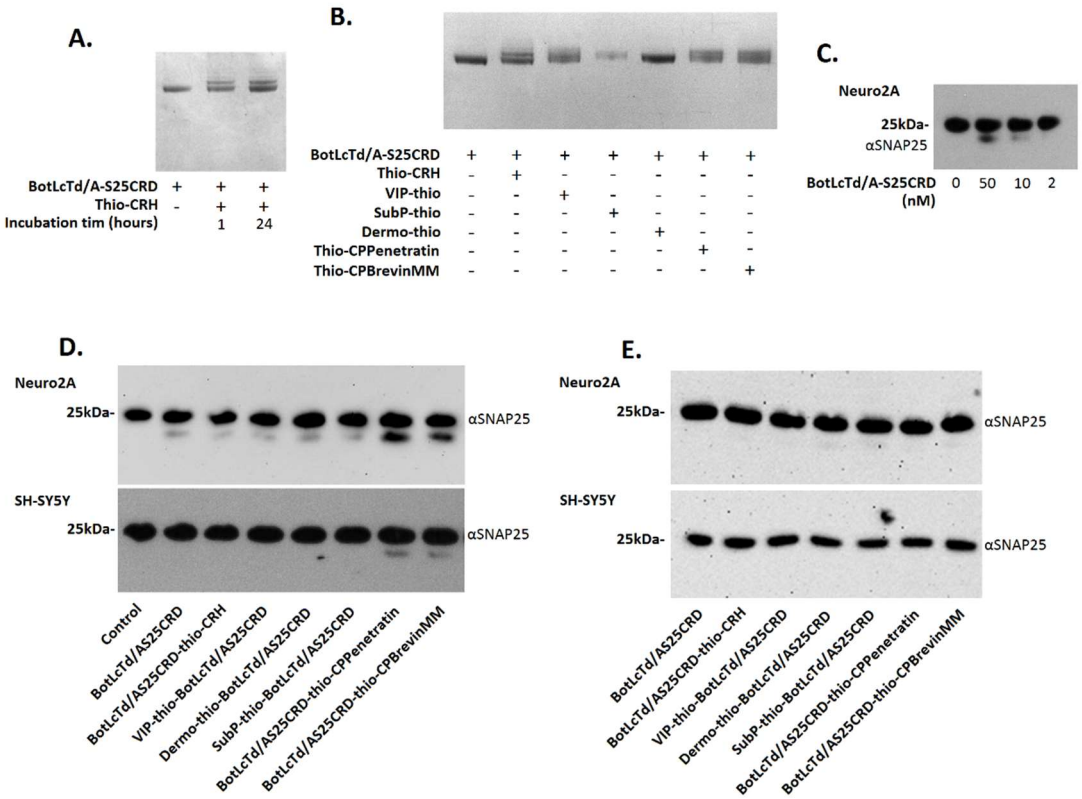

Figure 4.9 – Thio-CPPs conjugated to botulinumLcTd-S25CRD can increase SNAP25 cleavage.

A) SDS-PAGE showing conjugation between thio-CRH and botLcTd/A-S25CRD over 1 hour at RT and 24 hours at 4˚C (N=3). B) SDS-PAGE showing conjugation between a variety of thio-ligands and thio-CPPs to botLcTd/A-S25CRD over 1 hour (N=2). C) Western blot showing the SNAP25 and after incubating Neuro2A cells with botLcTd/A-S25CRD for 72 hours (N=2). D) Western blot showing SNAP25 cleavage of Neuro2A and SH-SY5Y cells incubated over 72 hours with ligand-conjugated botulinumLcTd-S25CRD samples at 10nM (N=3). E) Western Blot showing SNAP25 cleavage of Neuro2A and SH-SY5Y cells incubated for 24 hours with ligand-conjugated botulinumLcTd-S25CRD at 10nM (N=2).

4.2.10 Design and synthesis of diphtheriaLcTd with cysteines accessible for peptide-thio binding.

Having shown that LcTd domains of botulinum A was better at cleaving SNAP25 in neuroblastoma cells than the LC only, and that thio-CPP conjugation improved upon this in Neuro2A cells, it was then important to determine whether this was the case with diphtheria. As previously mentioned, dipLcTd does not have any free cysteines, therefore the conjugation of a cysteine rich domain is necessary. Because in both mCherry-S25CRD and botulinumLcTd-S25CRD there was never 100% conjugation it was decided that new cysteine containing domains should be explored. There have been other groups which have used a slightly different cysteine rich domain (CRD) for attachment, so this was used (Lalli & Schiavo 2002; Griffin et al. 1998). Additionally, it was proposed that the cysteine containing sequence from dipLC could also be used. A plasmid was constructed externally, containing the sequence for dipLcTd along with the 1cys domain from dipLC and also the CRD (fig. 4.10:A). When this was expressed there was very little produced. It appeared as a smudge above the better expressed dipLcTd (48 kDa) and it was difficult to purify through FPLC (fig 4:10:B). Whilst there was an increase in the band through SDS-PAGE when thio-CRH was added, it can be agreed that the protein produced could not be reliably synthesised or used (fig 4.10:C). The CRD was removed through restriction digest to form a diphtheriaLcTd-1cys sample; however, like the first sample, whilst there was evidence of conjugation, the protein could not be reliably produced (fig 4.10:D-F).

Another plasmid was constructed externally containing dipLcTd along with an additional LC (fig 4.10:G). This protein was successfully produced and mostly purified through FPLC where it was later shown that almost 100% of the protein could conjugate to thio-CRH, demonstrating it to be more efficient at conjugation than S25-CRD (fig. 4.10:H-I). This protein could therefore be a useful tool to conjugate to the ligands and confirm the data found in figure 4.9 that CPPs could increase LcTd uptake.

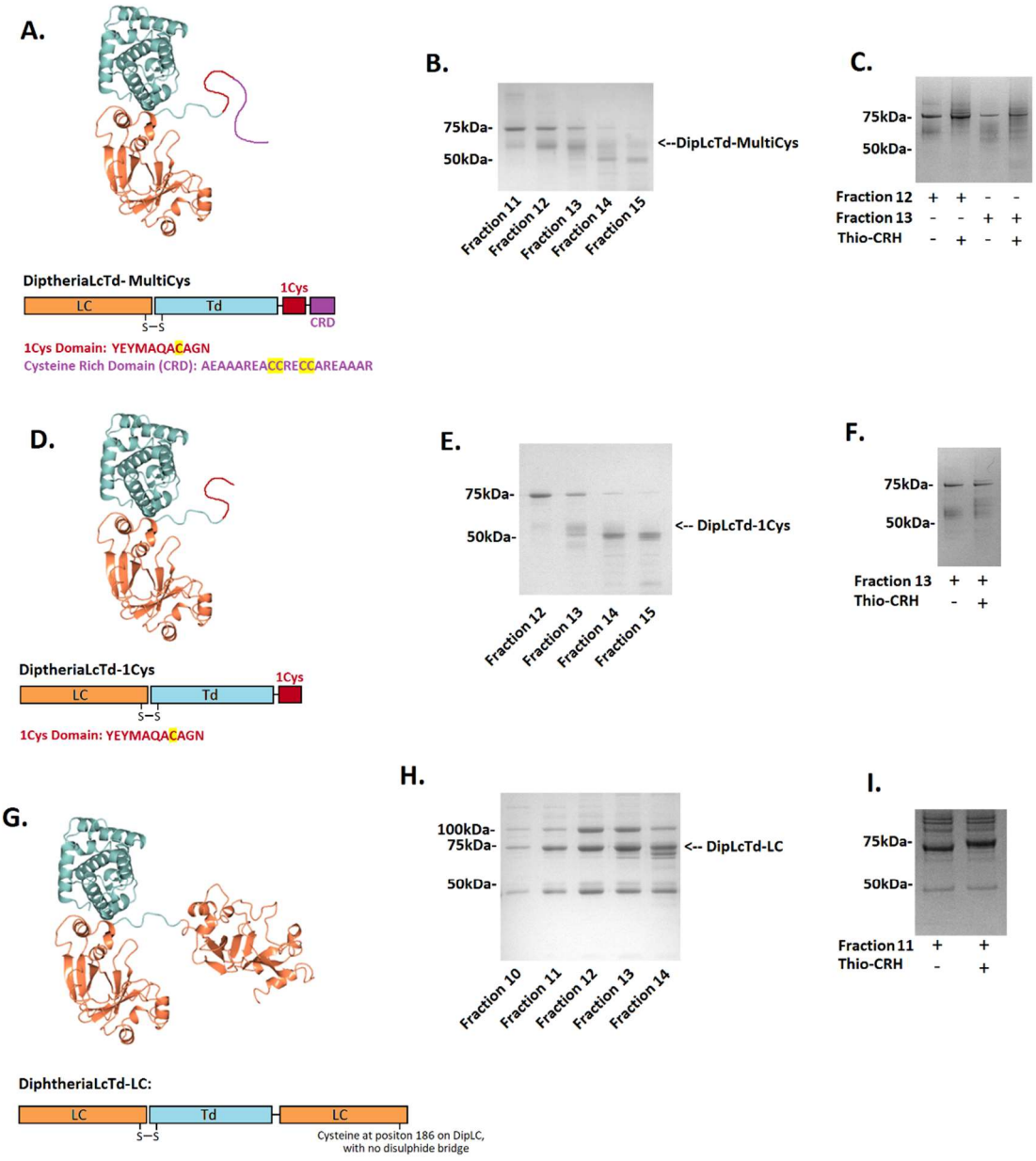

Figure 4.10 – Designing a diphtheriaLcTd protein with free cysteines for pyridyldithio conjugation

A) Schematic showing diphtheriaLcTd-MultiCys protein with cysteine domains highlighted. B) SDS-PAGE showing the FPLC fractions after production and attempted purification of diphtheriaLcTd-MultiCys. C) SDS-PAGE showing the thio-CRH conjugation to two of the expressed fractions. D) Schematic showing diphtheriaLcTd-1Cys protein with cysteines for binding highlighted. E) SDS-PAGE showing the FPLC fractions after production and attempted purification of diphtheriaLcTd-1Cys. F) SDS-PAGE showing the thio-CRH conjugation to one of the expressed fractions. G) Schematic showing diphtheriaLcTd-LC protein, with the unconjugated cysteine on the second LC indicated for protein conjugation. H) SDS-PAGE showing the FPLC fractions after production and attempted purification of diphtheriaLcTd-LC. I) SDS-PAGE showing the thio-CRH conjugation to one of the expressed fractions. Diphtheria domains PDB ID: 1SGK (McNicholas et al. 2011; Berman et al. 2000).

4.2.11 Utilising diphtheriaLcTd-LC for ligand binding and enhanced delivery.

Having successfully produced dipLcTd-LC and shown it could conjugate to thio-CRH, it was necessary to determine how well it was able to conjugate to the other thio-peptides in our possession before adding onto cells. Figure 4.11:A shows that all of the thio-peptides were able to conjugate to dipLcTd-LC with up to 100% efficiency at 1 hour incubation. This also had the advantage over the botLcTd/A-S25CRD conjugation because it appeared that all of the protein in the sample had the same amount of thio-peptide conjugated. The LC domain which was added to the existing LcTd was a catalytically active domain, therefore it poses the possibility that there could be an increase toxicity in between dipLcTd and dipLcTd-LC. Figure 4.11:B shows that there was no significant increase in toxicity between these two proteins. This was expected because the Td and the added LC are recombinantly fused, as the Td is proposed to form a pore to allow the disulphide bridged LC into the cytosol then the fused LC would remain attached to the Td within the endosomes.

All of the ligand conjugated dipLcTd-LC samples were then tested in Neuro2A and SH-SY5Y cells at concentrations best suited to the cell line based on figure 4.11:B. Figure 4.11:C and D show that, like figure 4.8, there was no apparent increase in the cytosolic translocation of the catalytic domain in all apart from those linked with CPPs. It was previously shown that SH-SY5Y cells were less sensitive to CPPs than Neuro2A, however, because SH-SY5Y is more sensitive to dipLcTd it was hoped that any effect would be amplified. This was not

the case however, as there was a significant difference at the higher concentrations of dipLcTdLC-thio-CPPs in Neuro2A cells but this was seen to a far lesser extent in SH-SY5Y cells (fig. 4.11:E-F). Together, this data shows that pyridyldithio-peptides are capable of binding and modifying proteins and their internalisation capabilities, but that careful considerations need to be made regarding the desired targeting motif, the necessity of a translocation domain and available SH residues.

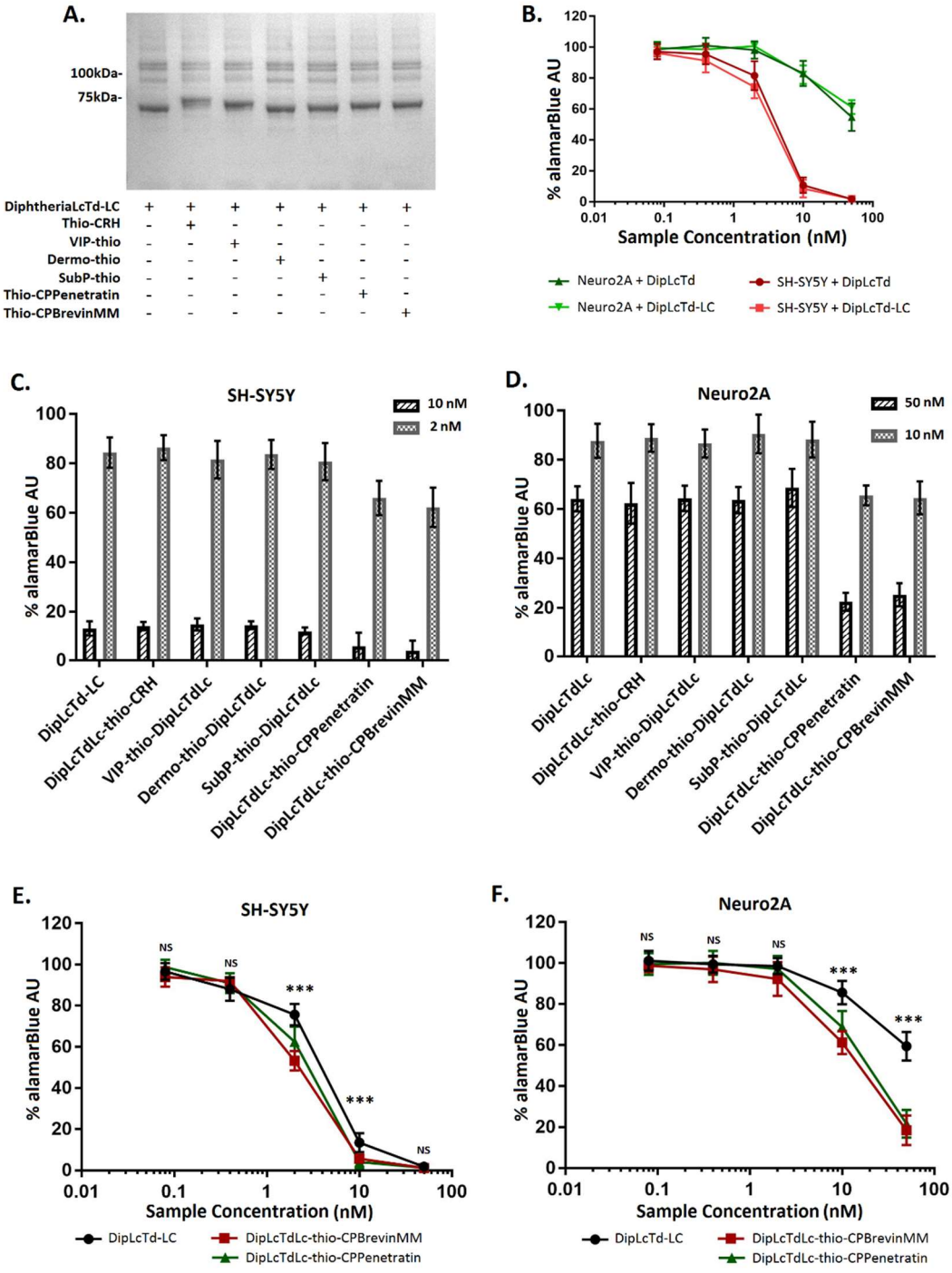

Figure 4.11 – Utilising diphtheriaLcTd-LC for thio-peptide directed cell entry

*A) SDS-PAGE (run time: 2 hours) showing conjugation between dipLcTd-LC and thio-peptides after incubating for 1 hour (N=3). B) AlamarBlue assay showing the relative toxicity between dipLcTd and dipLcTd-LC in Neuro2A and SH-SY5Y cell lines after 72 hours incubation. C-D) Bar graph showing the toxicity of dipLcTd-LC and the thio-peptide conjugated samples in SH-SY5Y and Neuro2A cell respectively after 72 hours incubation (n=3, N=2). E-F) AlamarBlue assay of titrations of dipLcTd-LC and the thio-CPP conjugated samples in SH-SY5Y and Neuro2A cell respectively after 72 hours incubation. Significance measured by one-way ANOVA for all sample values of the same concentration (n=3, N=3). Significance for statistical analysis: P>0.05 = NS P<0.05 = * P<0.01 = ** P<0.001=***.*

4.3 Discussion.

Within this chapter, it has been established that cell targeting or internalising peptides with pyridyl disulphide groups can be used to modify proteins with free cysteines and can alter internalisation. However, whilst these modifications do influence internalisation, this does not equate to cytosolic presence and catalytic function within cells. It has been shown here that native translocation domains can be used to further enhance cytosolic translocation and increase therapeutic function. Whilst this has been shown to be the case, it should be noted here that the ligands used were not sufficiently optimised, and because of this, disulphide mediated internalisation was not as efficient at it might have the potential to be. Any future attempts to target toxins to cells using ligands will be optimised before utilisation.

The CPPs were able to increase the presence of the toxins inside the cells through pyridyl disulphide binding. Additionally, it was shown that the S25-CRD which was fused to botLcTd/A in the last chapter was functional, and that through the recombinant fusion of a second dipLC the dipLcTd-LC was able to fully conjugate to the thio-peptides. Research into other cysteine rich domains may yet yield a sequence which is able to conjugate completely, without the need to fuse an entire 25 kDa domain. Because it was found that the CPPs did increase the SNAP25 cleavage when conjugated to botulinumLcTd-S25CRD with Neuro2A, it could be that the lack of function seen with OG-assisted conjugation is due to the ligand being hidden through folding into the protein when OG concentration

decreases. The thio-CPPs used were small peptides, therefore it would be interesting to see whether this would still be the case if the thio-CPPs contained a linker between the pyridyl disulphide residue and the CPP sequence, therefore the linker would be hidden through protein re-folding but potentially not the CPP. Another possibility is that the botulinum internal cysteines conjugated to the thio-peptide are necessary for function, although as of yet there are no reports of their importance (Pirazzini et al. 2017). However, this is dismissed as any disulphide bonds would be reduced intracellularly, allowing the enzyme to function. In conclusion, whilst OG can free internal cysteines as shown in the last chapter, the modification cannot be taken for granted as being functional.

As shown in the first few figures of this chapter, LC domains can be attached to CPPs but not always effectively internalised. DipLC was able to internalise into the cytosol more efficiently than ricinLC, both through thio-CPP conjugation and LF3000. This is not entirely understood, as conjugated thio-CPP uptake theoretically should have been equal in both dipLC and ricinLC, especially seeing at the EC_{50} for both LCs is approximately equal. It may be that dipLC has a mechanism to increase endosomal escape in a way which ricinLC does not, but this has not been explored. An alternative reason could be that ricinLC is able to enter into cells is a way that dipLC is not, therefore making CPP attachment redundant. There is a report where ricinLC was found to bind to a receptor on polymorphonuclear leucocytes, which share precursors with macrophages such as J774.2 (Arfilli et al. 2010). This would explain the reasons for ricinLC and dipLC having the same EC_{50} when dipLC has a higher catalytic activity than ricinLC, with one dipLC molecule capable of killing one cell (Moynihan & Pappenheimer 1981; Yamaizumi et al. 1978). It was interesting to see that after 24 hours of dipLC incubation there was so little cytotoxicity; it has been previously documented that diphtheria is not as quick as other toxins, such as ricin, for there to be cytotoxicity, with two days appearing to be sufficient (Kageyama et al. 2002; Yamaizumi et al. 1978).

Because it requires over 24 hours for the effects of dipLC to be seen, 3 days incubation for the cells with samples appeared to be the optimal timepoint for analysis using metabolic activity assays. By doing so, it was possible to see the toxicity of diphtheria and also, because of normal cell growth in the control wells, the differences between the dosed samples and the control results. However, there are pitfalls of using such assays. Whilst it was shown in the beginning of this chapter that both MTT and alamarBlue assay readings, used for measuring metabolic activity, were directly proportional to the number of cells

counted in the wells, it has not for instance been measured how diphtheria could influence metabolic activity in itself. Another flaw in these assays is that that 40% MTT AU does not mean that of 60% cells died, it means that some cells died within the three days and therefore were unable to produce progeny; therefore, the longer one incubates the cells the higher the chance of seeing differences between the incubated samples and the control. On the other hand, it has also been shown that lower cell densities could equal lower doubling times, this may mean that the surviving cells are proliferating faster to compensate. Nonetheless, these assays are the quickest ways of collecting a large amount of accurate data; however, careful interpretation of the data is required.

Within this chapter it was found that in all samples tested there was an increase in the catalytic activity within the cells when there was the native translocation domain conjugated. Interestingly, although the translocation domains between diphtheria and botulinum share a conserved sequence, they behaved completely differently terms of intracellular catalytic function (Trujillo et al. 2006). This was evident in the large differences in SH-SY5Y and Neuro2A sensitivity to both dipLcTd and botLcTd/A. Reasons for this are unclear, but it appears that there may be differing mechanisms within the endosomes of these cells which make the translocation domains differently interact with the membrane or form pores. This could be because of altered pH within the endosomal pathway, or in the case of dipLcTd there may have been differing reactions influencing endosomal maturation or numerous other mechanisms which have yet to be investigated (Nagahama et al. 2014; Antignani & Youle 2008). Even more interestingly, there was no consistency between the two cells, with Neuro2A internalising botLcTd/A more efficiently and likewise SH-SY5Y with dipLcTd.

It was unexpected that J774.2 cells did not show any difference in intracellular catalytic activity between dipLC and dipLcTd. This could be because the increased sensitivity to toxins shown by Rust and colleagues was not necessarily just because of increased internalisation, but because of increased endosomal leakage independent of translocation domains (Rust et al. 2015). On the other hand, the reason for this lack of difference between the dipLC and dipLcTd could be because the translocation domains are unable to function for unknown reasons in these cells. The latter may be more likely owing to unregulated endosomal escape potentially resulting in cell death, but this is not always the case (Scharf et al. 2012; Erazo-Oliveras et al. 2014). Nonetheless, here there are three different cell lines each with different sensitivities to translocation domains of different

proteins; this could be a strong indication that the factors which determine endosomal escape could be as varied and as cell-specific as those that determine cell internalisation. This data suggests that a 'one size fits all' approach to endosomal escape is limited, and therefore could present problems for increasing the efficiency of the cytosolic translocation of drugs because there is another dimension of mechanisms which need to be explored. On the flip side, research into such matters could increase specificity of drug targeting and function.

Whilst GALA has been shown in numerous reports to increase endosomal escape, here there was no increase in intracellular catalytic activity of the toxins doses (Kakudo et al. 2004; Futaki et al. 2005). This could be for a number of reasons; for instance that GALA and diphtheria was added in a 1:1 ratio, however there may be more GALA peptides needed to create bigger pores for diphtheria to get through. Therefore, there is the possibility that a higher ratio of GALA to protein would result in increased cytosolic escape, which could explain why GALA-coated nanoparticles have had some degree of success (Sasaki et al. 2008; Nishimura et al. 2014). Alternatively, a smaller protein may be more successful with this method.

The ligands used here were accumulated owing to evidence suggesting that one or more of them would be able to bind to receptors and internalise into cells, transporting the conjugated toxin. Unfortunately this was not the case for any of the ligands tested. One potential reason for this is the orientation of the pyridyldithio attachment; the data in figure 4.3:D showing the difference between thio-CPBrevinMM and CPBrevinMM-thio was not completed until after ordering most of the peptides. Another reason could be that the receptors were not present on any of the cells tested, but this is unlikely as there are reports using those ligands to measure effects in the exact cell lines used (Muller et al. 2006; Lutz et al. 2006).

A potential reason that CPPs were able to increase delivery and the ligands were not could be the difference in the way that CPPs and ligands interact with the cell. For instance, CPPs interact with the cell surface, supposedly in a non-specific way, and it is possible that because of the flexibility of CPP composition not even the full length of CPP needs to be available for this interaction to occur (Bashyal et al. 2016; Zhang et al. 2015). Ligands on the other hand specifically bind to receptors, which requires a particular sequence of amino acids to be available, and potentially space to interact efficiently. However, whilst these cysteines on the botulinum-S25CRD and the dipLcTd-LC are available for

pyridyldithio-peptide conjugation, it may be that the size or obstruction of the bacterial toxin could obscure the availability of some of the amino acids in the ligand sequence. For a specific ligand sequence, this could present problems in receptor-ligand binding, however because CPPs are more flexible in their interaction and sequence they are less affected. It would be interesting therefore to use these peptides again with botulinum-S25CRD and the dipLcTd-LC and to insert a short peptide linker in between the pyridyl disulphide residue and the ligand sequence to determine whether this improves the interaction and internalisation of the thio-conjugates.

On the other hand, ligand-receptor binding on the surface of the cell does not necessarily equal internalisation, as numerous receptors function through downstream pathways which are not directed by receptor endocytosis. Another consideration in the reason for lack of internalisation of thio-ligands is that there could have been degradation of the peptides or that some were not fully functional due to manufacturing issues, this is a possibility because previously this laboratory has found success using CRH to target botLcTd/A to SH-SY5Y cells (Arsenault et al. 2013). Although the results for the thio-ligand conjugation have not been desirable, as shown in the previous chapter and through CPP conjugated delivery, the methodology does hold potential. Therefore, through screening peptide libraries against desired cells it would theoretically be possible to find suitable peptides to modify and direct protein toxins; then, the pyridyl disulphide group and potentially a linker can be attached at a location which would not interfere with the cell binding.

There was a large difference across all three cell lines in the amount of FITC-CPP was present in the cells and the subsequent uptake of enzyme-thio-CPPs. This was surprising; although it has been reported that macrophages such as J774.2 have increased macropinocytosis, no difference was expected between Neuro2A and SH-SY5Y (Jones 2007). This points to the possibility of cell specificity, which is unexpected given the nature of CPPs. It could be that receptors exist on Neuro2A which do not on SH-SY5Y, or that some of the mechanisms of cell entry discussed in the introduction are more efficient in one cell than the other. This is supported by other studies comparing CPPs between cell lines and also finding a large variance in both the uptake efficiency and cytotoxicity of CPPs (Mussbach et al. 2011). This data highlights a requirement to further investigate the bioactive conformation of CPPs and how this influences the cell-uptake based on their specific biology and biochemistry.

The mCherry-S25CRD conjugated to CPPs was able to greatly increase the amount of mCherry-S25CRD into macrophages as shown in figure 4.5; however, it then begs the question of how this occurred given the size of mCherry. Looking back to Chapter 1, it was reasoned that there were most likely several mechanisms where CPPs internalise depending on type and concentration, although only a few of them appear to be compatible with the transportation of the conjoined protein. As all concentrations used were under 5 μM, enhanced macropinocytosis is likely used at least in part and it would have been possible for the conjugated protein to have been also taken up (Fischer et al. 2004; Chao & Raines 2011). Whilst it has been shown that CPPs can interact with the cell membranes and form pores, it is unlikely that this mechanism was used as the pore would not be big enough for the translocation of the toxin (Herce & Garcia 2007). On the other hand, the 'inverted-micelle' mechanism, where electrostatic reactions between the lipid bilayer and CPPs cause it to bind to the bilayer and resulting in encapsulation is another method where the CPP could have been internalised with the conjugated toxin (Alves et al. 2008).

Figure 4.5 may have shown increase in mCherry-S25CRD internalisation into macrophages when conjugated to thio-CPPs, however it also suggested that the problem with CPPs lies not in internalisation, but in endosomal escape. This data was supported by other figures in this chapter showing that the catalytic activity of the delivered toxins in the cells is not what it should be in the case of efficient delivery of such toxic proteins. There have been ways proposed to enhance the endosomal escape potential of CPPs, for instance, the addition of histidine to CPPs such as TAT increases endosmosis and subsequent endosome rupturing via proton buffering (Lo & Wang 2008). Endosomolytic agent would be potentially more capable of facilitating the endosomal escape of large toxins than pore-forming agents such as GALA, but could result increased undesirable cell toxicity (Lönn et al. 2016). On the other hand, the data did show that the addition of translocation domains was able to increase the amount of catalytic activity. So, maybe a three-pronged approach needs to be adopted for efficient drug delivery, with the toxin, the internalisation domain and the endosomal escape domain forming an effective multi-functioning protein complex.

In conclusion, through the conjugation of toxic protein domains to peptides via disulphide conjugation, it has been found that CPPs are able to deliver into the cells, however their mechanisms of endosomal escape are limited. By further exploring this, it was found that

translocation domains can enhance the intracellular catalytic activity of the toxic proteins, presumably by facilitating endosomal escape. Moreover, through cysteine attachment to toxin LcTd domains it was possible for CPPs to further enhance the delivery of the toxins, although there appears to be a degree of cell specificity with CPP delivery. Unfortunately, the thio-ligand delivery was unsuccessful, but owing to the CPP data and the conjugation data from the previous chapter, it appears that the methodology has potential; perhaps if ligands were screened or optimised with specific cells and then synthesised with long linkers before use there could be efficient delivery of toxin LcTds. One drawback to using translocation domains however is that it negates the necessity for a pyridyldithio-conjugated peptide; one of the main benefits of conjugating via pyridyl disulphide was the cleavable linker formed between the targeting domain and the toxin, however endogenous LcTd domains have a disulphide bond in between. Because the light chain will be cleaved from the translocation domain in the endosomes anyway, recombinant attachment of targeting proteins or peptides could be used. Nonetheless, thio-peptides could be useful as a library of modifications which could be added to a variety of proteins in a quick and stable way as a method of screening. As previously mentioned, this method only utilises peptide sequences for pyridyl disulphide attachment; therefore, for protein ligands a different strategy would be required. Moreover, there is still demand for a system where more than two domains can be conjugated at the same time, preferably in one reaction. Therefore, the SNARE stapling method will be investigated to determine whether these needs can be addressed.

Chapter 5: Utilising SNARE-linking as a platform for ligand dependant delivery.

5.1 Introduction

As previously discussed, a big limiting factor with the pyridyl disulphide conjugation method used in the previous chapter is that only peptides could be attached with the pyridyldithio group. However, by using the stapling proteins optimised in figures 3.9-11 it is possible to recombinantly bind either toxin domains or ligand proteins regardless of size. By doing so, it is hypothesised that complexes of two or three proteins can be linked together through SNARE stapling. As it can be seen from the introduction table 1.2, there are numerous different ligands that could be used to target these linked complexes to neuroblastoma cell lines and facilitate internalisation. As stated previously, protein ligands are good for targeting into cells as proof of concept because they bind to endogenous receptors efficiently and are easy to produce through plasmid expression in competent bacteria.

Up until this point, only ricinLC has been successfully conjugated to the SNARE complex both through recombinant and pyridyldithio attachment. Because of the data in the previous chapter, I will also be using translocation domains in this section to ensure more efficient delivery of toxins into the cytosol. It was decided that because of the translocation domain being attached to the light chain of both diphtheria and botulinum toxins through an endogenous disulphide bonds, that the stapling linkers could be recombinantly fused to the toxin translocation domains without interfering with the light chain catalytic function. Through the production of ligands and toxin domains with recombinantly fused staples (protein-staples), this chapter aims first to identify a potential ligand which can be used to target and internalise into neuroblastoma. Then, it will look at the construction of the SNARE complexes with chosen ligands and toxin LcTd domains. From this, the complexes can be incubated with cells to determine how relatively efficient they are at facilitating cytosolic catalytic function of the stapled toxin domains. The main objective of this chapter is to create a complex with three domains conjugated, for them to retain their functions and behave complementary to each other and to allow the binding and internalisation into specific cells, delivering linked toxic enzymes into the cytosol.

5.2 Results

5.2.1 Recombinant CNTF and EGF fused botulinumLcTd/A is able to cleave SNAP25 in neuroblastoma cell lines

In order to identify ligands which would be suitable to use with the selected cell types, recombinantly fused protein samples made in house were first run on an SDS-PAGE gel to check purify and size of the protein. Figure 5.1:A shows that because many of the peptides supposedly conjugated to botLcTd/A are 3kDa or less, there is no visible way of determining whether they are present. CNTF and EGF are both lager, and there is a difference in band migration between these samples and the control botLcTd/A. Unfortunately, both adrenomedullin and TNFα are 6kDa or larger and therefore a difference would be expected, however it is clear from the SDS-PAGE that they have not been successfully fused due to either breakdown or an error in expression. Nonetheless, the remaining samples were incubated at 20 nM with SH-SY5Y and Neuro2A cells for 72 hours before the cells were harvested and lysed to run on a western blot (fig. 5.1:B). The membrane showed that both Neuro2A and SH-SY5Y showed significant SNAP25 cleavage when exposed to recombinantly fused botLcTd/A-EGF, but botLcTd/A-CNTF only cleaved SNAP25 in SH-SY5Y cells. This result therefore gives the means to potentially target cells specifically owing to the different cell responses to the ligands. To complement this, LA-N-5 human neuroblastoma cell line was introduced and also incubated with both botLcTd/A-EGF and botLcTd/A-CNTF; in contrast to Neuro2A cells, only botLcTd/A-CNTF was able to cleave SNAP25 in these cells (fig. 5.1:C).

From this, to confirm suspicions that the ligands were internalising through the presence of endogenous cell surface receptors, the antibodies for both CNTFR and EGFR were acquired. The cell lysates of all three neuroblastoma cell lines were blotted with either antibodies, before the membranes were re-blotted with SNAP25 as a control. Because CNTF also can bind to IL-6, there was a concern that there could be little, if any, CNTFR present on SH-SY5Y or LA-N-5 cells; however, it was shown that both cells had CNTFR present. Interestingly, there was a small amount of CNTFR present in Neuro2A cells, however at this stage the location is undetermined. On the other hand, EGFR was shown to be highly present on both SH-SY5Y and Neuro2A cells. Both antibodies appeared to be clean with the expected band size and with little non-specific binding (fig 5.1:D).

Cells were then stained to visualise the presence of the receptors in the cells. Both CNTFR and EGFR appeared to be spread throughout SH-SY5Y cells, including presence in the

neurites. EGFR was also found throughout the Neuro2A cells, but CNTFR showed little presence in these cells. The inverse was true of LA-N-5 cells, where CNTFR presence was very evident, however not so with EGFR (fig 5.1:E).

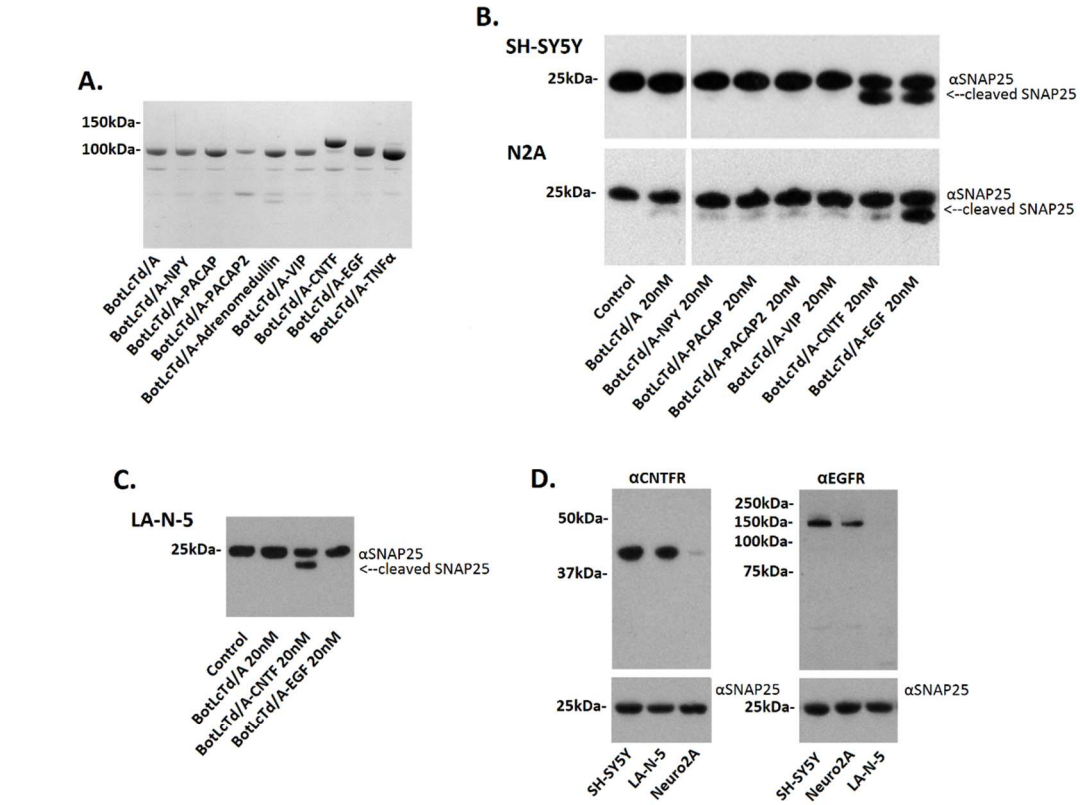

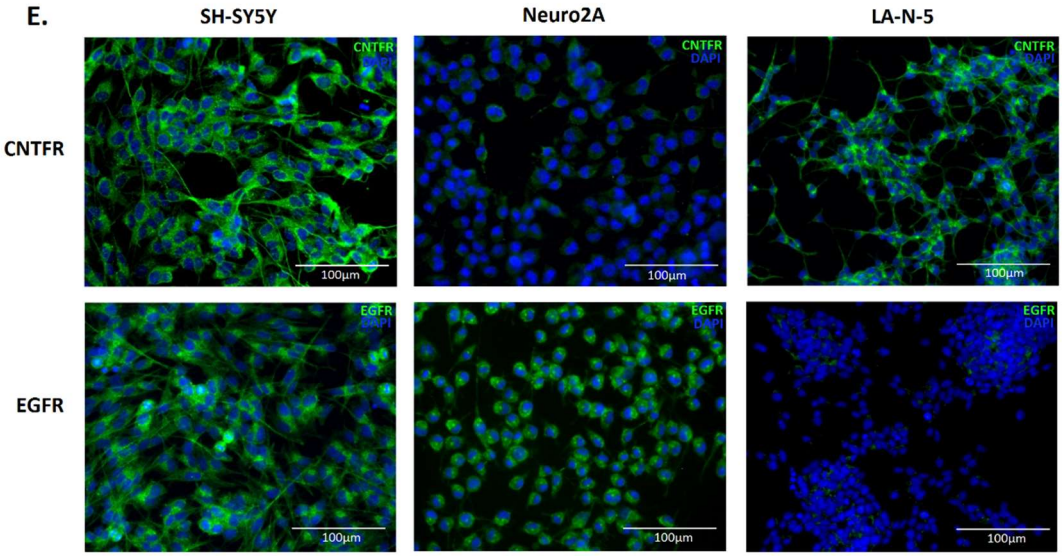

Figure 5.1 – Identification of ligands for potential use in targeting complexes to neuroblastoma cells

A) SDS-PAGE showing the recombinantly fused botLcTd/A-ligand proteins produced. B) Western blot showing SH-SY5Y and Neuro2A cells after 72 hours incubated with botLcTd/A-ligands (N=2). C) Western blot of LA-N-5 neuroblastoma cells after application of either botLcTd/A-EGF or botLcTd/A-CNTF (N=2). D) Western blot staining lysates of neuroblastoma cell lines with either EGFR or CNTFR with SNAP25 as control. E) Images taken using epifluorescent microscope of the SH-SY5Y, Neuro2A and LA-N-5 cells with CNTFR or EGFR staining. Hoechst: 20 ms, EGFR: 4000 ms, CNTF: 4000 ms. (N=2).

It has been shown here that both EGF and CNTF are potentially good candidates for targeting stapled complexes to specific neuroblastoma cell lines. However, it is important to consider the potential issues with these endogenous ligands; for example, EGF has been shown to activate cell proliferation (Ho et al. 2005). On the other hand, CNTF may increase differentiation in the cells causing decreased growth and increased spindle morphology (Sleeman et al. 2000). Therefore, both ligands will need to be tested to determine the effects they have on these neuroblastoma cells. Nonetheless, both ligand varieties show potential as proof of concept targeting domains for their own utilisation in neuroblastoma cell targeting as well as investigating the SNARE linking method.

5.2.2 Investigating CNTF and EGF controls with Neuro2A and SH-SY5Y cells

The desired individual components of the linked complexes were firstly made and applied to cells to determine any effect upon proliferation and morphology. As well as syntaxin, SNAP25 and brevin, recombinantly fused CNTF-syntaxin, CNTF-Brevin and EGF-Brevin (ligand-staples) were also produced (fig. 5.2:A). Figure 5.2:B indicates that there was no alteration in the growth of Neuro2A cells for any concentrations tested of any of the individual components; however, with SH-SY5Y cells there was increased proliferation with the addition of EGF containing proteins. The incubation of CNTF containing proteins did not appear to decrease the proliferation of cells. Moreover, images taken of SH-SY5Y cells with and without CNTF-brevin showed that there was no observable difference in neurite

outgrowth or soma size between the two samples, further indicating that differentiation of the cells is not occurring in these conditions (fig. 5.2:C).

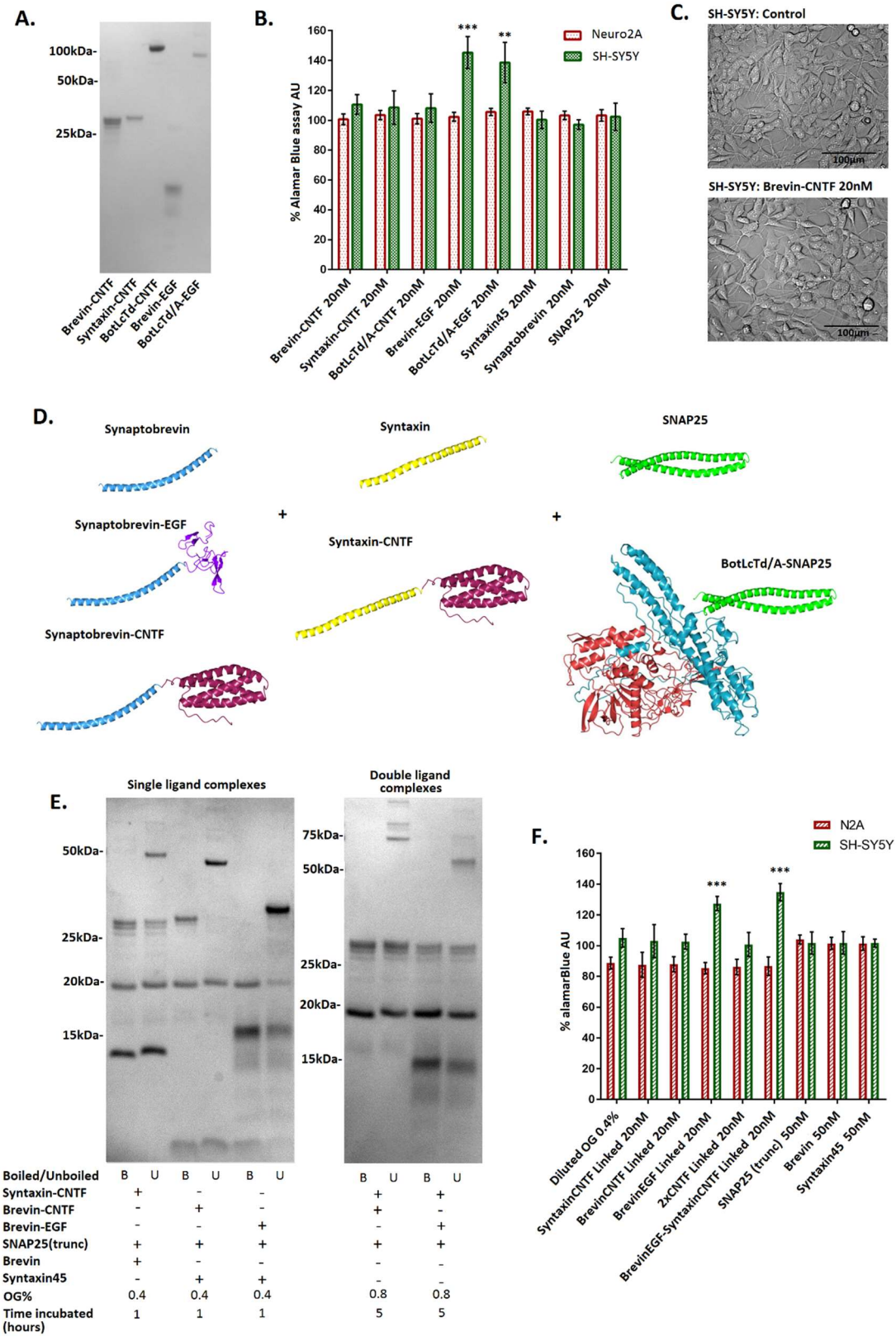

Figure 5.2 - Investigating the effects of CNTF and EGF have on SH-SY5Y and Neuro2A cells.

A) *SDS-PAGE showing the proteins to be used in SNARE formation. B) AlamarBlue assay with SH-SY5Y and Neuro2A cells where the SNARE components were incubated for 72 hours with the cells to determine whether there are any changes in proliferation. Significance measured by Student T-test for each concentration against the syntaxin45 20 nM sample (n=3, N=3). C) Brightfield images of SH-SY5Y cells either with or without incubating with Brevin-CNTF over 72 hours, showing no observable difference in neurite outgrowth or soma size. D) Schematic showing the SNARE peptides and the recombinantly fused proteins which have been successfully made and the possible combinations for complex linking. D) SDS-PAGE looking at the formation of both x1 and x2 ligand stapled complexes (N=3). E) AlamarBlue assay looking at how the addition of the linked complexes and mixed components influences alamarBlue AU % after 72 hours incubation. Significance of OG containing samples measured by Student T-test for each concentration against the 0.4% OG control sample (n=3, N=3). Significance for statistical analysis: P>0.05 = NS P<0.05 = * P<0.01 = ** P<0.001=***. CNTF PDB ID: 1CNT. EGF PDB ID: 1JL9. BotLcTd/A PDB ID: 3BTA. SNARE PDB ID: 5W5D (McNicholas et al. 2011; Berman et al. 2000).*

It was then important to determine whether linked complexes could be made from the ligand-staple proteins. Figure 5.3:D shows a schematic of the different versions of syntaxin, brevin and SNAP25 which were produced and the possible combinations of each of the three components that could be attempted. It was first decided to determine how well ligand-complexes formed without toxin attachment. After 1 hour incubation, successful linking could be seen in all three samples where one ligand-staple formed a complex with complementary SNARE proteins (fig. 5.2:E). It was apparent here that only CNTF-brevin was able to fully form into the complex, as the other samples showed a proportion of unlinked components of all three varieties remaining after 1 hour, especially CNTF-syx. Additionally, the linking of more than one ligand was attempted; discouragingly, it appeared that there was significantly less complex formation in these samples, even in the presence of increased OG % and an increased incubation time.

Nonetheless, the samples were diluted irrespective of complex formation and applied to SH-SY5Y and Neuro2A cells to determine whether the formation of complexes would influence cell growth. Because of the dilute nature of some of the ligand-staples produced,

samples of approximately 400 nM were the highest concentration which could be reliably made. Because of this, and the required 1 in 20 dilution of OG containing samples, 20 nM was the highest sample concentration applied to cells. All samples were made through incubation with 0.4% OG and 1 hour incubation. Aside from the influence of diluted OG on the Neuro2A cells, it appeared that there were no adverse effects on the cell lines when complexes or complex components combined were added (fig 5.2:F). Additionally, because complexes were being made often with the unconjugated SNARE proteins in excess, it was deemed prudent to observe whether these proteins influenced the cells at higher concentrations, which they did not.

5.2.3 CNTF-staples can be linked in a complex with botulinumLcTd/A and used to specifically target cell types.

Despite the less than desirable efficiency in forming the single and double ligand linked complexes in the previous section, it is possible that different combinations of different linking components may have alternative linking efficiencies. Therefore, botulinumLcTd/A-SNAP25 (botLcTd/A-S25) was produced and incubated with staple proteins to form complexes. It should be understood that this botLcTd/A is catalytically active and does cleave the 9 amino acids at the C-terminus of the fused SNAP25 which it is recombinantly fused to; however, it has been previously shown that provided the botLcTd/A is bound to the N-terminus of the protein there is no effect on SNARE formation (Arsenault et al. 2013; Ferrari et al. 2013). Figure 5.3:A shows that 100% of botLcTd/A-S25 was able to successfully form complexes. BotLcTd/A-S25 was then incubated with the CNTF-staples in order to successfully form linked CNTFbrev-botLcTd/A, linked CNTFsyx-botLcTd/A and linked CNTFx2-BotLcTd/A.

As described in the methods, using SDS-PAGE the concentration for each linked sample is measured by running alongside BSA standards. Therefore, through using band intensity analysis, the approximate mg/ml and the band size (kDa) can be used to work out the molar concentration before preparing samples for incubating with cells. In doing this one can also find out the % of the botLcTd/A-S25 which has been used up to make the linked complexes. In instances where the SNARE formation was less than 75% the sample was not used.

Successfully SNARE linked samples were then tested to determine whether the CNTF ligand was able to direct the botLcTd/A domain into SH-SY5Y cells in a way comparable to

recombinantly fused botLcTd/A-CNTF. There was no significant toxicity or observable alteration in cell morphology in any of the cell samples tested when incubated with SH-SY5Y cells for 3 days (fig 5.3:B-C). Figure 5.3:D investigated the SNAP25 cleavage of complex added Neuro2A and SH-SY5Y cells after 72 hours incubation. It was found that, as predicted, there was no increase in cleavage in any of the Neuro2A samples when botLcTd/A-S25 was linked to CNTF-staple. However, there was a large increase in the SNAP25 cleavage in SH-SY5Y when botLcTd/A linked constructs were directed with CNTF. There was no distinction between either of the two CNTFx1-botLcTd/A linked samples; because of this, the term 'linked CNTFx1-botLcTd/A' will refer to linked CNTFbrev-botLcTd/A henceforth unless otherwise stated.

Titrations of recombinantly fused botLcTd/A-CNTF up to a maximum of 50 nM showed that there was a plateauing in the cleavage of SNAP25 at higher concentrations (fig. 5.3:E-F). This could be for a number of reasons; for one, there was evidence of heterogeneity in the presence and location of CNTFR in figure 5.1 which could mean that some cells are unable to internalise CNTF-botLcTd/A complexes as much as others. It has already been established in the previous chapter that all of the SNAP25 within the cells has the potential to be cleaved (fig. 4.8); however, if there is a limitation to the amount of botLcTd/A entering the cells then there would be a limitation to the cleavage.

To determine whether this % SNAP25 cleavage could be improved upon, CNTFx1-botLcTd/A Linked was compared to the CNTFx2 version. Figure 5.3:G shows that there appeared to be an increase in SNAP25 cleavage between the two samples. These results were then quantified in Figure 5.3:H, showing that there was a significant increase in the SNAP25 cleavage at the same concentration between CNTFx1 and CNTFx2 linked botLcTd/A. Encouragingly, there was no significant difference between the CNTFx1-botLcTd/A linked and the recombinantly fused botLcTd/A-CNTF, indicating that the CNTF which is linked to the botLcTd/A-S25 remains fully functional. Moreover, because of the increase in the SNAP25 cleavage between the CNTFx1 and CNTFx2 directed botLcTd/A samples, it strongly indicated that both of the CNTF domains attached in the complex remain functional and are complementary to each other. This second linked CNTF domain evidently increased internalisation of the botLcTd/A, resulting in the increased % cleavage.

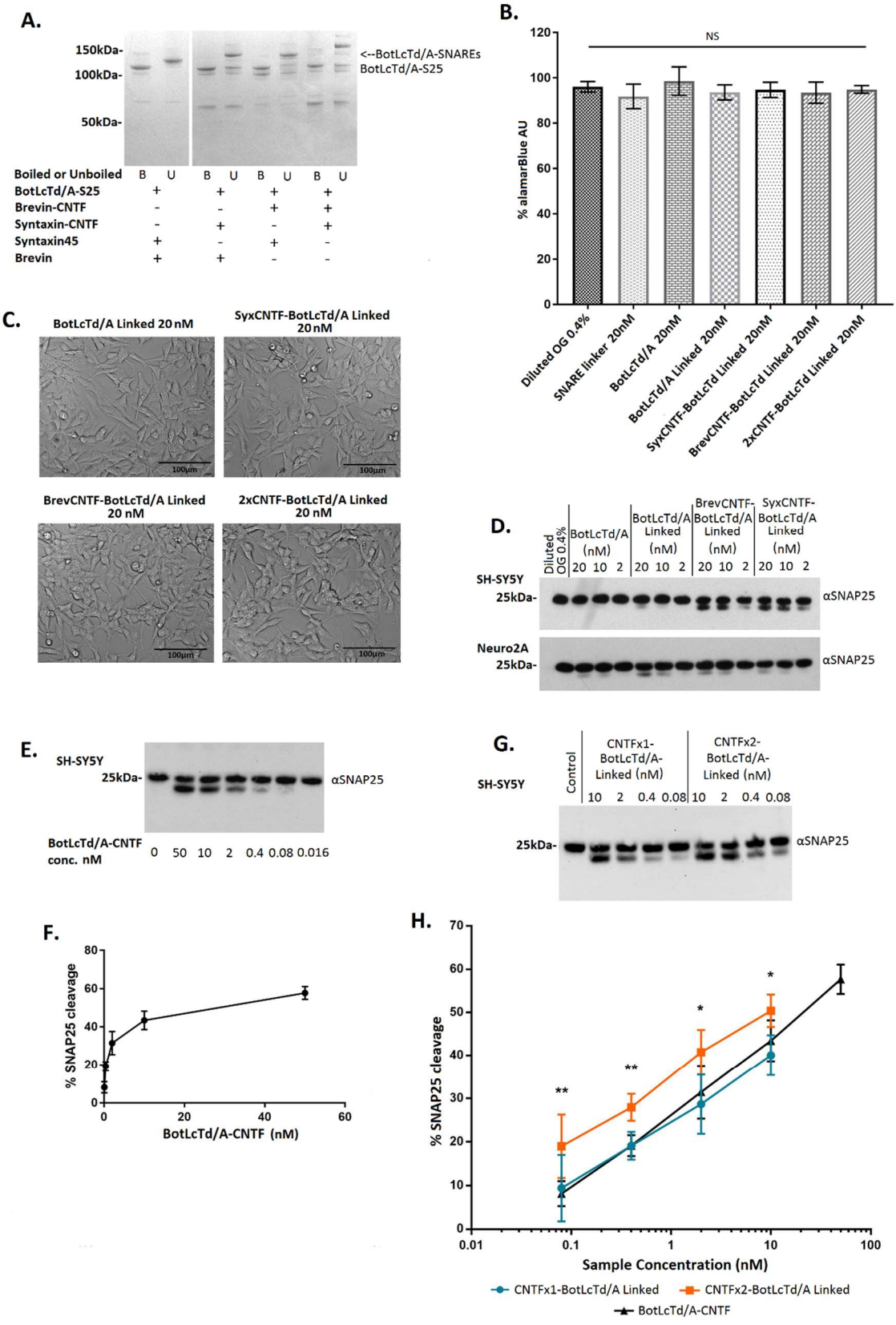
A.
150kDa-
100kDa-
50kDa-
<--BotLcTd/A-SNAREs
BotLcTd/A-S25
Boiled or Unboiled B U B U B U B U
BotLcTd/A-S25 + + + +
Brevin-CNTF - - + +
Syntaxin-CNTF - + - +
Syntaxin45 + - + -
Brevin + + - -
B.
NS
% alamarBlue AU
120
100
80
60
40
20
0
Diluted OG 0.4%
SNARE linker 20nM
BotLcTd/A 20nM
BotLcTd/A Linked 20nM
SyxCNTF-BotLcTd Linked 20nM
BrevCNTF-BotLcTd Linked 20nM
2xCNTF-BotLcTd Linked 20nM
C.
BotLcTd/A Linked 20 nM
SyxCNTF-BotLcTd/A Linked 20 nM
BrevCNTF-BotLcTd/A Linked 20 nM
2xCNTF-BotLcTd/A Linked 20 nM
100µm
D.
Diluted OG 0.4%
BotLcTd/A (nM)
BotLcTd/A Linked (nM)
BrevCNTF-BotLcTd/A Linked (nM)
SyxCNTF-BotLcTd/A Linked (nM)
20 10 2 20 10 2 20 10 2 20 10 2
SH-SY5Y
25kDa-
αSNAP25
Neuro2A
25kDa-
αSNAP25
E.
SH-SY5Y
25kDa-
αSNAP25
BotLcTd/A-CNTF conc. nM
0 50 10 2 0.4 0.08 0.016
G.
Control
CNTFx1-BotLcTd/A-Linked (nM)
CNTFx2-BotLcTd/A-Linked (nM)
10 2 0.4 0.08 10 2 0.4 0.08
SH-SY5Y
25kDa-
αSNAP25
F.
% SNAP25 cleavage
80
60
40
20
0
0 20 40 60
BotLcTd/A-CNTF (nM)
H.
% SNAP25 cleavage
70
60
50
40
30
20
10
0
0.01 0.1 1 10 100
Sample Concentration (nM)
CNTFx1-BotLcTd/A Linked
CNTFx2-BotLcTd/A Linked
BotLcTd/A-CNTF

Figure 5.3 – CNTFx2-BotLcTd/A-SNARE increases SNAP25 cleavage compared to CNTFx1-BotLcTd/A-SNARE

A) *SDS-PAGE showing the formation of linked botLcTd/A complexes with CNTF-staples (N>3). B) AlamarBlue assay showing the cell growth of samples incubated with botLcTd/A-SNAREs and CNTF-BotLcTd/A-SNAREs for 72 hours. Significance measured by one-way ANOVA across all values (n=3, N=3). C) Images of cells after incubating with samples for 3 days. D) Western blot showing cleavage of SNAP25 after 3 day incubation with linked botLcTd/A and both CNTFx1-botLcTd/A linked varieties (N=2). E-F) Western Blot and subsequent quantification of SNAP25 cleavage after 72 hours incubation with botLcTd/A-CNTF (N=3). G) Western blot showing SNAP25 cleavage after 72 hours incubation with CNTFx1-botLcTd/A linked and CNTFx2-botLcTd/A linked. H) Quantification of subfigures E and G combined. Significance measured by one-way ANOVA for each concentration (N=3). Significance for statistical analysis: P>0.05 = NS P<0.05 = * P<0.01 = ** P<0.001=***.*

5.2.4 Investigating the optimum time point and effects of accumulation for CNTF-BotLcTd/A-SNARE SNAP25 cleavage

To determine whether 72 hours was the optimum timepoint for analysing SNAP25 cleavage, it was decided stagger the addition of both linked CNTFx1-BotLcTd/A and CNTFx2-BotLcTd/A into cell wells over 3 days. It was found that there was no cleavage after 6 hours incubation and there was little at 24 hours for either complex (fig. 5.4:A-B). Therefore, this data supports the use of 72 hours as the optimum timepoint for analysis

As well as incubating doses for a 72 hour timepoint, it was decided to attempt to increase SNAP25 cleavage by adding an additional sample at 24 hours. This cumulative addition of samples onto cells did not increase SNAP25 cleavage as there was no significant difference between cells with samples added at 72 hours and those added at 72 and 24 hours (fig. 5.4:C-D).

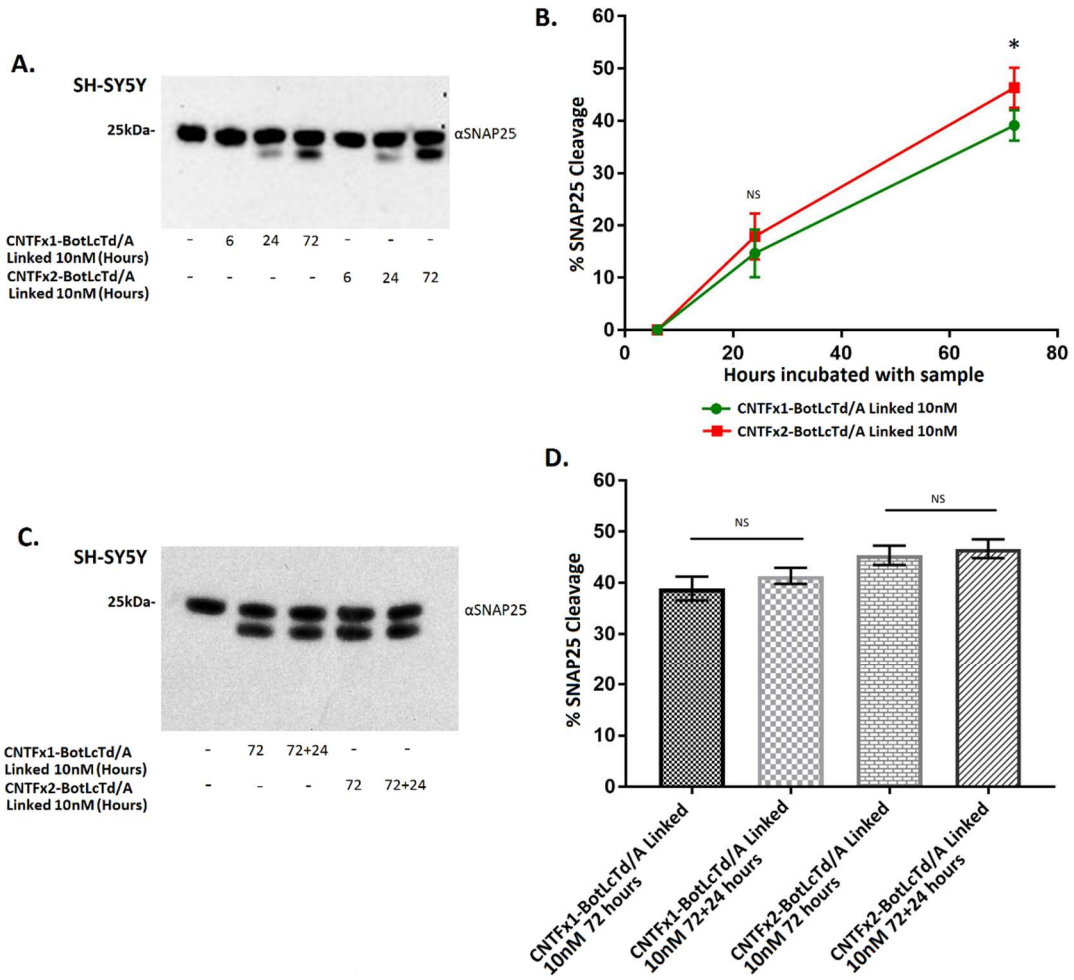

Figure 5.4 - Investigating the timepoints and accumulation of CNTF linked botLcTd/A complexes

A) *Western blot showing the timepoints of cells incubated with CNTFx1-botLcTd/A linked and CNTFx2-botLcTd/A linked. B) Quantification of subfigure A. Significance measured by Student T-test between samples of the same concentration (N=3). C) Western blot showing the effects of SNAP25 cleavage though cumulative addition of CNTFx1-botLcTd/A linked and CNTFx2-BotLcTd/A linked at 10 nM at 72 hours and 24 hours. D) Quantification of subfigure C. Significance measured by Student T-test between samples added at 72 and 72+24 hours (N=3). Significance for statistical analysis: P>0.05 = NS P<0.05 = * P<0.01 = ** P<0.001=***.*

5.2.5 SH-SY5Y culture is a heterogeneous population.

In order to investigate the reason for % SNAP25 cleavage plateauing at high concentrations of CNTF linked botLcTd/A and recombinantly fused botLcTd/A-CNTF, an antibody was obtained which was specific to the cleaved form of SNAP25 from botLcTd/A (αC-SNAP25) (fig. 5.5:A). This was then used alongside a mouse total αSNAP25 antibody and both used for immunocytochemistry (ICC) (fig. 5.5:B). Both of the secondary antibodies used did not show any background in SH-SY5Y cells when used without primary antibodies (fig. 5.5:C).

SH-SY5Y cells were either incubated with buffer A, 2 nM botLcTd/A or 2 nM linked CNTFx2-botLcTd/A for 72 hours and were then stained with both αSNAP25 and αC-SNAP25 and imaged by confocal microscope. It was shown that the total αSNAP25 presence within cells was not homogenous in any of the cell populations, but was present in every cell. αC-SNAP25 staining was not observed in the buffer A incubated cells and there was negligible staining in the 2 nM non-ligand attached botLcTd/A incubated cells (fig 5.5:D-E). On the other hand, there was significant αC-SNAP25 staining in the 2 nM CNTFx2-BotLcTd/A stapled sample; whilst there appeared to be SNAP25 cleavage in most of these cells, the presence was heterogeneous. This staining of αC-SNAP25 appeared to be independent of the amount of SNAP25 in the cells. These images support the hypothesis that the SH-SY5Y cells are a heterogeneous population in their internalisation of CNTF linked botLcTd/A, and that this is at least in part the reason for the plateauing of partial SNAP25 cleavage.

To further determine the nature of this heterogeneity, images were taken with SH-SY5Y cells stained with CNTFR antibody with αSNAP25 as control. In undosed control cells, the presence of CNTFR appeared to be throughout the cells, with there being a large amount in the neurites and at the cell surface (as indicated); however it should be noted that some cells appeared to have a higher presence of CNTFR than others (fig. 5.6:A). There was no observable difference between the control cells and those treated with non-ligand linked botLcTd/A 2 nM for 72 hours (fig. 5.6:B). When cells had been incubated with linked CNTFx2-botLcTd/A 2 nM there was a substantial decrease in the CNTFR quantity accompanied with a shift in the location of CNTFR mostly from the cell surface and neurites into the soma (as indicated) (fig. 5.6:C).

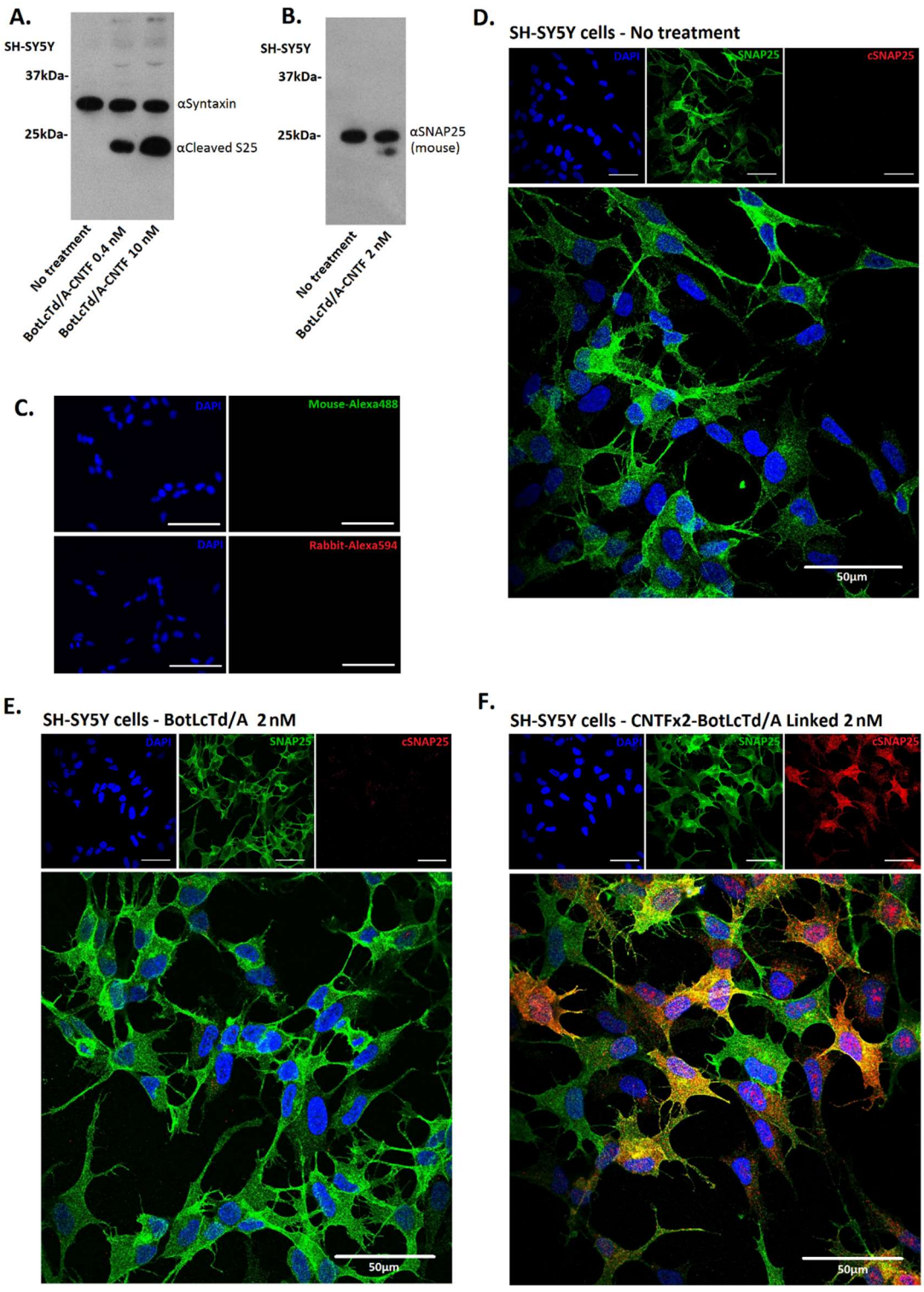
A.
SH-SY5Y
37kDa-
25kDa-
αSyntaxin
αCleaved S25
No treatment
BotLcTd/A-CNTF 0.4 nM
BotLcTd/A-CNTF 10 nM
B.
SH-SY5Y
37kDa-
25kDa-
αSNAP25
(mouse)
No treatment
BotLcTd/A-CNTF 2 nM
C.
DAPI
Mouse-Alexa488
DAPI
Rabbit-Alexa594
D.
SH-SY5Y cells - No treatment
DAPI
SNAP25
cSNAP25
50µm
E.
SH-SY5Y cells - BotLcTd/A 2 nM
DAPI
SNAP25
cSNAP25
50µm
F.
SH-SY5Y cells - CNTFx2-BotLcTd/A Linked 2 nM
DAPI
SNAP25
cSNAP25
50µm

Figure 5.5 – SH-SY5Y culture is a heterogeneous sample.

A-B) Western blot showing the αCleavedSNAP25 (αC-SNAP25) rabbit and total αSNAP25 mouse antibodies with SH-SY5Y cell lysates, with αSyntaxin1 used as a loading control. C) Images showing secondary antibodies Mouse-Alexa488 and Rabbit-Alexa594 with DAPI on cells without primary antibodies (epifluorescent microscope: 4000 ms. Obj. x40. Scale bars 100µm). D-F) Buffer A, 2 nM botLcTd and 2 nM CNTFx2-BotLcTd/A linked complex treated SH-SY5Y cells (72 hours), stained with αSNAP25 (mouse) and αC-SNAP25 (Rabbit) and DAPI. Inset scale bars 50 µm (see methods section 2.5 for details of confocal microscopy).

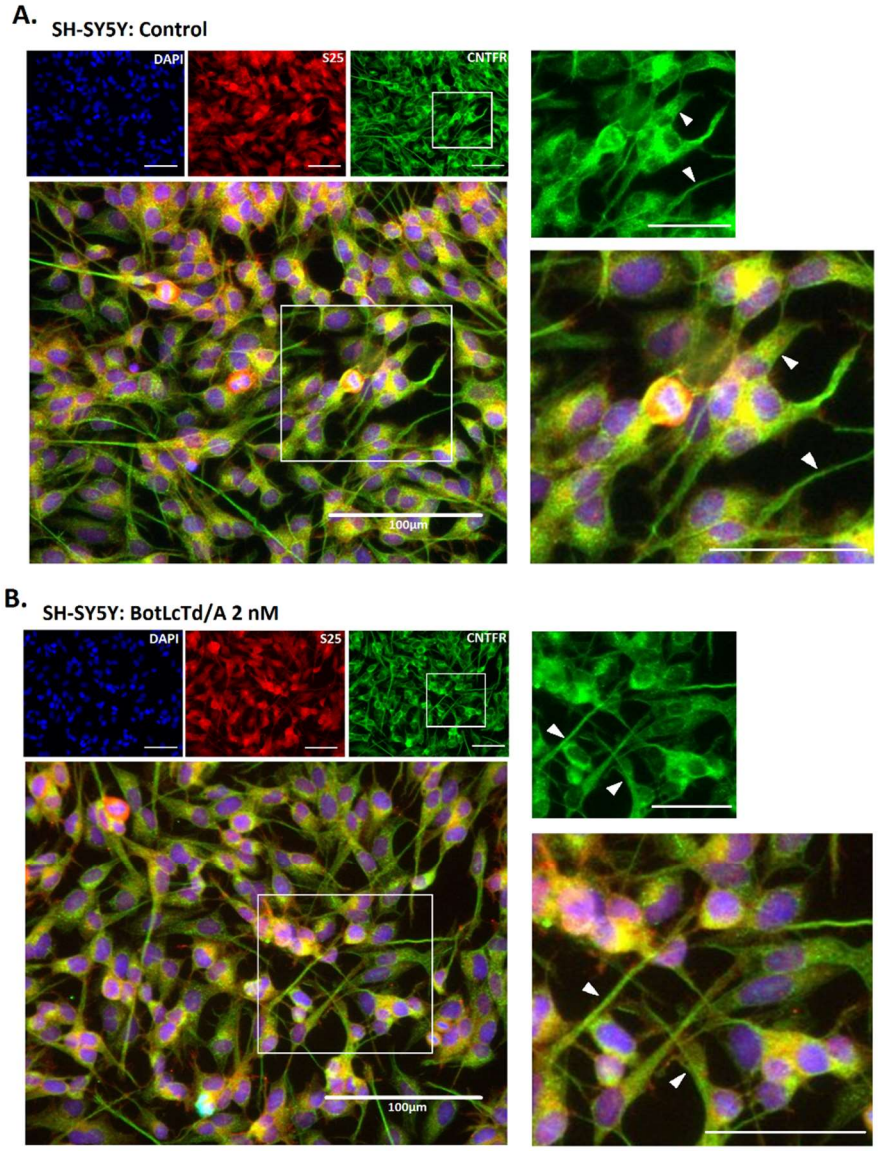

C.

SH-SY5Y: CNTFx2-botLcTd/A 2 nM

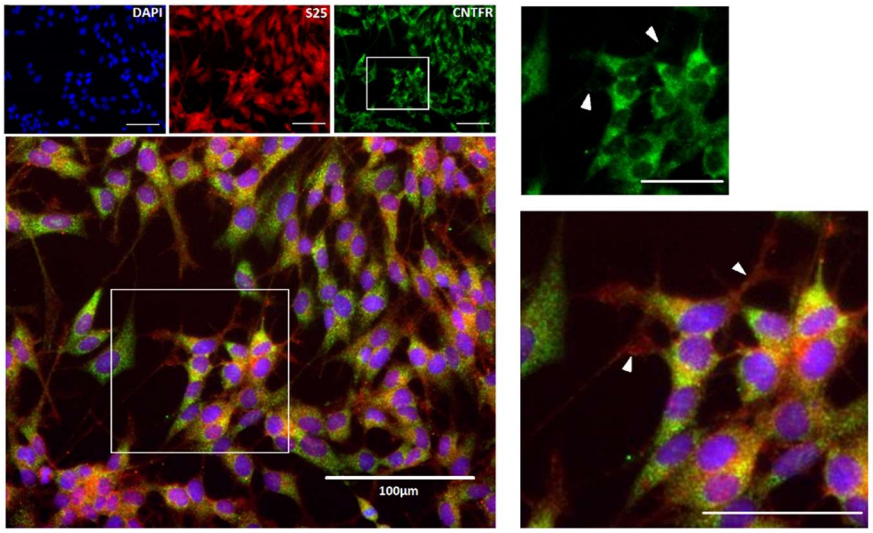

D.

SH-SY5Y: BrevinCNTF 2 nM

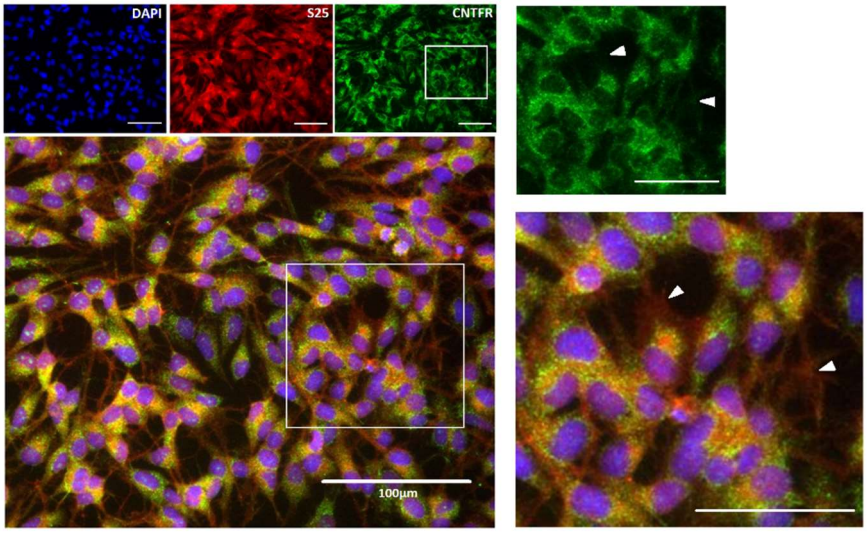

E.

SH-SY5Y: BotLcTd/A-EGF 2 nM

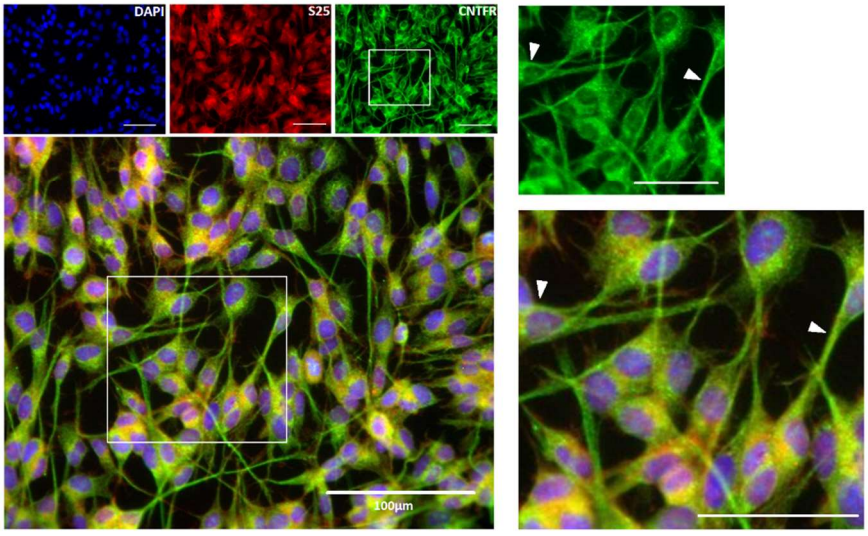

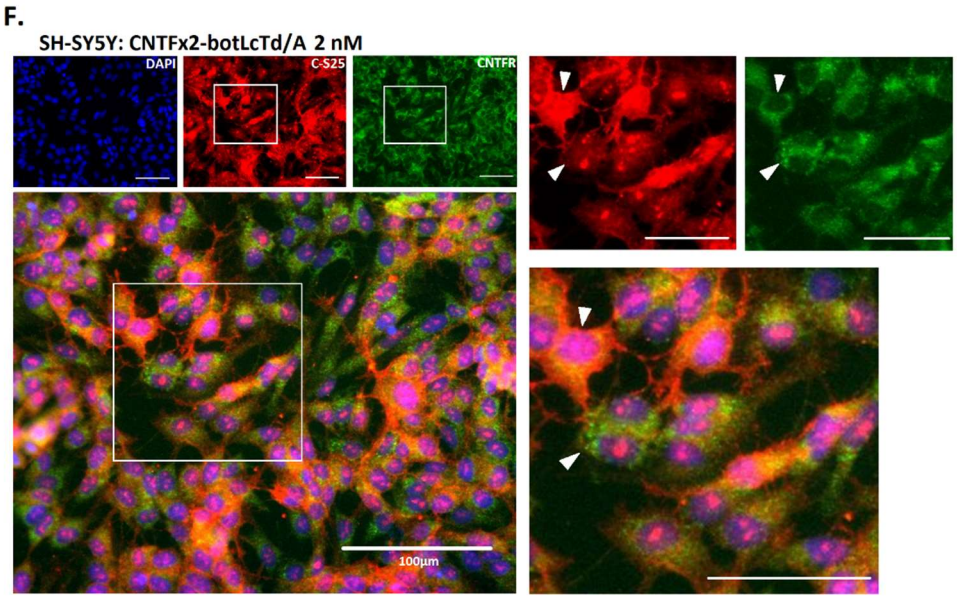

Figure 5.6 – Imaging CNTFR staining in treated cells

A-E) Images taken using epifluorescent microscope of αCNTFR staining (4000 ms) and control αSNAP25 staining (200 ms) in SH-SY5Y cells when incubated for 72 hours with various samples at 2 nM, showing relative quantity and presence of CNTFR in cell membranes and neurites. Neurites and cell edges indicates with arrows (N=2). F) Images taken using epifluorescent microscope of αCNTFR staining (4000 ms) and αC-SNAP25 staining (200 ms) in SH-SY5Y cells after incubating with CNTFRx2-botLcTd/A linked 2 nM for 72 hours. Arrows indicate heterogeneity of αC-SNAP25 and the consistency of αCNTFR staining. All inset scale bars 50 µm, all obj. x40.

To determine whether the shift in the presence and location of CNTFR was dependant on botLcTd/A internalisation or CNTF binding, CNTF-brevin 2 nM was incubated with the cells, as well as recombinant botLcTd/A-EGF separately. It can be seen in figure 5.6:D that when CNTF-brevin 2 nM was applied there was an internalisation of the CNTFR in a way similar to that seen in figure 5.6:C. Moreover, when botLcTd/A-EGF 2 nM was incubated there was no difference observed in the location of CNTFR when compared to the control or botLcTd/A 2 nM samples (fig. 5.6:E). In those cells which were treated with CNTF containing samples, the presence of CNTFR appeared to be less heterogeneous than those without CNTF (as indicated). From this, there appeared to be no difference in CNTFR presence

between those cells which showed high amounts of cleaved SNAP25 and those which showed no or little cleaved SNAP25 (fig. 5.6:F). Therefore, it cannot be concluded whether those cells with initially high CNTFR were more likely to have high SNAP25 cleavage.

5.2.6 EGF linked complexes are unable to internalise in SH-SY5Y or Neuro2A cells.

As figure 5.1 had previously demonstrated by immunoblotting that recombinantly fused botLcTd/A-EGF was able to cleave SNAP25 in both SH-SY5Y and Neuro2A cells, it was decided that this warranted further investigation. Fused botLcTd/A-EGF titrations were incubated with both SH-SY5Y and Neuro2A cell lines and it was found that there was successful SNAP25 cleavage in both which could be observed at 2 - 0.4 nM (fig. 5.7:A). Interestingly, there was a higher gradient at the higher concentrations on the graph relating botLcTd/A-EGF and % cleaved SNAP25 than when compared to botLcTd/A-CNTF (fig. 5.7:B). It could be that this decreased plateauing is due to differences in location and expression of EGFR compared to CNTFR.

Using brevin-EGF, linked complexes were made to bind EGF to botLcTd/A-S25 and CNTF-syntaxin. It was found that whilst EGF-BotLcTd/A linked was able to form efficiently, there was little formation of EGF-CNTF-BotLcTd/A (fig. 5.7:C). This was unfortunate as it would have been interesting to see whether a complex with two different linked ligands could target the two separate cell lines and how this would have influenced SNAP25 cleavage. Nonetheless, EGF-BotLcTd/A linked was applied to both Neuro2A and SH-SY5Y; it was found through western blotting that there was little or no cleavage in any of the samples (fig 5.7:D). This was an unexpected observation, as it was clear that EGF-BotLcTd/A linked was able to successfully form. EGF-brevin is believed to bind to receptors and be functional because of its influence on SH-SY5Y growth in figure 5.2. However, a possible reason for the lack of stapled-complex effects could have been that EGF is smaller than CNTF and therefore when the complex is formed the EGF binding domain is smothered by the formed complex. It is a useful demonstration that it is not just complex linking which is a factor in SNARE stapling success, as it is possible that even successful stapling can result in malformed complexes.

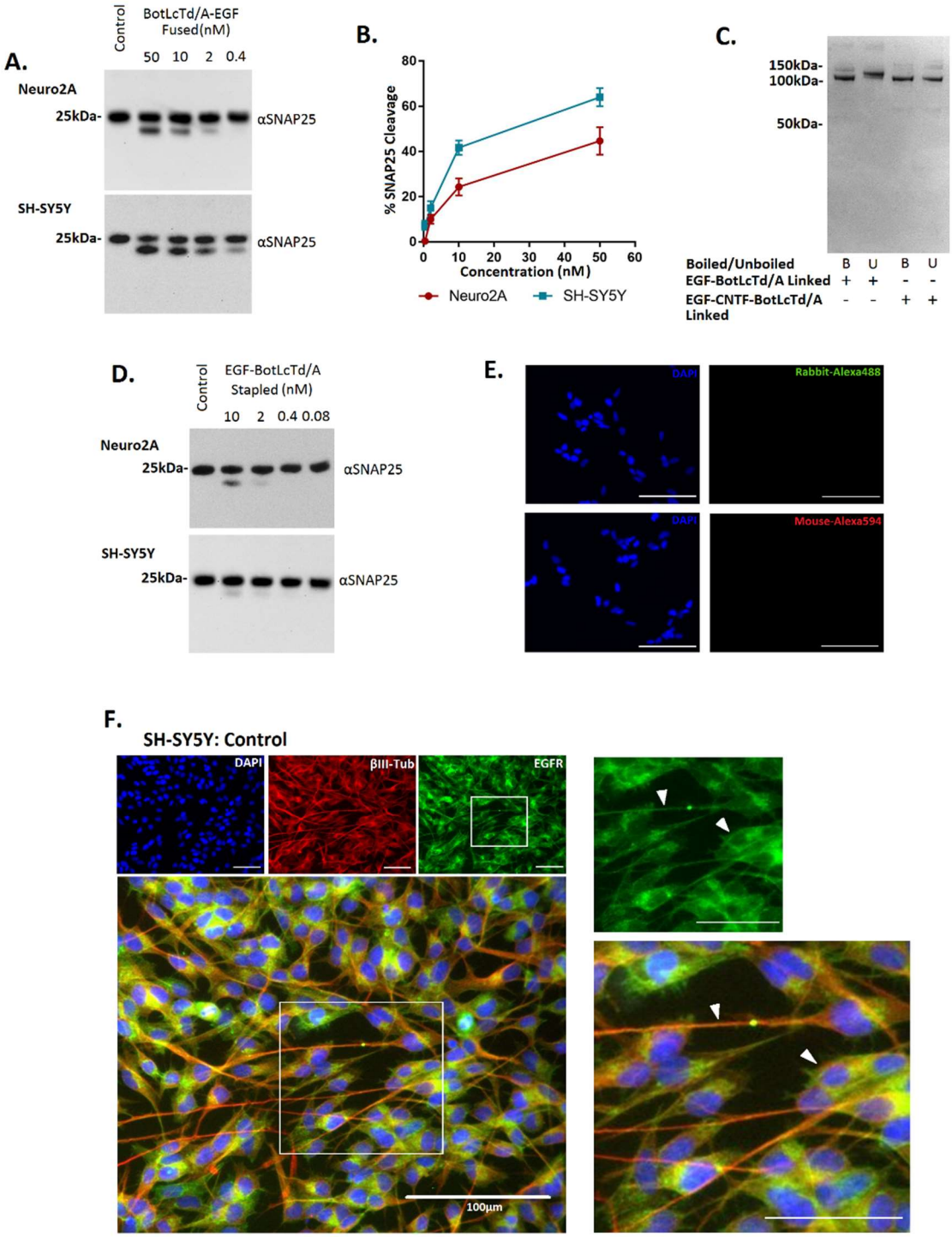
A.
Control
BotLcTd/A-EGF Fused(nM)
50 10 2 0.4
Neuro2A
25kDa-
αSNAP25
SH-SY5Y
25kDa-
αSNAP25
B.
% SNAP25 Cleavage
0
20
40
60
80
0 10 20 30 40 50 60
Concentration (nM)
Neuro2A
SH-SY5Y
C.
150kDa-
100kDa-
50kDa-
Boiled/Unboiled B U B U
EGF-BotLcTd/A Linked + + - -
EGF-CNTF-BotLcTd/A Linked - - + +
D.
Control
EGF-BotLcTd/A Stapled (nM)
10 2 0.4 0.08
Neuro2A
25kDa-
αSNAP25
SH-SY5Y
25kDa-
αSNAP25
E.
DAPI
Rabbit-Alexa488
DAPI
Mouse-Alexa594
F.
SH-SY5Y: Control
DAPI
βIII-Tub
EGFR
100μm

G.

SH-SY5Y: BotLcTd/A-EGF Fused 10 nM

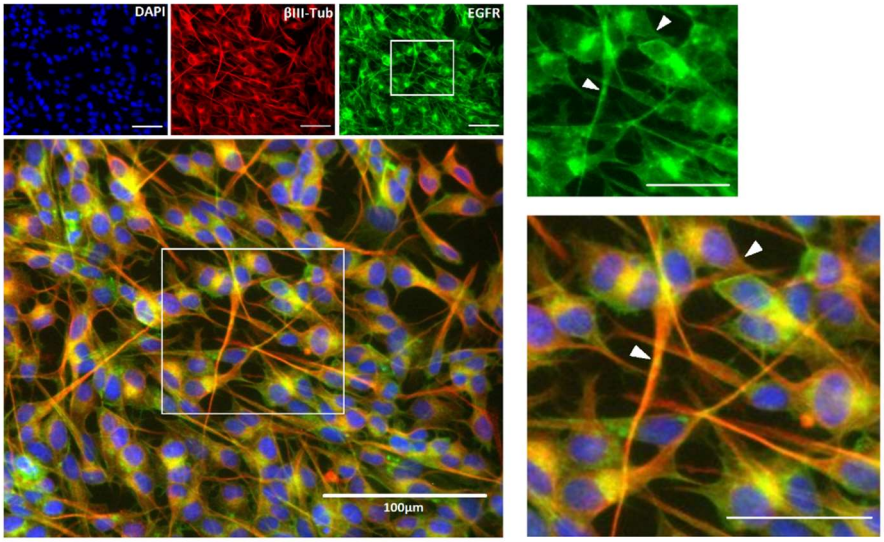

H.

Neuro2A: Control

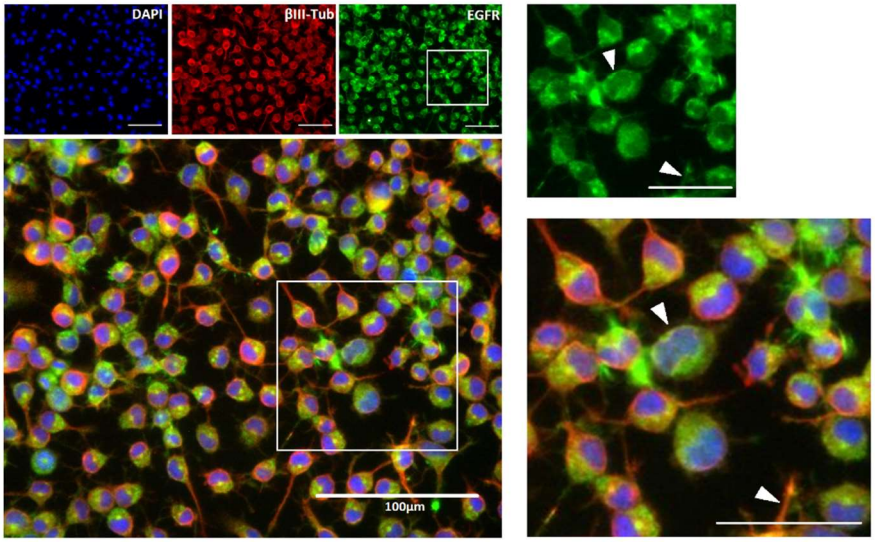

I.

Neuro2A: BotLcTd/A-EGF Fused 10 nM

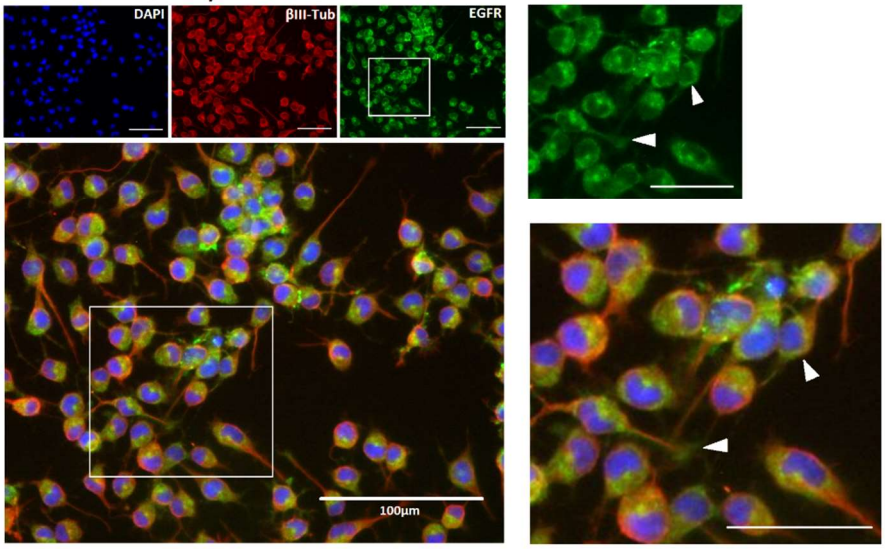

Figure 5.7 – Synthesis of EGF-linked botLcTd/A complexes and investigation of EGFR in EGF-dosed cells

A) Western blot showing the cleavage of SNAP25 in Neuro2A and SH-SY5Y cells when incubated with titrations of botLcTd/A-EGF for 72 hours. B) Quantification of SNAP25 cleavage in A (N=2). C) SDS-PAGE showing the formation of EGF-botLcTd/A linked complex and the lack of formation of linked CNTF-EGF-botLcTd/A (N=3). D) Western blot showing the cleavage of SNAP25 in Neuro2A and SH-SY5Y cells when incubated with titrations of linked EGF-botLcTd/A for 72 hours (N=3). E) Images taken showing the lack of non-specific staining of secondary antibodies used without the presence of primary antibodies (epifluorescent microscope: 4000 ms. Scale bars 100µm). F-G) Images taken showing SH-SY5Y cells both with and without recombinantly fused botLcTd/A-EGF addition after 72 hours, fixed and stained with EGFR (rabbit) (4000 ms) and βIII-tubulin control (mouse) (200 ms) (N=2). H-I) Images taken showing Neuro2A cells both with and without recombinant botLcTd/A-EGF addition after 72 hours, fixed and stained with EGFR (rabbit) (4000 ms) and βIII-tubulin control (mouse) (200 ms) (N=2). Arrows indicating EGF presence in the neurites and at the edges of cells in both cell lines. All inset scale bars in F-I: 50 µm, obj. x40.

Despite the lack of success with the delivery of botLcTd/A using EGF stapled complexes, it was still desirable to determine whether the quantity and location of the EGFR was the reason for the difference from CNTF in plateauing at higher concentrations. Figure 5.7:E shows that neither of the secondary antibodies used here showed any non-specific binding without the presence of primary antibodies in SH-SY5Y cells. SH-SY5Y cells which had been either incubated with buffer A or recombinantly fused botLcTd/A-EGF 10 nM were fixed and stained with EGFR and βIII-tubulin as a control. It was found that there was no observable difference in the location or quantity of EGFR between control and sample incubated cells (fig. 5.7:F-G) (as indicated). Potentially, it is this lack of significant receptor internalisation and expression inhibition once activated which is the reason for the difference between the % SNAP25 cleavage gradient between CNTFR and EGFR. It can be seen in figure 5.7:H-I that a similar lack of change in EGFR presence or location is seen in Neuro2A cells when incubated with recombinantly fused botLcTd/A-EGF.

5.2.7 SNAP25 cleavage through stapled botLcTd/A delivery directly influences H3-Noradrenaline exocytosis

As discussed in the introduction, botulinum neurotoxins can be used for pain relief because they inhibit the exocytosis of neurotransmitters, but there is also an argument that it can be used for cancer treatment (Bandala et al. 2015; Karsenty et al. 2009) Numerous cancer varieties use paracrine and autocrine pathways to enhance growth and increase vasculature (Chanthery et al. 2012; Chaban et al. 2013); these signals are made and released by cells and therefore to inhibit them could potentially be advantageous.

SH-SY5Y are commonly used for noradrenaline exocytosis studies and therefore are a good cell line in which to determine whether the cleavage of SNAP25 by botLcTd/A is capable of inhibiting this exocytosis (Atcheson et al. 1994; Vaughan et al. 1995; Géraldine et al. 2010). It has been found previously in literature that botulinum A SNAP25 cleavage is capable of inhibiting stimulated release in differentiated cells and nerve terminals, but the investigation of the effects of SNAP25 cleavage on undifferentiated neuroblastoma remains limited (Arsenault et al. 2013; Raciborska et al. 1998; Huang et al. 1998). It was decided to measure the quantity of noradrenaline release through radioactive labelling ([H3]-NA), with the hypothesis that increased SNAP25 cleavage through CNTFx1 and CNTFx2 linked construct botLcTd/A delivery would decrease the stimulated release of [H3]-NA. It was hoped that there would be a difference in the stimulated release of [H3]-NA between the CNTFx1 and CNTFx2 linked constructs.

In order to determine this hypothesis, the protocol must first my optimised. Quantification of radiation was done through a scintillation counter, which measures the radioactive decay of samples in counts per minute (CPM). However, for low energy decay not all events are recorded because of quenching in the scintillation fluid, therefore the CPM is different to the actual value of disintegrations per minute (DPM). Because tritium is known for having significant quenching, titrations of known radioactive concentrations diluted in basal buffer was made (fig. 5.8:A). It was shown that the quench had a consistent level of around 20% from between 5500000 to 1000 DPM, this is consistent with other reported tritium data (fig. 5.8:B) (Thomson 2001).

At the end of release experiments it was desirable to harvest and lyse the remaining cells to determine the overall % of tritium that was released and how much was left behind in the cell; it had to be considered whether cell lysates and the number of cells in the lysates could influence quench. Therefore, trypsin was first used, then basal buffer with 0.4%

triton and 0.2% nuclease benzonase was mixed and left for a further 5 minutes before making up to 1ml in basal buffer and placing in the scintillation vial. When samples each containing the lysates of $1.2x10^5$ cells were added to titrations of known radioactive concentrations it was found that there was a decrease in quench% as the DPM decreased. Therefore the amount of CPM found in the lysis buffer needed to be considered before working out the % quench to use for calculating the DPM (fig. 5.8:C). Additionally, it was found that in lysates containing between $8x10^4$ and $3x10^5$ cells there was no observable trend in the degree of quench when 10^5 DPM [H3]-NA was added (fig. 5.8:D). Because of the variance in this data, the % quench for the lysates was measured in each experiment.

It was also important to consider the drugs and buffers that would be used whilst incubating with [H3]-NA and stimulating release. The basal buffers and release buffers are shown in section 2.1.2, where the release buffer uses 70 mM KCl, balanced by NaCl, to stimulate cell release. It was decided based on similar experiments that $2.775x10^6$ DPM [H3]-NA would be incubated in basal buffer with the SH-SY5Y cells for 45 minutes before being removed and the wells washed; either basal buffer or release buffer is then added to the cells for 5 minutes before collecting to determine basal or stimulated release. The buffers with no additional drugs were found to cause the basal release of 5% and the stimulated release of 10%, this is comparable to other papers which have used SH-SY5Y cells in the same way (Géraldine et al. 2010) (fig. 5.8:E)

Pargyline is a monoamine oxidase (MAO) inhibitor which prevents the breakdown of noradrenaline. Therefore pargyline at a concentration of 20 mM (with ascorbic acid 0.2 mM) was added to the basal buffer with [H3]-NA during incubation (Atcheson et al. 1994; Davletov et al. 1998). It was found that there was no significant difference in either basal or release buffer between the cells incubated with or without pargyline (fig. 5.8:E). Desipramine, on the other hand, can be used to inhibit the re-uptake of noradrenaline (Géraldine et al. 2010). 1 mM desipramine was added to the basal buffer used for washing the SH-SY5Y cells after [H3]-NA incubation, however in doing so there was a large increase in the proportion of radiation that was being detected in both the basal and release samples. On observation, it appeared that the reason for this large detection was because the cells were dying and coming away from the plate into the media. This increase in cell death was also observed at significantly lower than recommended concentrations (fig. 5.8:E). It was therefore decided that only pargyline only was to be used in the incubation of [H3]-NA.

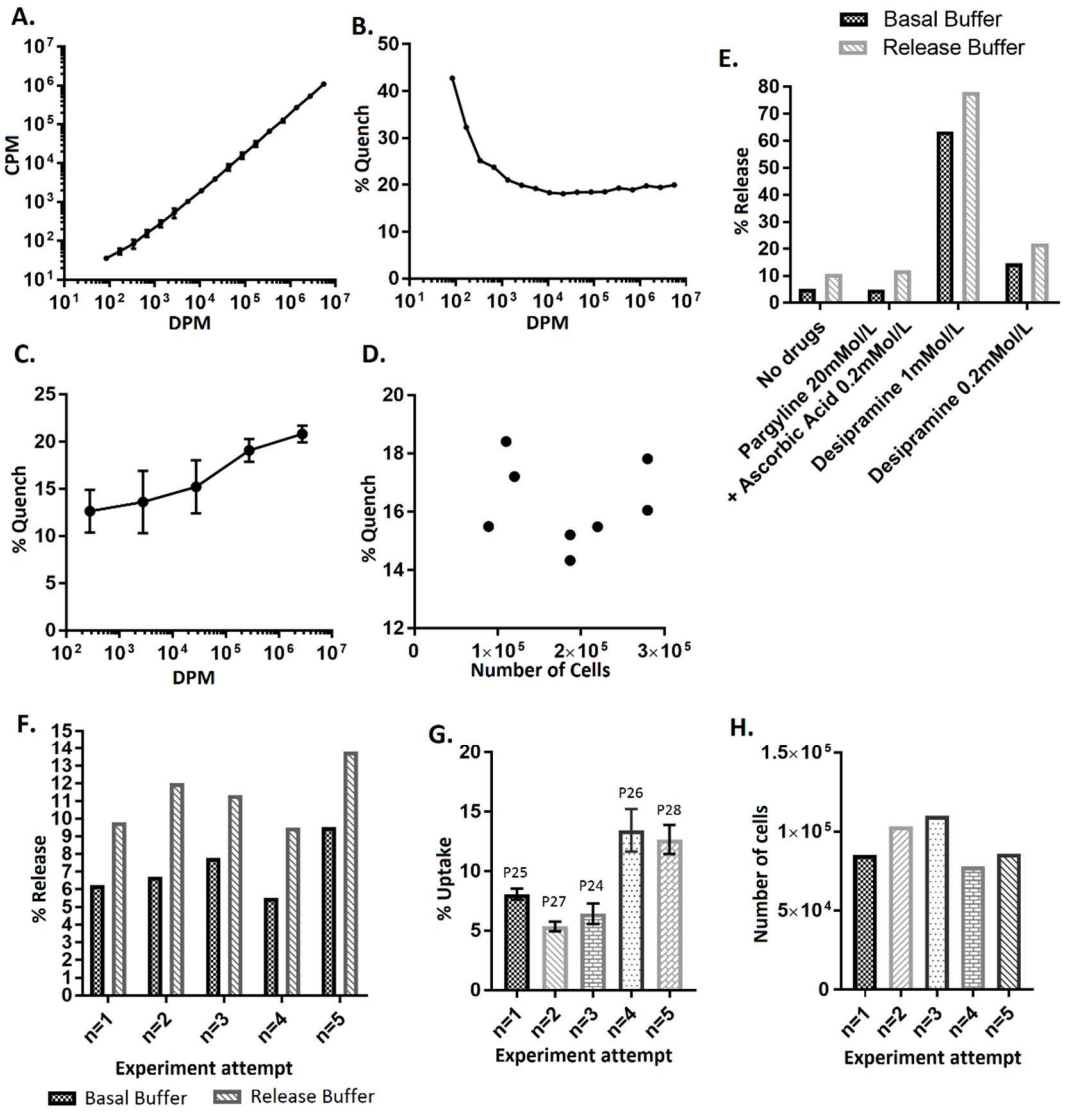

Figure 5.8 – Control experiments for establishing a [H3]-Noradrenaline assay

A) Standard curve using known DPM concentrations of [H3]-Noradrenaline ([H3]-NA) and plotting against the measured CPM from the scintillation counter (N=3). B) Graph plotting the DPM against the % quench when measuring the CPM (N=3). C) Graph measuring the % quench with 1.2x10^5 cell lysates when mixed with a known DPM of [H3]-NA (N=3). D) Scatter plot determining whether % quench in radioactive cell lysate samples is dependent on the number of cells lysed (N=3). E) Optimisation of the protocol and determining the drugs and concentrations to be used (N=2). F) The % basal and stimulated release of the control cells in the 5 experiments which were completed. G) The % uptake of the 2.775x10^6 DPM of radiation which was incubated with for 45 minutes. Passage numbers (P) are also displayed (Note: SH-SY5Y cells frozen at P21). H) Bar chart showing the number of cells counted in each experiment.

Upon establishing the assay conditions, wells containing adherent SH-SY5Y cells were incubated for three days with different concentrations of CNTF linked botLcTd/A complexes before undergoing analysis. Figure 5.8:F shows the basal and stimulated release of the control cells in each of the 5 experiments. Even though there were similar values for each experiment there was concern that the differences would interfere with detecting any subtle changes in radioactive release. Therefore, in each experiment, the basal and stimulated release of each condition would be given as a relative percentage of the control stimulated release. Approximately 2.5x10^4 cells were seeded into 24 well plates and the number of cells measured before experiments. Neither passage number (P) nor number of cells at 72 hours appeared to influence uptake or the amount of NA-[H3] release from cells (fig 5.8:G-H). It was ensured that all experiments were done within 10 passages of defrosting.

After protocol optimisation, SH-SY5Y cells were incubated with differing concentrations of CNTFx1 and CNTFx2-botLcTd/A linked complexes, before [H3]-NA was added. After washing away excess [H3]-NA, it was possible to stimulate exocytosis through KCl-rich buffer and compare this to basal release. It was hypothesised that increased SNAP25 cleavage through CNTFx1 and CNTFx2 linked construct botLcTd/A delivery would decrease the stimulated release of [H3]-NA, and that potentially there would be a difference in the stimulated release of [H3]-NA between the CNTFx1 and CNTFx2 linked constructs.

The stimulation buffer was incubated for 1,3 and 5 minutes and compared to 5 minute incubation in basal buffer and it was found that there was no stimulated release plateau before 5 minutes (fig. 5.9:A). It was undesirable to incubate the buffers for more than 5 minutes because of potential re-uptake of the [H3]-NA and the eventual escape of [H3]-NA] in the basal buffer down the concentration gradient. Therefore 5 minutes incubation of basal and release buffer with cells before the buffer was removed and analysed quantitatively for radioactive [H3]-NA.

The stimulated and basal release from the control samples were then compared to those which had been treated with the CNTF linked botLcTd/A complexes. There was a strong correlation between the increase in the concentrations of CNTF-BotLcTd/A linked samples added to cells and the decrease in the amount of radiation in samples with stimulated release. An issue with linked CNTF-BotLcTd/A complexes there it has not resulted in 100% SNAP25 cleavage in any of the concentrations incubated. To determine what would happen with enhanced SNAP25 cleavage, botLcTd/A+LF3000 was incubated over 72 hours;

it was shown here that there was no significant difference between basal and stimulated release in these samples, suggesting a complete blockade of stimulated release (fig. 5.9:B).

Whilst all the stimulated release points are significantly different from the control stimulated release, it should be noted that this is biased because the control stimulated release is at 100% with a standard deviation of 0, so almost any difference would have resulted in significance. Therefore, the focus here is the level of significance and the pattern which ensues when there is increased addition of CNTF-botLcTd/A linked complexes. There was no significant difference between the x1 and x2 CNTF linked release; however, there was significant difference between the value for CNTFx1-BotLcTd/A 0.4 nM and CNTFx2-BotLcTd/A 10 nM.

One criticism of this experiment was that it was impossible to measure the degree of SNAP25 cleavage in the samples which were analysed for release, by doing to it would have been possible to directly analyse SNAP25 cleavage against stimulated release. Taking the data from figure 5.3, where 10 nM CNTF-BotLcTd/A linked complexes resulted in just under 50% cleavage, a broad judgement can be made that around 50% of the cleavage results in 50% decrease in stimulated release. This was surprising as it was hypothesised that 50% cleavage would result in more than 50% release owing to numerous SNARE complexes needing to form for successful stimulated exocytosis, thereby if a proportion are disrupted then it is more likely that the whole process would be disrupted as has been previously reported (Huang et al. 1998; Raciborska et al. 1998). Because the SNAP25 cleavage appears to be in some cells more than others, as shown in figure 5.5, it is possible that through this some cells had very little stimulated release whilst others remained mostly undisrupted, which could explain these results. It could therefore be possible that through alternative or more efficient targeting moieties, a SNAP25 cleavage of 60-80% could be achieved uniformly across the cells and could result in a more significant decrease in stimulated release. Nonetheless, it has been suggested here that non-differentiated SH-SY5Y cells are able to have neurotransmitter release inhibited in a concentration dependant manner through botLcTd/A internalisation and SNAP25 cleavage, which could be of use for non-cytotoxic cancer strategies.

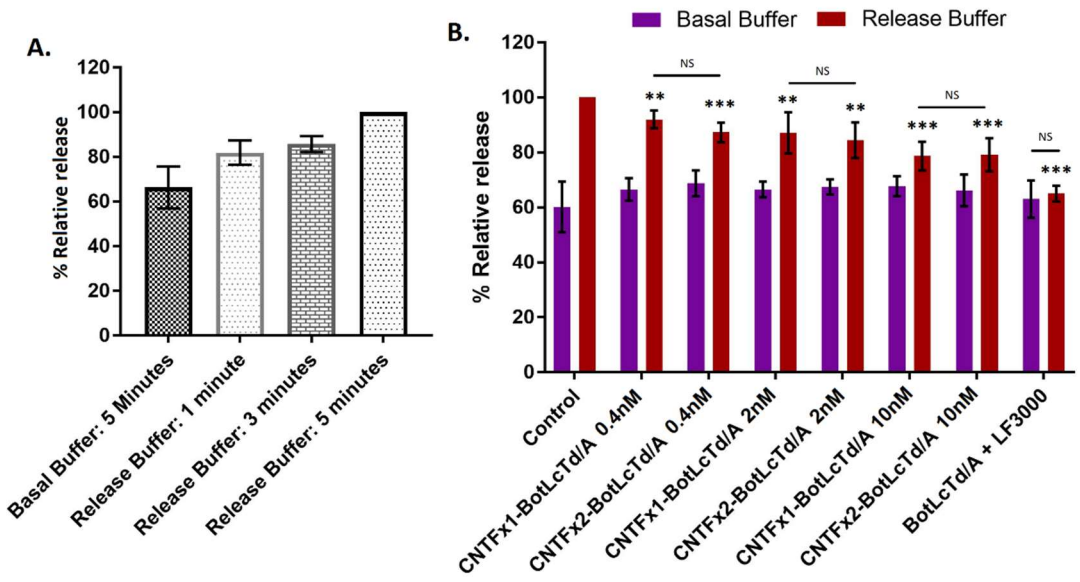

Figure 5.9 – Comparison of basal release and stimulated release in cells incubated with CNTF-linked complexes

*A) Bar chart showing the time points of incubation with release buffer and the resulting % release (N=2). B) Graph showing the basal and stimulated release of cells that had been incubated for 72 hours with different concentrations of CNTFx1-BotLcTd/A and CNTFx2-BotLcTd/A linked samples and with LF3000 (N>2 for each bar). Significance measured by Student T-test by comparing values to either the control stimulated release or between concentrations or conditions as drawn. Significance for statistical analysis: P>0.05 = NS P<0.05 = * P<0.01 = ** P<0.001=***.*

5.2.8 The effects of CNTFx1 and x2 linked botulinumLcTd/A can also be seen in LA-N-5 cells

Having established the internalisation of CNTFx1 and CNTFx2 linked botLcTd/A in SH-SY5Y cells, it was advantageous to investigate whether these effects could extend to other cells. LA-N-5 is another neuroblastoma cell line which exhibits more differentiated behaviours such as slow proliferation and robust neurite formation. As shown in figure 5.1, LA-N-5 cells were able to internalise botLcTd/A-CNTF to cleave SNAP25 but there was no cleavage when incubated with botLcTd/A-EGF. Furthermore, it was detected through Western blot and imaging that there was CNTFR presence in LA-N-5 comparable with that found on SH-

SY5Y, but that there was little EGFR detected (fig. 5.1). These properties therefore make LA-N-5 useful for further exploring CNTFx1 and CNTFx2 linked complexes. Figure 5.10:A-D shows that the cells had a very slow growing and doubling time when compared to the other cell lines used. However when grown at $2x10^4$ cells/well in a 96 well plate for 3 days they became 60-80% confluent and the alamarBlue assay can be successfully used to explore the effects of incubated samples on cell metabolism, and indirectly cell number, owing to the background being less than 10% of fluorescence (fig. 5.10:E-F).

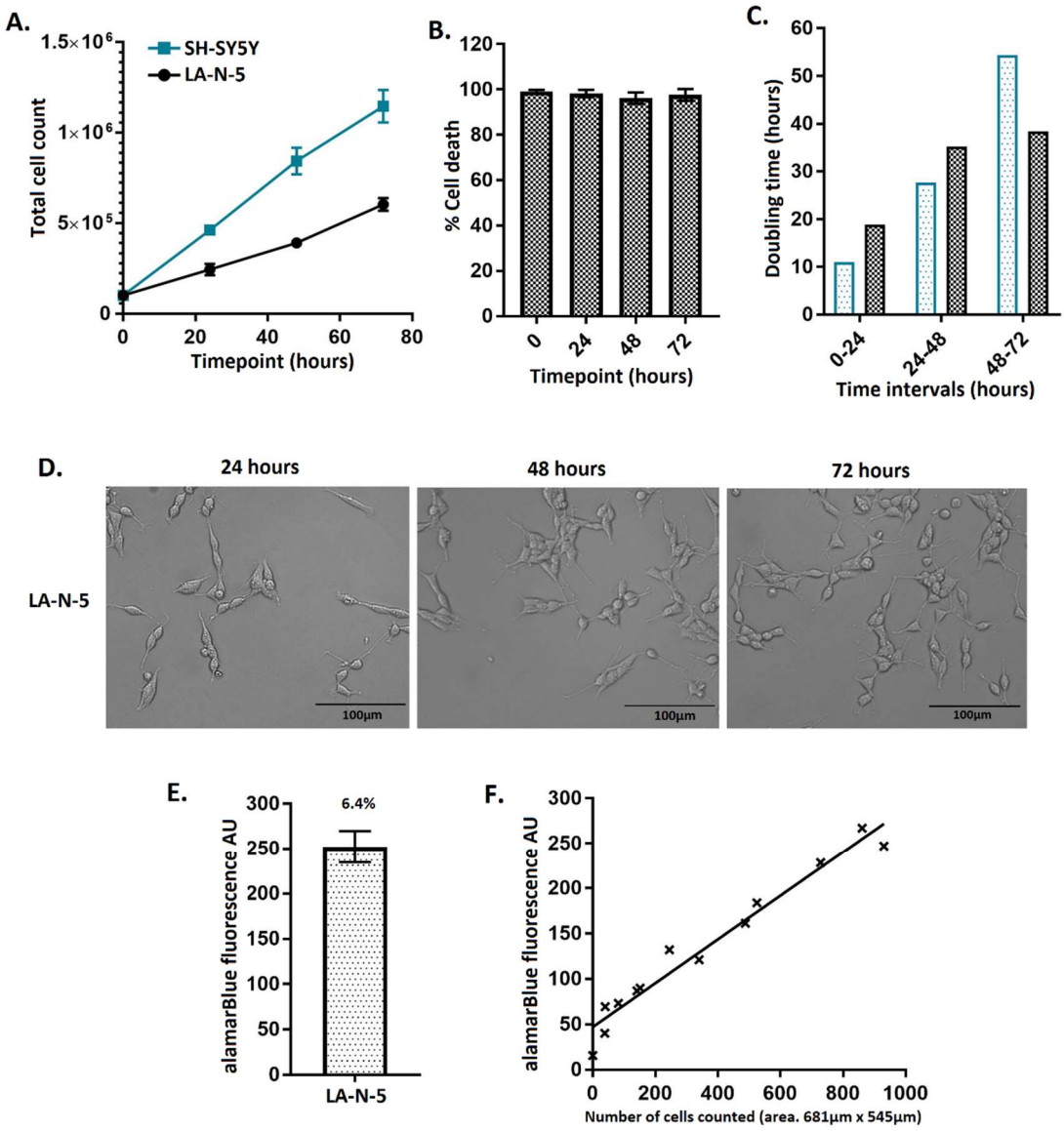

Figure 5.10 – Controls of LA-N-5 cells and confirmation of their suitability for CNTF experiments

A) Graph showing cell growth of LA-N-5, measuring at 24 hour timepoints through Bio-Rad automated cell counter and comparing to the SH-SY5Y data previously shown in figure 4.1 (n=2, N=3). B) Cell death% of the measured cells over 72 hours through Bio-Rad automated cell counter (n=2, N=3). C) Doubling time of the cells as calculated from formula in section 4.2.1 and comparing to the SH-SY5Y data previously shown in figure 4.1. D) Brightfield images of the LA-N-5 cells over 72 hours in culture (Obj. x40). E) AlamarBlue value and the % control of the cells after 72 hours of growth at approximately 60-80% confluency (n=3, N=3). F) The alamarBlue values and their relationship with manually counted cell number from images taken (n=2, N=12).

It has been previously shown that recombinantly fused BotLcTd/A-CNTF cleaved SNAP25 at 20 nM, it was then titrated to compare how the cleavage % compared with SH-SY5Y cells. Interestingly, it was found that the fused BotLcTd/A-CNTF was capable of cleaving SNAP25 at comparable concentrations to SH-SY5Y cells (fig. 5.11:A-B). Potential OG toxicity was found to be similar to that of Neuro2A cells with a maximum of 0.2% OG to be used (fig. 5.11:C). CNTFx1 and CNTFx2-botLcTd/A linked were then added in the same way as in figure 5.3. There was no toxicity or alteration of growth reported in any of the wells incubated with samples or linked complex components (fig. 5.11:D-E). The data found suggested that the % cleavage difference between CNTFx1 and CNTFx2 linked botLcTd/A complexes is similar to that seen in SH-SY5Y cells, as well as there being no significant difference between the recombinantly fused botLcTd/A-CNTF and the linked version at any of the points (fig. 5.11:G- H). Together, this data demonstrates that the internalisation of ligand-targeted toxin complexes as well as the enhanced effects between single and double ligand complexes is not unique to SH-SY5Y cells.

In addition to the quantitative data, it was desirable to stain LA-N-5 cells which had been incubated with either buffer A or linked CNTFx2-BotLcTd/A and determine what effects these samples had upon the location and presence of CNTFR. In figure 5.11:I it can be seen that like SH-SY5Y, CNTFR was strongly present in the cell neurites and throughout the cell (as indicated). On the other hand, when incubated with CNTFx2-BotLcTd linked, there was

a large decrease in the presence of CNTFR and a retraction away from the neurites and into the soma (fig. 5.11:J). This finding is comparable to that of SH-SY5Y. One difference however, is that it was noted that the cleaved SNAP25 antibody was far more homogenous in its location in linked CNTFx2-BotLcTd/A incubated LA-N-5 cells than in SH-SY5Y cells (fig 5.11:K). The reason for this may lie in that LA-N-5 cells exhibit far less cancerous behaviours than both SH-SY5Y and Neuro2A cells, such as decreased growth small soma with long neurites. Therefore, since heterogeneity is a hallmark of cancerous behaviour it is not impossible to hypothesise that LA-N-5 may be more homogenous than the other cell lines tested.

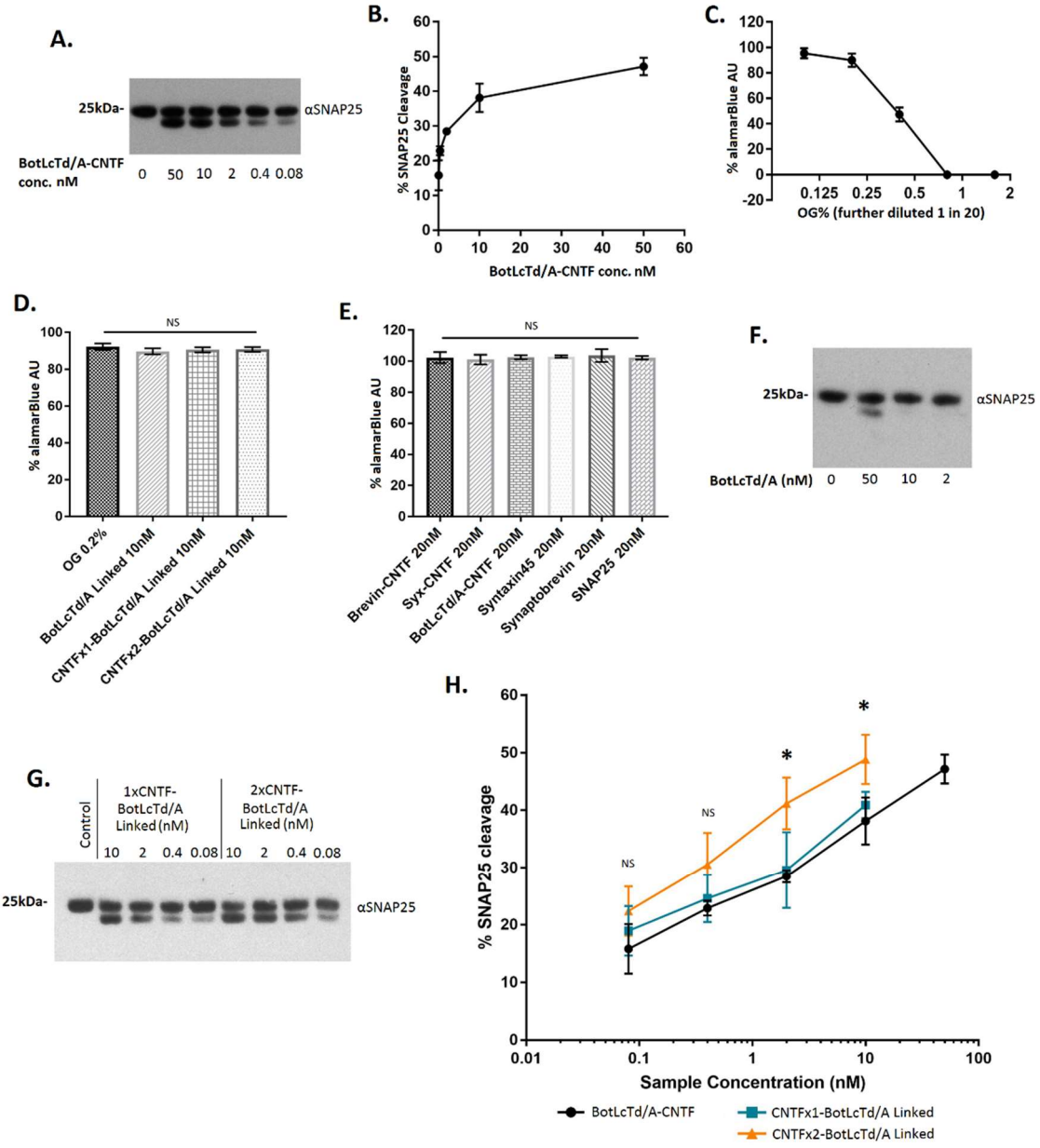

I. LA-N-5: Control

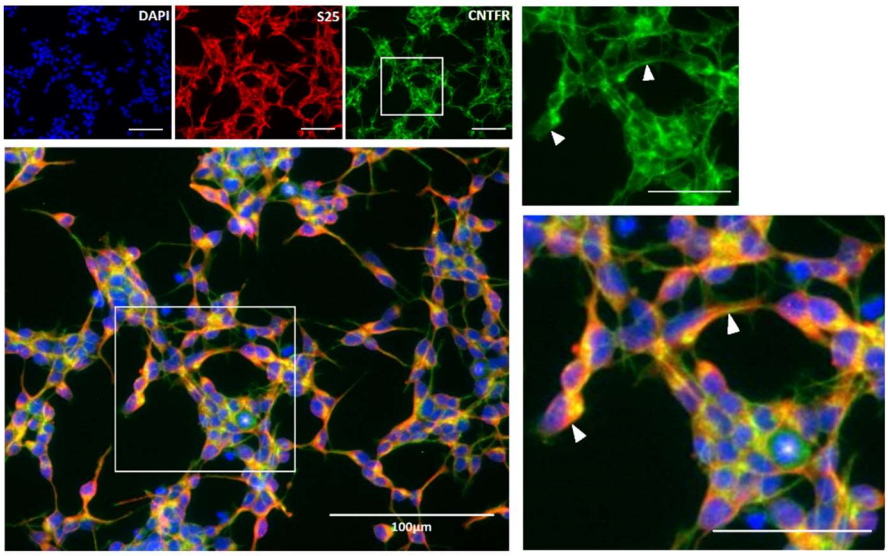

J. LA-N-5: CNTFx2-BotLcTd/A 2 nM

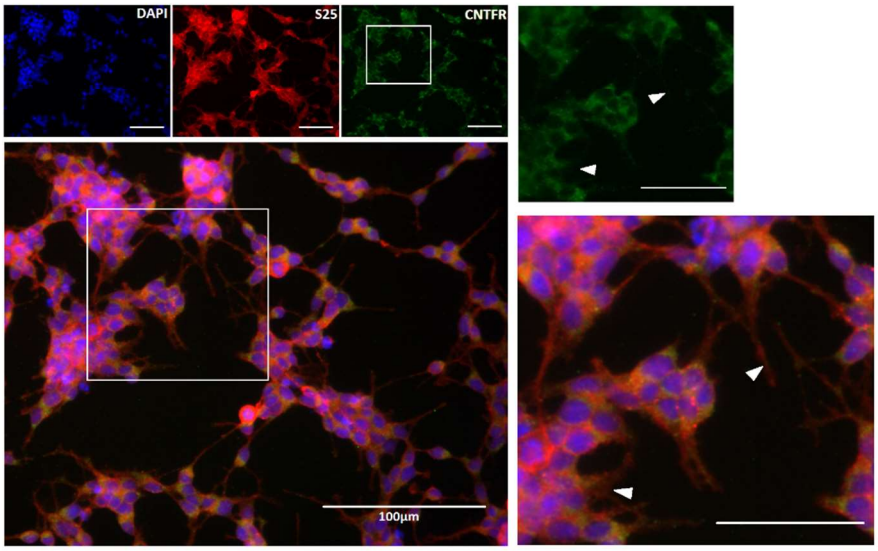

K. LA-N-5: CNTFx2-BotLcTd/A 2 nM

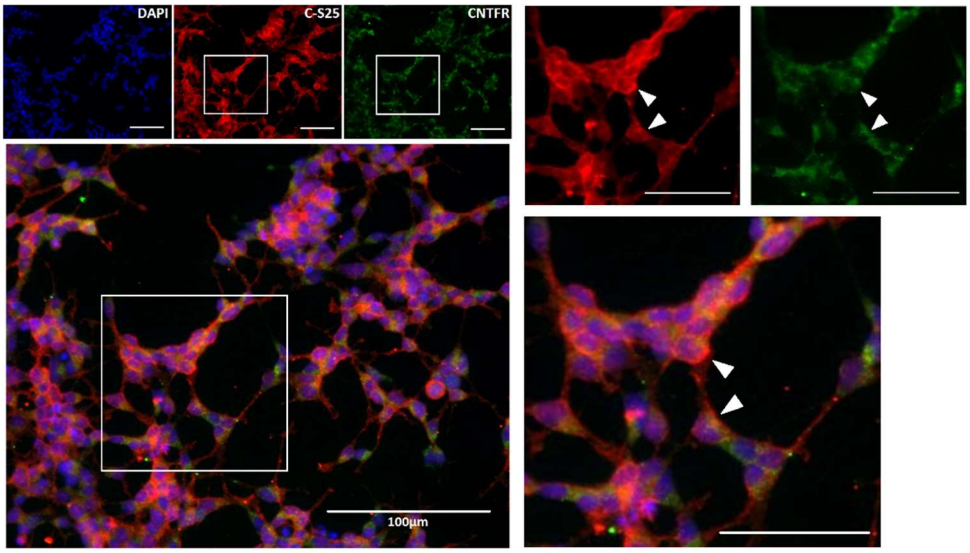

Figure 5.11 – Investigating CNTFx1 and x2 linked botLcTd/A complexes in LA-N-5 cells

A) *Representative Western blot showing SNAP25 cleavage in cells incubated with titrations of botLcTd/A-CNTF for 72 hours (N=3). B) Quantification of A using Bio-Rad band analysis. C) AlamarBlue assay showing the toxicity of OG concentrations at 1 in 20 dilution in LA-N-5 cells over 72 hours (N=3). D) Western blot showing SNAP25 and cleavage on incubation of LA-N-5 cells with botLcTd/A concentrations for 72 hours (N=2). E) Representative Western blot showing cleaved SNAP25 in cell lysates after cell incubation with CNTFx1 and CNTFx2 linked botLcTd/A complexes for 72 hours (N=3). F-G) AlamarBlue assays showing cells incubated with linked complexes and staple components for 72 hours. Significance measured through one-way ANOVA across all samples. H) Quantification of the SNAP25 cleavage shown in A and E. Significance measured through one-way ANOVA between sample values of the same concentration (N=3). I-J) Images of LA-N-5 cells incubated with either buffer A or linked CNTFx2-BotLcTd/A 2 nM for 72 hours then stained with CNTFR (4000 ms) and SNAP25 (200 ms). K) Image of LA-N-5 cells incubated for 72 hours with linked CNTFx2-BotLcTd/A 2 nM and stained with αCNTFR (4000 ms) and αC-SNAP25 (200 ms). Images taken from epifluorescent microscope. Arrows indicate neurites and cell edges to highlight differences in CNTFR location. Significance for statistical analysis: P>0.05 = NS P<0.05 = * P<0.01 = ** P<0.001=***. Obj. x40 for all images. Scale bars for all inset images 50 µm.*

5.2.9 DiphtheriaLcTd-S25 stapled to CNTFx1 and x2 sees an increase in cytotoxicity in SH-SY5Y cells

Having established that botTd/A can be delivered into cells and escape endosomes as shown by the cleavage of SNAP25, it is important to determine whether other enzymes can be delivered in a similar manner. DiphtheriaLcTd-S25 (DipLcTd-S25) was synthesised to determine this (fig. 5.12:A); diphtheria is useful as it kills cells and therefore theoretically cells should be more sensitive to the outcomes as once a cell succumbs to the toxicity there can be no progeny. DipLcTd-S25 was firstly incubated with brevin and syntaxin to ensure that it was able to form a linked complex (fig. 5.12:B). The toxicity of dipLcTd, recombinantly fused dipLcTd-S25 and linked dipLcTd complex was then compared in SH-SY5Y cells; it was shown that the linked and stapled versions were more toxic that the dipLcTd itself (fig. 5.12:C). This effect has also been observed independently elsewhere

within the Davletov laboratory, with potential reason being that the helices composing either the SNAREs or SNAP25 may interact with cell membranes and internalise in a way which is not possible by dipLcTd alone. This has been previously shown in figure 5.3:D, however was not noted at the time.

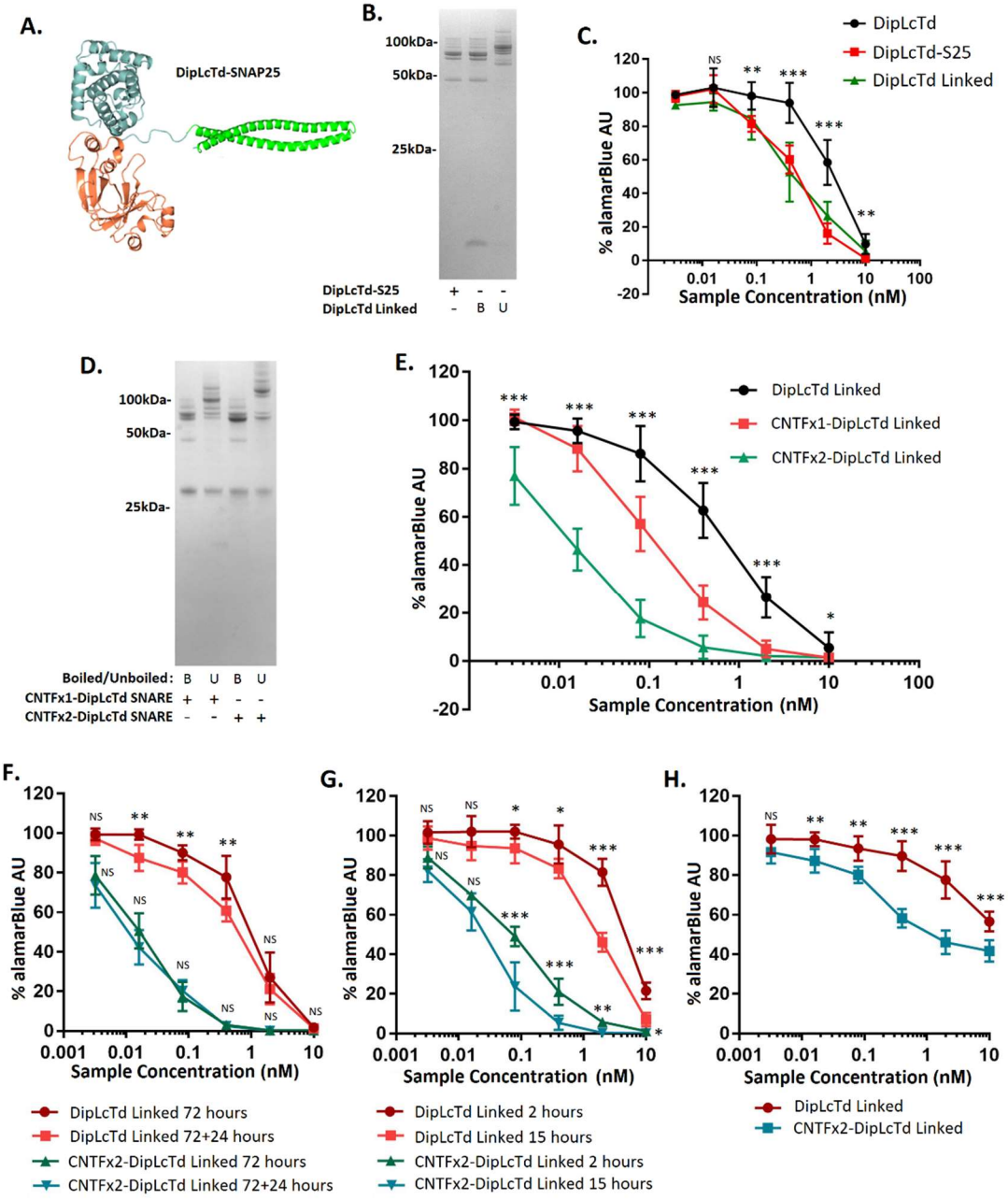

Figure 5.12 – Forming linked complexes with dipLcTd-S25

*A) Schematic of DipLcTd-S25. B) SDS-PAGE showing the DipLcTd-S25 formation into a linked complex (N=3). C) AlamarBlue Assay showing the relative toxicity of dipLcTd compared to dipLcTd-S25 and linked dipLcTd after 72 hours incubation. Significance was measured by one-way ANOVA for all values at each concentration (n=3, N=3). D) SDS-PAGE showing the formation of linked CNTFx1-dipLcTd and CNTFx2-dipLcTd (N=3). E) AlamarBlue assay showing the relative toxicity between linked complexes dipLcTd, CNTFx1-DipLcTd and CNTFx2-DipLcTd incubated for 72 hours. Significance was measured by one-way ANOVA for all values at each concentration (n=3, N=3). F) AlamarBlue assay of linked complexes dipLcTd and CNTFx2-DipLcTd added either at 72 hours or 72+24 hours (n=3, N=2). G) AlamarBlue assay of linked dipLcTd and CNTFx2-DipLcTd at 72 hours and media changed at either 2 hours or 15 hours. Significance for both F and G was measured by Student T-test between the values of the same samples at the same concentration, measuring between the different incubations (n=3, N=2). H) AlamarBlue assay of linked dipLcTd and CNTFx2-DipLcTd incubated for 24 hours and immediately analysed. Significance was measured by Student T-test between the values at the same concentration (n=3, N=2). Significance for statistical analysis: P>0.05 = NS P<0.05 = * P<0.01 = ** P<0.001=***. DipLcTd PDB ID: 1SGK. SNARE PDB ID: 5W5D (McNicholas et al. 2011; Berman et al. 2000).*

Figure 5.12:D showed that CNTFx1-dipLcTd linked and CNTFx2-dipLcTd linked could be successfully formed with brevin-CNTF and syntaxin-CNTF. The toxicity of the CNTF stapled complexes was then compared to linked DipLcTd complex without any ligand linked; it was found that both versions of the CNTF linked complexes significantly decreased the number of cells at lower concentrations, with the linked CNTFx2-dipLcTd being the most toxic (fig. 5.12:E). Whilst it was extremely encouraging seeing this large increase in cytotoxicity, it should be noted that the recombinantly fused version of dipLcTd/A-CNTF was not in our possession and therefore could not be compared.

Because of the substantial change in EC_{50} brought about through CNTFx2 linking, accumulation and timescale experiments were able to reveal more about the nature of the

linked complex internalisation and the toxicity of dipLcTd. Linked dipLcTd and CNTFx2-dipLcTd/A linked were added into SH-SY5Y cells at titrated concentrations for 72 hours, with a separate set of wells being dosed again at 24 hours before analysis. Figure 5.12:F shows that there was a significant difference between the single and double dosed samples with the linked dipLcTd but not with the CNTFx2-dipLcTd/A samples. This is most likely because of the passive way which dipLcTd-S25 enters the cells, therefore more protein will equal a higher degree of entry. On the other hand, the linked CNTFx2-dipLcTd/A binds and is internalised specifically by CNTF receptors; however, it has already been demonstrated that after CNTF addition there is internalisation of the receptors (fig. 5.6), which could account for the lack of increase in cell death through accumulation of a CNTF containing sample.

In a different experiment, samples were added to cells at 72 hours, before the media was changed to remove the complex after either 2 or 15 hours and the cells left to grow until analysis. Figure 5.12:G showed that the linked dipLcTd was only toxic at high concentrations after 2 hour sample incubation, and that there was a significant increase in cell death when the samples were incubated for 15 hours. The CNTFx2-dipLcTd/A linked samples also showed an increase in toxicity between the 2 hour and 15 hour sample incubated cells. What is particularly interesting about this data is that the linked dipLcTd alamarBlue assay values for both 2 hours and 15 hours were different to those shown in figure 5.12:F for 72 hours, whereas the 15 hour incubation for CNTFx2-DipLcTd/A linked samples were not significantly different from the 72 hour values. This strongly indicates that the internalisation of CNTF linked complexes is far quicker than the dipLcTd linked complexes without attached targeting domain, with all internalisation occurring before 15 hours. On the other hand, linked dipLcTd appears to be internalised passively over the whole of the 72 hours.

In figure 4.3 it was proposed that the reason for the lack of PI staining of dipLC incubated cells at 24 hours was because of the length of time required for diphtheria to trigger cell death. This was investigated by adding linked dipLcTd or CNTFx2-dipLcTd into cells over 24 hours before immediately analysing. Figure 5.12:H showed that there was a small degree of cell death in the higher concentrations of both samples, however this result is significantly less than what is seen at 72 hours. This shows that even where it is known that dipLcTd has efficiently internalised within 24 hours, as demonstrated in figure 5.12:G, that it takes more than 24 hours for effective cell death to occur.

5.2.10 Stapling EGF and CNTF together with dipLcTd can internalise into a wider variety of neuroblastoma cells than one ligand alone.

Following the apparent success of using CNTF linked dipLcTd complexes, it was decided to attempt using brevin-EGF to link and target complexes to SH-SY5Y cells. Figure 5.13:A shows that linked EGF-DipLcTd was successfully formed; moreover, unlike the botLcTd-S25, dipLcTd-S25 was able to form a complex with both EGF and CNTF. When SH-SY5Y cells were incubated with the EGF linked complexes it was found that both EGF and EGF with CNTF linked dipLcTd has increased toxicity compared to CNTFx2-dipLcTd (values taken from fig. 5.12:E as a comparison) at lower concentrations (fig. 5.13:B). Whilst the EGF and EGF-CNTF stapled dipLcTd complex results were similar, it is apparent that at the lowest concentrations that linked EGF-CNTF-dipLcTd was not as toxic as linked EGF-dipLcTd. This could be for a number of reasons; for one, because CNTF internalisation might not be as efficient as EGF, therefore the CNTF binding to CNTFR could distract from EGF-EGFR interactions. Another possibility is that there is crowding around the SNARE staple, meaning that EGF could interfere with CNTF or vice versa at a protein level.

Because it was possible to link together brevin-EGF, Syntaxin-CNTF and dipLcTd-S25, it then needs to be seen how these complexes behave in alternative neuroblastoma cell lines compared to complexes with only one ligand. For instance, Neuro2A cells do not appear to internalise CNTF-linked complexes and LA-N-5 cells do not appear to internalise EGF-linked complexes; therefore, a good test of double ligand function is to determine whether the construct with both CNTF and EGF linked is able to internalise into both cells.

It was important to firstly investigate was that sensitivity of both LA-N-5 and Neuro2A cells to dipLcTd-S25. Unlike SH-SY5Y, there was very little difference in toxicity between dipLcTd and dipLcTd-S25 or linked dipLcTd (fig 5.14:A,C). As expected, there was little in the way of increased toxicity when CNTFx1 or CNTFx2 linked dipLcTd was incubated with Neuro2A cells, however when linked EGF-dipLcTd or EGF-CNTF-dipLcTd was applied there was a significant shift in the EC_{50} of the samples. Likewise, when LA-N-5 cells were incubated with linked EGF-dipLcTd there was little alteration in toxicity, but when any of the CNTF containing samples were added there was a shift in the EC_{50} (fig. 5.14:B,D).

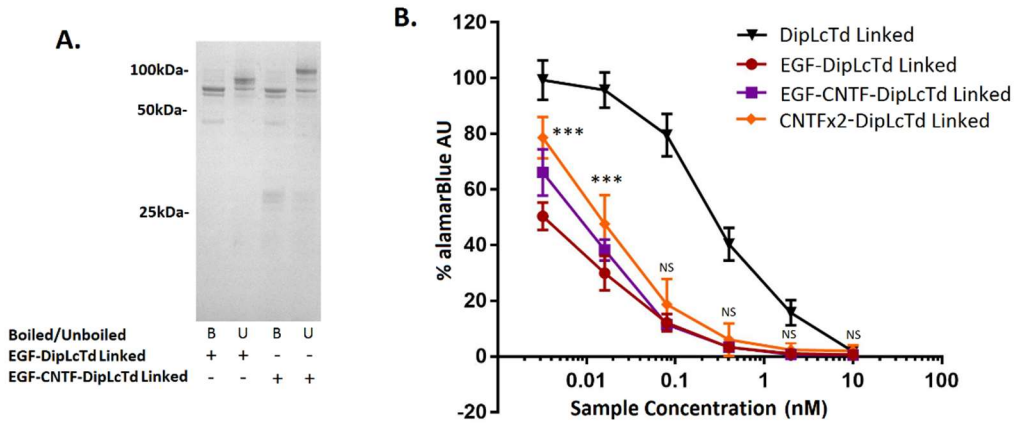

Figure 5.13 – Formation and utilisation of EGF linked dipLcTd complexes in SH-SY5Y cells

A) *SDS-PAGE showing formation of linked EGF-dipLcTd and EGF-CNTF-dipLcTd (N=3). B) AlamarBlue assay of titrations of ligand targeted linked dipLcTd samples for 72 hours (n=3, N=3). The linked CNTFx2-dipLcTd readings were those taken from figure 5.12:E. Significance was measured by one-way ANOVA for all values excluding dipLcTd linked at each concentration. Significance for statistical analysis: P>0.05 = NS P<0.05 = * P<0.01 = ** P<0.001=***.*

Here it was found that in LA-N-5 cells the same decrease in toxicity was observed between linked CNTF-dipLcTd and EGF-CNTF-dipLcTd as in SH-SY5Y cells; a likely reason for this could be protein interference between both ligand domains. Whilst it is clear that all three domains remain functional and can evidently target both cell lines through their individual receptors, it is worth being cautious about the addition of other ligand varieties until more is understood about how the ligand proteins fit around the SNARE staple and whether modifications to the ligand-staples would improve upon the efficiency of double ligand complexes. For example, the addition of a long protein linker between the ligand and the staple domain of one of the ligand-staples may function to allow the protein domains to better fit around the staple.

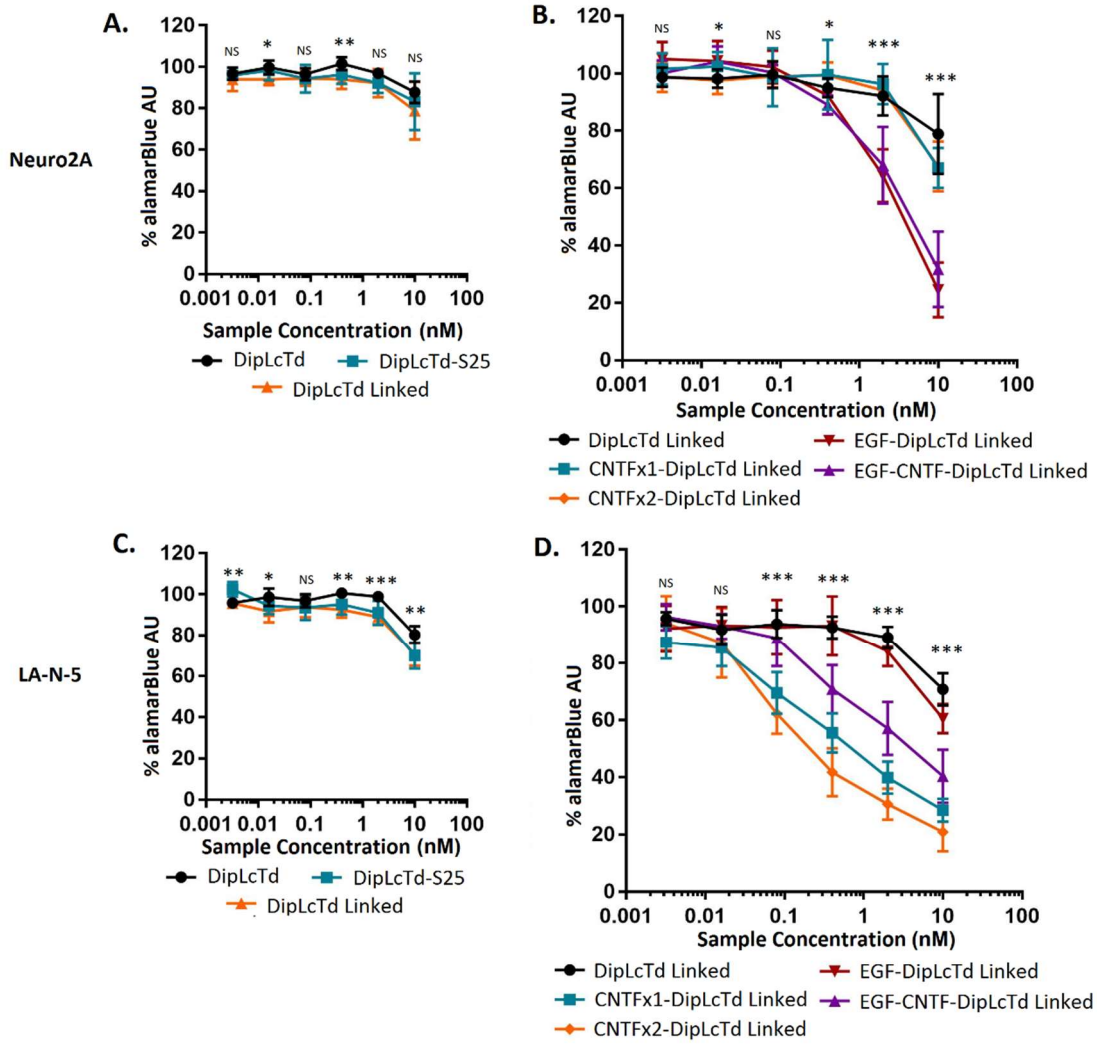
A.
B.
C.
D.
Neuro2A
LA-N-5
% alamarBlue AU
Sample Concentration (nM)
DipLcTd
DipLcTd-S25
DipLcTd Linked
EGF-DipLcTd Linked
CNTFx1-DipLcTd Linked
EGF-CNTF-DipLcTd Linked
CNTFx2-DipLcTd Linked

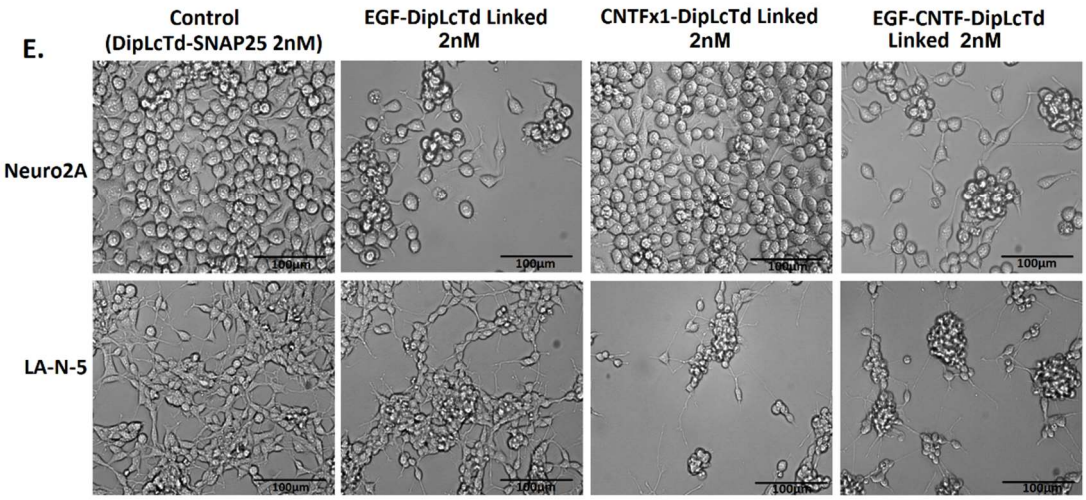
E.
Control (DipLcTd-SNAP25 2nM)
EGF-DipLcTd Linked 2nM
CNTFx1-DipLcTd Linked 2nM
EGF-CNTF-DipLcTd Linked 2nM
Neuro2A
LA-N-5
100µm

Figure 5.14 – Comparing the targeting and internalisation of dual-ligand linked dipLcTd complexes

*A) AlamarBlue assay of Neuro2A cells with dipLcTd control samples (n=3, N=3). B) AlamarBlue assay of ligand linked dipLcTd complexes in Neuro2A cells (n=3, N=3). C) AlamarBlue assay of LA-N-5 cells with dipLcTd control samples (n=3, N=3). D) AlamarBlue assay of ligand linked dipLcTd complexes in LA-N-5 cells (n=3, N=3). Significance of A-D measured by one-way ANOVA for all sample values of the same concentration). E) Representative brightfield images of wells incubated with ligand-linked dipLcTd samples (N=2) (Obj. x40). All conditions shown here were after sample incubation for 72 hours. Significance for statistical analysis: P>0.05 = NS P<0.05 = * P<0.01 = ** P<0.001=***.*

Both Neuro2A and LA-N-5 were observed to have similar responses to both dipLcTd alone and linked dipLcTd, therefore it was deemed appropriate to use imaging to visualise the differences between the ligand linked dipLcTd complexes at the same concentrations. Figure 5.14:E shows the morphology and density of both cell lines in control conditions. Imaged then show cells which have been incubated for 72 hours linked EGF-dipLcTd. In these images there is no visible alteration of LA-N-5 cells, however there is a significant decrease in the number of Neuro2A cells seen in these conditions. The inverse is true when the cells are incubated with linked CNTF-dipLcTd. This shows that ligand-linked complexes can target and internalise into specific cells based on their receptor make-up. When both ligands are linked to the dipLcTd complex then both cells show a significant decrease in cell density, and morphology in the case of LA-N-5, than when compared to the control. This therefore demonstrates that SNARE linking can be utilised to link together domains into a tri-functional complex. Together, this shows that SNARE linking could address not just the need to mix and match protein combinations together, but also that it is possible for it to become a successful conjugation strategy to merge with the current research in dual-targeting therapies.

5.3 Discussion

Within this chapter there have been a large variety of protein-staples used to make numerous complexes. This versatility in itself is demonstration of the niche which SNARE linking occupies as a strategy for building and exploring different combinations of proteins. It has also been successfully demonstrated that three different domains can be linked together in a co-operative tri-functioning complex which has been shown to improve the range of cells that can be specifically targeted for drug delivery.

There has been a degree of variance in the formation and success of the formed complexes. For instance, it is uncertain as to why the double ligand linked complexes in figure 5.2 did not form, yet were able to form efficiently in the presence of botLcTd-SNAP25. Moreover, in figure 5.7 it was demonstrated with brevin-EGF that sometimes linking into complexes does happen very efficiently, but there is not the desired function when tested. Nonetheless, all of the individual protein-staples were found to be functional on their own and all were able to form into complexes of some kind, but it is not currently known why some linked complexes form better than others. On the flip side, there is the advantage that if one protein-staple does not work then there is the option to use a different one. For instance, brevin-CNTF was able to form complexes more efficiently than syntaxin-CNTF in most instances, so in single CNTF complexes, brevin-CNTF was more often used. This diversity opens up a new avenue of protein complex building to aid in successful formation and delivery.

Within these experiments, correct protein concentration calculations were relied upon to ensure the correct ratio of the individual components. This was because the complexes were often made in such small amounts that it was not possible to filter or purify, however, because of the size differences of all the components, if a large enough stock was made it would be possible to filter out the excess. Nonetheless, it was shown in figure 5.2 that most of the protein-staples had no influence on cell morphology or proliferation. But there is concern, especially with CNTF, that excess ligand could bind and internalise receptors, therefore there would be undesirable competitive inhibition of the receptors.

Whilst both botulinum and diphtheria toxic domains used could have their intracellular catalytic effects measured over the 72 hour experiments, it is difficult to determine how functional the enzyme itself is across the 3 days as it is possible that through internalisation and degradation there is no functional toxin left by day 3. A way of potentially measuring this is to remove the sample containing media at particular timepoints during incubation

and dose it onto fresh cells, but this would only measure the presence of functional toxin remaining in the media. However, without doing this, it can be seen from figure 5.12:G that when linked dipLcTd was removed after 15 hours there was significantly less cell death than there was when the linked dipLcTd was incubated for the full 72 hours in figure 5.12E-F. This suggests that there was still functioning dipLcTd in the media between 15 and 72 hours to facilitate that increase in toxic effect. Additionally, figure 5.4:A shows that at 24 hours there was very little SNAP25 cleavage, whereas there was significantly more botulinum mediated SNAP25 cleavage at 72 hours so therefore there must have been active botLcTd/A linked to CNTF either in the media or inside the cells between the two timepoints.

It has been shown here that the recombinant attachment of the translocation domains of toxins to stapling proteins does not influence the protein function. In fact, as found in figure 5.12, the attachment of SNAP25 to the proteins actually significantly enhanced the uptake. It was surprising that there was no decrease in the effectiveness of the protein, this is because of the nature of the translocation domain inserting into the endosomes and forming pores to allow the light chain domain to escape into the cytosol. One would have hypothesised that the recombinant fusing could have interfered with this mechanism but there was no interference and there have been other groups which have used this technique successfully (Fuentes et al. 2015; Nugent et al. 2017). This quelled initial fears raised in figure 3.11 regarding the method of attachment of toxins to stapling proteins as light chains need to be cleaved in order to function. Because of the translocation domain being attached to the light chain via a disulphide bond there is no need to attach the staples via disulphide binding. On the other hand, if there were proteins without translocation domains that one would want to link, it is possible that a disulphide bound staple would be more effective.

Another issue to address with SNARE linked complexes is that they require 0.4% OG to form and this is toxic to cells if not diluted properly. The toxicity was successfully managed through careful diluting and dosing into plates. It should be noted that in this lab samples containing 0.4% OG have been injected into rats (including vehicle control) without dilution and that no adverse effects have been observed in any of the quantities tested (observations from Charlotte Leese and Rebecca Bresnahan of the Davletov lab). Whilst there was initial concern that the OG could permeabilise cells and increase toxin entry

there was no difference in the function of either botLcTd/A or dipLcTd between OG positive and negative samples at the dilutions incubated.

Given that the main pitfalls of the previous chapter surrounded the lack of an efficient targeting sequence, it was especially important here that an effective domain was found which could be linked to the complex and successfully facilitate specific internalisation. Here, two were found. EGFR and its ligands have been previously established as a receptor pathway with potential for targeting numerous cancer varieties cells, however CNTF has not yet been fully realised. Whilst most cells express some degree of EGFR, approximately 30% cancer types have been reported to express up to 200 fold more receptors, significantly increasing targeting potential and highlighting the reason for a trend in research utilising EGFR for cancer specific drug delivery (Herbst & Shin 2002; Seshacharyulu et al. 2013). On the other hand, cancers which respond to CNTF are limited to neuroblastoma and other glioma (Kuroda et al. 2001; Weis et al. 1999). The presence of CNTF signalling in neuroblastoma however is often a hallmark of more well differentiated and less aggressive cancers, which could explain why it was found in the two least proliferative cell lines (Rossino et al. 1995; Negro et al. 1997). Nonetheless, both CNTF and EGF were able to satisfy the requirements for receptor-mediated specific internalisation domains.

It was especially encouraging that by linking two CNTF ligands to toxin-staples complexes there was an increase in measurable catalytic activity, presumably as the result of increased internalisation. Both complexes containing either diphtheria or botulinum A domains linked with CNTF showed a significant increase in cytosolic enzyme activity compared to the complexes without ligand attachment; however, it is worth noting that the significance here is slightly biased. This is because assays used to measure diphtheria toxin were done in triplicate as well as repeated individually 3 times, meaning that there were 9 readings taken; on the other hand, the western blots used to measure SNAP25 cleavage for the botulinum toxin only produced 3 values from the 3 individual experiments. Both ANOVA and Student's T-test take into account the number of values in a sample size when determining significance; therefore, because there were more values taken for the diphtheria experiments over the botulinum ones, there is more likely to be significance calculated.

One of the potential reasons for there being a higher amount of SNAP25 cleavage or toxicity in double ligand complex incubated cells could be because there is a higher rate of

association between the complex and the cell surface receptors. For instance, if both CNTF ligands can bind at the same time to CNTFR, it means that if one dissociates the other could still remain. On the other hand there are studies that show that CNTF and EGF receptors can often dimerise on the cell surface, therefore, dual ligand binding may influence the receptor mechanics or alter the rate of internalisation (Neugart et al. 2009; Songtawee et al. 2015).

One of the remarkable features of some of the cells was the level of heterogeneity, not just between the different cancer cell lines but also within the cell populations in regard to the differences in SNAP25 cleavage between SH-SY5Y cells. Interestingly, LA-N-5 cells did not express heterogeneity to this degree, but this could be explained through its other less cancerous behaviours such as slow growth and more differentiated morphology. It is not uncommon for cancer populations to express heterogeneity; there have been many reports alluding to the benefits of such behaviour, including the increased tendency for drug resistance and more efficient tumour propagation. It has been observed that within numerous tumour microenvironments exists a hierarchy of cells which can have separate roles; for instance some cells main attribute is their extensive growth and proliferation, whilst another population within the tumour functions to sustain this growth through paracrine signalling. This co-operative functioning between cancer cell populations can be the driving force behind aggressive tumours (Cleary et al. 2014; Meacham & Morrison 2013). Because of this, the task of successfully targeting an aggressive cancer cell population is a challenging prospect.

It is therefore advantageous that the SNARE linking method developed in this chapter has been shown to be able to target and internalise different receptors on different cells, which could be a useful strategy for addressing heterogeneity in cancer. This sort of tri-linked protein drug construction is something which has not previously been demonstrated as the chemistry can be difficult and the control of differing domain ratios is a challenge. This method has been successful in exploring the parameters required for efficient drug delivery and identified some of the challenges which have to be overcome. It has also been a useful tool for further understanding both the function and potential that botulinum and diphtheria toxins have as therapeutic enzymes for cancer. It concludes that this SNARE linking is a versatile conjugation platform which has the potential to be utilised with numerous proteins, to ‘mix and match’ different components allowing easy drug domain optimisation for targeting specific cells and delivering desired therapeutic domains.

Chapter 6: General Discussion

The objectives of this project were to investigate pyridyl disulphide conjugation and SNARE linking, using these methods to explore drug design by taking apart the therapeutic components and re-constructing them in novel ways to best exploit their therapeutic potential. Within this, it was also hoped to further understand the nature of particular therapeutic toxins, identify cell internalisation peptides or proteins for neuroblastoma targeting, and investigate how to enhance cytosolic translocation through endosomal escape. This project has touched upon all these key areas with some yielding more success than others; however, even where there has not been the desired outcome there have still been findings of interest which need to be further contemplated and discussed to determine the best course of action for potential future research.

Two methods of conjugation were investigated: one to modify proteins with peptides and the other for protein-protein linking and for triple domain complexes to form. Firstly, pyridyldithio conjugation was successful in modifying proteins through the addition of small peptides, but had severe limitations in the size of the peptides which could be used. There is the possibility that the chemistry exists where proteins could be conjugated to pyridyldithio group, but steps would need to be taken to prevent the chemical linker containing the pyridyldithio domain from being a limiting factor in stability. The pyridyl disulphide conjugation is similar in its efficiency and stability to other methods utilised within 'Click chemistry', which are numerous chemical reactions that are also used for the bioconjugation of peptides in a stereospecific and high yielding reaction in simple reactive conditions (H. Li et al. 2013; McKay & Finn 2014). However, one drawback of Click chemical reactions over pyridyl disulphide conjugation is that they are mostly non-cleavable linkers which cannot be reduced by enzymes once inside cells, which could pose issues with therapeutic efficacy. It could be possible that pyridyl disulphide attached peptides or small molecules may be a new way to specifically bind to antibodies to develop antibody drug conjugates (ADCs). One of the reasons for the extensive use of maleimide in ADCs is the lack of available cysteines partnered with an excess of lysines. However, researchers have now identified the issues of instability and heterogeneity associated with maleimide-lysine conjugation in ADC development and are looking into new ways to modify therapeutic antibodies to allow conjugation via cysteines (Jackson et al. 2014; Behrens et al. 2015; Deonarain et al. 2015).

SNARE linking on the other hand addressed alternative protein linking requirements to pyridyl disulphide conjugation, but whilst it was able to work with protein-protein conjugation there too were issues which arose. Although protein-staples can be used like Lego building blocks as an identification tool for good protein combinations, linking together three separate components significantly increases complexity. For instance, one issue identified here is that there are occasions where functional SNARE proteins simply don't form in a complex with particular other SNAREs, another is that even if they do form there was an example (EGF-botLcTd/A linked) where there was not any complex functionality. Additionally, as a consequence of three protein components coming together there is more excess unlinked protein. Whilst most of the complexes have successfully formed and functioned it could be that excess unlinked protein could result in competitive inhibition at particular concentrations. Although here there has been no attempt to filter the complexes, Charlotte Leese within the Davletov lab has attempted to purify complexes through dialysis membranes, however this resulted in aggregation and dilution of the complexes. It may be possible that other methods could be used for filtering larger or more concentrated stocks, or that molar ratios of the added components could be maintained, making filtering unnecessary.

One way to prevent there being so much unlinked protein at the end of a reaction has been to recombinantly fuse SNARE peptides syntaxin and synaptobrevin together with a desired proteins into a protein termed a 'nanolock'. Thereby, when SNAP25-protein is added the supercoiled complex linker forms with all four helices but there being only two separate components instead of three. Whilst this is successful with linking together two proteins domains, it has not been attempted with three and it would be difficult to do so. Nonetheless, if the SNARE stapling method is only to be utilised to link together two protein domains it would be desirable to use nanolock to reduce protein waste and the need for filtering. On the other hand, it is possible that more than three protein domains could be attached to the SNARE complex. In this instance the SNAP25 can be split into two helixes and each utilised as separate SNARE-staples. Alternatively, for some protein domains it could be possible to attach to both the N and C termini of the staple proteins; however, neither of these methods have been attempted. Based on the observations made regarding the triple linked complexes in chapter 5 and the hypothesised inter-domain interference, it is recommended not to attempt further domain linking until more is known about how to best conserve space around the SNARE linker or to prevent domain interference.

Another advantage of note in SNARE linking is that unlike the possibility of pyridyldithio being used with proteins, SNAREs can be used with peptides. Complexes consisting of x1 and x2 SubstanceP-staple domains were successfully formed and also linked with botLcTd-S25, however this data was not shown here owing to there being no internalisation into any of the cell lines tested. Nonetheless, it may be that alternative internalisation peptides for particular cells could also be efficiently linked together via SNARE complex and function successfully. It was hoped that there would be a suitable peptide sequence identified in chapter 4 pyridyl disulphide conjugation investigations that could have been carried over into SNARE linking so that a direct comparison could have been made between the two methods. Unfortunately, whilst CNTF was successful at targeting SH-SY5Y and LA-N-5 cells, it could not have been used attached to pyridyl disulphide because of its size. Human EGF is 53 amino acids in length which was longer than anything that was pyridyldithio attached, it is possible that it could have been successful, but it would not have been without expense or risk. On the other hand, although CPPs did improve toxin uptake through pyridyl disulphide conjugation they were not good enough to warrant staple attachment. Nonetheless, hypothetically if a peptide library was available and a suitable sequence was found it would have been interesting to directly compare the two methods in terms of easiness of conjugation and internalisation efficiency.

Here, both peptide and proteins were investigated for their receptor targeting and cell internalisation properties, as well as their ability to direct proteins and complexes. Whilst peptide targeting yielded limited success, protein targeting produced far better results; this is mostly because of the optimisation steps and the investigation of receptor presence which was done at the beginning of chapter 5. In addition to CNTF and EGF, there are other proteins which were not tested but could have resulted in a similar level of internalisation; interleukins for instance have already proved their success in neuroblastoma as has transferrin and EGF (Louis & Shohet 2015; Ho et al. 2005; Nakamura et al. 2012). However, it was desirable to uncover a novel neuroblastoma targeting domains. Although CNTFR has been previously shown to be present on neuroblastoma cells and CNTF is able to influence particular factors within neuroblastoma, it has not been before established the particulars of using CNTF to target cancer therapeutic domains (Arsenault et al. 2013; Johnson et al. 1994). Here is was successful, but this was only in two out of the three cell lines; this is most likely because CNTFR has been reported to be most present on the least aggressive cancer cells (Garcia et al. 2009; Kuroda et al. 2001). A note of concern is that CNTFR appears

to internalise once activated and it is currently unknown the conditions or timepoint where it may be recycled to the cell surface.

Internalisation of proteins is dependent on kinetics and affinity of the ligand to the receptor, so once specific receptors on diseased tissue are identified then ligands can be modified to improve upon their internalisation. For instance the human CNTF derived protein Axokine has been developed as a therapy for amyotrophic lateral sclerosis and overeating; whilst there has been no FDA approval, it has been reported that Axokine is up to five times more potent than CNTF in both *in vivo* and *in vitro*, as well as having increased stability (Sleeman et al. 2000; Sleeman et al. 2003; Schuster et al. 2003; Marshal & Barbosa 2005). It would therefore be interesting to determine whether Axokine conjugation via linking to toxins would increase delivery. On the other hand, although CNTF is capable of being utilised for toxin targeting to neuroblastoma cells, it is also present on a number of other healthy neural tissues, such as the hypothalamus and the optic nerve (Liu et al. 2007; Severi et al. 2012). Despite this, relative presence of CNTFR has not been directly measured between the healthy tissue and the neuroblastoma, so there still could be potential for CNTF targeting.

Had there been time and resources, it would have been interesting to determine the compatibility of both conjugation methods with antibody targeting. For instance, the monoclonal antibody dinutuximab which targets glycolipid GD2 expressed on neuroblastoma cells and is currently the only antibody therapy approved for neuroblastoma. However, dinutuximab is not an antibody-drug conjugate (ADC), it is an antibody-dependent cell-mediated cytotoxicity drug (ADCC), which means that it does not have a group for drug attachment (Ploessl et al. 2016; Hoy 2016). One of the major drawbacks of ADCs is that they are most often based of ADCCs because they are easier to develop, however there is an issue surrounding antibody therapies because of intellectual property. This makes it difficult for researchers outside the company holding the patent for the approved ADCC to research ADCs. Other ways of creating specific receptor binding domains are emerging which have the specificity and size of ligands, but the non-activation and library selection of antibodies. DARPins (Designed Ankyrin repeat proteins) are derived from ankyrin repeat proteins, the most numerous protein family found in the human genome (Stumpp et al. 2008; Plückthun 2015). These can be built into libraries and because of their variability and size of between 14-21 kDa, they are far more penetrative into tissue than antibodies and are therefore being used as an alternative targeting platform

(Brauchle et al. 2014; Stahl et al. 2013; Boersma et al. 2011). Therefore, as technology for targeting domains evolves so must the conjugation strategies. There is potential that, given the circumstances, SNARE linking or pyridyl disulphide conjugation could be utilised with the ever changing parameters for cell internalisation.

As well as investigating novel sequences for neuroblastoma internalisation, both conjugation methods were also utilised to reveal the potencies and behaviours of toxins. In doing so it was highlighted how long both toxins required before the effect of the cytosolic catalytic activity could be measured. It was analysed that both diphtheria and botulinum LcTd domains required over 24 hours before effects were seen, this was later found to be the case with diphtheria in wider literature however remained unexpected with botulinum neurotoxin A (Kageyama et al. 2002; Yamaizumi et al. 1978). It should be noted that although botulinum required 24 hours here before cleavage was seen, it has been observed by Charlotte Leese within the Davletov lab that when the same botLcTd-S25 was linked to x2 of the native receptor binding domain for botulinum neurotoxin A (Rbd/A) and delivered into differentiated neuroblastoma cells there was approximately 50% SNAP25 cleavage at 8 hours and 80% cleavage at 24 hours (data unpublished). This suggests that botLcTd/A is capable of quickly cleaving SNAP25 within cells, but it does depend on the targeting domain which is used to internalise.

Botulinum neurotoxin was used here because of its link with pain and its potential as an anti-cancer agent, however it also made a good enzyme for assaying cytosolic escape due to the unique effect of SNAP25 cleavage and the lack of cleaved SNAP25 breakdown by the cell (Huang et al. 1998). Diphtheria toxin cytosolic presence on the other hand results in cell death, which is not as specific. It is important to clarify the following point: botLcTd-s25 cleaves the SNAP25 9 amino acids at the C-terminus (aa.197-206), but there is still SNARE formation, this has been previously documented (Huang et al. 1998; Montecucco et al. 2005). However, when endogenous SNAP25 is cleaved it is also still able to form complexes; it is proposed that the reason for the decrease in exocytosis observed here and in other botulinum therapies is because the formed SNARE complex has significantly decreased its responsiveness to cytosolic Ca^{2+} release which stimulates exocytosis (Sørensen et al. 2006; Trudeau et al. 1998; Sakaba et al. 2015).

It was originally intended to use BLF once the delivery of other toxins had been established; this would have been useful as a further investigation of how BLF could potentially target cells and inhibit growth without killing them, thereby being a useful drug whilst reducing

cancer side effects (Rust et al. 2015). However, due to difficulties in synthesis and the lack of translocation domain this was not successful. It would also have been interesting to see how two different non-toxic enzymes behaved when linked together through SNARE stapling, for instance, whether BLF and botLcTd could have been used together to prevent growth and signalling.

Within this project endosomal escape was identified as a major limiting step; whilst this was anticipated, there are still relatively few papers which look dedicatedly at endosomal escape (Fuchs et al. 2016; Varkouhi et al. 2011). This is maybe because understanding still needs to be developed, which presents problems because cytosolic translocation is difficult to research independently of cell internalisation. Moreover, it is apparent that different cell lines have different internalisation pathways and mechanisms. The data here suggest that endosomal escape could also hold a degree of cell specificity; however, this is hard to conclude because in the system here the factors influencing internalisation and the eventual endosomal escape could not be reliably separated. It could be important to further understand factors which influence endosomal escape as specific translocation domains may be more preferential depending on the cell line or toxin used. Whilst this was suggested with dipLcTd in its difference in EC_{50} between Neuro2A and SH-SY5Y cells, it was less apparent with botLcTd, but there could be numerous other examples of cells and translocation domains showing preference. It should be noted that patents do exist which specify the invention of combining clostridial neurotoxins and diphtheria catalytic and translocation domains in order to enhance delivery into neuronal cells (Sutton & Shone 2004; Shone et al. 2003). These modified protein constructs could reveal more about the nature of translocation domain preference in cells, and whether translocation domain function is transferrable between toxins.

For future experimentation, it would be useful to conclude whether a Td-staple linked to a toxinLC-staple would still be able to enhance cytosolic translocation in the same way that the translocation domain would if it was directly attached. Based on current data, it is difficult to speculate; the translocation domain could still interact with the endosomal membrane and form pores. However, on the other hand, the translocation domain stability without the attached light chain is unknown, and there is data which suggests that the diphtheria translocation domain functions as a chaperone as well as a pore (Chassaing et al. 2011; Hammond et al. 2002). It has not been determined whether this chaperone activity would still exist with a long linker in between the two domains.

One of the drawback of the method of assaying the drug complexes is that it is very one-dimensional. Whilst there is evidence of specific targeting and stability, real cancer exists in 3 dimensions with environmental factors (e.g. circulation, inflammation etc.) which are not mimicked in these experiments. Therefore, these results are unlikely to be representative of the results found in an *in vivo* environment. Whilst this is impossible to fully do *in vitro*, an improvement could have been made by using special microplates which encourage the 3D growth of cells, this would aid in testing the penetrative nature of the complexes in tissue (Ravi et al. 2015; Edmondson et al. 2014). It should be noted that colleagues (Rebecca Bresnahan – Davletov Lab) have successfully injected botLcTd/A containing samples linked to RbdA (200 ng in 30 µL) into rat hind-paw and cleaved SNAP25 was found in surrounding tissue as well as in spinal cord at day 7. This strongly suggests that these linked complexes are capable of being used *in vivo* for specific delivery, with their action being dependant on the attached delivery domain.

As well as the development of the conjugation techniques over the course of this project it has been interesting seeing how the understanding of efficient internalisation of protein toxins has been enhanced throughout through investigation into endosomal escape, internalisation domains and how these can all be exploited by the linking platform and cell type. For instance, the dipLC internalisation of chapter 4 in SH cells has worked methodically up to the efficient internalisation of linked CNTFx2-dipLcTd in SH cells at the end of chapter 5. In conclusion, this project has shown how taking a conjugation focused approach to investigating efficient internalisation has enabled a large variety of findings from a different perspective. Additionally, it has identified how these methods of conjugation address currently unmet needs within drug research as well as the limitations that other researchers would need to consider in order to effectively exploit both methods.

References

Allen, T.M., 2002. Ligand-targeted therapeutics in anticancer therapy. *Nature Reviews Cancer*, 2(10), pp.750–763. Available at: http://www.nature.com/doifinder/10.1038/nrc903.

Alves, I.D. et al., 2008. Membrane interaction and perturbation mechanisms induced by two cationic cell penetrating peptides with distinct charge distribution. *Biochimica et Biophysica Acta - General Subjects*, 1780(7–8), pp.948–959.

Antignani, A. & FitzGerald, D., 2013. Immunotoxins: The role of the toxin. *Toxins*, 5(8), pp.1486–1502.

Antignani, A. & Youle, R.J., 2008. Endosome fusion induced by diphtheria toxin translocation domain. *Proceedings of the National Academy of Sciences of the United States of America*, 105(23), pp.8020–5. Available at: http://www.pubmedcentral.nih.gov/articlerender.fcgi?artid=2430352&tool=pmcentrez&rendertype=abstract.

Arap, W., Pasqualini, R. & Ruoslahti, E., 2012. Cancer Treatment by Targeted Drug Delivery to Tumor Vasculature in a Mouse Model Cancer Treatment by Targeted Drug Delivery to Tumor Vasculature in a Mouse Model. *Science*, 377(1998), pp.377–380.

Araye, A. et al., 2016. The Translocation Domain of Botulinum Neurotoxin A Moderates the Propensity of the Catalytic Domain to Interact with Membranes at Acidic pH. *PLoS ONE*, 11(4), pp.1–20.

Arfilli, V. et al., 2010. Shiga toxin 1 and ricin A chain bind to human polymorphonuclear leucocytes through a common receptor. *Biochem. J*, 432, pp.173–180.

Ariansen, S. et al., 1993. Membrane translocation of diphtheria toxin A-fragment: role of carboxy-terminal region. *Biochemistry*, 32(1), pp.83–90. Available at: http://www.ncbi.nlm.nih.gov/pubmed/8418864.

Arnold, P.B. et al., 2009. Modification of blood vessel diameter following perivascular application of botulinum toxin-A. *Hand*, 4(3), pp.302–307.

Arsenault, J. et al., 2013. Stapling of the botulinum type A protease to growth factors and neuropeptides allows selective targeting of neuroendocrine cells. *Journal of Neurochemistry*, 126(2), pp.223–233. Available at: http://doi.wiley.com/10.1111/jnc.12284.

Arttamangkul, S. et al., 2000. Binding and internalization of fluorescent opioid peptide conjugates in living cells. *Molecular Pharmacology*, 58(6), pp.1570–80. Available at: http://eutils.ncbi.nlm.nih.gov/entrez/eutils/elink.fcgi?dbfrom=pubmed&id=11093798&retmode=ref&cmd=prlinks%5Cnhttp://www.ncbi.nlm.nih.gov/pubmed/11093798.

Arunachalam, B. et al., 2000. Enzymatic reduction of disulfide bonds in lysosomes: characterization of a gamma-interferon-inducible lysosomal thiol reductase (GILT). *Proceedings of the National Academy of Sciences of the United States of America*, 97(2), pp.745–750.

Atcheson, R. et al., 1994. Studies on the mechanism of [3H]-noradrenaline release from SH- SY5Y cells: The role of Ca2+ and cyclic AMP. *Br.J.Pharmacol.*, 111, pp.787–792.

Badescu, G. et al., 2014. Bridging disulfides for stable and defined antibody drug conjugates. *Bioconjugate Chemistry*, 25(6), pp.1124–1136.

Baluna, R. et al., 1999. Evidence for a structural motif in toxins and interleukin-2 that may be responsible for binding to endothelial cells and initiating vascular leak syndrome. *Proceedings of the National Academy of Sciences of the United States of America*, 96(7), pp.3957–62. Available at: http://www.pubmedcentral.nih.gov/articlerender.fcgi?artid=22402&tool=pmcentrez&rendertype=abstract.

Bandala, C. et al., 2015. Botulinum neurotoxin type A inhibits synaptic vesicle 2 expression in breast cancer cell lines. *International journal of clinical and experimental pathology*, 8(7), pp.8411–8. Available at: http://www.pubmedcentral.nih.gov/articlerender.fcgi?artid=4555739&tool=pmcentrez&rendertype=abstract.

Bashyal, S. et al., 2016. Cell penetrating peptides as an innovative approach for drug delivery; then, present and the future. *Journal of Pharmaceutical Investigation*, 46(3), pp.205–220.

Bechara, C. & Sagan, S., 2013. Cell-penetrating peptides: 20years later, where do we stand? *FEBS Letters*, 587(12), pp.1693–1702. Available at: http://linkinghub.elsevier.com/retrieve/pii/S0014579313003268.

Beck, A. & Reichert, J.M., 2014. Antibody-Drug Conjugates: Present and future. *mAbs*, 6(1), pp.15–17.

Becker, N. & Benhar, I., 2012. Antibody-Based Immunotoxins for the Treatment of Cancer. *Antibodies*, 1(3), pp.39–69. Available at: http://www.mdpi.com/2073-4468/1/1/39/.

Behrens, C.R. et al., 2015. Antibody-Drug Conjugates (ADCs) Derived from Interchain Cysteine Cross-Linking Demonstrate Improved Homogeneity and Other Pharmacological Properties over Conventional Heterogeneous ADCs. *Molecular Pharmaceutics*, 12(11), pp.3986–3998.

Bell, C.E. & Eisenberg, D., 1996. Crystal structure of diphtheria toxin bound to nicotinamide adenine dinucleotide. *Biochemistry*, 35(4), pp.1137–49. Available at: http://www.ncbi.nlm.nih.gov/pubmed/8573568.

Berman, H.M. et al., 2000. The protein data bank. *Nucleic acids research*, 28(1), pp.235–242.

Biedler, J.L. et al., 1978. Multiple neurotransmitter synthesis by human neuroblastoma cell lines and clones. *Cancer research*, 38(11), pp.3751–7. Available at: http://www.ncbi.nlm.nih.gov/pubmed/29704.

Bigatto, V. et al., 2015. TNF-a promotes invasive growth through the MET signaling pathway. *Molecular Oncology*, 9(2), pp.377–388. Available at: http://dx.doi.org/10.1016/j.molonc.2014.09.002.

Boersma, Y.L. et al., 2011. Bispecific Designed Ankyrin Repeat Proteins (DARPins) targeting epidermal growth factor receptor inhibit A431 cell proliferation and receptor recycling. *Journal of Biological Chemistry*, 286(48), pp.41273–41285.

Böhme, D. & Beck-Sickinger, A.G., 2015. Drug delivery and release systems for targeted tumor therapy. *Journal of Peptide Science*, 21(3), pp.186–200.

De Boisvilliers, M. et al., 2016. VIP and PACAP analogs regulate therapeutic targets in high-risk neuroblastoma cells. *Peptides*, 78, pp.30–41. Available at:

http://dx.doi.org/10.1016/j.peptides.2016.01.014.

Bornstein, G.G., 2015. Antibody Drug Conjugates: Preclinical Considerations. *The AAPS Journal*, 17(3), pp.525–534. Available at: http://link.springer.com/10.1208/s12248-015-9738-4.

Bostad, M. et al., 2015. Light-controlled endosomal escape of the novel CD133-targeting immunotoxin AC133-saporin by photochemical internalization - A minimally invasive cancer stem cell-targeting strategy. *Journal of Controlled Release*, 206, pp.37–48. Available at: http://dx.doi.org/10.1016/j.jconrel.2015.03.008.

Braakman, I. & Hebert, D.N., 2013. Protein folding in the endoplasmic reticulum. *Cold Spring Harbor Perspectives in Biology*, 5(5), p.a013201.

Brauchle, M. et al., 2014. Protein interference applications in cellular and developmental biology using DARPins that recognize GFP and mCherry. *Biology Open*, 3(12), pp.1252–1261. Available at: http://bio.biologists.org/cgi/doi/10.1242/bio.201410041.

Cardoso, A.M.S. et al., 2012. S4(13)-PV cell-penetrating peptide induces physical and morphological changes in membrane-mimetic lipid systems and cell membranes: Implications for cell internalization. *Biochimica et Biophysica Acta - Biomembranes*, 1818(3), pp.877–888.

Carlsson, J., Drevin, H. & Axén, R., 1978. Protein thiolation and reversible protein-protein conjugation. *The Biochemical journal*, 173(3), pp.723–737.

Chaban, V. V. et al., 2013. Physically disconnected non-diffusible cell-to-cell communication between neuroblastoma SH-SY5Y and DRG primary sensory neurons. *American Journal of Translational Research*, 5(1), pp.69–79.

Chanthery, Y.H. et al., 2012. Paracrine Signaling Through MYCN Enhances Tumor-Vascular Interactions in Neuroblastoma. , 4(115), pp.1–21.

Chao, T.Y. & Raines, R.T., 2011. Mechanism of ribonuclease a endocytosis: Analogies to cell-penetrating peptides. *Biochemistry*, 50(39), pp.8374–8382.

Chassaing, A. et al., 2011. Solution and membrane-bound chaperone activity of the diphtheria toxin translocation domain towards the catalytic domain. *FEBS Journal*, 278(23), pp.4516–4525.

Chen, S., 2012. Clinical uses of botulinum neurotoxins: Current indications, limitations and future developments. *Toxins*, 4(10), pp.913–939.

Chen, X., Zaro, J.L. & Shen, W.-C.C., 2014. Fusion Protein Linkers: Property, Design and Functionality. *Advanced Drug Delivery Reviews*, 65(10), pp.1357–1369. Available at: http://dx.doi.org/10.1016/j.addr.2012.09.039.

Chester, C. et al., 2015. Dual antibody therapy to harness the innate anti-tumor immune response to enhance antibody targeting of tumors. *Current Opinion in Immunology*, 33, pp.1–8. Available at: http://dx.doi.org/10.1016/j.coi.2014.12.010.

Christie, R.J. et al., 2015. Stabilization of cysteine-linked antibody drug conjugates with N-aryl maleimides. *Journal of Controlled Release*, 220, pp.660–670.

Chu, J. & Pelletier, J., 2014. Targeting the eIF4A RNA helicase as an anti-neoplastic approach. *Biochim Biophys Acta*, 1849(7), p.doi:10.1016/j.bbagrm.2014.09.00. Available at: http://www.ncbi.nlm.nih.gov/pubmed/25234619.

Cleary, A.S. et al., 2014. Tumour cell heterogeneity maintained by cooperating subclones in Wnt-driven mammary cancers. *Nature*, 508(7494), pp.113–117. Available at: http://www.nature.com/doifinder/10.1038/nature13187.

Cohen, K.A. et al., 2005. Safety evaluation of DT388IL3, a diphtheria toxin/interleukin 3 fusion protein, in the cynomolgus monkey. *Cancer Immunology, Immunotherapy*, 54(8), pp.799–806. Available at: http://link.springer.com/10.1007/s00262-004-0643-4.

Cruz-Migoni, A. et al., 2011. A Burkholderia pseudomallei toxin inhibits helicase activity of translation factor eIF4A. *Science (New York, N.Y.)*, 334(6057), pp.821–4. Available at: http://science.sciencemag.org/content/334/6057/821.abstract.

Darios, F. et al., 2010. SNARE tagging allows stepwise assembly of a multimodular medicinal toxin. *Proceedings of the National Academy of Sciences of the United States of America*, 107(42), pp.18197–18201.

Davletov, B.A. et al., 1998. Vesicle exocytosis stimulated by α-latrotoxin is mediated by latrophilin and requires both external and stored Ca2+. *EMBO Journal*, 17(14), pp.3909–3920.

Deeks, E.D., 2016. Certolizumab Pegol: A Review in Inflammatory Autoimmune Diseases.

BioDrugs, 30(6), pp.607–617.

Delaroche, D. et al., 2007. Tracking a new cell-penetrating (W/R) nonapeptide, through an enzyme-stable mass spectrometry reporter tag. *Analytical Chemistry*, 79(5), pp.1932–1938.

Deonarain, M.P. et al., 2015. Emerging formats for next-generation antibody drug conjugates. *Expert Opinion on Drug Discovery*, 10(5), pp.463–481.

Derossi, D. et al., 1994. The third helix of the Antennapedia homeodomain translocates through biological membranes. *Journal of Biological Chemistry*, 269(14), pp.10444–10450.

Dever, T.E. & Green, R., 2012. The elongation, termination, and recycling phases of translation in eukaryotes. *Cold Spring Harbor Perspectives in Biology*, 4(7), pp.1–16.

Ding, X. et al., 2013. VIP-targeted Cytotoxic Nanomedicine for Breast Cancer. *Drug Delivery and Translational Research*, 16(3), pp.387–393.

Dressler, D. & Benecke, R., 2007. Pharmacology of therapeutic botulinum toxin preparations. *Disability and Rehabilitation*, 29(23), pp.1761–1768. Available at: http://www.tandfonline.com/doi/full/10.1080/09638280701568296.

Ducry, L. & Stump, B., 2017. Antibody-Drug Conjugates : Linking Cytotoxic Payloads to Monoclonal Antibodies Antibody - Drug Conjugates : Linking Cytotoxic Payloads to Monoclonal Antibodies. *Bioconjugate Chemistry*, 21(January), pp.5–13.

Dunican, D.J. & Doherty, P., 2001. Designing cell-permeant phosphopeptides to modulate intracellular signaling pathways. *Biopolymers*, 60(1), pp.45–60. Available at: http://doi.wiley.com/10.1002/1097-0282(2001)60:1%3C45::AID-BIP1003%3E3.0.CO;2-9.

Duvic, M. & Tapur, R., 2008. Optimizing denileukin diftitox (Ontak(registered trademark)) therapy. *Future Oncology*, 4(13), pp.457–469. Available at: http://www.embase.com/search/results?subaction=viewrecord&from=export&id=L352606371.

Eby, J.K. et al., 2012. Polymer micelles with pyridyl disulfide-coupled antigen travel through lymphatics and show enhanced cellular responses following immunization. *Acta Biomaterialia*, 8(9), pp.3210–3217. Available at:

http://dx.doi.org/10.1016/j.actbio.2012.06.007.

Edmondson, R. et al., 2014. Three-Dimensional Cell Culture Systems and Their Applications in Drug Discovery and Cell-Based Biosensors. *Assay Drug Dev Technol*, 12(4), pp.207–218. Available at: http://dx.doi.org/10.1089/adt.2014.573.

Elmquist, A., Lindgren, M. & Bartfai, T., 2001. VE-Cadherin-Derived Cell-Penetrating Peptide , p VEC , with Carrier Functions. *Experimental Cell Research*, 244, pp.237–244.

Endo, Y. & Tsurugi, K., 1987. RNA N-glycosidase activity of ricin A-chain. Mechanism of action of the toxic lectin ricin on eukaryotic ribosomes. *Journal of Biological Chemistry*, 262(17), pp.8128–8130.

Erazo-Oliveras, A. et al., 2014. Protein delivery into live cells by incubation with an endosomolytic agent. *Nature methods*, 11(8), pp.861–867.

Falktoft, B., Georg, B. & Fahrenkrug, J., 2009. Signaling pathways in PACAP regulation of VIP gene expression in human neuroblastoma cells. *Neuropeptides*, 43(5), pp.387–396. Available at: http://dx.doi.org/10.1016/j.npep.2009.08.002.

Farkhani, S.M. et al., 2014. Cell penetrating peptides: Efficient vectors for delivery of nanoparticles, nanocarriers, therapeutic and diagnostic molecules. *Peptides*, 57, pp.78–94.

Ferrari, E. et al., 2011. Re-assembled botulinum neurotoxin inhibits CNS functions without systemic toxicity. *Toxins*, 3(4), pp.345–355.

Ferrari, E. et al., 2013. Synthetic self-assembling clostridial chimera for modulation of sensory functions. *Bioconjugate Chemistry*, 24(10), pp.1750–1759. Available at: http://pubs.acs.org/doi/abs/10.1021/bc4003103.

Fischer, A. et al., 2012. Beltless translocation domain of botulinum neurotoxin A embodies a minimum ion-conductive channel. *Journal of Biological Chemistry*, 287(3), pp.1657–1661.

Fischer, A. et al., 2008. Botulinum neurotoxin devoid of receptor binding domain translocates active protease. *PLoS Pathogens*, 4(12).

Fischer, R. et al., 2004. A Stepwise Dissection of the Intracellular Fate of Cationic Cell-

penetrating Peptides. *Journal of Biological Chemistry*, 279(13), pp.12625–12635.

Fontaine, S.D. et al., 2015. Long-term stabilization of maleimide-thiol conjugates. *Bioconjugate chemistry*, 26(1), pp.145–52. Available at: http://www.ncbi.nlm.nih.gov/pubmed/25494821.

Frankel, A.E., Tagge, E.P. & Willingham, M.C., 1995. Clinical trials of targeted toxins. *Seminars in cancer biology*, 6(5), pp.307–17. Available at: http://www.ncbi.nlm.nih.gov/pubmed/8562908.

Fuchs, H., Weng, A. & Gilabert-Oriol, R., 2016. Augmenting the efficacy of immunotoxins and other targeted protein toxins by endosomal escape enhancers. *Toxins*, 8(7), pp.1–28.

Fuentes, A.C. et al., 2015. Denileukin Diftitox (Ontak) as Maintenance Therapy for Peripheral T-Cell Lymphomas: Three Cases with Sustained Remission. *Case reports in oncological medicine*, 2015, p.123756. Available at: http://www.ncbi.nlm.nih.gov/pubmed/26240767%5Cnhttp://www.pubmedcentral.nih.gov/articlerender.fcgi?artid=PMC4512602.

Futaki, S. et al., 2005. Unique features of a pH-sensitive fusogenic peptide that improves the transfection efficiency of cationic liposomes. *Journal of Gene Medicine*, 7(11), pp.1450–1458.

Gao, H. et al., 2014. RGD and Interleukin-13 Peptide Functionalized Nanoparticles for Enhanced Glioblastoma Cells and Neovasculature Dual Targeting Delivery and Elevated Tumor Penetration. *Molecular Pharmaceutics*, 11(3), pp.1042–1052. Available at: http://pubs.acs.org/doi/abs/10.1021/mp400751g.

Garcia, J. et al., 2009. Comprehensive profiling of the cell surface proteome of Sy5Y neuroblastoma cells yields a subset of proteins associated with tumor differentiation. *Journal of Proteome Research*, 8(8), pp.3791–3796.

Garnacho, C., 2016. Intracellular drug delivery: Mechanisms for cell entry. *Current Pharmaceutical Design*, 22(9), pp.1210–1226.

Géraldine, M. et al., 2010. DHA enhances the noradrenaline release by SH-SY5Y cells. *Neurochemistry International*, 56(1), pp.94–100.

Glaser, T. et al., 1981. Dermorphins, opioid peptides from amphibian skin, act on opioid

receptors of mouse neuroblastoma x rat glioma hybrid cells. *Journal of Neurochemistry*, 36(6), pp.1613–1617.

Greenfield, L. et al., 1983. Nucleotide sequence of the structural gene for diphtheria toxin carried by corynebacteriophage beta. *Proceedings of the National Academy of Sciences of the United States of America*, 80(22), pp.6853–7. Available at: http://www.pubmedcentral.nih.gov/articlerender.fcgi?artid=390084&tool=pmcentrez&rendertype=abstract.

Griffin, B.A., Adams, S.R. & Tsien, R.Y., 1998. Specific Covalent Labeling of Recombinant Protein Molecules Inside Live Cells. *Science*, 281(1998), p.269.

Guardiola, S. et al., 2015. Peptides targeting EGF block the EGF-EGFR interaction. *ChemBioChem*, p.n/a-n/a. Available at: http://doi.wiley.com/10.1002/cbic.201500525.

Guidotti, G., Brambilla, L. & Rossi, D., 2017. Cell-Penetrating Peptides: From Basic Research to Clinics. *Trends in Pharmacological Sciences*, 38(4), pp.406–424. Available at: http://dx.doi.org/10.1016/j.tips.2017.01.003.

Haas, D.H. & Murphy, R.M., 2004. Design of a pH-sensitive pore-forming peptide with improved performance. *Journal of Peptide Research*, 63(1), pp.9–16.

Halling, K.C. et al., 1985. Genomic cloning and characterization of a ricin gene from Ricinus Communis. *Nucleic Acids Research*, 13(22), pp.8019–8033.

Hammond, K., Caputo, G.A. & London, E., 2002. Interaction of the membrane-inserted diphtheria toxin T domain with peptides and its possible implications for chaperone-like T domain behavior. *Biochemistry*, 41(9), pp.3243–3253.

Hartley, R.W., 1989. Barnase and barstar: two small proteins to fold and fit together. *Trends in Biochemical Sciences*, 14(11), pp.450–454.

Hayon, T. et al., 2003. Appraisal of the MTT-based assay as a useful tool for predicting drug chemosensitivity in leukemia. *Leuk Lymphoma*, 44(11), pp.1957–62.

Herbst, R.S. & Shin, D.M., 2002. Monoclonal antibodies to target epidermal growth factor receptor-positive tumors a new paradigm for cancer therapy. *Cancer*, 94(5), pp.1593–1611.

Herce, H.D. et al., 2009. Arginine-rich peptides destabilize the plasma membrane, consistent with a pore formation translocation mechanism of cell-penetrating peptides. *Biophysical Journal*, 97(7), pp.1917–1925. Available at: http://dx.doi.org/10.1016/j.bpj.2009.05.066.

Herce, H.D. & Garcia, A.E., 2007. Molecular dynamics simulations suggest a mechanism for translocation of the HIV-1 TAT peptide across lipid membranes. *Proceedings of the National Academy of Sciences*, 104(52), pp.20805–20810. Available at: http://www.pnas.org/cgi/doi/10.1073/pnas.0706574105.

Herce, H.D., Garcia, A.E. & Cardoso, M.C., 2014. Fundamental Molecular Mechanism for the Cellular Uptake of Guanidinium-Rich Molecules. *Journal of the American Chemical Society*, 136, pp.17459–67. Available at: http://www.hdherce.com/articles/JACS2014/Herce_JACS_2014.pdf.

Herschman, R., 1984. The role of binding ligand in toxic hybrid proteins: a comparison of EGF-ricin, EGF-ricin A-chain, and ricin. *Biochemical and Biophysical Research Communications*, 124(2), pp.551–557.

Hill, D.P. & Robertson, K.A., 1998. Differentiation of LA-N-5 neuroblastoma cells into cholinergic neurons: Methods for differentiation, immunohistochemistry and reporter gene introduction. *Brain Research Protocols*, 2(3), pp.183–190.

Ho, R. et al., 2005. Proliferation of human neuroblastomas mediated by the epidermal growth factor receptor. *Cancer Research*, 65(21), pp.9868–9875.

Hogle, J.M., 2002. Poliovirus cell entry: common structural themes in viral cell entry pathways. *Annual review of microbiology*, 56, pp.677–702. Available at: http://www.pubmedcentral.nih.gov/articlerender.fcgi?artid=1500891&tool=pmcentrez&rendertype=abstract%5Cnhttp://www.ncbi.nlm.nih.gov/pubmed/12142481%5Cnhttp://www.pubmedcentral.nih.gov/articlerender.fcgi?artid=PMC1500891.

Hoy, S.M., 2016. Dinutuximab: A Review in High-Risk Neuroblastoma. *Targeted Oncology*, 11(2), pp.247–253.

Hruskova, K. et al., 2011. Synthesis and initial in vitro evaluations of novel antioxidant aroylhydrazone iron chelators with increased stability against plasma hydrolysis. *Chemical Research in Toxicology*, 24(3), pp.290–302.

Huang, X. et al., 1998. Truncated SNAP-25 (1-197), like botulinum neurotoxin A, can inhibit insulin secretion from HIT-T15 insulinoma cells. *Molecular endocrinology (Baltimore, Md.)*, 12(7), pp.1060–1070.

Huennekens, F., 1994. Tumor targeting: activation of prodrugs by enzyme-monoclonal antibody conjugates. *TIBTECH*, 12, pp.234–239.

Ignatovich, I.A. et al., 2003. Complexes of Plasmid DNA with Basic Domain 47-57 of the HIV-1 Tat Protein Are Transferred to Mammalian Cells by Endocytosis-mediated Pathways. *Journal of Biological Chemistry*, 278(43), pp.42625–42636.

Jackson, D. et al., 2014. In vitro and in vivo evaluation of cysteine and site specific conjugated herceptin antibody-drug conjugates. *PLoS ONE*, 9(1).

Järver, P. et al., 2007. Applications of cell-penetrating peptides in regulation of gene expression. *Biochem. Soc. Trans.*, 35(Pt 4), pp.770–774. Available at: http://www.ncbi.nlm.nih.gov/pubmed/17635145.

Jiang, J. et al., 2015. Atomic structure of anthrax protective antigen pore elucidates toxin translocation. *Nature*, 521(7553), pp.545–549. Available at: http://www.nature.com/doifinder/10.1038/nature14247.

Johnson, R.M. et al., 1994. Recombinant human ciliary neurotrophic factor stimulates the metabolic activity of SH-SY5Y cells as measured by a cytosensor microphysiometer. *Brain research*, 646(2), pp.327–331.

Jones, A.T., 2007. Macropinocytosis: Searching for an endocytic identity and role in the uptake of cell penetrating peptides. *Journal of Cellular and Molecular Medicine*, 11(4), pp.670–684.

Jost, W. et al., 2015. Clinical and pharmacological properties of incobotulinumtoxinA and its use in neurological disorders. *Drug Design, Development and Therapy*, 9, p.1913. Available at: http://www.dovepress.com/clinical-and-pharmacological-properties-of-incobotulinumtoxina-and-its-peer-reviewed-article-DDDT.

Kageyama, A. et al., 2002. Comparison of the apoptosis-inducing abilities of various protein synthesis inhibitors in U937 cells. *Bioscience, biotechnology, and biochemistry*, 66(4), pp.835–839. Available at: http://www.ncbi.nlm.nih.gov/pubmed/12036057.

Kakimoto, S. et al., 2009. The conjugation of diphtheria toxin T domain to poly(ethylenimine) based vectors for enhanced endosomal escape during gene transfection. *Biomaterials*, 30(3), pp.402–408. Available at: http://dx.doi.org/10.1016/j.biomaterials.2008.09.042.

Kakudo, T. et al., 2004. Transferrin-Modified Liposomes Equipped with a pH-Sensitive Fusogenic Peptide: An Artificial Viral-like Delivery System. *Biochemistry*, 43(19), pp.5618–5628.

Kalia, J. & Raines, R.T., 2007. Catalysis of imido-group hydrolysis in a maleimide conjugate. *Bioorganic & medicinal chemistry letters*, 17(22), pp.6286–6289. Available at: http://www.ncbi.nlm.nih.gov/pmc/articles/PMC2245990/%5Cnhttp://www.ncbi.nlm.nih.gov/pmc/articles/PMC2245990/pdf/nihms33056.pdf.

Karsenty, G. et al., 2009. Botulinum Toxin Type A Inhibits the Growth of LNCaP Human Prostate Cancer Cells In Vitro and In Vivo. *The Prostate*, 69(11), pp.1143–1150. Available at: http://doi.wiley.com/10.1002/pros.20958.

Kitagishi, H., Kawasaki, H. & Kano, K., 2015. Bioconjugation of Serum Albumin to a Maleimide-appended Porphyrin/Cyclodextrin Supramolecular Complex as an Artificial Oxygen Carrier in the Bloodstream. *Chemistry - An Asian Journal*, 10(8), pp.1768–1775. Available at: http://doi.wiley.com/10.1002/asia.201500451.

Kitson, S.L. et al., 2013. Antibody-Drug Conjugates (ADCs) – Biotherapeutic bullets. *Chemistry Today*, 31(August), pp.30–36.

Koley, D. & Bard, A.J., 2010. Triton X-100 concentration effects on membrane permeability of a single HeLa cell by scanning electrochemical microscopy (SECM). *Proceedings of the National Academy of Sciences of the United States of America*, 107(39), pp.16783–7. Available at: http://www.ncbi.nlm.nih.gov/pubmed/20837548%5Cnhttp://www.pubmedcentral.nih.gov/articlerender.fcgi?artid=PMC2947864.

Kontermann, R.E., 2012. Dual targeting strategies with bispecific antibodies. *Landes Bioscience*, 4(2), pp.182–197.

Koren, E. & Torchilin, V.P., 2012. Cell-penetrating peptides: Breaking through to the other side. *Trends in Molecular Medicine*, 18(7), pp.385–393. Available at:

http://dx.doi.org/10.1016/j.molmed.2012.04.012.

Koriazova, L.K. & Montal, M., 2009. Translocation of botulinum neurotoxin light chain protease by the heavy chain protein-conducting channel. *Toxicon*, 54(5), pp.565–569.

Kovaříková, P., Mrkvičková, Z. & Klimeš, J., 2008. Investigation of the stability of aromatic hydrazones in plasma and related biological material. *Journal of Pharmaceutical and Biomedical Analysis*, 47(2), pp.360–370.

Kreitman, R., 1998. Immunotoxins for targeted cancer therapy. *Adv Drug Deliv Rev*, 31(1–2), pp.53–88.

Kuczynski, E.A., Sargent, D.J. & Kerbel, R.S., 2015. Implications for Drug Resistance. *Nat Rev Clin Oncol*, 10(10), pp.571–587. Available at: %5C%5Cgbkenpfsphg0001%5CResolute%5CDATA%5CPurpleHat%5Cclients.ph%5CMerckSerono%5CAdmin%5CReferences%5CCRC%5CKuczynski_Nat Rev Clin Oncol_2013.pdf.

Kunwar, S. et al., 2010. Phase III randomized trial of CED of IL13-PE38QQR vs Gliadel wafers for recurrent glioblastoma. *Neuro-Oncology*, 12(8), pp.871–881.

Kuroda, H. et al., 2001. Signaling Pathway of Ciliary Neurotrophic Factor in Neuroblastoma Cell Lines. *Medical and Pediatric Oncology*, 121, pp.118–121.

Lalli, G. & Schiavo, G., 2002. Analysis of retrograde transport in motor neurons reveals common endocytic carriers for tetanus toxin and neurotrophin receptor p75NTR. *Journal of Cell Biology*, 156(2), pp.233–239.

Lee, M.H. et al., 2013. Disulfide-Cleavage-Triggered Chemosensors and Their Biological Applications. *Chemical Reviews*, (113), pp.5071–5109.

Lee, S.H. et al., 2007. Burkholderia pseudomallei animal and human isolates from Malaysia exhibit different phenotypic characteristics. *Diagnostic Microbiology and Infectious Disease*, 58(3), pp.263–270.

Leriche, G., Chisholm, L. & Wagner, A., 2012. Cleavable linkers in chemical biology. *Bioorganic and Medicinal Chemistry*, 20(2), pp.571–582. Available at: http://dx.doi.org/10.1016/j.bmc.2011.07.048.

Levary, D.A. et al., 2011. Protein-Protein Fusion Catalyzed by Sortase A. *PLoS ONE*, 6(4), pp.3–8.

Lewis, D., 2014. Using Polymers as Endosomal Escape Agents for siRNA Delivery in vivo.

Li, H., Aneja, R. & Chaiken, I., 2013. Click Chemistry in Peptide-Based Drug Design Huiyuan. *Molecules*, 18(8), pp.9797–9817.

Li, J. et al., 2015. Neuropeptide y Y1 receptors meditate targeted delivery of anticancer drug with encapsulated nanoparticles to breast cancer cells with high selectivity and its potential for breast cancer therapy. *ACS Applied Materials and Interfaces*, 7(9), pp.5574–5582.

Li, M. et al., 2009. Anti-tumor activity and immunological modification of ribosome-inactivating protein (RIP) from Momordica charantia by covalent attachment of polyethylene glycol. *Acta biochimica et biophysica Sinica*, 41(9), pp.792–799.

Li, W., Nicol, F. & Szoka, F.C., 2004. GALA: A designed synthetic pH-responsive amphipathic peptide with applications in drug and gene delivery. *Advanced Drug Delivery Reviews*, 56(7), pp.967–985.

Li, X.-X. et al., 2015. Standard chemotherapy with cetuximab for treatment of colorectal cancer. *World journal of gastroenterology : WJG*, 21(22), pp.7022–35. Available at: http://www.pubmedcentral.nih.gov/articlerender.fcgi?artid=4462745&tool=pmcentrez&rendertype=abstract.

Li, X. & Mao, C., 2014. Using Phage as a Platform to Select Cancer Cell-Targeting Peptides. *Methods in molecular biology*, 1108, pp.57–68. Available at: http://link.springer.com/10.1007/978-1-62703-751-8.

Li, Y.M., Vallera, D.A. & Hall, W.A., 2013. Diphtheria toxin-based targeted toxin therapy for brain tumors. *Journal of Neuro-Oncology*, 114(2), pp.155–164.

Lim, K.J. et al., 2013. A Cancer Specific Cell-Penetrating Peptide, BR2, for the Efficient Delivery of an scFv into Cancer Cells. *PLoS ONE*, 8(6).

Lin, Y.Z. et al., 1995. Inhibition of nuclear translocation of transcription factor NF-kB by a synthetic peptide containing a cell membrane-permeable motif and nuclear localization sequence. *Journal of Biological Chemistry*, 270(24), pp.14255–14258.

Liou, J.S. et al., 2012. Protein transduction in human cells is enhanced by cell-penetrating peptides fused with an endosomolytic HA2 sequence. *Peptides*, 37(2), pp.273–284. Available at: http://dx.doi.org/10.1016/j.peptides.2012.07.019.

Liu, C.C. et al., 2014. Biotoxins for cancer therapy. *Asian Pacific Journal of Cancer Prevention*, 15(12), pp.4753–4758.

Liu, X., Clark, A.F. & Wordinger, R.J., 2007. Expression of ciliary neurotrophic factor (CNTF) and its tripartite receptor complex by cells of the human optic nerve head. *Molecular vision*, 13(May), pp.758–763.

Lo, L.S. & Wang, S., 2008. An endosomolytic Tat peptide produced by incorporation of histidine and cysteine residues as a nonviral vector for DNA transfection. *Biomaterials*, 29(15), pp.2408–2414.

Lönn, P. et al., 2016. Enhancing Endosomal Escape for Intracellular Delivery of Macromolecular Biologic Therapeutics. *Scientific Reports*, 6(1), p.32301. Available at: http://www.nature.com/articles/srep32301.

Lopes, F.M. et al., 2010. Comparison between proliferative and neuron-like SH-SY5Y cells as an in vitro model for Parkinson disease studies. *Brain Research*, 1337, pp.85–94. Available at: http://dx.doi.org/10.1016/j.brainres.2010.03.102.

Louis, C.U. & Shohet, J.M., 2015. Neuroblastoma : Molecular Pathogenesis and Therapy. *Annu Rev. Med.*, (66), pp.49–63.

Lu, C. et al., 2010. Neuropeptide Y and its Y2 receptor: potential targets in neuroblastoma therapy. *Oncogene*, 29(41), pp.5630–5642. Available at: http://www.nature.com/doifinder/10.1038/onc.2010.301.

Lundholt, B.K., Scudder, K.M. & Pagliaro, L., 2003. A Simple Technique for Reducing Edge Effect in Cell-Based Assays. *Journal of Biomolecular Screening*, 8(5), pp.566–570. Available at: http://journals.sagepub.com/doi/10.1177/1087057103256465.

Lunov, O. et al., 2011. Differential Uptake of Functionalized Polystyrene Nanoparticles by Human Macrophages and a Monocytic Cell Line. *ACS Nano*, 5(3), pp.1657–1669.

Lutz, E.M. et al., 2006. Characterization of novel splice variants of the PAC1 receptor in human neuroblastoma cells: Consequences for signaling by VIP and PACAP. *Molecular and Cellular Neuroscience*, 31(2), pp.193–209.

Luvisetto, S. et al., 2015. Botulinum toxin type a as a therapeutic agent against headache and related disorders. *Toxins*, 7(9), pp.3818–3844.

Lyon, R.P. et al., 2014. Self-hydrolyzing maleimides improve the stability and pharmacological properties of antibody-drug conjugates. *Nature Biotechnology*, 32(10), pp.1059–62. Available at: http://www.ncbi.nlm.nih.gov/pubmed/25194818.

Ma'ayan, A. et al., 2009. Neuro2A Differentiation by Gαi/o Pathway. *Sci Signal.*, 2(54), pp.1–7.

Ma, Y. et al., 2012. Direct cytosolic delivery of cargoes in vivo by a chimera consisting of D- and L-arginine residues. *Journal of Controlled Release*, 162(2), pp.286–294. Available at: http://dx.doi.org/10.1016/j.jconrel.2012.07.022.

Madani, F. et al., 2013. Modeling the endosomal escape of cell-penetrating peptides using a transmembrane pH gradient. *Biochimica et Biophysica Acta (BBA) - Biomembranes*, 1828(4), pp.1198–1204. Available at: http://linkinghub.elsevier.com/retrieve/pii/S0005273612004403.

Mandal, M. & Lee, K.D., 2002. Listeriolysin O-liposome-mediated cytosolic delivery of macromolecule antigen in vivo: Enhancement of antigen-specific cytotoxic T lymphocyte frequency, activity, and tumor protection. *Biochimica et Biophysica Acta - Biomembranes*, 1563(1–2), pp.7–17.

Manjappa, A.S. et al., 2011. Antibody derivatization and conjugation strategies: Application in preparation of stealth immunoliposome to target chemotherapeutics to tumor. *Journal of Controlled Release*, 150(1), pp.2–22.

Marshal, S. & Barbosa, M., 2005. Ciliary Neurotrophic Factor variants. , p.US 2005/0064555 A1.

Master, A.M. & Gupta, A. Sen, 2012. EGF receptor-targeted nanocarriers for enhanced cancer treatment. *Nanomedicine*, 7(12), pp.1895–1906.

McCombs, J.R. & Owen, S.C., 2015. Antibody drug conjugates: design and selection of linker, payload and conjugation chemistry. *The AAPS journal*, 17(2), pp.339–51. Available at: http://www.ncbi.nlm.nih.gov/pubmed/25604608.

McKay, C.S. & Finn, M.G., 2014. Click Chemistry in Complex Mixtures: Bioorthogonal Bioconjugation. *Chem Biol*, 21(9), pp.1075–1101.

McNicholas, S. et al., 2011. Presenting your structures: The CCP4mg molecular-graphics software. *Acta Crystallographica Section D: Biological Crystallography*, 67(4), pp.386–394.

Meacham, C.E. & Morrison, S.J., 2013. Tumour heterogeneity and cancer cell plasticity. *Nature*, 501(7467), pp.328–337. Available at: http://www.nature.com/doifinder/10.1038/nature12624.

Medina-Kauwe, L.K., 2003. Endocytosis of adenovirus and adenovirus capsid proteins. *Advanced Drug Delivery Reviews*, 55(11), pp.1485–1496.

Megison, M.L., Gillory, L. a & Beierle, E. a, 2013. Cell Survival Signaling in Neuroblastoma. *Anticancer Agents Med Chem*, 13(4), pp.563–575.

Merck, 2017. *Benzonase ® Nuclease Brochure*, Nottingham.

Miller, D.K. et al., 1983. Cell killing by lysosomotropic detergents. *Journal of Cell Biology*, 97(6), pp.1841–1851.

Mitchell, D.J. et al., 2000. Polyarginine enters cells more efficiently than other polycationic homopolymers. *The journal of peptide research : official journal of the American Peptide Society*, 56(5), pp.318–325.

Montal, M., 2010. Botulinum Neurotoxin: A Marvel of Protein Design. *Annual Review of Biochemistry*, 79(1), pp.591–617. Available at: http://www.annualreviews.org/doi/abs/10.1146/annurev.biochem.051908.125345.

Montecucco, C. & Molgó, J., 2005. Botulinal neurotoxins: Revival of an old killer. *Current Opinion in Pharmacology*, 5, pp.274–279.

Montecucco, C., Schiavo, G. & Pantano, S., 2005. SNARE complexes and neuroexocytosis: How many, how close? *Trends in Biochemical Sciences*, 30(7), pp.367–372.

Montrose, K. et al., 2013. Xentry, a new class of cell-penetrating peptide uniquely equipped for delivery of drugs. *Scientific Reports*, 3(1), p.1661. Available at: http://www.nature.com/articles/srep01661.

Moon, H. et al., 2016. Plug-and-playable fluorescent cell imaging modular toolkits using the bacterial superglue, SpyTag/SpyCatcher. *Chem. Commun.*, 52(97), pp.14051–14054. Available at: http://xlink.rsc.org/?DOI=C6CC07363H.

Morandat, S. & El Kirat, K., 2007. Solubilization of supported lipid membranes by octyl glucoside observed by time-lapse atomic force microscopy. *Colloids and Surfaces B: Biointerfaces*, 55(2), pp.179–184.

Moynihan, M.R. & Pappenheimer, A.M., 1981. Kinetics of Adenosinediphosphoribosylation of Elongation Factor 2 in Cells Exposed to Diphtheria Toxin. *Infection and Immunity*, 32(2), pp.575–582.

Muller, J.M. et al., 2006. The VIP-receptor system in neuroblastoma cells. *Regulatory Peptides*, 137(1–2), pp.34–41.

Muñoz, M. et al., 2005. The NK1 receptor is involved in the antitumoural action of L-733,060 and in the mitogenic action of substance P on neuroblastoma and glioma cell lines. *Neuropeptides*, 39(4), pp.427–432.

Murphy, J.R., 2011. Mechanism of diphtheria toxin catalytic domain delivery to the eukaryotic cell cytosol and the cellular factors that directly participate in the process. *Toxins*, 3(3), pp.294–308.

Mussbach, F. et al., 2011. Transduction of peptides and proteins into live cells by cell penetrating peptides. *Journal of Cellular Biochemistry*, 112(12), pp.3824–3833.

Mustafa, G., Anderson, E. & Caudle, R., 2008. Anti-nociceptive effect of a conjugate of substance P and light chain of botulinum neurotocin type A. *Pain*, 42(2), pp.157–162.

Nagahama, M. et al., 2014. Intracellular trafficking of Clostridium botulinum C2 toxin. *Toxicon*, 82, pp.76–82. Available at: http://linkinghub.elsevier.com/retrieve/pii/S0041010114000531.

Nakamura, Y. et al., 2012. Transferrin receptor-1 suppresses neurite outgrowth in neuroblastoma Neuro2A cells. *Neurochemistry International*, 60(5), pp.448–457. Available at: http://dx.doi.org/10.1016/j.neuint.2011.08.018.

Negro, A. et al., 1997. CNTF up-regulation of TIMP-2 in neuroblastoma cells. *Molecular Brain Research*, 48, pp.30–36.

Neugart, F. et al., 2009. Detection of ligand-induced CNTF receptor dimers in living cells by fluorescence cross correlation spectroscopy. *Biochimica et Biophysica Acta - Biomembranes*, 1788(9), pp.1890–1900. Available at:

http://dx.doi.org/10.1016/j.bbamem.2009.05.013.

Neundorf, I. et al., 2009. Fusion of a short HA2-derived peptide sequence to cell-penetrating peptides improves cytosolic uptake, but enhances cytotoxic activity. *Pharmaceuticals*, 2(2), pp.49–65.

Ngan, E.S., 2015. Heterogeneity of neuroblastoma. *Oncoscience*, 2(10), p.837. Available at: http://impactjournals.com/oncoscience/index.php?abs=216.

Nicklin, S.A. et al., 2000. Selective Targeting of Gene Transfer to Vascular Endothelial Cells by Use of Peptides Isolated by Phage Display. *Circulation*, 102, p.231.

Nicol, F., Nir, S. & Szoka, F.C., 2000. Effect of phospholipid composition on an amphipathic peptide-mediated pore formation in bilayer vesicles. *Biophysical journal*, 78(2), pp.818–29. Available at: http://www.sciencedirect.com/science/article/pii/S0006349500766392.

Nischan, N. et al., 2015. Covalent attachment of cyclic TAT peptides to GFP results in protein delivery into live cells with immediate bioavailability. *Angewandte Chemie - International Edition*, 54(6), pp.1950–1953.

Nishimura, Y. et al., 2014. A display of pH-sensitive fusogenic GALA peptide facilitates endosomal escape from a Bio-nanocapsule via an endocytic uptake pathway. *Journal of Nanobiotechnology*, 12(1), p.11. Available at: http://www.jnanobiotechnology.com/content/12/1/11 [Accessed September 18, 2014].

Nugent, M. et al., 2017. Conjugate of an IgG binding domain with botulinum neurotoxin A lacking the acceptor moiety targets its SNARE protease into TrkA-expressing cells when coupled to anti-TrkA IgG or Fc-βNGF. *Bioconjugate Chemistry*, p.acs.bioconjchem.7b00157. Available at: http://pubs.acs.org/doi/abs/10.1021/acs.bioconjchem.7b00157.

Oshima, H. et al., 2014. TNF-α/TNFR1 signaling promotes gastric tumorigenesis through induction of Noxo1 and Gna14 in tumor cells. *Oncogene*, 33(29), pp.3820–9. Available at: http://www.ncbi.nlm.nih.gov/pubmed/23975421.

Oyler, G.A. et al., 1989. The identification of a novel synaptosomal-associated protein, SNAP-25, differentially expressed by neuronal subpopulations. *Journal of Cell*

Biology, 109(6 I), pp.3039–3052.

Pack, D.W., Putnam, D. & Langer, R., 2000. Design of imidazole-containing endosomolytic biopolymers for gene delivery. *Biotechnology and Bioengineering*, 67(2), pp.217–223.

Parente, R.A., Nir, S. & Szoka, F.C., 1988. pH-dependent fusion of phosphatidylcholine small vesicles. Induction by a synthetic amphipathic peptide. *Journal of Biological Chemistry*, 263(10), pp.4724–4730.

Pastan, I. et al., 1993. Immunotoxin therapy of cancer. *Oncology (Williston Park, N.Y.)*, 7(5), pp.69-78-80, 83–86.

Patil, N.A. et al., 2015. Cellular disulfide bond formation in bioactive peptides and proteins. *International Journal of Molecular Sciences*, 16(1), pp.1791–1805.

Pence, J. & Shorter, N., 1992. Autoregulation of neuroblastoma growth by vasoactive intestinal peptide. *Journal of Pediatric Surgery*, 27(8), pp.935–944.

Perez, H.L. et al., 2014. Antibody-drug conjugates: Current status and future directions. *Drug Discovery Today*, 19(7), pp.869–881. Available at: http://dx.doi.org/10.1016/j.drudis.2013.11.004.

Pinto, N.R. et al., 2015. Advances in risk classification and treatment strategies for neuroblastoma. *Journal of Clinical Oncology*, 33(27), pp.3008–3017.

Pirazzini, M. et al., 2017. Botulinum Neurotoxins : Biology , Pharmacology , and Toxicology. *pharmacological reviews*, 69, pp.200–235.

Ploessl, C. et al., 2016. Dinutuximab: An Anti-GD2 Monoclonal Antibody for High-Risk Neuroblastoma. *Annals of Pharmacotherapy*, 50(5), pp.416–422.

Plückthun, A., 2015. Designed Ankyrin Repeat Proteins (DARPins): Binding Proteins for Research, Diagnostics, and Therapy. *Annual Review of Pharmacology and Toxicology*, 55(1), pp.489–511. Available at: http://www.annualreviews.org/doi/10.1146/annurev-pharmtox-010611-134654.

Polito, L. et al., 2011. Immunotoxins and other conjugates containing saporin-s6 for cancer therapy. *Toxins*, 3(6), pp.697–720.

Polito, L., Djemil, A. & Bortolotti, M., 2016. Plant Toxin-Based Immunotoxins for Cancer

Therapy: A Short Overview. *Biomedicines*, 4(2), p.12. Available at: http://www.mdpi.com/2227-9059/4/2/12.

Ponte, J.F. et al., 2016. Understanding How the Stability of the Thiol-Maleimide Linkage Impacts the Pharmacokinetics of Lysine-Linked Antibody-Maytansinoid Conjugates. *Bioconjugate Chemistry*, 27(7), pp.1588–1598.

Pooga, M. et al., 1998. Cell penetration by transportan ¨. *The FASEB journal : official publication of the Federation of American Societies for Experimental Biology*, 12(1), pp.67–77.

Quadros, E. V, Nakayama, Y. & Sequeira, J.M., 2013. Saporin Conjugated Monoclonal Antibody to the Transcobalamin Receptor TCblR/CD320 Is Effective in Targeting and Destroying Cancer Cells. *Journal of Cancer Therapy*, 4(6), pp.1074–1081.

Raciborska, D., Trimble, W. & Charlton, M., 1998. Presynaptic protein interactions in vivo: evidence from botulinum A, C, D and E action at frog neuromuscular junction. *The European journal of neuroscience*, 10(8), p.2617–28. Available at: papers3://publication/uuid/B100E67F-9E70-455B-8555-2981E5B3E487.

Rampersad, S.N., 2012. Multiple applications of alamar blue as an indicator of metabolic function and cellular health in cell viability bioassays. *Sensors (Switzerland)*, 12(9), pp.12347–12360.

Ramsey, J.D. & Flynn, N.H., 2015. Cell-penetrating peptides transport therapeutics into cells. *Pharmacology and Therapeutics*, 154, pp.78–86. Available at: http://dx.doi.org/10.1016/j.pharmthera.2015.07.003.

Rangger et al., 2013. Tumor targeting and imaging with dual-peptide conjugated multifunctional liposomal nanoparticles. *International Journal of Nanomedicine*, 8, p.4659. Available at: http://www.dovepress.com/tumor-targeting-and-imaging-with-dual-peptide-conjugated-multifunction-peer-reviewed-article-IJN.

Raso, V. & Basala, M., 1984. A highly cytotoxic human transferrin-ricin A chain conjugate used to select receptor-modified cells. *The Journal of biological chemistry*, 259(2), pp.1143–9. Available at: http://www.ncbi.nlm.nih.gov/pubmed/6319379.

Ravi, M. et al., 2015. 3D cell culture systems: Advantages and applications. *Journal of Cellular Physiology*, 230(1), pp.16–26.

Reddington, S.C. & Howarth, M., 2015. Secrets of a covalent interaction for biomaterials and biotechnology: SpyTag and SpyCatcher. *Current Opinion in Chemical Biology*, 29, pp.94–99. Available at: http://dx.doi.org/10.1016/j.cbpa.2015.10.002.

Reissmann, S., 2014. Cell penetration: scope and limitations by the application of cell-penetrating peptides. *Journal of Peptide Science*, 20(10), pp.760–784. Available at: http://doi.wiley.com/10.1002/psc.2672.

Rossi, E.A., Goldenberg, D.M. & Chang, C.H., 2012. The dock-and-lock method combines recombinant engineering with site-specific covalent conjugation to generate multifunctional structures. *Bioconjugate Chemistry*, 23(3), pp.309–323.

Rossino, P. et al., 1995. Ciliary Neurotrophic Factor-Induced Gene Expression in Human Neuroblastoma Cell Lines. *Neurochemical Research*, 20(6), pp.675–680.

Roth, V., 2006. Doubling Time Computing. , p.http://www.doubling-com/compute.php.

Rust, A. et al., 2015. Two complementary approaches for intracellular delivery of exogenous enzymes. *Sci. Rep.*, 5, pp.1–9. Available at: http://dx.doi.org/10.1038/srep12444%5Cn10.1038/srep12444%5Cnhttp://www.nature.com/srep/2015/150724/srep12444/abs/srep12444.html#supplementary-information.

Saffarian, P. et al., 2016. TAT-BoNT/A(1–448), a novel fusion protein as a therapeutic agent: analysis of transcutaneous delivery and enzyme activity. *Applied Microbiology and Biotechnology*, 100(6), pp.2785–2795.

Sakaba, T. et al., 2015. Distinct Kinetic Changes in Neurotransmitter Release after SNARE Protein Cleavage. *Science*, 309(5733), pp.491–494.

Sandvig, K. & van Deurs, B., 2005. Delivery into cells: lessons learned from plant and bacterial toxins. *Gene therapy*, 12(11), pp.865–872.

Sasaki, K. et al., 2008. An artificial virus-like nano carrier system: Enhanced endosomal escape of nanoparticles via synergistic action of pH-sensitive fusogenic peptide derivatives. *Analytical and Bioanalytical Chemistry*, 391(8), pp.2717–2727.

Scharf, B. et al., 2012. Annexin A2 binds to endosomes following organelle destabilization by particulate wear debris. *Nature Communications*, 3(2012), p.755. Available at: http://www.nature.com/doifinder/10.1038/ncomms1754.

Schmohl, J.U. et al., 2015. Mutagenic deimmunization of diphtheria toxin for use in biologic drug development. *Toxins*, 7(10), pp.4067–4082.

Schrot, J., Weng, A. & Melzig, M.F., 2015. Ribosome-inactivating and related proteins. *Toxins*, 7(5), pp.1556–1615.

Schuster, B. et al., 2003. Signaling of human ciliary neurotrophic factor (CNTF) revisited: The interleukin-6 receptor can serve as an α-receptor for CNTF. *Journal of Biological Chemistry*, 278(11), pp.9528–9535.

Scott, A.M., Wolchok, J.D. & Old, L.J., 2012. Antibody therapy of cancer. *Nature Reviews Cancer*, 12(4), pp.278–287. Available at: http://www.nature.com/doifinder/10.1038/nrc3236.

Seshacharyulu, P. et al., 2013. Targeting the EGFR signaling pathway in cancer therapy. *Expert Opinion on Therapeutic Targets*, 16(1), pp.15–31.

Severi, I. et al., 2012. Constitutive expression of ciliary neurotrophic factor in mouse hypothalamus. *Journal of Anatomy*, 220(6), pp.622–631.

Shastry, P., Basu, A. & Rajadhyaksha, M.S., 2000. Neuroblastoma Cell Lines-A Versatile in Vztro Model in Neurobiology. *International Journal of Neuroscience*, 108, pp.109–126.

Shete, H.K., Prabhu, R.H. & Patravale, V.B., 2014. Endosomal escape: a bottleneck in intracellular design. *Journal of Nanoscience and Nanotechnology*, 14, pp.460–474.

Shi, M., Lu, J. & Shoichet, M.S., 2009. Organic nanoscale drug carriers coupled with ligands for targeted drug delivery in cancer. *Journal of Materials Chemistry*, 19(31), p.5485.

Shimamura, T. et al., 2010. Interleukin 13 Mediates Signal Transduction through Interleukin 13 Receptor 2 in Pancreatic Ductal Adenocarcinoma: Role of IL-13 Pseudomonas Exotoxin in Pancreatic Cancer Therapy. *Clinical Cancer Research*, 16(2), pp.577–586. Available at: http://clincancerres.aacrjournals.org/cgi/doi/10.1158/1078-0432.CCR-09-2015.

Shone, C.C. & Melling, J., 1992. Inhibition of calcium-dependent release of noradrenaline from PC12 cells by botulinum type-A neurotoxin: Long-term effects of the neurotoxin on intact cells. *European Journal of Biochemistry*, 207(3), pp.1009–1016.

Shone, C.C., Sutton, J.M. & Silman, N., 2003. Constructs for the delivery of therapeutic agents to neuronal cells. , p.Pub. No.: US 2003/0147895A1.

Siegall, C., 1994. Targeted toxins as targeted anticancer agents. *Targeted Toxins*, 74(3), pp.1006–1012.

Sleeman, M.W. et al., 2003. Ciliary neurotrophic factor improves diabetic parameters and hepatic steatosis and increases basal metabolic rate in db/db mice. *Proceedings of the National Academy of Sciences*, 100(24), pp.14297–14302. Available at: http://www.pnas.org/cgi/doi/10.1073/pnas.2335926100.

Sleeman, M.W. et al., 2000. The ciliary neurotrophic factor and its receptor, CNTFR alpha. *Pharmaceutica Acta Helvetiae*, 74(2–3), pp.265–72. Available at: http://www.ncbi.nlm.nih.gov/pubmed/10812968%5Cnhttp://ac.els-cdn.com/S0031686599000503/1-s2.0-S0031686599000503-main.pdf?_tid=cccff8a6-0e53-11e3-b754-00000aacb361&acdnat=1377524063_9120befa4a8f18d61b4e4031e4610785%5Cnhttp://www.ncbi.nlm.nih.gov/pubmed/108.

Słomińska-Wojewódzka, M. & Sandvig, K., 2013. Ricin and Ricin-Containing Immunotoxins: Insights into Intracellular Transport and Mechanism of action in Vitro. *Antibodies*, 2(2), pp.236–269. Available at: http://www.mdpi.com/2073-4468/2/2/236/.

Smaglo, B.G., Aldeghaither, D. & Weiner, L.M., 2014. The development of immunoconjugates for targeted cancer therapy. *Nat Rev Clin Oncol*, 11(11), pp.637–648.

Sollner, T. et al., 1993. A Protein Assembly-Disassembly Pathway In-Vitro That May Correspond to Sequential Steps of Synaptic Vesicle Docking, Activation, and Fusion. *Cell*, 75(3), pp.409–418.

Songtawee, N., Bevan, D.R. & Choowongkomon, K., 2015. Molecular dynamics of the asymmetric dimers of EGFR: Simulations on the active and inactive conformations of the kinase domain. *Journal of Molecular Graphics and Modelling*, 58, pp.16–29. Available at: http://dx.doi.org/10.1016/j.jmgm.2015.03.002.

Sørensen, J.B. et al., 2006. Sequential N- to C-terminal SNARE complex assembly drives priming and fusion of secretory vesicles. *The EMBO Journal*, 25(5), pp.955–966.

Available at: http://emboj.embopress.org/cgi/doi/10.1038/sj.emboj.7601003.

Srinivasarao, M., Galliford, C. V. & Low, P.S., 2015. Principles in the design of ligand-targeted cancer therapeutics and imaging agents. *Nature Reviews Drug Discovery*, 14(February), pp.1–17. Available at: http://www.nature.com/doifinder/10.1038/nrd4519.

Stahl, A. et al., 2013. Highly potent VEGF-A-antagonistic DARPins as anti-angiogenic agents for topical and intravitreal applications. *Angiogenesis*, 16(1), pp.101–111.

Stephanopoulos, N. & Francis, M.B., 2011. Choosing an effective protein bioconjugation strategy. *Nature Chemical Biology*, 7, pp.876–884.

Stuchbury, T. et al., 1975. A reporter group delivery system with both absolute and selective specificity for thiol groups and an improved fluorescent probe containing the 7-nitrobenzo-2-oxa-1,3-diazole moiety. *Biochem J*, 151(2), pp.417–432. Available at: http://www.ncbi.nlm.nih.gov/entrez/query.fcgi?cmd=Retrieve&db=PubMed&dopt=Citation&list_uids=3168.

Stumpp, M.T., Binz, H.K. & Amstutz, P., 2008. DARPins: A new generation of protein therapeutics. *Drug Discovery Today*, 13(15–16), pp.695–701.

Sudhof, T.C. & Rothman, J.E., 2009. Membrane Fusion: Grappling with SNARE and SM Proteins. *Science*, 323(5913), pp.474–477. Available at: http://www.sciencemag.org/cgi/doi/10.1126/science.1161748.

Sun, J. et al., 2004. Membrane destabilization by ricin. *European Biophysics Journal*, 33(7), pp.572–579.

Sutton, J.M. & Shone, C.C., 2004. Pharmaceutical use for secreted bacterial effector proteins. , p.Pub. No.: US 2004/0208889 A1.

Thomas, A., Teicher, B.A. & Hassan, R., 2016. Antibody-drug conjugates for cancer therapy. *The Lancet Oncology*, 17(6), pp.e254–e262.

Thompson, D.E. et al., 1990. The complete amino acid sequence of the Clostridium botulinum type A neurotoxin, deduced by nucleotide sequence analysis of the encoding gene. *European journal of biochemistry / FEBS*, 189(1), pp.73–81. Available at: http://www.ncbi.nlm.nih.gov/pubmed/2185020.

Thomson, J., 2001. Use and Preparation of Quench Curves in Liquid Scintillation Counting. *Packard BioScience Company, Meriden, Connecticut*, pp.1–6. Available at: http://www.scar.utoronto.ca/~gurd/BgyC23/quench_curves.pdf.

Tighe, A.P. & Schiavo, G., 2013. Botulinum neurotoxins: Mechanism of action. *Toxicon*, 67, pp.87–93. Available at: http://linkinghub.elsevier.com/retrieve/pii/S0041010112008069.

Toporkiewicz, M. et al., 2015. Toward a magic or imaginary bullet? Ligands for drug targeting to cancer cells: Principles, hopes, and challenges. *International Journal of Nanomedicine*, 10, pp.1399–1414.

Tortorella, S. & Karagiannis, T.C., 2014. Transferrin Receptor-Mediated Endocytosis: A Useful Target for Cancer Therapy. *The Journal of Membrane Biology*, 247(4), pp.291–307. Available at: http://link.springer.com/10.1007/s00232-014-9637-0 [Accessed September 9, 2014].

Trudeau, L.E., Fang, Y. & Haydon, P.G., 1998. Modulation of an early step in the secretory machinery in hippocampal nerve terminals. *Proc Natl Acad Sci U S A*, 95(12), pp.7163–7168. Available at: http://www.pnas.org/content/95/12/7163.full.pdf.

Trujillo, C. et al., 2006. Trojan horse or proton force: Finding the right partner(s) for toxin translocation. *Neurotoxicity Research*, 9(2–3), pp.63–71.

Tumey, L.N. et al., 2014. Mild method for succinimide hydrolysis on ADCs: Impact on ADC potency, stability, exposure, and efficacy. *Bioconjugate Chemistry*, 25(10), pp.1871–1880.

Tünnemann, G. et al., 2006. Cargo-dependent mode of uptake and bioavailability of TAT-containing proteins and peptides in living cells. *The FASEB journal : official publication of the Federation of American Societies for Experimental Biology*, 20(11), pp.1775–1784.

Tyagi, N. et al., 2015. Potential therapeutic applications of plant toxin-ricin in cancer: challenges and advances. *Tumor Biology*, pp.8239–8246. Available at: http://link.springer.com/10.1007/s13277-015-4028-4.

Vaidyanathan, V. V. et al., 1999. Proteolysis of SNAP-25 isoforms by botulinum neurotoxin types A, C, and E: Domains and amino acid residues controlling the

formation of enzyme- substrate complexes and cleavage. *Journal of Neurochemistry*, 72(1), pp.327–337.

Varkouhi, A.K. et al., 2011. Endosomal escape pathways for delivery of biologicals. *Journal of Controlled Release*, 151(3), pp.220–228. Available at: http://dx.doi.org/10.1016/j.jconrel.2010.11.004.

Vaughan, P.F., Peers, C. & Walker, J.H., 1995. The use of the human neuroblastoma SH-SY5Y to study the effect of second messengers on noradrenaline release. *General pharmacology*, 26(6), pp.1191–201. Available at: http://www.ncbi.nlm.nih.gov/pubmed/7590107.

Vingerhoeds, M.H. et al., 1996. Targeted delivery of diphtheria toxin via immunoliposomes: efficient antitumor activity in the presence of inactivating anti-diphtheria toxin antibodies. *FEBS letters*, 395(2–3), pp.245–50. Available at: http://www.ncbi.nlm.nih.gov/pubmed/8898105.

Vives, E., Brodin, P. & Lebleu, B., 1997. A Truncated HIV-1 Tat Protein Basic Domain Rapidly Translocates through the Plasma Membrane and Accumulates in the Cell Nucleus A Truncated HIV-1 Tat Protein Basic Domain Rapidly Translocates through the Plasma Membrane and A. *The Journal of biological chemistry*, 272(25), pp.16010–16017.

Van Der Vlies, A.J. et al., 2010. Synthesis of pyridyl disulfide-functionalized nanoparticles for conjugating thiol-containing small molecules, peptides, and proteins. *Bioconjugate Chemistry*, 21(4), pp.653–662.

Walsh, M.J., Dodd, J.E. & Hautbergue, G.M., 2013. Ribosome-inactivating proteins: Potent poisons and molecular tools. *Virulence*, 4(8), pp.774–84. Available at: http://www.pubmedcentral.nih.gov/articlerender.fcgi?artid=3925711&tool=pmcentrez&rendertype=abstract.

Wang, L. et al., 2014. Adrenomedullin is a therapeutic target in colorectal cancer. *International Journal of Cancer*, 134(9), pp.2041–2050.

Wei, C. et al., 2016. Where did the linker-payload go? – A quantitative investigation on the destination of the released linker-payload from an antibody-drug conjugate with a maleimide linker in plasma. *Analytical Chemistry*, p.acs.analchem.6b00976. Available at: http://pubs.acs.org/doi/abs/10.1021/acs.analchem.6b00976.

Weis, J. et al., 1999. CNTF and its Receptor Subunits in Human Gliomas. *Journal of Neuro-Oncology*, 44(3), pp.243–253.

Weldon, J.E. & Pastan, I., 2012. A guide to taming a toxin: recombinant immunotoxins constructed from Pseudomonas exotoxin A for the treatment of cancer. *FEBS journal*, 278(23), pp.4683–4700.

Wiley, D.C. & Skehel, J.J., 1987. The structure and function of the hemagglutiin membrane glycoprotein of influenza virus. *Structure*, 56, pp.365–394.

Wu, X.Y. et al., 2015. Hypoxia-induced apoptosis is blocked by adrenomedullin via upregulation of Bcl-2 in human osteosarcoma cells. *Oncol Rep*, 34(2), pp.787–794. Available at: http://www.ncbi.nlm.nih.gov/pubmed/26035796.

Yamaizumi, M. et al., 1978. One molecule of diphtheria toxin fragment a introduced into a cell can kill the cell. *Cell*, 15(1), pp.245–250.

Yang, S.T. et al., 2010. Cell-penetrating peptide induces leaky fusion of liposomes containing late endosome-specific anionic lipid. *Biophysical Journal*, 99(8), pp.2525–2533. Available at: http://dx.doi.org/10.1016/j.bpj.2010.08.029.

Yeh, F.L. et al., 2011. Retargeted clostridial neurotoxins as novel agents for treating chronic diseases. *Biochemistry*, 50(48), pp.10419–10421.

Yotsumoto, F. et al., 2009. Efficacy of ligand-based targeting for the EGF system in cancer. *Anticancer research*, 29(11), pp.4879–85. Available at: http://www.ncbi.nlm.nih.gov/pubmed/20032451.

Young Kim, H. et al., 2015. Discovery of a non-cationic cell penetrating peptide derived from membrane-interacting human proteins and its potential as a protein delivery carrier. *Scientific Reports*, 5(October 2014), p.11719. Available at: http://www.nature.com/doifinder/10.1038/srep11719.

Yu, X. et al., 2016. Improved delivery of Cas9 protein/gRNA complexes using lipofectamine CRISPRMAX. *Biotechnology Letters*, 38(6), pp.919–929.

Zahid, M. & Robbins, P.D., 2015. Cell-type specific penetrating peptides: Therapeutic promises and challenges. *Molecules*, 20(7), pp.13055–13070.

Zakeri, B. et al., 2012. Peptide tag forming a rapid covalent bond to a protein, through

engineering a bacterial adhesin. *Proceedings of the National Academy of Sciences*, 109(12), pp.E690–E697. Available at: http://www.pubmedcentral.nih.gov/articlerender.fcgi?artid=3311370&tool=pmcentrez&rendertype=abstract.

Zhang, Q., Gao, H. & He, Q., 2015. Taming Cell Penetrating Peptides: Never Too Old to Teach Old Dogs New Tricks. *Molecular Pharmaceutics*, 12(9).

Zhang, X. et al., 2016. Stability, folding dynamics, and long-range conformational transition of the synaptic t-SNARE complex. *Proceedings of the National Academy of Sciences*, 113(50), pp.E8031–E8040. Available at: http://www.pnas.org/lookup/doi/10.1073/pnas.1605748113.

Appendix

Appendix 1: Amino acid sequences.

All sequences are taken from the point of GST cleavage from thrombin.

Diphtheria Light Chain (aa.1-189) Translocation Domain (aa.194-388)

GSGADDVVDSSKSFVMENFSSYHGTKPGYVDSIQKGIQKPKSGTQGNYDDDWKGFYSTDNKYDAA
GYSVDNENPLSGKAGGVVKVTYPGLTKVLALKVDNAETIKKELGLSLTEPLMEQVGTEEEFIKRFGDG
ASRVVLSLPFAEGSSSVEYINNWEQAKALSVELEINFETRGKRGQDAMYEYMAQACAGNLVPRGSV
GSSLSCINLDWDVIRDKTKTKIESLKEHGPIKNKMSESPNKTVSEEKAKQYLEEFHQTALEHPELSELKT
VTGTNPVFAGANYAAWAVNVAQVIDSETADNLEKTTAALSILPGIGSVMGIADGAVHHNTEEIVAQS
IALSSLMVAQAIPLVGELVDIGFAAYNFVESIINLFQVVHNSYNRPAYSPGHKTQPGILD

Diphtheria Light Chain Thrombin cleavage site

Diphtheria Translocation domain

Diphtheria Light Chain (aa.1-189) Translocation Domain (aa.194-388) – SNAP25B

GSGADDVVDSSKSFVMENFSSYHGTKPGYVDSIQKGIQKPKSGTQGNYDDDWKGFYSTDNKYDAA
GYSVDNENPLSGKAGGVVKVTYPGLTKVLALKVDNAETIKKELGLSLTEPLMEQVGTEEEFIKRFGDG
ASRVVLSLPFAEGSSSVEYINNWEQAKALSVELEINFETRGKRGQDAMYEYMAQACAGNLVPRGSV
GSSLSCINLDWDVIRDKTKTKIESLKEHGPIKNKMSESPNKTVSEEKAKQYLEEFHQTALEHPELSELKT
VTGTNPVFAGANYAAWAVNVAQVIDSETADNLEKTTAALSILPGIGSVMGIADGAVHHNTEEIVAQS
IALSSLMVAQAIPLVGELVDIGFAAYNFVESIINLFQVVHNSYNRPAYSPGHKTQPGILDSMGRLEGAS
GGGGASSAGGASGGGGASSAGAEDADMRNELEEMQRRADQLADESLESTRRMLQLVEESKDAGIR
TLVMLDEQGEQLERIEEGMDQINKDMKEAEKNLTDLGKFAGLAVAPANKLKSSDAYKKAWGNNQD
GVVASQPARVVDEREQMAISGGFIRRVTNDARENEMDENLEQVSGIIGNLRHMALDMGNEIDTQN
RQIDRIMEKADSNKTRIDEANQRATKMLGKLIHRD

Diphtheria Light Chain Thrombin cleavage site

Diphtheria Translocation domain Mouse SNAP25B (2-204)

Diphtheria Light Chain (aa.1-189) Translocation Domain (aa.194-388) - Diphtheria Light Chain (aa. 1-190)

GSGADDVVDSSKSFVMENFSSYHGTKPGYVDSIQKGIQKPKSGTQGNYDDDWKGFYSTDNKYDAA
GYSVDNENPLSGKAGGVVKVTYPGLTKVLALKVDNAETIKKELGLSLTEPLMEQVGTEEEFIKRFGDG
ASRVVLSLPFAEGSSSVEYINNWEQAKALSVELEINFETRGKRGQDAMYEYMAQACAGNLVPRGSV
GSSLSCINLDWDVIRDKTKTKIESLKEHGPIKNKMSESPNKTVSEEKAKQYLEEFHQTALEHPELSELKT
VTGTNPVFAGANYAAWAVNVAQVIDSETADNLEKTTAALSILPGIGSVMGIADGAVHHNTEEIVAQS
IALSSLMVAQAIPLVGELVDIGFAAYNFVESIINLFQVVHNSYNRPAYSPGHKTQPGILDSMGRLEGAS
GGGGASSAGGADDVVDSSKSFVMENFSSYHGTKPGYVDSIQKGIQKPKSGTQGNYDDDWKGFYST
DNKYDAAGYSVDNENPLSGKAGGVVKVTYPGLTKVLALKVDNAETIKKELGLSLTEPLMEQVGTEEFI
KRFGDGASRVVLSLPFAEGSSSVEYINNWEQAKALSVELEINFETRGKRGQDAMYEYMAQACAGNR
KLIHRD

Diphtheria Light Chain Thrombin cleavage site Diphtheria Translocation domain

Diphtheria Light Chain (aa.1-189) Translocation Domain (aa.194-388) – Diphtheria (aa. 179-190) – Cysteine rich domain

GSGADDVVDSSKSFVMENFSSYHGTKPGYVDSIQKGIQKPKSGTQGNYDDDWKGFYSTDNKYDAA
GYSVDNENPLSGKAGGVVKVTYPGLTKVLALKVDNAETIKKELGLSLTEPLMEQVGTEEEFIKRFGDG
ASRVVLSLPFAEGSSSVEYINNWEQAKALSVELEINFETRGKRGQDAMYEYMAQACAGNLVPRGSV
GSSLSCINLDWDVIRDKTKTKIESLKEHGPIKNKMSESPNKTVSEEKAKQYLEEFHQTALEHPELSELKT
VTGTNPVFAGANYAAWAVNVAQVIDSETADNLEKTTAALSILPGIGSVMGIADGAVHHNTEEIVAQS
IALSSLMVAQAIPLVGELVDIGFAAYNFVESIINLFQVVHNSYNRPAYSPGHKTQPGILDSMGGASGG
GGASSAGYEYMAQACAGNRSMGGRLGASGGGGASSAGAEAAAREACCRECCAREAAARGRLLELK
LIHRD

Diphtheria Light Chain Thrombin cleavage site Diphtheria Translocation domain Diphtheria (aa. 179-190) Cysteine rich domain

Botulinum/A Light Chain Translocation Domain (aa. 1-852)

GSPGMPFVNKQFNYKDPVNGVDIAYIKIPNAGQMQPVKAFKIHNKIWVIPERDTFTNPEEGDLNPPP
EAKQVPVSYYDSTYLSTDNEKDNYLKGVTKLFERIYSTDLGRMLLTSIVRGIPFWGGSTIDTELKVIDTN
CINVIQPDGSYRSEELNLVIIGPSADIIQFECKSFGHEVLNLTRNGYGSTQYIRFSPDFTFGFEESLEVDTN
PLLGAGKFATDPAVTLAHELIHAGHRLYGIAINPNRVFKVNTNAYYEMSGLEVSFEELRTFGGHDAKFI
DSLQENEFRLYYYNKFKDIASTLNKAKSIVGTTASLQYMKNVFKEKYLLSEDTSGKFSVDKLKFDKLYKM
LTEIYTEDNFVKFFKVLNRKTYLNFDKAVFKINIVPKVNYTIYDGFNLRNTNLAANFNGQNTEINNMNF
TKLKNFTGLFEFYKLLCVRGIITSKTKSLDKGYNKAKSLVPRGSQALNDLCIKVNNWDLFFSPSEDNFTN
DLNKGEEITSDTNIEAAEENISLDLIQQYYLTFNFDNEPENISIENLSSDIIGQLELMPNIERFPNGKKYEL
DKYTMFHYLRAQEFEHGKSRIALTNSVNEALLNPSRVYTFFSSDYVKKVNKATEAAMFLGWVEQLVY
DFTDETSEVSTTDKIADITIIIPYIGPALNIGNMLYKDDFVGALIFSGAVILLEFIPEIAIPVLGTFALVSYIAN
KVLTVQTIDNALSKRNEKWDEVYKYIVTNWLAKVNTQIDLIRKKMKEALENQAEATKAIINYQYNQYT
EEEKNNINFNIDDLSSKLNESINKAMININKFLNQCSVSYLMNSMIPYGVKRLEDFDASLKDALLKYIYD
NRGTLIGQVDRLKDKVNNTLSTDIPFQLSKYVDNQRLLSTFTEYIKNIRSGILDSMGRLELKLNSS

BoNT/A Lc (1-449) Thrombin cleavage site Optimized BoNT/A Td (449-872)

Botulinum/A Light Chain Translocation Domain (1-852) – SNAP25B

GSPGMPFVNKQFNYKDPVNGVDIAYIKIPNAGQMQPVKAFKIHNKIWVIPERDTFTNPEEGDLNPPP
EAKQVPVSYYDSTYLSTDNEKDNYLKGVTKLFERIYSTDLGRMLLTSIVRGIPFWGGSTIDTELKVIDTN
CINVIQPDGSYRSEELNLVIIGPSADIIQFECKSFGHEVLNLTRNGYGSTQYIRFSPDFTFGFEESLEVDTN
PLLGAGKFATDPAVTLAHELIHAGHRLYGIAINPNRVFKVNTNAYYEMSGLEVSFEELRTFGGHDAKFI
DSLQENEFRLYYYNKFKDIASTLNKAKSIVGTTASLQYMKNVFKEKYLLSEDTSGKFSVDKLKFDKLYKM
LTEIYTEDNFVKFFKVLNRKTYLNFDKAVFKINIVPKVNYTIYDGFNLRNTNLAANFNGQNTEINNMNF
TKLKNFTGLFEFYKLLCVRGIITSKTKSLDKGYNKAKSLVPRGSQALNDLCIKVNNWDLFFSPSEDNFTN
DLNKGEEITSDTNIEAAEENISLDLIQQYYLTFNFDNEPENISIENLSSDIIGQLELMPNIERFPNGKKYEL
DKYTMFHYLRAQEFEHGKSRIALTNSVNEALLNPSRVYTFFSSDYVKKVNKATEAAMFLGWVEQLVY
DFTDETSEVSTTDKIADITIIIPYIGPALNIGNMLYKDDFVGALIFSGAVILLEFIPEIAIPVLGTFALVSYIAN
KVLTVQTIDNALSKRNEKWDEVYKYIVTNWLAKVNTQIDLIRKKMKEALENQAEATKAIINYQYNQYT
EEEKNNINFNIDDLSSKLNESINKAMININKFLNQCSVSYLMNSMIPYGVKRLEDFDASLKDALLKYIYD
NRGTLIGQVDRLKDKVNNTLSTDIPFQLSKYVDNQRLLSTFTEYIKNIRSMAEDADMRNELEEMQRR
ADQLADESLESTRRMLQLVEESKDAGIRTLVMLDEQGEQLERIEEGMDQINKDMKEAEKNLTDLGKF

AGLAVAPANKLKSSDAYKKAWGNNQDGVVASQPARVVDEREQMAISGGFIRRVTNDARENEMDE
NLEQVSGIIGNLRHMALDMGNEIDTQNRQIDRIMEKADSNKTRIDEANQRATKMLGSG

BoNT/A Lc (1-449) Thrombin cleavage site Optimized BoNT/A Td (449-872)

Mouse SNAP25 (1-206)

SNAP25B- Cysteine rich domain (S25-CRD)

GSPGISGGGGGILDSMEAEKNLTDLGKFCGLCVCPCNKLNSS

SNAP25 trunc (aa.2-204)

GSPGISGGGGGILDAEDADMRNELEEMQRRADQLADESLESTRRMLQLVEESKDAGIRTLVMLDEQ
GEQLERIEEGMDQINKDMKEAEKNLTDLGKFAGLAVAPANKLKSSDAYKKAWGNNQDGVVASQPA
RVVDEREQMAISGGFIRRVTNDARENEMDENLEQVSGIIGNLRHMALDMGNEIDTQNRQIDRIME
KADSNKTRIDEANQRATKMLGLDSMDLEEL

Synaptobrevin (28-84) – Ciliary neurotrophic factor (Brevin-CNTF)

GSNLTSNRRLQQTQAQVDEVVDIMRVNVDKVLERDQKLSELDDRADALQAGASQFETSAAKLGILD
SMGRLEGGSGGGGSGGMAFTEHSPLTPHRRDLCSRSIWLARKLRSDLTALTESYVKHQGLNKNINLD
SADGMPVASTDQWSELTEAERLQENLQAYRTFHVLLARLLEDQQVHFTPTEGDFHQAIHTLLLQVAA
FAYQIEELMILLEYKIPRNEADGMPINVGDGGLFEKKLWGLKVLQELSQWTVRSIHDLRFISSHQTGIP
ARGSHYIANNKKM

Synaptobrevin (28-84) Ciliary neurotrophic factor

Syntaxin 3 (195-253) -Ciliary neurotrophic factor (Syx-CNTF)

GSPGISGGGGGILDEGRHKDIVRLESSIKELHDMFMDIAMLVENQGEMLDNIELNVMHTVDHVEKA
RDETKRALDSMGRLEGGSGGGGSGGMAFTEHSPLTPHRRDLCSRSIWLARKLRSDLTALTESYVKHQ
GLNKNINLDSADGMPVASTDQWSELTEAERLQENLQAYRTFHVLLARLLEDQQVHFTPTEGDFHQA
IHTLLLQVAAFAYQIEELMILLEYKIPRNEADGMPINVGDGGLFEKKLWGLKVLQELSQWTVRSIHDLR
FISSHQTGIPARGSHYIANNKKM

Syntaxin 3 (195-253) Ciliary neurotrophic factor

Appendix 2: Designing and establishing CP-BrevinMM

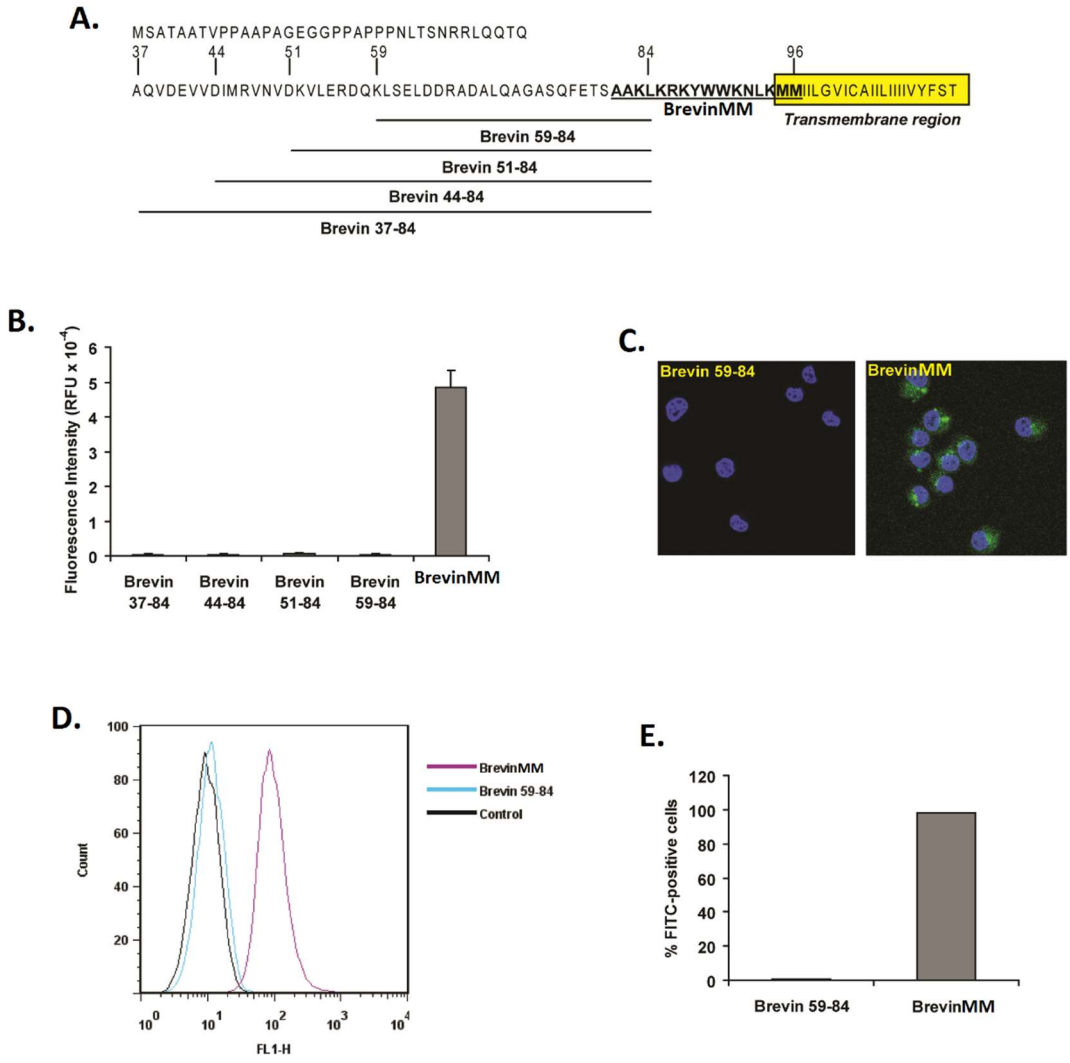

Appendix 2 - Design of a new cell-penetrating peptide: CP-BrevinMM.

A) Synaptobrevin 2 sequence, full-length rat vesicle-associated membrane protein 2. Short peptides (Brevins 37-84, 44-84, 51-84 and 59-84) used as a negative control. Brevin, lysine-enriched peptide from juxtamembrane region of synaptobrevin 2 as a cell-penetrating peptide. B) The ability of these peptides to act as CPPs was tested in RAW 264.7. Cells were treated with 1 µM of FITC-labelled peptides for 1 h and the amount of fluorescence inside the cells was determined after cell lysis by measurement of fluorescence intensity (excitation 490 nm / emission 525 nm). Cells were treated with for 1h with FITC-peptides and the uptake of 1 µM Brevin 59-84 and Brevin was analysed by confocal microscopy (C). The amount of Brevin inside cells (D) and the percentage of cells containing the peptide (E) were estimated by FACS. – All data here was done by Violeta Ruipérez.